FC Ciências ULisboa

Nanoporous carbons from sisal residues and their application in hybrid TiO$_2$/carbon photocatalysts for the removal and degradation of phenol in solution

Doutoramento em Química
Química Tecnológica

Marta Videira Amaral Santos Andrade

Tese orientada por:
Prof. Doutora Ana Paula Carvalho
Doutora Maria Concepción Ovín Ania

Documento especialmente elaborado para a obtenção do grau de doutor

2015

This page is intentionally left blank.

"I am among those who think that science has great beauty.
A scientist in his laboratory is not only a technician:
he is also a child placed before natural phenomena
which impress him like a fairy tale."

"Life is not easy for any of us. But what of that?
We must have perseverance and above all confidence in ourselves.
We must believe that we are gifted for something
and that this thing must be attained."

Marie Curie

Aos meus pais,

ao Luis e ao Vicente

AGRADECIMENTOS

Um agradecimento especial às minhas orientadoras de tese, sem as quais este trabalho não teria sido possível. À Professora Ana Paula Carvalho, agradeço-lhe a sua confiança, o seu apoio incondicional, o entusiasmo pelas novas descobertas, o seu vasto conhecimento e a sua amizade. À Conchi, obrigada pelos novos conhecimentos que me transmitiu, pelo seu dinamismo, por todo o apoio e por me ter proporcionado a realização deste trabalho que se revelou tão enriquecedor. Um muito obrigada ao Juan Matos por toda a sua ajuda nos ensaios fotocatalíticos.

Um agradecimento muito especial à Ana (Mestre), pela sua valiosa amizade ao longo destes anos, pelos seus conselhos, incentivo e confiança, e pela sua contribuição para este trabalho.

Obrigada a todos os colegas do grupo de Adsorção, pelo bom ambiente de trabalho, pela amizade e carinho, em especial à Guida e à Cristina, e também ao Nuno, pelo seu companheirismo e ajuda.

Gostaria de agradecer ao Parra, à Marta, à Rocío, à Leticia, à Nausika, por todo o apoio e carinho que me deram nas minhas idas ao INCAR, a Oviedo, e que de tudo fizeram para que sentisse um pouco em casa. Obrigada também à Alicia pelos ensaios de actinometria.

À Ana, pela sua amizade já tão duradoura, e à Patrícia pelo apoio que me deu nestes últimos meses. Um obrigada ainda a todos os amigos e familiares que me apoiaram durante o decorrer destes últimos anos. Um agradecimento muito especial à minha mãe, que tem sido incansável e que tanto me tem apoiado, estando sempre disponível e acreditando sempre em mim.

E obrigada a ti, Luis, por partilhares todos estes momentos comigo e me ajudares a acreditar que posso sempre fazer melhor, e a ti Vicente, por tornares a minha vida mais colorida, pelos teus beijinhos, sorrisos e abraços.

Obrigada a todos.

Dezembro de 2015

INDEX

LIST OF FIGURES

LIST OF TABLES

ABBREVIATIONS

2,4-DCP	2,4-dichlorophenol
AA	Annual Average
ACF	Activated Carbon Fibers
AOP	Advanced Oxidation Processes
APA	Agência Portuguesa do Ambiente
BDDT	Brunauer, Deming, Deming and Teller
BET	Brunauer, Emmet and Teller
BJH	Barrett, Joyner and Halenda
BOD	Biological Oxygen Demand
CAS	Chemical Abstracts Service
CB	Conduction Band
COD	Chemical Oxygen Demand
DFT	Density Functional Theory
DR	Dubinin-Raduskhevich
EC_{50}	Effective Concentration that reduces by 50 % the response of a certain population of organisms, after a specified exposure duration
EEA	European Environment Agency
ELV	Emission Limit Value
EDX	Energy Dispersive X-ray Spectroscopy
EU	European Union
FTIR	Fourier Tranform Infrared Spectroscopy
GAC	Granular Activated Carbon
GC-MS	Gas Chromatography-Mass Spectrometry
HPLC	High Performance Liquid Chromatography
ICP-OES	Inductively Coupled Plasma-Optical Emission Spectrometry
INCAR	Instituto Nacional del Carbón
IR	Infrared
IUPAC	International Union of Pure and Applied Chemistry
LH	Langmuir-Hinshelwood
MBR	Membrane Bioreactor
MF	Microfiltration
NF	Nanofiltration
NP-10	Nonylphenol decaethoxylate

ppb	parts per billion
ppm	parts per million
PAC	Powdered Activated Carbon
PMV	Permissible Maximum Value
PZC	Point of Zero Charge
QY	Quantum Yield
RMV	Recommended Maximum Value
RO	Reverse Osmosis
SEM	Scanning Electron Microscopy
SHE	Standard Hydrogen Electrode
TEM	Transmission Electron Microscopy
TG	Thermogravimetry
TOC	Total Organic Carbon
TPR	Temperature Programmed Reduction
TU	Toxicity Unit
TVFM	Theory of Volume Filling of Micropores
UF	Ultrafiltration
USEPA	United States Environmental Protection Agency
UV	Ultraviolet (electromagnetic radiation in the range λ: 100-400 nm)
UVA	Ultraviolet A (electromagnetic radiation in the range λ: 315-400 nm)
UVC	Ultraviolet C (electromagnetic radiation in the range λ: 100-280 nm)
UV-vis	Ultraviolet-visible
VB	Valence Band
WDS	Wavelength Dispersive X-Ray Spectroscopy
WWTP	Wastewater Treatment Plant
XPS	X-ray Photoelectron Spectroscopy
XRD	X-ray Diffraction

SYMBOLS

A	adsorption potential
Abs	absorbance
A_{BET}	specific apparent area determined by the BET method
a_m	mean area occupied by a molecule in the monolayer
c_{BET}	BET constant
C	concentration
C_o	initial concentration
C/C_o	relative concentration
C_e	concentration at the equilibrium
d	Interplanar distance
e^-	electron
eV	electron Volt
E	characteristic energy of the system under study
E_o	characteristic energy that depends on the adsorbent
E_1	adsorption molar energy for the first layer
E_L	liquefaction energy
E_{bg}	energy band gap
h^+	hole
$\hbar$	Planck´s constant
h	initial adsorption rate
hkl	Miller indexes
k_1	pseudo-first order constant rate
k_2	pseudo-second order constant rate
k_{app}	apparent constant rate
K_{ab}	absorption rate constant
K_e	equilibrium constant
K_s	dispersion rate constant
L_o	mean pore radius
m	slope
m/z	mass-to-charge ratio
n^{ads}	adsorbed amount at pressure p
n_m	monolayer capacity
N_A	Avogrado's constant
p	pressure
$p°$	saturation pressure
$p/p°$	relative pressure

pH_{PZC}	pH at the point of zero charge
pKa	acid dissociation constant
P	radiant power
q_e	adsorbed amount at equilibrium
q_P	photon flux, chemical basis
$q_{n,p}$	photon flux, amount basis
q_t	adsorbed amount at time t
r	reaction rate
R	gas constant
R_L	relative reflectance
re	removal efficiency
t	time
$t_{1/2}$	half-life time obtained by the pseudo-second order equation
T	temperature
V	volume
V_{meso}	mesoporous volume
V_{micro}	microporous volume
V_{total}	total pore volume
w	weigth of dry carbon
$W_{0,N2}$	microporous volume obtained by the application of the DR equation to the N_2 adsorption isotherm at $-196\,°C$
$W_{0,CO2}$	microporous volume obtained by the application of the DR equation to the CO_2 adsorption isotherm at $0\,°C$
β	affinity coeficient
Δabs	absorbance variation
ΔG	Gibbs free energy variation
ΔS	entropy variation
ΔH	enthalpy variation
ε	molar absorption coefficient
λ	wavelength
ν	frequency
θ	Bragg angle

ABSTRACT

The main aim of this PhD thesis was the development of nanoporous adsorbents and catalysts using industrial by-products of low commercial value as precursors and to investigate their application in advanced remediation technologies for the removal and/or degradation of aromatic pollutants in aqueous solution.

The first stage of this study consisted on investigating the valorization of rope industry´s wastes through the analysis of their pyrolytic behaviour. The thermal characterization of the residues confirmed that although most decomposition occurs at 400 ∘C, some pyrolytic reactions take place above 550 ∘C. The yields of the different fractions were 22 wt. % of a carbonaceous residue (char), 50 wt. % tars and a gas fraction at 800 ∘C. From the analysis of the different fractions, it was possible to conclude that the produced oil was rich in hydrocarbons and alcohols, while the gas fraction is mainly composed of CO_2, CO and CH4, and the carbonaceous solid residue displayed somewhat porous features, with a more developed porous structure as the pyrolysis temperature increased.

Further on, the synthesis of copper-doped activated carbons from sisal residues was explored, using a wet impregnation and low temperature calcination procedure. The incorporation of copper was also performed in a bituminous coal for comparison purposes. The role of copper on the physicochemical and structural features of the materials has shown to be strongly dependent on the nature of the carbon matrix. The dual role of copper on the reactivity of the carbons was observed; on one hand, favouring the development of microporosity in the case of the coal-derived activated carbon, due to the catalysed air gasification of the material at a very low temperature (i.e., 325 ℃); on the other hand, the immobilization of copper on the sisal-derived carbon, acted as a combustion retardant during the calcination step, protecting the carbon matrix. In both cases, a homogenous distribution of copper within the carbon matrix, and a good preservation of large textural properties were observed.

The incorporation of copper on the carbon material was also carried out through a different approach, via impregnation of the carbon precursor followed by activation. This allowed to obtain carbon materials displaying a well-developed nanoporous texture (although comparatively with a marked inhibition of the textural development), and a homogeneous dispersion of copper particles, predominantly as Cu(II) species. These materials were used in the photocatalytic degradation of phenol from solution under visible light, as hybrid titania/Cu-carbon composites. The photo-oxidation tests showed the outstanding role of copper under visible light, in terms of increased phenol conversion, mineralization degree and degradation rate. Similar overall conversions were obtained with half of the amount of the photoactive semiconductor (1:1 composites). The beneficial effect of copper loading was also observed in

the marked regioselectivity of the intermediates, towards the preferential formation of catechol. Furthermore, the copper-loaded photocatalyst was found to be stable upon long irradiation exposure.

The nanoporous carbons prepared from the activation of sisal wastes were also used as additives to TiO_2 powders. The incorporation of the carbon material in the formulation of the photocatalyst (TiO_2/carbon) proved to increase the photocatalytic performance of TiO_2 regardless the studied illumination conditions, although the effect was more pronounced at λ > 200 nm. The photocatalytic runs performed using the carbon alone as catalyst confirmed a certain level of self photoactivity under different irradiation conditions (λ > 200 nm or λ > 360 nm). An evident deactivation of the carbon photocatalyst was observed after 60 min of irradiation, most likely due to the consumption of the photoactive sites. As for the photo-oxidation mechanism for the carbon component, a marked regioselectivity towards the ortho-substitution was also observed at high energy photons, confirming the strong effect of both the composition of the catalyst and the illumination conditions on the nature of the degradation intermediates of phenol.

RESUMO

O principal objetivo do trabalho que se apresenta nesta tese de doutoramento foi o desenvolvimento de adsorventes e catalisadores nanoporosos usando como precursores subprodutos industriais de baixo valor comercial e avaliar o seu desempenho em tecnologias avançadas para a remediação (remoção e/ou degradação) de poluentes aromáticos em solução aquosa.

A primeira etapa do estudo consistiu em investigar a valorização de resíduos de sisal provenientes da indústria de cordoaria. O sisal (*Agave sisalana*) é uma das fibras naturais de origem lenhinocelulósica mais utilizadas em todo o mundo, devido às suas excelentes características relacionadas com o baixo custo e densidade, boas propriedades mecânicas e ausência de toxicidade. O processo de manufatura de cordas gera uma quantidade elevada de desperdícios, que são claramente subaproveitados, sendo utilizados apenas na produção de cordas de qualidade inferior ou como combustível. Dado o interesse crescente em explorar novas aplicações para estes resíduos, a análise feita neste trabalho relativamente ao seu comportamento pirolítico, permitiu avaliar a potencialidade das fibras de sisal para outras aplicações que não as tradicionais.

A caracterização térmica destes desperdícios confirmou que embora a reação de pirólise se inicie a 250 °C, ocorrendo a maioria da decomposição até 400 °C, algumas reações pirolíticas ocorrem acima de 550 °C. Os rendimentos obtidos para as diferentes frações foram de 22 % de um resíduo carbonáceo (carbonizado), 50 % de alcatrão e uma fração gasosa a 800 °C. A partir da análise das diferentes frações, foi possível concluir que o óleo produzido é rico em hidrocarbonetos e álcoois, enquanto que a fração gasosa é composta maioritariamente por CO_2, CO e CH_4.e O resíduo sólido exibe alguma porosidade, observando-se um maior desenvolvimento da estrutura porosa com o aumento da temperatura de pirólise.

Seguidamente foi explorada a modificação da química superficial de dois carvões ativados resultantes de ativação física dos precursores, resíduos de sisal e carvão betuminoso, com dióxido de carbono e vapor de água, respetivamente. Os carvões foram dopados com cobre através de um processo de impregnação em solução e subsequente calcinação feita a uma temperatura baixa.

A influência do cobre sobre as características físico-químicas e estruturais dos materiais mostrou ser altamente dependente da natureza da matriz de carbono. Verificou-se que a influência do cobre na modificação da estrutura depende da reatividade dos carvões, tendo-se constatado que no caso do carvão betuminoso o cobre favorece o desenvolvimento da microporosidade, catalisando a reação de gaseificação do material a uma temperatura muito

baixa (325 °C); enquanto que a imobilização de cobre no carvão derivado de sisal, atuou como um retardante de combustão durante o passo de calcinação, protegendo a matriz de carbono. Em ambos os casos, foi observada uma distribuição homogénea de cobre no interior da matriz de carbono, e uma boa preservação das propriedades texturais.

A incorporação de cobre na matriz carbonácea foi também realizada através de uma abordagem diferente, por meio de impregnação do precursor, seguida de ativação. Para tal, impregnaram-se pedaços de sisal primeiro com uma solução de $Cu(NO_3)_2.3H_2O$ (de modo a obter uma concentração de Cu final de 5%) e seguidamente com uma solução de K_2CO_3, de acordo com a proporção sisal: K_2CO_3 de 2:1. Os materiais preparados apresentaram uma textura nanoporosa bem desenvolvida, embora para o carvão dopado com cobre se observe uma marcada inibição do desenvolvimento estrutural, comparativamente com o carvão não-dopado. Através da aplicação de diversas técnicas, como espectroscopia fotoeletrónica de raios X, difração de raios X e redução a temperatura programada, foi possível concluir que as partículas de cobre apresentam uma dispersão homogénea na matriz de carbono, e são predominantemente espécies de Cu(II).

Estes materiais foram utilizados no processo de fotocatálise heterogénea, uma das tecnologias mais promissoras para a degradação e mineralização de compostos orgânicos recalcitrantes, em meio aquoso. Este processo, que tem sido amplamente estudado na área ambiental, integra os denominados Processos de Oxidação Avançados (POAs), que se baseiam na formação de espécies altamente reativas, como por exemplo, os radicais hidroxilo ($^\bullet OH$), que vão atacar as moléculas orgânicas através de reações sucessivas, até à obtenção de dióxido de carbono e água como produtos finais.

Estudou-se a degradação fotocatalítica de fenol, o qual foi escolhido como molécula modelo, uma vez que é frequentemente detetado em águas residuais, nomeadamente em águas provenientes de diversas indústrias. Dada a sua persistência, baixa biodegradabilidade e toxicidade, alguns compostos fenólicos são considerados poluentes prioritários pelas agências ambientais.

Inicialmente ensaiou-se a degradação de fenol em solução sob irradiação com luz visível, usando como catalisador TiO_2, o semicondutor mais investigado em processos fotocatalíticos e misturas de dióxido de titânio com carvão dopado com cobre, e com carvão não-dopado. Dada a elevada porosidade apresentada pelos carvões ativados, todos os ensaios fotocatalíticos foram precedidos por uma etapa de pré-adsorção de fenol, de modo a eliminar a contribuição do processo de adsorção na reação de fotocatálise.

Os testes de fotooxidação demonstraram o papel fundamental do cobre para, sob irradiação com luz visível, promover o aumento da conversão de fenol, do grau de mineralização Os resultados obtidos mostraram os compósitos 1:1 (i.e. onde se tem apenas metade da quantidade do semicondutor fotoativo da utilizada ao ensaiar apenas o semicondutor) permitem alcançar conversões globais semelhantes. O resultado mais elevado para a mineralização de fenol após 6 h de irradiação foi obtido para o fotocatalisador híbrido TiO_2/Cu-carvão (cerca de 42 %), quase o dobro da mineralização obtida para o compósito TiO_2/carvão não-modificado. O efeito benéfico da presença de cobre foi também observado na regiosselectividade acentuada dos compostos aromáticos intermediários, com a formação preferencial de catecol, considerada um percurso reacional preferencial de oxidação de fenol,

em relação à formação de quinonas, uma vez que se gera um menor número de intermediários, sendo assim mais efetiva para alcançar a mineralização completa (conversão em CO_2 e H_2O). Além disso, o fotocatalisador com cobre mostrou ser estável após um tempo relativamente longo de exposição à irradiação, sem ocorrência de lixiviação ou fotorredução das espécies de cobre.

A interpretação dos resultados considerou que as espécies de cobre dispersas na matriz de carbono poderão criar um meio de transferência eletrónica rápida, minimizando a recombinação dos pares eletrão/lacuna criados com a iluminação do semicondutor e também sítios hidrofóbicos, nos quais o oxigénio molecular dissolvido é facilmente adsorvido, o que favorecerá a formação de espécies radicais de oxigénio.

Os carvões nanoporosos preparados a partir da ativação dos resíduos de sisal foram também utilizados como aditivos ao TiO_2. A incorporação do material de carbono na formulação do fotocatalisador (TiO_2/carvão) provou aumentar o desempenho fotocatalítico do TiO_2 na degradação e mineralização de fenol, independentemente das condições de iluminação estudadas. Contudo o um efeito é mais pronunciado para $\lambda > 200$ nm, dada a presença de fotões mais energéticos e de um fluxo fotónico mais elevado, o qual foi medido por actinometria química. Para estas condições de irradiação a mineralização de fenol com o catalisador TiO_2/carvão é 1.5 vezes superior ao que obteve usando apenas TiO_2, sendo de salientar que no caso da mistura, a quantidade de TiO_2 é apenas metade utilizada para o ensaio com apenas o semicondutor.

Os testes fotocatalíticos realizados utilizando como catalisador apenas o carvão confirmaram um certo nível de fotoatividade sob diferentes condições de irradiação ($\lambda > 200$ nm ou $\lambda > 360$ nm). No entanto, quando a luz é filtrada a $\lambda > 360$ nm, após 60 minutos de irradiação é observada uma clara desativação do fotocatalisador, provavelmente devida ao consumo dos locais fotoativos. Quanto ao mecanismo de fotooxidação para o componente de carbono, no caso de fotões de elevada energia foi também observada uma regiosseletividade marcada relativamente à substituição na posição orto, o que confirma a forte influência da composição do catalisador e das condições de iluminação sobre a natureza dos intermediários de degradação de fenol.

Palavras-chave: sisal, carvão, fenol, fotocatálise, TiO_2

CHAPTER 1

WORK CONTEXTUALIZATION

Water scarcity has become a global issue, triggered by the continuous population growth and increasing standards of living, the climate changes, the industrialization, the intensive agriculture and urbanization. The decrease in water resources worldwide combined with the increasing attention of the authorities regarding environmental protection has led to a continuous search for new water treatment processes capable not only of eliminating the contaminants already recognized as problematic for the environment and public health, but also of providing a solution to emerging pollutants. Polluted water from inadequate wastewater management contributes to the contamination of freshwater and coastal ecosystems, compromising the access to safe drinking water and providing a major health and environmental management challenge. The stringent standards on drinking water quality have favoured the development of alternative technologies to conventional water treatment processes, which are not effective for the treatment of persistent pollutants that remain in the discharged effluents of wastewater treatment plants, and hence reach water courses (Comninellis, Kapalka, *et al.*, 2008; Poyatos, Muñio, *et al.*, 2010; Sanz, Lombraña, *et al.*, 2013).

Advanced Oxidation Processes, which are based on the formation of powerful and non-selective oxidizing agents, have emerged as effective technologies for the degradation of pollutants, as they may lead to their complete mineralization, obtaining carbon dioxide, water and some inorganic compounds as the final products. Among them, heterogeneous photocatalysis based on semiconductors is one of the most promising technologies for wastewater treatment, providing an effective response for the treatment of persistent and recalcitrant compounds. The most widely investigated semiconductor is TiO_2, due to its cost effectiveness, low toxicity and high chemical stability. However, it also presents several drawbacks which are mainly related to the low surface area, low activity under visible light, high recombination rate of photo-generated electron-hole pairs, and recovery and reutilization issues. To overcome these limitations different approaches have been investigated, and the incorporation of a carbon component in the composition of the catalyst appears as an adequate strategy to improve the efficiency of the semiconductor photocatalyst.

Activated carbons are the most commonly applied adsorbents in environmental remediation processes, both in liquid and gas phase. Integrating a wide array of wastewater treatment processes, these materials have recently raised interest concerning their application in photocatalytic processes. Despite carbons are strong light absorbing materials, their incorporation in hybrid carbon/semiconductor composites has been reported as an interesting

strategy to obtain high photoconversion efficiencies in the degradation of a wide variety of pollutants. The enhanced performance of TiO_2/carbon composites has been attributed to several factors associated to an enhanced visible light absorption, the porosity of the carbon support, strong interfacial electronic effects, and/or to the intrinsic photochemical activity of certain carbons (Faria and Wang, 2009; Ania, Velasco, *et al.*, 2012).

Nanoporous carbons are versatile materials that can be easily prepared from diverse industrial and agricultural residues, allowing to obtain added-value products from low-cost and readily available precursors, thus presenting a clear advantage from the economical point of view. Their shape, textural and surface chemistry properties can also be easily modified through different approaches, to meet the requirements of a specific end-application. Thus, activated carbons remain as an important topic in the field of materials research and environmental remediation, with prospects of an increasing demand in the world wastewater management market in the near future.

CHAPTER 2

OBJECTIVES

This dissertation addresses an important environmental issue with implications for public health, as is the problematic of wastewater contamination by phenolic compounds, major contaminants of industrial effluents. These pollutants are not effectively removed by conventional treatments at wastewater treatment plants, due to their persistence and low biodegradability. The aim of this thesis was the development of nanoporous adsorbent materials from industrial by-products of low commercial value, with properties suitable to integrate environmental remediation technologies for the removal/degradation of this type of pollutants in liquid phase.

The first stage of this study consisted on the valorization of lignocellulosic wastes discarded from the rope industry, which were used as precursors for the preparation of the nanoporous carbon adsorbents. These residues are frequently either recycled for the production of low quality ropes or used as fuel. In this sense, the potential of this waste to be transformed in an added-value product was investigated through the pyrolytic behaviour of sisal wastes, with the analysis of the different fractions (gases, tars, solids) originated in this process.

The second part of this study focused on the photocatalytic degradation of a model pollutant, phenol, in aqueous solution. Different methodologies for the preparation of activated carbons using sisal residues as precursors were evaluated, either by physical or chemical activation, with steam or potassium carbonate, respectively. The incorporation of a transition metal, namely copper, in the carbon matrix was also envisaged, with a focus on the subsequent application of these materials in photocatalytic processes. This modification was carried out either using a post-synthesis approach in the preparation of the materials or through the impregnation of the raw sisal waste before the carbonization and activation steps. The synthesized activated carbons were thoroughly characterized by different techniques regarding textural and surface chemistry properties, along with copper content, dispersion, and speciation.

Regarding the photocatalytic degradation of phenol, the goal was to explore the role of the nanoporous and copper containing carbons as additives to TiO_2 in hybrid photocatalysts, under visible light irradiation, by comparing their photocatalytic activity with that of metal-free carbons and TiO_2 alone. Given the porous nature of the carbon materials, the different processes taking place during the experimental procedure, photolysis, photocatalysis and adsorption, were considered. Phenol conversion and mineralization were assessed, as well as the identification and quantification of the degradation intermediates originated during the process. The influence of the irradiation wavelength (UV-visible *vs* visible light) on the photo-

-oxidation mechanism and degradation intermediates of phenol was also investigated for the hybrid TiO$_2$/carbon photocatalysts.

CHAPTER 3

ACTIVATED CARBONS AND ADVANCED PROCESSES FOR WASTEWATER TREATMENT

Wastewater treatment philosophy dates back to thousands of years ago, making part of many ancient civilizations, such as Rome and the Indus Valley. Near the Indus River, in an ancient Indian region, it was located one of the oldest known wastewater management systems dating from about 1500 BC (Chanan, Vigneswaran, *et al.*, 2013; Ranade and Bhandari, 2014). At that time, the local population was established near rivers, thus ensuring an easier water supply and discharge. It is believed that these old communities possessed water supply and sewage systems.

Modern sewage treatment systems date back only a few centuries ago, around the sixteenth century. The development of biological, physical and chemical treatments began gradually. The twentieth century saw the main thrust in this area, and the understanding and knowledge of wastewater treatment evolved since 1900 to date. Currently, industrial wastewater treatment involves primary, secondary and tertiary stages of treatment, and it also tends to employ a combination of chemical and biological treatment methods, in order to satisfy the treated water discharge standards.

In general, wastewater treatment requires a large amount of chemicals, multiple transactions and a very high degree of process control and regular maintenance. The contemporary economic development has also led to the growth of many water-intensive industries that represent the most water polluting sectors. Among them, phenolic compounds are pollutants frequently detected in industrial wastewaters that cause great concern due to its persistence, ecotoxicity, and low biodegradability. Indeed, phenolic compounds are refractory compounds and thus conventional wastewater treatments are not able to effectively remove them from water. So, advanced treatments such as adsorption with activated carbon and advanced oxidation processes are required.

The aim of this chapter is to present an overview of the current state of the scientific knowledge on the occurrence, fate and the available remediation technologies for phenolic compounds in the aquatic environment. The fate of such compounds during conventional wastewater treatment processes along with a review of recent advances in the development of treatment methodologies in environmental waters focused on their mitigation is addressed, highlighting the role of activated carbon adsorption and advanced oxidation processes, namely heterogeneous photocatalysis.

3.1 Freshwater scarcity: a problem at a global scale

 "All people have the right to safe drinking water, sanitation, shelter and basic services."

"Universal access to safe drinking water and water resources is an imperative that cuts across all internationally agreed development objectives, including the Millennium Development Goals."

Ban Ki-moon
Secretary-General of the United Nations

Water is crucial for all aspects of life, the defining feature of our planet. Water is essential to all living organisms on Earth, from the smallest microorganism to the largest living mammal. However, although two-thirds of the world are covered by water, only about 2.5 % of this volume corresponds to fresh water, most of which located in the polar ice caps, glaciers and as permanent snow. Less than 0.7 % of the water found in rivers, lakes and underground water can be used directly for human consumption.

Although it plays a crucial role in maintaining a high quality of life, having an indisputable impact on health and an enormous effect on the economic and social development, this natural resource has become increasingly scarce. According to the Intergovernmental Panel on Climate Change, the four main factors responsible for the water shortage aggravation are population growth, the increase in the number and size of urban areas in developing countries, excessive consumption and climate changes.

The global population is expected to exceed 9 billion people by 2050. Urban populations may rise nearly twice as fast, projected to nearly double from current 3.4 billion to 6.4 billion by 2050. This population increase will mean a greater demand for food, which will be by far the largest contributor to the increase in water consumption, since the food industry uses 70-90 % of the available fresh water (Shiklomanov, 2000; UN, 2009). Climate change will also have a significant impact on the sustainability of water supply in the coming decades, leading to a huge variability in water resources worldwide (Oki and Kanae, 2006).

In addition to these factors, it is important to remember that global water consumption continues to grow at an unsustainable rate, increasing twice as fast as population growth. Considering that 1.2 billion people lack access to safe drinking water, 2.6 billion have little or no sanitation, and millions of people die each year (3900 children a day) due to diseases transmitted through contaminated water, and that this number will rapidly increase, it is easy to anticipate that, as oil is these days, water may soon become the subject of an international conflict. Aware of the importance of water to humanity, in December 2010, following the proposal initiated by Tajikistan and submitted by a group of countries, the United Nations General Assembly declared 2013 as the United Nations International Year of Water Cooperation (A/RES/65/154).

Fresh water shortage is a problem that has been taking major proportions worldwide. The over-exploitation of water resources and recurrent droughts that occurred in recent years are the sources of water scarcity. A recent United Nations report indicates that by the year 2025, two-thirds of the world's population could face water scarcity (UN, 2012). This shortage may be

in the form of physical scarcity, with limited availability of water, or in the form of economic scarcity, whereas although there is water availability, there will exist no facilities and infrastructures that can provide water with the required quantity and quality (Figure 3.1).
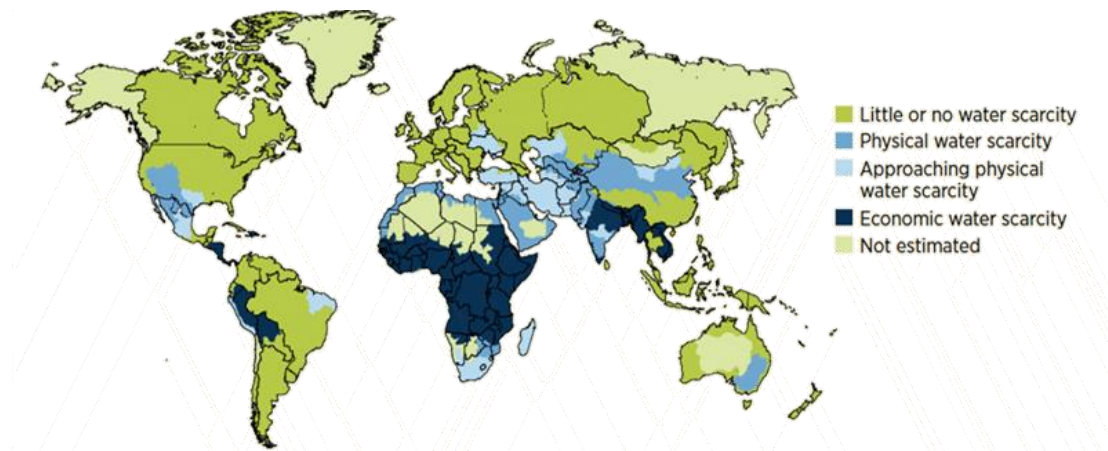
Figure 3.1- Global map of physical and economical water scarcity. Source: UN, 2012.

Since water distribution throughout the world is not uniform, the origin of this shortage can be naturally occurring in some regions due to the reduction of rain or climatic changes. The human factor, however, is also quite critical in the aggravation of this problem, through water waste, pollution of water resources, and/or inadequate management of these resources.

The high fresh water consumption in developed and developing countries originates large volumes of wastewater, which in many cases are highly contaminated with thousands of industrial and natural chemicals. According to recent reports (Corcoran, Nellemann, *et al.*, 2010), it is estimated that the total wastewater-combining sewer, industrial and agricultural wastewaters- which is discharged worldwide rises to tens of million cubic meters per day.

In addition, a significant portion of all wastewater discharges in developing countries is not subject to any treatment, resulting in a high pollution load of rivers and other watercourses, thus putting at risk all living species, including the surrounding population dependent on these water sources. It is estimated that almost 90 % of all sewage in developing countries is discharged without any treatment, polluting rivers, lakes and coastal areas (Figure 3.2) (Corcoran, Nellemann, *et al.*, 2010).

Considering both aspects, it is clear that freshwater contamination is one of the critical environmental problems currently faced by humanity. Water management is thus one of the most significant challenges in environmental protection and sustainability. The best resolution for this issue lies on waste management, through effective treatment, recycling and reuse.

Water supply is naturally regulated by the hydrological cycle, which continually renews watercourses. Surface water flow to the soil (infiltration and percolation) allows the removal of some compounds, not being however, usually sufficient to remove the large variety of undesirable chemical species (e.g., pesticides, solvents, pharmaceuticals, household chemicals, etc.) that can be found in all kinds of water (Kolpin, Furlong, *et al.*, 2002). The leaching of compounds which are present in the soil has also to be taken into account as a factor of water contamination.

In this context, the water treatment industry is a fast-growing market in both developed and developing countries, being the five largest contributors to this growth, as follows:
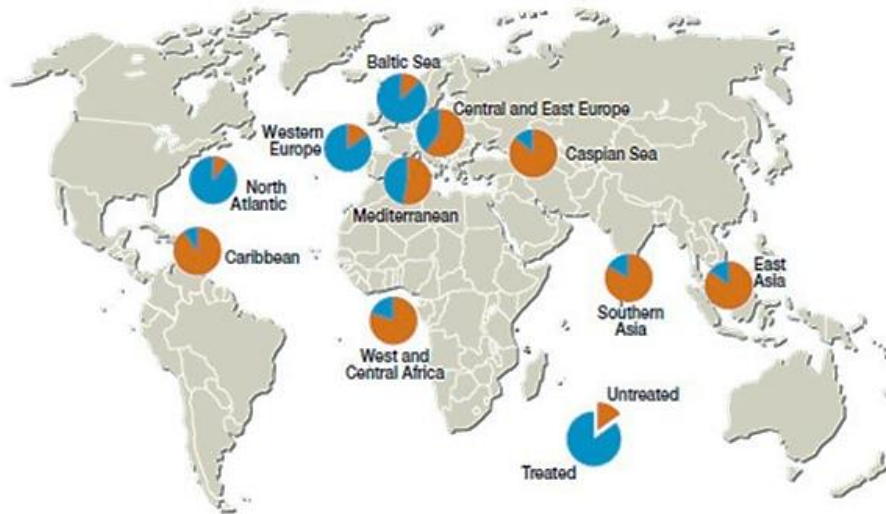
Figure 3.2- The ratio of untreated to treated wastewater reaching water bodies in 10 regions. Source: UNEP/GRID-Arendal. Author: Hugo Ahlenius.

1. The increase in gross domestic product which leads to an increase in water demand (through the expansion of industry);

2. More restrict rules for drinking water and wastewater, due to the implementation of higher quality standards;

3. Increasing drinking water demand with higher health and environmental monitoring standards in developing countries, especially in China and India;

4. The growth of the intensive use of water for the production of alternative energy sources (biofuels);

5. New technologies in the industrial segment, requiring high standards of water purity or increased water reuse.

3.2 Wastewater

3.2.1 Water usage in industry

Water is an important requirement in many industrial processes, for example, heating, cooling, production, cleaning and rinsing. Although these figures may vary considerably between different regions and countries, the industrial (including energy) and domestic sectors represent 20 % and 10 % of the total use of the world's freshwater withdrawals, respectively (Guterres and de Aquim, 2013; UN, 2014a). On average, 44 % of total water abstraction in Europe is used for agriculture, 40 % for industry and energy production (cooling in power plants), and 15 % for public water supply. The main water consumption sectors are irrigation, urbanization, and manufacturing industry.

The percentage of a country's industrial sector water demands is generally proportional to the average income level, representing only ~ 5 % of water withdrawals in low-income countries, compared to over 40 % in some high-income countries (Shiklomanov, 2000; UN, 2014b). Although, at a global scale, industry uses relatively little water in comparison to the agriculture

sector, it requires an accessible, reliable and environmentally supply of consistent and acceptable quality.

Furthermore, water withdrawals for industry are most often reported in combination with those for energy. In addition, the water required for small-scale industry and commerce is often confused with domestic consumption. As a result, surprisingly little is known about how much water is actually withdrawn and consumed by industry for its purposed manufacturing, transformation and production needs.

This observation suggests that the level of a country's or a region's economic development is an important driver of its industrial water use, and may ultimately have as much influence on water use as its population growth. Industry is generally accustomed to have water available at a relatively inexpensive price. Increasing water scarcity, however, will result in higher charges, including additional taxes for water treatment and discharge.

Nowadays, environmental contamination by hazardous and toxic chemicals is considered as one of the major problems faced by industrialized countries. Industry generates a substantial proportion of wastewater that, if unregulated, has the potential to be a highly toxic source of pollution. The vast array of complex organic compounds and heavy metals used in modern industrial processes, if released into the environment can cause both human health and environmental disasters.

Chemical and allied process industries use water extensively, thus making them water-intensive industries (Ranade and Bhandari, 2014). The main uses of water in the industry sector are listed in Table 3.1.

Table 3.1- Typical water uses in chemical and allied industries (Ranade and Bhandari, 2014).

Usage	Volume	Extent of contamination
Reactant	Low	High
Solvent	Low	High
Cleaning/stripping agent	Medium	Medium
Cooling water	Large	Low
Boiler water	Large	Low

These needs for water are satisfied using the following sources:

• Surface water/groundwater
• Seawater
• Recycled water (industrial wastewater/urban sewage).

The industries with the greatest concerns in terms of wastewater are chemical and petrochemical (refineries), pharmaceuticals, pulp and paper, food, fertilizers, tanneries, textile and municipal wastewater treatment plants (Hancock, 1999; Guterres and de Aquim, 2013; Ranade and Bhandari, 2014). In general, the most water-intensive industries are the highest contributors to industrial wastewater generation. For example, the normal paper industry consumes ~ 300 m^3 of water per ton of product, generating a similar amount of wastewater.

The chemical fertilizers industry also contributes greatly to water consumption, requiring up to 270 m^3 of water per ton of product, while the high-quality paper industry needs a maximum

amount of water up to 1000 m³ per ton of product and is one of the most water-intensive in the industry sector. The most water-polluting industries have to be managed through environmental pollution control measures. These industries also represent industry sectors in which a strategy for wastewater treatment, recycling and reuse is crucial (Ranade and Bhandari, 2014).

3.2.2 Wastewater characterization

Wastewater characterization is the first step in the seek for solutions to its treatment, recycling, and reuse. Typically wastewater is characterized in terms of its biological, chemical and physical properties. The major constituents of consideration in wastewater treatment are included in the following categories: suspended solids, biodegradable organic pollutants, pathogenic organisms, nutrients, priority pollutants, refractory organic pollutants, heavy metals and inorganic dissolved solids (Table 3.2) (Tchobanoglous, Burton, *et al.*, 2004a; Guterres and de Aquim, 2013).

Table 3. 2- Principal constituents of concern in wastewater treatment (Tchobanoglous, Burton, *et al.*, 2004a).

Constituents	Reason for importance
Suspended solids	Suspended solids can lead to the development of sludge deposits and anaerobic conditions when untreated wastewater is discharged in the aquatic environment
Biodegradable organics	Composed principally of proteins, carbohydrates, and fats, biodegradable organics are measured most commonly in terms of BOD and COD. If discharged untreated to the environment, their biological stabilization can lead to the depletion of natural oxygen resources and to the development of septic conditions
Pathogens	Transmittable diseases by pathogenic organisms that may be present in wastewater
Nutrients	Both nitrogen and phosphorus, along with carbon, are essential nutrients for growth. When discharged to the aquatic environment, these nutrients can lead to the growth of undesirable aquatic life. When discharged in excessive amounts on land, they can also lead to the pollution of groundwater
Priority pollutants	Organic and inorganic compounds selected on the basis of their known or suspected carcinogenicity, mutagenicity, teratogenicity, or high acute toxicity. Many of these compound are found in wastewater
Refractory organics	These organics tend to resist to conventional methods of wastewater treatment. Typical examples include surfactants, phenols, and agricultural pesticides
Heavy metals	Heavy metals are usually added to wastewater from industrial activities and may have to be removed if the wastewater is to be reused
Dissolved inorganics	Inorganic constituents such as calcium, sodium and sulfate are added to the original domestic water supply as a result of water use and may have to be removed if the wastewater is to be reused

BOD- Biological Oxygen Demand; COD- Chemical Oxygen Demand.

The characterization of wastewater includes the evaluation of separate and independent parameters. The analysis of organic matter in wastewater comprises a number of organic constituents which can not be distinguished separately (Guterres and de Aquim, 2013). Despite being desirable a complete wastewater characterization for devising a treatment methodology, most of the times, only few parameters are measured and monitored. Some of the most important parameters for industrial wastewaters are discussed here.

To analyse the high levels of organic matter (higher than 1 mg L^{-1}), methods commonly used in laboratories include biochemical oxygen demand (BOD), chemical oxygen demand (COD) and total organic carbon (TOC). The BOD value is representative of the total oxygen requirement for oxidizing those chemicals that can be oxidized by bacterial means. These are typically biodegradable substances such as organic matter. Since not all chemicals are biodegradable, another comprehensive parameter that can account for the pollution due to organics is needed. This parameter is COD, which represents the oxygen requirement for oxidizing all the chemicals in the wastewater. In recent years, the TOC measurement, which represents the total organic fraction in terms of carbon, is also a very widespread technique for better accuracy and evaluation of wastewater quality.

Due to the enormous number of potentially polluting substances contained in wastewater, a chemical-specific approach is insufficient to provide the necessary information on water quality. Therefore, biological test systems with living cells or organisms give a global response to the pool of micropollutants present in the sample. The measurement of biochemical responses to chemical contaminants may help improve the assessment of biologically significant exposures to toxic chemicals and enhance the ability to assess the risk of effects on the health and survival of toxicant exposed populations. The need for effluent toxicity evaluation is being acknowledged and toxicity tests have been included in regulatory requirements. The maximum toxicity level of a final effluent allowed to be discharged is calculated based on the effluent dilution rate in the river and its ecotoxicity.

Ecotoxicity tests on several trophic level using, for example, the following organisms are recommended: producer organisms – algae (e.g., *Scenedesmus subspicatus*, *Chlorella vulgaris*,), primary consumers – microcrustaceans (e.g., *Daphnia magna*, *Cladocera*), secondary consumers – like fish (*Danio rerio*, *Brachydanio rerio*), and decomposers – bacteria (*Vibrio fischeri*). The crustacean *Daphnia magna* is the most commonly used organism in the study and control of water quality and is used in biological assays to determine the toxicity of wastewater.

One of the purposes of ecotoxicological tests is to determine the maximum concentration which does not affect a given relevant parameter of the test organisms. Ecotoxicity is generally expressed as toxicity units, obtained from the equation TU=$100/EC_{50}$, where EC_{50} (expressed in % *v/v*) is the effective concentration of toxicant (in mg L^{-1}) that reduces by 50 % the response of a certain population of organisms, after a specified exposure duration. For example, the ecotoxicity assessment performed by the bioluminescence inhibition of the bacterium *Vibrio fischeri* using the Microtox® equipment, has been adopted in the official standards of several countries. In this case, the EC_{50} value corresponds to a decrease of light emission by 50 % after a contact time of 5, 15 or 30 minutes.

3.2.3 Wastewater treatment processes

As the availability of water for years to come is severely compromised, it is imperative to start designing industrial processes to minimize and avoid, as much as possible, the generation of wastewater. However, in the meantime it becomes necessary to deal with wastewater resulting from the existing industrial facilities, for which the most suitable destination is a wastewater treatment plant (WWTP), so promoting public health and preserving water resources in order to avoid contamination. The processing of industrial wastewater often requires a combination of different methods, since the use of a single method is rarely satisfactory. Currently, the treatment of industrial wastewater generally comprises a three-step process designated as primary, secondary and tertiary, tending to employ a combination of biological and chemical treatment methods, in order to comply with the standards for discharge of treated effluent (Tchobanoglous, Burton, et al., 2004b).

The choice of a treatment methodology will depend on various factors, such as qualitative and quantitative composition of the wastewater, the system location and quality objectives to be achieved, as well as the imposition of the degree of treatment (Ikehata, 2013). Generally, treatment of industrial wastewater requires a large amount of chemicals, multiple operations and configurations, a high degree of process control and regular maintenance, as it is exemplified in Table 3.3. All this complexity leads to high treatment costs.

Table 3.3- Typical unit processes in WWTP and target wastewater constituents (Ikehata, 2013).

Type	Unit process	Target constituent
Pre-treatment	Flow equalization, maceration	-
	Screens, grit removal	Large solid objects (stones, plastics, …)
Primary treatment	Sedimentation	Heavy solids
	Flotation	Light solids (oil, wax, fibers,…)
Secondary treatment	Activated sludge, biological filters, rotating biological contactors, membrane bioreactors	Biodegradable organics
Tertiary treatment	Filtration	Suspended solids, including pathogenic microorganisms
	Biological nutrients removal	Nitrogen and phosphorus, more recalcitrant organics
Advanced treatment	Chemical oxidation (ozonation, UV/H_2O_2 AOP)	Recalcitrant organics, pathogenic microorganisms
	Membrane filtration (NF, RO)	Dissolved and suspended solids, recalcitrant organics, pathogenic microorganisms
Disinfection	Chlorination	Pathogenic microorganisms
	UV disinfection	Pathogenic microorganisms
Low-rate treatment	Stabilization pounds, aerated lagoons, constructed wetlands	Suspended solids, nutrients, biodegradable organics, some pathogenic microorganisms

NF- Nanofiltration; RO- Reverse Osmosis; UV/H_2O_2 AOP- Ultraviolet/Hydrogen Peroxide Advanced Oxidation Process.

The first step of the treatment process, designated as a **primary or pre-processing treatment**, involves the physical screening and gravity sedimentation of heavy solids or soft solids float, such as oil, grease and fibers. This stage consists mainly on filtering solids, sand and other floating materials - usually sent to landfill - removing oil and grease using sedimentation and primary clarifiers. Chemical coagulants and flocculants can be used before the sedimentation/flotation in order to improve the solid/liquid separation. Although some pathogenic organisms can be removed in the primary treatment, this is usually insufficient for the removal of viruses and bacteria. Furthermore, only the metals in particulate form can be removed by gravity separation. A more elaborate treatment (secondary or tertiary treatment followed by disinfection) and/or additional security measures would be required when using the primary effluent for irrigation of crops and fish farms. The proper discharge of the sludge is also needed to prevent the spread of pathogens and other contaminants in the soil and watercourses.

The **secondary (or biological) treatment** is a combination of biological and physical-chemical treatments, consisting in the removal of biodegradable soluble organic substances using microorganisms (bacteria). Aerobic processes are commonly used, in which the effluent is clarified by separation of the microorganisms from the treated effluent, which is then discharged into waterways or subjected to a tertiary treatment. Secondary treatment systems are generally classified as fixed film (where the biomass grows on media and the sewage passes over its surface) or growth suspension systems (or activated sludge, wherein the biomass is mixed with sewage).

There is currently a wide variety of commercially available conventional and advanced biological treatment processes, such as activated sludge sequencing batch reactors, oxidation ditches, trickling filters, rotating biological contactors, and membrane bioreactors (MBR). When combined with proper disinfection, wastewater with a secondary treatment may be considered safe for discharge and for a variety of non-potable applications, including irrigating crops, recreational restricted dams and groundwater recharge via basin infiltration.

Yet, certain restrictions are suggested when reclaimed water is used in places where direct contact or incidental ingestion could occur, such as parks, golf courses and recreational lakes, and for irrigation of food crops. As in the case of primary sludge, secondary sludge also contains high levels of metals, organic compounds and pathogens. Furthermore, proper treatment is required for sludge disposal, soil application and reuse.

Biological processes are most commonly used in the treatment of domestic and urban wastewaters, but may also be employed in the treatment of industrial wastewater. In these cases, if the concentration of organic compounds is too high or if these are refractory, adaptations in the process are required, like introducing a pretreatment or even replacement by other techniques (Tchobanoglous, Burton, *et al.*, 2004b).

Given the wide variety of organic compounds that has been detected after secondary wastewater treatment, the purpose of **tertiary or advanced treatments** is to improve the quality of this effluent before discharge, although they are less implemented on a large scale. Advanced treatment technologies include diverse operations, such as chemical or biological removal of nutrients and pathogens agents through granular media or membrane filtration such as microfiltration (MF), ultrafiltration (UF), and nanofiltration (NF), reverse osmosis (RO),

disinfection with ultraviolet (UV) radiation, ozone and chlorine and/or adsorption technologies with activated carbon and advanced oxidation processes (AOPs).

Membrane filtration processes are a rapidly growing tertiary treatment technology. Due to their very small pore sizes (< 1 mm), membranes can substantially remove all pathogenic organisms, including viruses. In many urban water reuse projects, filters are also used as a pre-treatment of advanced treatments and in combination with the secondary treatment. However, in the case of most persistent pollutants (e.g., phenols, pesticides, solvents, household chemicals and drugs, etc.), to produce water with acceptable levels, it is often necessary the application of AOPs. This kind of processes are recommended when wastewater components have a high chemical stability and/or low biodegradability (Mantzavinos and Psillakis, 2004; Lafi and Al-Qodah, 2006).

Even though conventional treatments, such as decantation, filtration, coagulation and flocculation, and biological process are not able to completely face the problem of water pollution, they continue however to be the most used, and are still quite effective. In addition, they can operate together with new processing techniques for even greater efficiencies, both in terms of removing pollutants and in economic terms.

In Europe, the wastewater treatment process has undergone considerable changes over the past decades, as depicted in Figure 3.3. Modifications have been observed towards the implementation of tertiary systems in wastewater treatment in the countries of North and Central Europe, and, to a lesser extent, also in the South and East. In the South East and West Balkan countries, the % of population connected to wastewater collection is very small, and tertiary systems represent a small part of the treatment process.
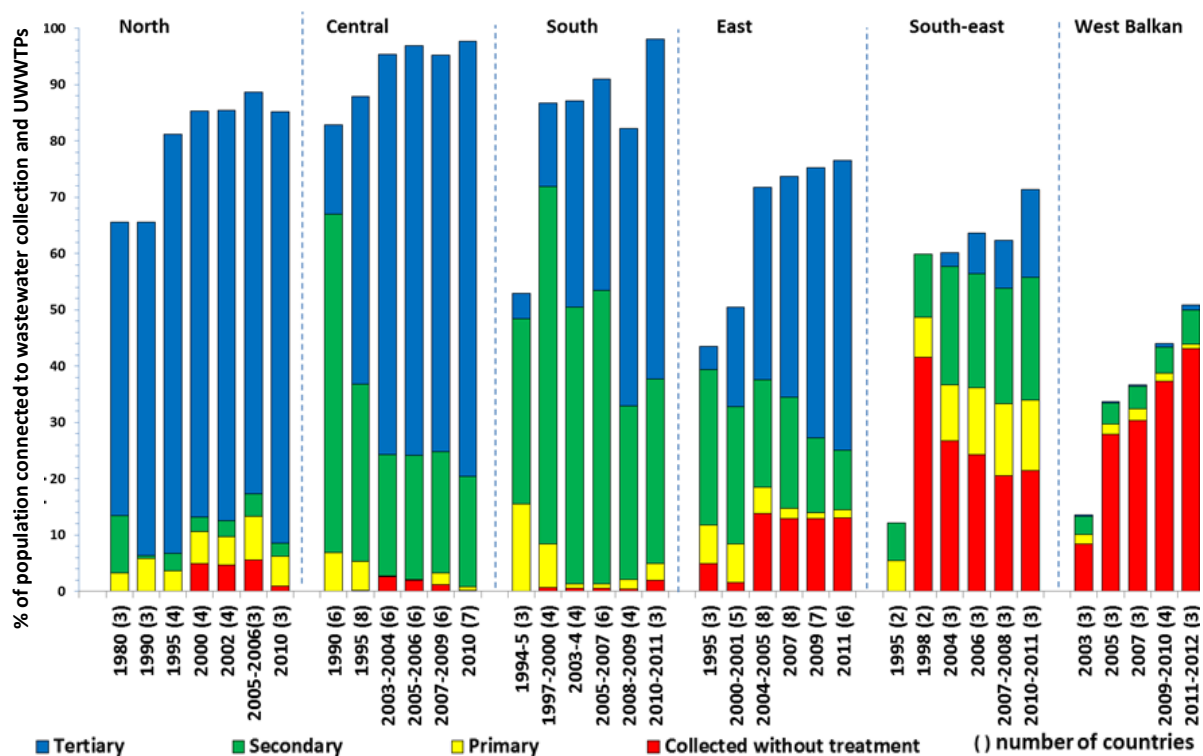
Figure 3. 3- Modifications in the wastewater treatment process in Europe. Source: European Environment Agency.

Yet, in the context of sewerage in Portugal, and other countries, tertiary treatment is considered in some ways a "luxury". In fact, in Portugal the reusability of treated water for direct human consumption has not yet been reached, but the available techniques (primary and secondary treatments) allow to safely reuse treated water for various purposes, such as irrigation.

Summarizing, the aim of wastewater management is to promote the effective and responsible use of water (including reuse), treatment and discharge, as well as protect public health and environment. The different types and levels of risk existing in different wastewater management scenarios, are shown in Figure 3.4:
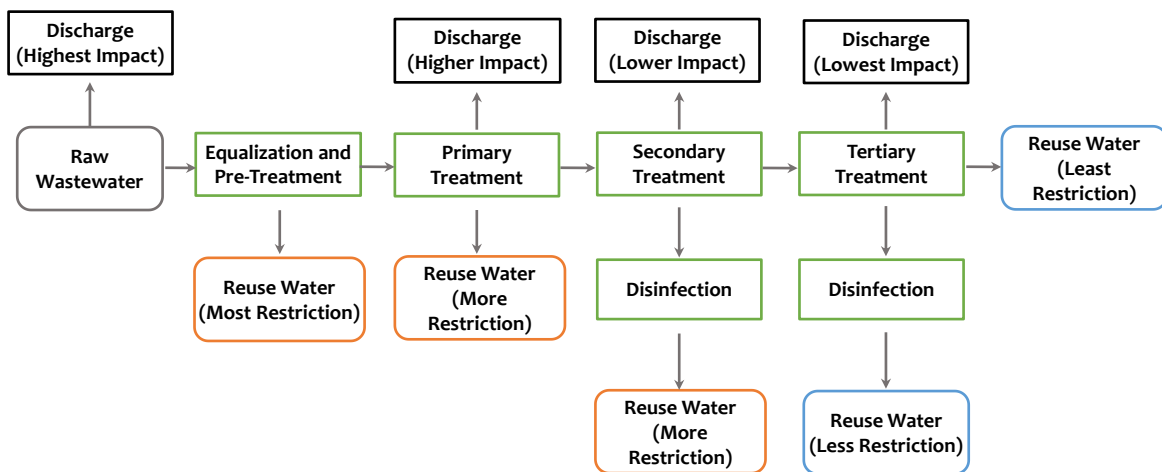
Figure 3.4- Simplified wastewater treatment, discharge, and reuse schemes (adapted from Ikehata, 2013).

In the following sections, adsorption technologies with activated carbons and AOPs for wastewater treatment will be the subject of a more detailed discussion.

3.3 Activated carbons

3.3.1 Historical aspects

Activated carbons are currently considered the most effectively adsorbents used in sewage and drinking water treatment plants, removing many classes of pollutants, such as surfactants, pesticides, dyes and aromatic compounds. The good performance of these materials results from the unique combination of a highly developed porous network (surface areas and pore volumes) and of the presence of heteroatoms (i.e., atoms other than carbon), creating a great variety of surface functional groups (Bandosz and Ania, 2006; Marsh and Rodríguez-Reinoso, 2006).

The first use of carbons dates back to 3750 BC, being used by the Egyptians and Sumerians in the reduction of copper, zinc, and tin minerals in the bronze manufacturing process, and also as smokeless fuel (Derbyshire, Jagtoyen , *et al.*, 2001; Przepiórski, 2006). At that time, the materials were charred wood, coal or simply a partially devolatilized coals, and not what is now known as activated carbons. In the Cave of Altamira, in Spain, that represents the apogee of Paleolithic cave art that was developed across Europe, from 35000 to 11000 BC, outstanding illustrations drawn using charcoal were found.

The first proof of the medicinal use of carbons was found in Thebes (Greece), in an Egyptian papyrus dated of 1550 BC. The therapeutic value of carbon was explored later by the Greeks and Romans in the treatment of various diseases. By the year 500 BC, the Greek scientist Hippocrates recommended that the water for consumption should be filtered with carbonized wood before its consumption, so as to eliminate bad flavor and odor (Figure 3.5) (Menéndez-Diaz and Martín-Gullón, 2006). Recent studies also indicate that in Phoenicians ships, water was stored in carbonized wood barrels, a practice that was continued until the eighteenth century. The first application of activated carbons as adsorbents in gas phase, occurred only in 1793, when coal was used to mitigate the odors emanating by gangrene.
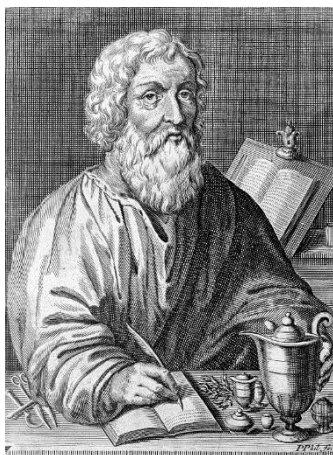
Figure 3. 5- Hippocrates, an early protagonist in the use of charcoal.

The introduction of activated carbons in industrial processes took place in England, in 1794, when these adsorbents were applied as bleaching agents in the production of sugar. The first large-scale application in gas phase took place in 1854 (Menéndez-Diaz and Martín-Gullón, 2006), with the installation of carbon filters in the sewage ventilation systems in London. In 1872, carbons filters were also used in masks on chemical industries for preventing the inhalation of mercury vapors.

Activated carbon, as it is currently known, was produced by R. von Ostrejko, who is considered the father and/or this type of materials, having patented in 1901, two different methods for their production:

- The carbonization of lignocellulosic materials with metallic chlorides (the base of the chemical activation process);

- The slight gasification of chars with water vapor or carbon dioxide at elevated temperatures (thermal or physical activation).

The starting point for the great development in the production and application of activated carbons was undoubtedly World War I, when these materials were used in gas masks (Menéndez-Diaz and Martín-Gullón, 2006). The increasing medical and scientific knowledge, the restrict environmental regulations referring to water resources, and the applications in the purification of gases and recovery of chemical compounds with high economic value boosted the use of these materials, increasing its production decade after decade. (Menéndez-Diaz and Martín-Gullón, 2006). In the last three decades, the use of activated carbons as a support for

metallic catalysts has also been quite widespread (Rodríguez-Reinoso and Sepúlveda-Escribano, 2009; Figueiredo and Pereira, 2009).

Although the development and utilization of activated carbons as adsorbents has brought enormous benefits to humanity, only recently there has been to a growing interest in the development and application of new carbon materials, as for example activated carbon fibers and carbon nanotubes. In this regard, recent advances in the design of carbon materials with controlled porosity and also a better understanding of their physical, chemical and mechanical properties, opened new horizons and created opportunities for a more vast application.

3.3.2 Structure and properties

At atomic scale and from a structural point of view, carbon materials can be considered as carbon atoms grouped into layers of fused aromatic rings (graphene layers), with a certain degree of planarity, which depends upon the degree of graphitization. Thus, carbon materials exhibit a high content of sp^2-hybridized carbon, which is responsible for at least a two-dimensional order in the carbon structure. These graphene layers are stacked by weak van der Waals forces either in an ordered (i.e., graphite and graphitizable carbons) or turbostratic - disordered stacking- structure (i.e. activated carbons, carbon blacks) (Henning, 1966). From structural and chemical viewpoints, a clear distinction can be made between basal-plane and edge carbon atoms in the graphene layers.

The reactivity of carbon surfaces is defined by the basal to edges ratio; the edges have higher reactivity than the basal planes, and it is associated to chemisorption of heteroatoms giving rise to stable surface functionalities (Radovic and Bockrath, 2005).

The main chemical features of the graphene sheets are: i) the surface functionalities either located at the edges (predominantly) or inserted in the basal-plane, and ii) the free edge sites. These free sites are associated to armchair (carbyne-like) and zig-zag (carbene type) configuration carbon atoms (rather than H-terminated or free radicals as generally assumed for a long time), and account for the surface reactivity of carbons to chemisorb heteroatoms or in gasification reactions (Radovic, Silva-Villalobos, *et al.*, 2011).

Due to their electronic structure ($1s^2$, $2s^2$, $2p^2$), carbon atoms present a flexible coordination chemistry and unique bonding ability, both with carbon atoms or other elements. All this results in a wide spectrum of materials and allotropic forms. For instance, depending on the hybridization state of carbon atoms bond to other carbon atoms, major carbon allotropic forms are: diamond (sp3 hybridization with tetrahedral stereochemistry), graphene (2D sheet of sp^2 carbon atoms), graphite (layered structure of sp2 carbon atoms with a planar trigonal stereochemistry) and fullerenes (spherical structure of sp2+x carbon atoms, being 0<x<1).

At the microscopic scale, carbon materials exhibit very different structures, some of these having a preferred arrangement in certain directions, such as synthetic graphite, while others disordered microstructures are features of carbonized or activated carbons (Marsh and Rodríguez-Reinoso, 2006).

3.3.2.1 Physical properties

Generally, activated carbons can be considered as an irregular array of two-dimensional microcrystals arranged in parallel planes. Each microcrystal is formed by crystalline planes of

carbon atoms grouped in hexagonal aromatic condensed rings, constituing a structure formed by 5 to 15 aromatic layers, also called basal planes or graphenic layers (Figure 3.6).

Figure 3.6- Schematic representation of the microstructure of activated carbons (Bansal, Donnet, *et al.*, 1988).

This microcrystalline structure begins to form during the carbonization process, in which the regular arrangement of carbon bonds on the surface of the crystallites is broken. The structure of an activated carbon can be visualized as a stack of undeveloped aromatic leaves, cross-linked and distributed in a random fashion, separated by disorganized carbonaceous and inorganic matter (ash) derived from the raw material. During the activation process the spaces between the crystallites become unobstructed of carbonaceous material and the resulting channels, together with the inside and parallel cracks, constitute the pore network. This porous structure consists of pores of different sizes, which according to the International Union of Pure and Applied Chemistry (IUPAC) (Rouquerol, Avnir, *et al.*, 1994), can be classified into three categories: micropores, mesopores and macropores (Figure 3.7). The micropores have apertures less than 2 nm, mesopores have openings between 2 and 50 nm and in the case of macropores the opening is greater than 50 nm.
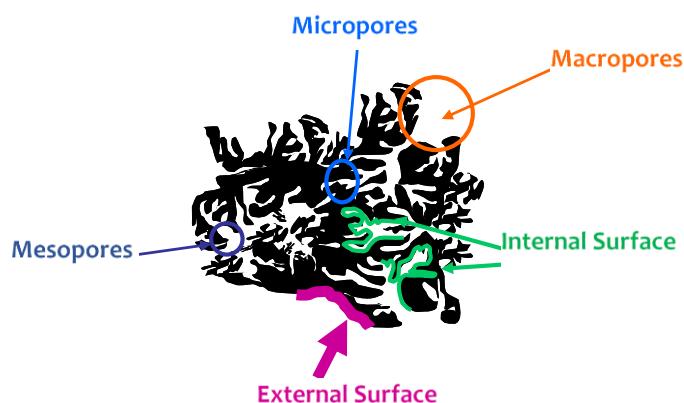
Figure 3.7- Schematic representation of the pore structure of an activated carbon.

The micropores in activated carbons are considered to be slit-shaped, in which the size corresponds to the width, the distance between opposite walls. These pores, that are most of the internal area of the activated carbon, can be further subdivided into ultramicropores (pores with sizes less than 0.7 nm) and supermicropores (pore size between 0.7 and 2 nm). Although the most significant part of adsorption on activated carbon occurs in the micropores, meso- and macropores also play an important role in this process, acting as transport pores, allowing the access of the adsorbate to the micropores.

Porosity, that may be defined as the ratio of the volume of pores and voids to the volume occupied by the solid can not be regarded as a characteristic of a simple material, since it

depends on the method used for its determination. In a way that is necessarily arbitrary, it is considered that the external area corresponds to the area of the protuberances and cavities which are wider than deep, and the internal area to the area inside the walls of the pores and cracks having a depth greater than the width. For porous solids the internal area is much higher than the external.

3.3.2.2 Chemical Properties

The knowledge of the surface chemistry of carbon materials is of paramount importance, since its physical and chemical properties are strongly dependent of the presence of chemical species on the surface. The presence of heteroatoms, even in small amounts, can have a significant influence on the physical and chemical properties of these materials, and, consequently, on the desired properties for a specific application.

The versatile surface chemistry of carbons provides a useful and unlimited tool to design materials to face new challenges, and thus has become a topic of growing interest among researchers. In this regard, a large number of studies have demonstrated the role of surface chemistry of carbons in the adsorption of aromatic compounds, dyes, heavy metals, and pharmaceutical compounds in solution (Mestre, Marques, *et al.*, 2012; Galhetas, Mestre, *et al.*, 2014). In the field of catalysis, whether used as catalyst support and or even as catalyst, the role of surface chemistry of activated carbons in relation to the dispersion of the catalyst or the catalytic activity has also been investigated (Bandosz and Ania, 2006; Menéndez-Diaz and Martín-Gullón, 2006; Fernandes, Andrade, *et al.*, 2012; Ania, 2013). From the point of view of their reactivity, two kinds of activated carbon surfaces can be considered:

• A flat, non-polar, which comprises the center of the carbon surface, the graphenic layers. Adsorption occurs on this surface through van der Waals forces of dispersive character, which play a very important role in adsorption processes.

• A surface formed by the unsaturated carbon atoms located at the edges of the basal planes. On these edges are located functional groups (carbon-oxygen, carbon-nitrogen, etc.) as well as highly reactive free radicals.

Oxygen is unquestionably the most abundant heteroatom present on the surface of activated carbons, originating, by itself or in combination with hydrogen, the vast majority of functional groups that characterize the surface chemistry of carbon materials. The reason for the abundance of oxygen-containing functionalities on carbon surfaces is linked to the strong affinity of carbons to interact with oxygen when exposed to air (O_2 chemisorption occurs even at low temperature) (Henning, 1966), although oxygen may also be incorporated from the chemistry of the precursor.

The relatively high area of the edges of the activated carbon results in a strong propensity to oxygen chemisorption. The dissociation of molecular oxygen atoms leads to a chemical reaction with carbon atoms to form oxygenated compounds on the surface. This oxidation process is of particular importance for pre-treated carbons at elevated temperatures, which have a highly reactive surface. The oxygen surface groups can also be formed by reaction with other oxidizing gases such as ozone, nitric oxide, carbon dioxide, etc., and oxidizing solutions such as nitric acid, hydrogen peroxide, etc.

3.3.2.2 Chemical properties

The different types of oxygen functional groups which may be present on the surface of carbon are shown in Figure 3.8. For some of the schematized functions such as quinone and pyrone-type some other arrangements can also be proposed. These highly reactive centers are responsible for the ability of activated carbons to participate in halogenation, hydrogenation, and oxidation reactions and/or act as catalysts in many chemical reactions.

Activated carbons also contain other heteroatoms, which may arise from the raw materials used, the agent added during activation or some post-synthesis modification. The relatively simple and quite numerous methods that are currently known to modify the surface chemistry of activated carbons, are quite useful in optimizing several conventional applications as well as for the search of new applications. The surface chemistry of the activated carbon can be modified by oxidation with various agents, creating oxygen functionalities or by heat treatment to promote selective or complete removal of such groups.
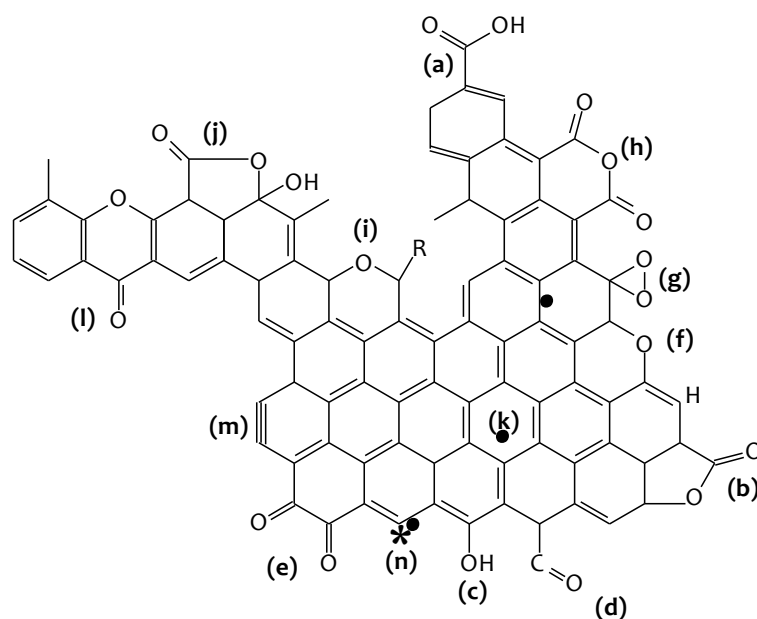
Figure 3.8- Schematic representation of the typical O-containing surface groups of carbon materials, including free edge sites and carbon-hydrogen complexes: (a) carboxyl groups, (b) lactone, (c) hydroxyl, (d) carbonyl, (e) quinone, (f) ether, (g) epoxyde, (h) carboxylic anhydride, (i) chromene, (j) lactol, (k) π electron density on carbon basal planes, (l) pyrone, (m) carbyne, and (n) carbene sites (adapted from Ania, 2013).

The remaining elements after complete combustion constitute the ashes, whose amount and composition is widely variable, depending on the precursor used in the preparation of the adsorbent (Marsh and Rodríguez-Reinoso, 2006). The ash content can vary from less than 1 wt. % for materials prepared from relatively pure precursors, to more than 10 wt. % for activated carbons prepared from coal. In the case of lignocellulosic materials, the major constituents of the ash are silicon, magnesium, calcium, iron, aluminum and sodium oxides. These compounds may play an important role in adsorption and catalytic processes, since they can modify i) the interactions between the surface of the carbon adsorbent/catalyst and the molecule to be adsorbed, and ii) the catalytic performance of the supported phases by electronic or structural interactions (Rodríguez-Reinoso and Sepúlveda-Escribano, 2001).

Another important effect of the presence of inorganic matter on the carbon precursor is, as an example, a possible catalytic effect on the gasification reaction during the activation. The

presence of iron, calcium and alkali compounds may catalyse the reaction of carbon atoms with carbon dioxide and water vapor (Marsh and Rodríguez-Reinoso, 2006). This catalytic effect has strong effect on the pore size distribution of the activated carbon; usually a larger porosity is obtained in the presence of ashes, than that for materials from which inorganic matter has been removed by an acid treatment.

According to the nature of their surface functional groups, activated carbons can be classified as:

Acidic carbons- Carbons that present an acidic character when reacting with appreciable amounts of bases, but do not react with acids, are designated acidic carbons. Generally, an acidic carbon is obtained when an activated carbon degassed at elevated temperature, in vacuum or inert atmosphere, is exposed to a stream of oxygen at moderate temperatures. They can also be obtained by oxidation by other oxidizing agents in gaseous or aqueous phase (e.g. HNO_3);

Basic carbons- Carbons that have a basic character when reacting with considerable quantities of acids, but do not react with bases are considered basic carbon. Activated carbons obtained by traditional methods usually have a basic character, although the structure of the functional groups responsible for this fact is not known with accuracy. It is considered that certain oxides, amine groups and also coal graphene layers are responsible for this basic character.

3.3.3 Activated carbon production

The industrial production of activated carbon is essentially based on two steps: carbonization of the raw material at a high temperature in the absence of air and activation of the carbonized product (Figure 3.9).

The carbonization step consists in the controlled heat treatment at a final temperature between 500 and 800 °C, in which the decomposition of the precursor occurs, eliminating elements such as hydrogen, nitrogen, oxygen and sulfur. The more volatile compounds with low molecular weight are eliminated first, followed by light aromatics, and finally hydrogen. The carbonization product (or char) is generally a material with a relatively low specific surface area (< 500 m^2 g^{-1}). During activation the incipient porous structure of the char is significantly developed.
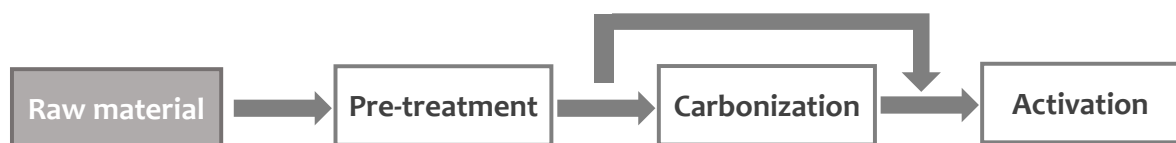
Figure 3. 9- General scheme of the production of activated carbons.

3.3.3.1 Precursors

Activated carbons can be produced from almost any raw material rich in carbon. There are many low cost materials with a low content of inorganic impurities that can be used in the production of activated carbons, such as wood, nut shells and fruit pits, lignite, bituminous coal and coke (Table 3.4).

Table 3.4- Properties of common precursors for the production of activated carbons (Marsh and Rodríguez-Reinoso, 2006).

Raw material	Carbon (wt. %)	Volatiles (wt. %)	Density (cm³ g⁻¹)	Ash (wt. %)	Texture of activated carbons
Soft wood	40-50	55-60	0.4-0.5	0.3-1.1	Soft, large pore volume
Hard wood	40-42	55-60	0.55-0.80	0.3-1.2	Soft, large pore volume
Lignin	35-40	58-60	0.3-0.4		Soft, large pore volume
Nutshells	30-45	55-60	1.4		Hard, large micropore volume
Lignite	55-70	25-40	1.0-1.35	5-15	Hard, small pore volume
Soft coal	65-80	20-30	1.25-1.50	2-12	Medium hard, medium pore volume
Petroleum coke	70-85	15-20	1.35	0.5-0.7	Medium hard, medium pore volume
Hard coal	70-75	10-15	1.45	5-15	Hard, large pore volume
Anthracite	85-95	5-10	1.5-1.8	2-15	Hard, large pore volume

The choice of the appropriate precursor is based on the following criteria (Menéndez-Diaz and Martín-Gullón, 2006):

• The possibility of originating materials with good adsorptive capacity, high density and hardness.

• Low inorganic matter content. The presence of these compounds reduces adsorption capacity, since it is expressed per unit mass.

• Availability and cost. As with any product, the price of the raw material affects the final cost, so a high availability is important to have to ensure stable prices. The yield of the process must also be taken into account, since significant mass losses may occur. Preparation yields can vary considerably, reaching very low values, such as 5-10 % for carbon made from wood.

Most lignocellulosic materials meet these requirements, occupying a prominent position as precursors in the production of activated carbons, representing about 45 wt. % of the total raw materials used in activation processes (Marsh and Rodríguez-Reinoso, 2006). Materials with low density and a high content of volatile constituents (for example, wood) lead to carbons with a high pore volume, but with a low density. Moreover, the use of materials with a higher density (for example, peel or fruit pits) allows to obtain granular activated carbons with a high pore volume, which can be used in different applications. The lignocellulosic materials are preferably used in chemical activation processes, while the use of peat, lignite, and various types of coal is more common on physical activation processes.

3.3.3.2 Pre-treatment

The precursor, or raw material, may have to be subjected to some pre-treatments before the activation process, in order for the desired particle size to be obtained by milling and screening, especially when the starting material is not quite homogeneous. Sometimes a washing step is also applied, using water or acid to remove any dirt and reduce the content of mineral matter (ash).

3.3.3.3 Carbonization

The pre-treatment step is followed by carbonization, a critical step in the overall process of activated carbons production, during which the formation of the microporous structure is initiated. The obtained material consists of a solid with an enriched content in carbon and aromaticity, but with a low adsorption capacity. The main experimental parameters that influence the process and determine the final yield are the carbonization temperature and the heating rate.

3.3.3.4 Thermal or physical activation

Physical activation takes place in two steps: thermal carbonization of the raw material and char activation by oxidizing gases such as water vapor, carbon dioxide, air or mixtures of both. After the first step, a more carbon enriched matrix is obtained, while in the second step, the char is gasified with the oxidizing agent at elevated temperatures (800-1000 °C). During activation, the active oxygen of the oxidizing agent eliminates the more reactive carbon atoms (more unsaturated), such as carbon monoxide. The activation will create additional porosity, and extend the existing porosity, "activating" the char.

The most used activating agents are carbon dioxide, water vapor and mixtures of the two, but other activating agents, such as air or oxygen, may be used (Marsh and Rodríguez-Reinoso, 2006). The most reactive agent is oxygen and the less reactive carbon dioxide. These gases will react with the carbon and remove some of the mass of the inner surface of the solid, creating a material with a highly developed porosity. Some blocked internal micropores may also become accessible due to the selective removal of carbon atoms.

The reaction of **oxygen** with carbon is highly exothermic and much faster than with carbon dioxide or water vapor, and therefore more difficult to control (Rodríguez-Reinoso and Sepúlveda-Escribano, 2001). Due to the high reactivity of oxygen, activated carbons with a low development of porosity and wider pores are obtained upon activation under oxygen atmosphere. For these reasons, this type of activation is not used at an industrial scale.

The gasification of the char with **steam**, **carbon dioxide or mixtures of both** usually occurs at 800-1000 °C (reactions 3.1 and 3.2). Activation with water vapor is the most used method for activated carbon preparation, allowing to obtain micro and mesoporous materials, with specific surface areas > 1000 $m^2\,g^{-1}$ (Marsh and Rodríguez-Reinoso, 2006). For samples prepared by activation with water vapor, the burn-off is directly related to the development of porosity. The partial formation of mesopores is reported only when with very high levels of burn-off (80 %).

$$C+CO_2 \rightarrow 2\ CO \qquad \Delta H= +159\ kJmol^{-1} \qquad reaction\ 3.1$$

$$C+H_2O \rightarrow CO+H_2 \qquad \Delta H= +117\ kJmol^{-1} \qquad reaction\ 3.2$$
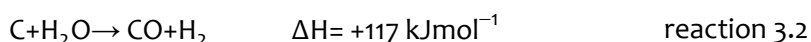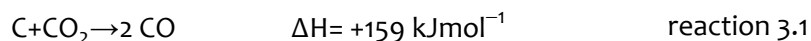
The endothermic nature of these reactions requires the direct heating to maintain the reaction temperatures. The heat supply is generated by the introduction of controlled amounts of air in the furnace in order to burn the gases produced during activation, according to the following reactions:

$$CO + \frac{1}{2}O_2 \rightarrow CO_2 \qquad \Delta H = 285 \text{ kJmol}^{-1} \qquad \text{reaction 3.3}$$

$$H_2 + \frac{1}{2}O_2 \rightarrow H_2O \qquad \Delta H = -238 \text{ kJmol}^{-1} \qquad \text{reaction 3.4}$$
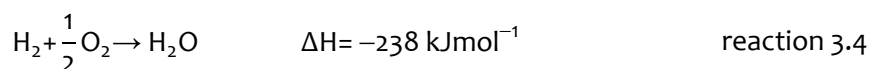
Comparing the porosity of two activated carbons prepared from the same precursor, activated with water vapor or CO_2, with similar burn-off values, it is apparent that both materials will reach similar adsorption capacities. However, the porosity developed by CO_2 is somewhat narrower than that of the sample activated with water vapor (Menéndez-Diaz and Martín-Gullón, 2006). Thus, the choice of the oxidizing agent will depend on the intended end-application.

3.3.3.5 Chemical Activation

Chemical activation involves the co-carbonization of the precursor with a chemical reagent, known as activating agent, under inert atmosphere, followed by removal of the resulting chemical compounds by exhaustive washing. The most commonly used activating agents in the industry are zinc chloride, phosphoric acid and potassium hydroxide. The development of porosity during the heat treatment occurs in an inert atmosphere at temperatures in the range of 400 to 900 °C (Marsh and Rodríguez-Reinoso, 2006).

The impregnation step may be performed in solution (the most common method) or by physical impregnation. In the first case, the dried precursor is mixed with a solution of an appropriate concentration of the activating agent for a certain contact time at a given temperature, and the mixture is then dried. In a physical mixture, different amounts of solid activating agent are mixed with defined amounts of the dried precursor, without any addition of water, at room temperature. After the chemical activation, it is necessary to grind the obtained carbon, and to perform a washing step to remove the excess of activating agent and its soluble degradation products.

The activation mechanism differs according to the chosen agent, resulting in a very distinct pore development. For example, zinc chloride promotes the extraction of water molecules from the structure of the lignocellulosic feedstock (Marsh and Rodríguez-Reinoso, 2006). The activation mechanism with potassium hydroxide is more complex involving the disintegration (almost explosive) of the structure, followed by intercalation by and gasification the oxygen of the hydroxide. The presence of oxygen is not essential (but can be a help) for this form of activation (Marsh and Rodríguez-Reinoso, 2006).

Zinc chloride was one of the most commonly used chemicals in the preparation of activated carbons in the 70's, and its use has declined due to environmental problems caused by zinc waste. The activation of lignocellulosic material with zinc chloride yields activated carbons having a porosity well developed in one step, resulting in considerable yields.

Phosphoric acid is perhaps the most commonly used activating agent, preferably in the activation of lignocellulosic material, leading to carbons with a well-developed porosity. Activation with this activating agent allows to obtain materials with a micro- and mesoporosity and high surface areas.

Alkali hydroxides and carbonates have been used in the preparation of activated carbons with high surface areas and developed porosity. These materials, referred to as super activated

carbons, with extremely high surface areas (> 3000 m^2 g^{-1}) were produced for the first time in the 70's and commercialized in the late 80's (Menéndez-Diaz and Martín-Gullón, 2006).

The use of raw materials with a low content of volatile compounds and a high carbon content is more appropriate for this activating agent. KOH reacts with the carbon backbone, yielding solid and liquid products, and in parallel, carbon consumption develops porosity. During the reaction that occurs above 600 °C, hydrogen and metallic potassium are formed, as well as CO and CO$_2$ (from the carbon matrix) and potassium oxide, according to the proposed mechanism (Lillo-Ródenas, Cazorla-Amorós, *et al.*, 2003) (reaction 3.5), followed by the decomposition of potassium carbonate in CO$_2$ and K$_2$O. The ratio KOH/precursor seems to be the factor with the greatest influence on the adsorption capacity of the obtained material (Linares-Solano, Lozano-Castelló, *et al.*, 2008).

$$6\ KOH+2\ C \leftrightarrow 2\ K+3\ H_2+2\ K_2CO_3 \qquad \text{reaction 3.5}$$
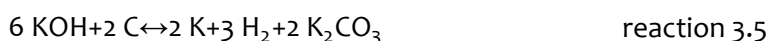
Specific areas higher than 1500 m^2 g^{-1} can be obtained with average KOH/precursor proportions (0.5, 1, 2); increasing this ratio, the porosity becomes more developed (more than 3000 m^2 g^{-1}), but the micropore size distribution becomes wider, including pores ranging from very large micropores to small mesopores (Linares-Solano, Lozano-Castelló, *et al.*, 2008). The use of very high KOH/precursor ratios results in the disintegration of the carbon granules due to gasification reactions (Marsh and Rodríguez-Reinoso, 2006). The final temperature treatment can also have some influence on the adsorption capacity developed.

The use of KOH and NaOH is relatively expensive, but above all hazardous and corrosive. Compared to these, sodium and potassium carbonates present lower costs, offering the advantage of being harmless chemicals, given the use of K$_2$CO$_3$ in the food industry as an additive (Adinata, Daud, *et al.*, 2007). Activation with K$_2$CO$_3$ can thus be considered a cleaner and more economic production technology.

This agent has been increasingly used in chemical activation processes, obtaining in the same experimental conditions activated carbons with better yields than with the use of KOH, and sometimes even higher surface areas (Carvalho, Gomes, *et al.*, 2004; Carrott, Carrott, *et al.*, 2006;. Tay, Ucar, *et al.*, 2009). Different precursors, such as agricultural wastes, lignin, coal, biomass, plastic and newspapers waste, and resins, have been chemically activated with K$_2$CO$_3$. Several studies highlight the comparable, or even better results than those obtained with commercial samples (Carvalho, Gomes, *et al.*, 2004; Carvalho, Mestre, *et al.*, 2006; Suhas, Carrott, *et al.*, 2007).

The first step of the degradation process of the raw material consists in the intercalation of Na or K atoms, originated by the reduction of alkali hydroxides or carbonates. This process causes the expansion of the graphenic layers of carbon, requiring however, an increase in temperature which causes the exit of the metal from the intercalated system. The porosity of the activated carbon will be determined by the strength of this process (Marsh and Rodríguez-Reinoso, 2006).

While in severe conditions, the carbon material can be completely disintegrated by potassium hydroxide, to yield a flocculent carbon with high adsorption capacities, under the same conditions, a less extensive pore development is observed, for activation with potassium

carbonate (Mestre, Tyszko, *et al.*, 2015). For milder conditions, no significant activation with potassium carbonate occurs, due to the larger size of the carbonate ion, which prevents its entry into the micropores of the starting material.

Due to the ionic nature of the solution, potassium ions can not diffuse into the porosity, without its counter ion. Activation mechanisms require the presence of potassium as well as oxygen species, otherwise a significant activation is not possible. Another reason for this fact is that, although potassium carbonate is able to diffuse through the microporosity, the formation of surface oxygen complexes from the carbonate ion is not a favoured reaction. The presence of carbonate induces an increased amount of CO_2, which confirms that the decomposition of the carbonate occurs. Potassium carbonate reacts with the carbon, releasing CO_2 from the carbonate (reaction 3.6).

$$K_2CO_3 \rightarrow K_2O + CO_2 \uparrow \qquad \text{reaction 3.6}$$

The increase in the gasification rate is attributed to the formation of potassium complexes, for example, phenoxy groups $C\text{-}O\text{-}K^+$, which can be considered as a kind of K^+ well dispersed species. The activation process is more effective as smaller the thermal stability of the carbonate in the presence of carbon. Potassium carbonate and potassium oxide from the decomposition of the first will react with carbon, reducing at temperatures above 700 °C, according to reactions 3.7 and 3.8:

$$K_2CO_3 + 2\ C \rightarrow 2\ K + 3\ CO \uparrow \qquad \text{reaction 3.7}$$

$$K_2O + C \rightarrow 2\ K + CO \uparrow \qquad \text{reaction 3.8}$$

3.3.4 Classification of activated carbons

The classification of activated carbons is a difficult task, given the complexity of these materials. One possible classification can be made considering its particle size, or shape. In Figure 3.10, different morphologies of activated carbons are presented.

Figure 3.10- Carbon materials obtained in different morphologies: grains, powders, pellets, films and coatings on monolith and foam structures (Morales-Torres, Carrasco-Marín, *et al.*, 2015).

Powdered activated carbons (PAC) present a fine granulometry/grain size < 100 micrometers and an average diameter between 15 and 25 micrometers (Bansal, Donnet, *et al.*, 1988). They have relatively high external areas, being preferably used in adsorption processes in liquid phase, in which the solute may have diffusional problems, instead of granular activated carbons, which might require higher equilibrium times. Included in this group are carbons used for municipal and industrial wastewater treatment, discoloration, food industry and pharmaceutical applications.

Granular activated carbons (GAC) present an average particle size between 1 and 5 mm (Bansal, Donnet, *et al.*, 1988). These materials present an increased particle size compared to PAC, and a smaller external area. Most applications in gas phase (gas purification, solvent recovery, masks and air filters for gases, gas separation by pressure swing adsorption, catalysis, etc.) use granular activated carbons, those having replaced PAC in many liquid phase applications, as for example, in the extraction of precious metals and in water treatment. Compared with PAC, GAC have lower pressure drops which facilitates their regeneration and reuse. However, granular carbons should also have a high bulk density and a low hardness and abrasion index.

Activated carbon fibers (ACF) and cloths are basically carbonized carbon fibers which are subsequently subjected to a heat treatment in an oxidizing atmosphere. The ACF development started in 1970, along with carbon cloths. These materials present all the characteristics of activated carbons, such as high specific surface area, high adsorption capacity, uniform and essentially microporous pore size distribution (1-40 μM), being soft and moldable (Donnet and Bansal, 1990). Although representing a small portion of the market, activated carbons in the form of fabrics or filters screen, have a number of additional advantages directly related to their structural characteristics such as high efficiency of contact, very low pressure drop, high adsorption rate in dynamic tests, as well as ease in handling and flexibility. Besides the internal area, the porous network of these materials is also determined by their fibrous (open) structure, ensuring a much faster adsorption kinetics. Consequently, diffusion resistance associated to the accessibility of the adsorbates to the active centers is much lower.

Monolithic carbon structures will likely be the base of the next generation of adsorption processes for environmental applications. These structures have the potential to overcome many of the limitations of the granular carbon beds in terms of low pressure drops, more regenerability, dusting elimination and abrasion (Menéndez-Diaz and Martín-Gullón, 2006). These benefits can lead to substantial reductions in capital cost and power consumption along with increased operability. The solid monoliths are used in various applications such as storage and gas separation, adsorption and as catalyst support.

Activated carbon membranes are mainly used in molecular separation processes of gases based on the differences in molecular size and shape. Activated carbon membranes allow the separation of N_2/O_2 from air, H_2/C_xH_y from mixtures of light hydrocarbons or CO_2/CH_4 from biogas (Menéndez-Diaz and Martín-Gullón, 2006). Besides this type of membranes, referred to as molecular sieve membranes, there are also adsorbent membranes that allow the separation of gases according to their textural and surface chemistry properties. Two types of membranes have been prepared: unsupported and supported. The unsupported materials offer high selectivity, although suffering from an extreme fragility. This disadvantage can be avoided by forming carbon layers on supports, such as porous graphite, sintered stainless steel and ceramic supports. The fast development of this technology and a more thorough investigation will certainly lead to large-scale production of activated carbon membranes.

3.3.5 Regeneration of activated carbons

Once the adsorption capacity of an activated carbon is exhausted, two options can be taken: the carbon can be disposed, by incineration or landfill, or can be regenerated for reuse. The second option seems to offer clear advantages, such as lower carbon consumption and the possibility of recovering an adsorbed product of potential economic value (Rodríguez-Reinoso,

McEnaney, *et al.*, 2002). However, the regeneration of exhausted carbon also entails costs, which in some cases are not lower than the production cost of a new activated carbon. Furthermore, in most regeneration processes, after a certain number of regeneration cycles, the adsorption capacity of the material decreases to a level at which the carbon can no longer be regenerated (Roskill Report, 1998; Ania, Menéndez, *et al.*, 2004; Ania, Parra, *et al.*, 2005; Ania, Parra, *et al.*, 2007). The regeneration step is almost exclusively carried out with GAC; PAC are typically discarded after use given the difficulties associated to the regeneration of fine powders, leading to high carbon losses.

There exist several methods for the regeneration of exhausted activated carbons, involving thermal treatments on different atmospheres (CO_2, steam, hot inert gases), chemical or biological processes, electrochemically-assisted, desorption under vacuum, with supercritical fluids, microwave-assisted, and more important, the use of conventional liquid solvents (Marsh and Rodríguez-Reinoso, 2006; Ania and Béguin, 2008; Çalışkan, Bermúdez, *et al.*, 2012; Guo and Du, 2012; Foo and Hamed, 2012; Cazetta, Junior, *et al.*, 2013).

3.3.6 Applications of activated carbons

Activated carbons are the most versatile adsorbent materials due to their high surface areas, developed porous structure (of essentially micropores), high adsorption capacity and variable surface chemistry. These multifunctional materials are used in a wide range of applications in numerous productive sectors such as the energy sector and the environment, the aircraft industry, electronics, medicine, etc. (Przepiórski, 2006). A summary of the major applications of activated carbon divided into applications in liquid or gas phase adsorption processes is shown in Table 3.5.

3.3.6.1 Applications in adsorption processes

Liquid phase applications account for about 80 % of total consumption of the activated carbon produced (Marsh and Rodríguez-Reinoso, 2006). Both GAC and PAC are largely used; GAC are mainly applied in continuous (dynamic adsorption carbon beds) processes due to their capacity to be regenerated, while PAC are mainly used in batch processes (being separated from the coal liquid after the completion of process and discarded or eluate). As an example, almost 60 wt. % of the activated carbon used in the United States in liquid phase applications is PAC, due to the need for a rapid distribution of liquid to the interior of the carbon particles.

In liquid phase applications, activated carbons act as adsorbents, eliminating substances of variable concentration, composition and size, with the aim of improving the taste and odor of water, as well as reducing natural organic matter, limiting thus the maximum formation of disinfection and/or oxidation by-products, as trihalomethanes. This topic will be the subject of further discussion in section 3.3.7.

3.3.6.2 Applications in catalysis

Activated carbons are also employed as catalysts and catalyst supports in a wide number of reactions (Faria and Wang, 2009; Figueiredo and Pereira, 2009) due to their versatility of forms and architectures. Their physical and chemical properties can be easily adapted to develop a high surface area on which the active phase can be dispersed, while an appropriate pore size distribution facilitates the diffusion of reactants and products to and from the surface. The acidic/basic character necessary to achieve the best performance can also be tailored.

Table 3.5- Industrial applications of activated carbons in adsorption processes (Przepiórski, 2006).

Application field	Common use
Adsorption from liquid phase	
Drinking water treatment	Removal of dissolved organics, control of taste and odor, lead, chlorine, color
Soft drinks and brewing	Removal of chlorine and dissolved organic contaminants from potable water, after disinfection with chlorine
Food industry	Decolorization of liquid sugars (glucose, maltose)
Pharmaceutical	Purification and separation of antibiotics, vitamins, hormones, etc.
Semiconductors	Production of ultra-high purity water
Petrochemical	Removal of oil and hydrocarbon contaminations from recycled steam condensate for boiler feed water
Groundwater	Reduction of total organic halogens and adsorbable organic halogens
Wastewater treatment	Process effluent treatment
Swimming pools	Removal of residual ozone and control of chloramine levels
Adsorption from gas phase	
Solvent recovery	Control of vapor emissions and recovery of organic solvents
Carbon dioxide production	Purification of carbon dioxide from fermentation processes
Gas purification	Purification of industrial off-gases
Waste disposal	Removal of heavy metals and dioxins from flue gas formed during incineration of various wastes
Tobacco manufacturing	Removal of some harmful substances (nicotine and tar)
Air conditioning	Removal of contaminants from air subjected to heating, ventilation, and air conditioning in airports, offices, hospitals
Semiconductors production	Production of ultra-high purity air
Toxic gas removal	Purification of greenhouse gases
Fridge deodorizers	Removal of general food odors

Although catalysts supported on activated carbons are considered the best choice for a large number of reactions (Rodríguez-Reinoso and Sepúlveda-Escribano, 2001), a few large-scale processes currently use these systems, and less than 1 % of the world production of activated carbon is used as catalyst support. This may be due to the lack of reproducibility that sometimes is associated with this type of catalysts as a result of a lack of the knowledge of the properties that might influence their behaviour.

However, the growing number of scientific publications on this subject has contributed to a better understanding of the behaviour of this type of catalysts. Many types of carbonaceous materials have been used as catalysts and catalyst support: graphite, carbon black, activated carbons, carbon fibers and fabrics fullerenes, nanotubes, among others (Rodríguez-Reinoso and Sepúlveda-Escribano, 2001). Among them, the most important are undoubtedly activated carbons with high surface areas and carbon blacks. Carbon materials may act as supported

catalysts in about 50 reactions of industrial interest from a list of 69 reactions catalysed by noble metals according to "The Catalytic Reaction Guide" published by Johnson Matthey, leader of catalysts suppliers worldwide (Rodríguez-Reinoso and Sepúlveda-Escribano, 2001). One of the first applications of activated carbons as a catalyst support was in the hydroprocessing of petroleum raw materials, and still remains as a major area of research and application in this field. Other areas of interest are hydrogenation reactions, ammonia synthesis and environmental catalysis, including the reduction of NO with CO (Rodríguez-Reinoso and Sepúlveda-Escribano, 2001; Rodríguez-Reinoso and Sepúlveda-Escribano, 2009).

Although the primary use of carbon materials in catalytic processes is as a porous support, several industrial reactions use activated carbons themselves as catalysts (Figueiredo and Pereira, 2009). An example of this fact is the production of carbonyl chloride (phosgene) by combining CO and Cl_2 over a carbon catalyst. The reactions catalysed by different carbons range from hydrogenation reactions by oxidation and reduction, polymerization and chlorination. Examples of such reactions include oxidative dehydrogenation reactions, cumene oxidation, H_2S oxidation, alcohols dehydration and dehydrogenation. For the performance of carbon as catalyst both the textural and surface chemistry properties are of great importance. However, it is difficult to distinguish the role played by each of these two factors.

Activated carbons are also of great importance in photocatalytic processes. In this regard, the use of activated carbons in carbon/semiconductor composites has become an important area of research in recent years, due to the increase of the efficiency of photocatalytic semiconductors (Faria and Wang, 2009; Ania, Velasco, *et al.*, 2012). New materials prepared through the immobilization of the active semiconductor on the porous carbon have been explored due to the good results observed for these composites in the photocatalytic degradation of environmental pollutants in liquid or gaseous phase. The increase in the photocatalytic efficiency is attributed to several factors related to the absorption of visible light, strong interfacial textural properties and electronic effects (Faria and Wang, 2009).

More recently, the photocatalytic activity of certain carbon materials, in the absence of a semiconductor has also been demonstrated (Ania, Velasco *et al.*, 2012). These results mark a starting point for future research in this field, offering the possibility of coupling the photocatalytic degradation of refractory pollutants to classical adsorption technologies based on activated carbon. This topic will be the subject of further discussion in section 3.4.6.4.

3.3.7 Nanoporous carbons in wastewater treatment

As it was already stated, water purification is the most important application of activated carbons in liquid phase. The use of these materials as adsorbents is of fundamental importance in industrialized societies, being cited by the United States Environmental Protection Agency (USEPA) as one of the best environmental control technologies available (Radovic, Moreno-Castilla, *et al.*, 2000).

Adsorption on activated carbon has been widely used for the removal of odor and taste of drinking water, and persistent organic pollutants (priority and emerging) of sewage, both in classical adsorption methods (Marsh and Rodríguez-Reinoso, 2006) or coupled to advanced techniques (Carvalho, Mestre, *et al.*, 2013). In developed countries, where there is a high water sanitation coverage, activated carbons are used in the final stages of wastewater treatment

(tertiary treatment), allowing the removal of both priority and emerging pollutants. On the other hand, in areas with a low health coverage, where the process water treatment consists in applying only primary or secondary treatments, the removal of most contaminants is usually not effective.

The adsorption of micropollutants onto activated carbon can be implemented either as a line-end technology or added to an existing technology in wastewater treatment plants, such as activated carbon in a bioreactor in a pumped-bed membrane (Dosoretz and Böddeker, 2004; Li, Hai, *et al.*, 2011). Although most activated carbons are generally used in sewage treatment plants in the final stages of the treatment process (tertiary treatment), this technology can also be positioned at an early stage in the process (Figure 3.11), especially in the case of highly polluted influent, thus preserving the biological treatment facility. According to the literature, about two thirds of the water treatment facilities in the United States and Canada have the ability to use activated carbons in a pre- and/or post-treatment when necessary (Snyder, Adham, *et al.*, 2007). Activated carbons may also be added to the biological treatment tank, thus improving the removal of conventional and emerging pollutants (Delgado, Charles, *et al.*, 2012; Stoquart, Servais, *et al.*, 2012). The greater efficiency of these hybrid systems for the removal of pharmaceutical compounds has recently been studied (Rúa-Gomez, Guedez, *et al.*, 2012).
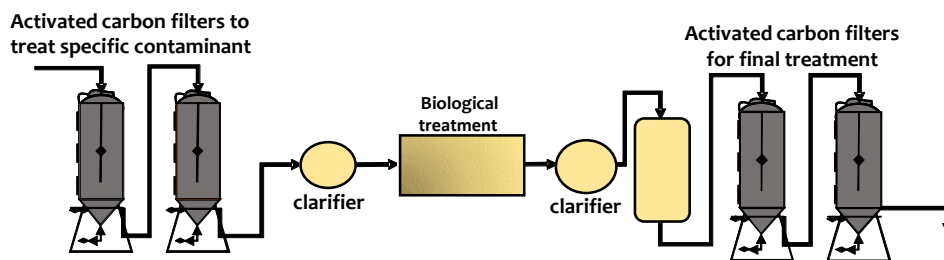
Figure 3. 11- Simplified scheme of a wastewater treatment plant with activated carbons adsorption as a pre and/or post-treatment (adapted from Carvalho, Mestre, *et al.*, 2013).

There are many available technologies for the implementation of activated carbons in wastewater treatment (Ternes and Joss, 2006; Rúa-Gómez, Guedez, *et al.*, 21012). After the secondary treatment, GAC can be applied through columns (Figure 3.12A), or added in the form of powder to the ultrafiltration membrane module of MBR systems, as it is schematized in Figure 3.12B. The fact that MBR systems produce free suspended solids effluent, makes them especially suitable to be coupled to of activated carbons technology, since that the presence of natural organic matter reduces the adsorption capacity of the activated carbon due to competitive adsorption (Cho, Huang, *et al.*, 2011; Bui and Choi, 2010; Pastrana-Martinez, López -Ramón, *et al.*, 2009).

Over the last few years the application of activated carbon adsorption in laboratory, pilot and full scale water treatment plants has been increasing, with satisfactory results for the removal of some micropollutants, including phenols, pesticides, solvents, pharmaceuticals and personal care products (Ahmaruzzaman and Sharma, 2005; Dias, Alvim-Ferraz, *et al.*, 2007; Ahmaruzzaman, 2008; El-Naas, Al-Zuhair, *et al.*, 2010; Baransi, Dubowski, *et al.*, 2012; Mailler, Gasperi, *et al.*, 2015).

A large number of studies on the mechanism of adsorption of contaminants on activated carbon can be found in the literature (Salame and Bandosz, 2003; Moreno-Castilla, 2004; Mestre, Pires, *et al.*, 2007; Velasco and Ania, 2011; Carvalho, Mestre, *et al.*, 2013). The main objective of these studies is to obtain a deeper knowledge of the adsorption mechanism and to evaluate the potential use of new carbon materials in water treatment processes. The use of green or eco-friendly carbons, raises a special interest in this field considering the low economic viability associated with manufacturing and regeneration costs of activated carbons, which in many cases restricts the implementation of these materials in large-scale industrial processes.
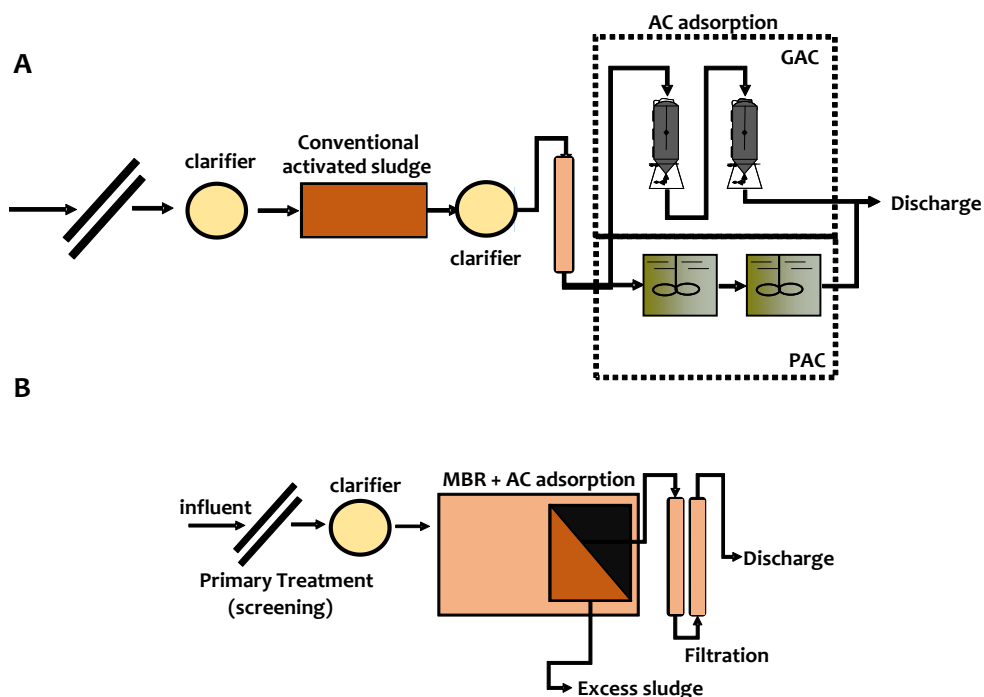
Figure 3.12- Schematic diagrams of the use of activated carbons in water treatment plants at different stages in the form of GAC or PAC: (A) Adsorption on activated carbon as sludge post-treatment; (B) Addition of activated carbon to the MBR system (adapted from Carvalho, Mestre, *et al.*, 2013).

Carbon materials synthesized from several agricultural or industrial waste, as for example, cork (Mestre, Pires, *et al.*, 2007), sisal (Mestre, Bexiga, *et al.*, 2011), olive pomace (Baccar, Sarrà, *et al.*, 2012) and Artemisia (Dubey, Dwivedi, *et al.*, 2010), and municipal waste such as plastics (Mestre, Pires, *et al.*, 2009) have been tested in the removal of emerging pollutants in aqueous medium, achieving removal efficiencies, in many cases, comparable to those obtained with activated carbons commercially available.

The importance of these studies lies not only in the search for new low-cost materials of high performance, but it is also of fundamental importance for disclosing the mechanisms of the adsorption of micropollutants. This is a highly complex process, dependent on many factors, including the texture (specific surface area and pore size distribution) and surface chemistry (presence of functional groups) of the activated carbon, the physical and chemical properties of the target compound and operational conditions (such as the solution pH and temperature).

Municipal and industrial wastewater treatment plants are examples of large scale activated carbon consumer markets, for which carbons are considered the best adsorbent materials (Przepiórski, 2006). The environmental concerns about water quality will surely keep the high demand for carbon materials in WWTP, and wastewater treatment with activated carbon will be mandatory in certain countries. Also the need for further treatment for recycling water, especially in cities, will increase the demand for activated carbon.

The available results demonstrate the effectiveness of the adsorption processes based on activated carbon to deal with the removal of pollutants at trace level. The non-specificity of these materials allows them to be effective adsorbents for a variety of micropollutants with different physical and chemical properties. Thus, activated carbons are used in different phases of the wastewater treatment process, as an independent process or coupled to another treatment process.

3.4 Advanced Oxidation Processes

In the course of the last decade there has been an increase in research in the field of AOPs for the removal and degradation of recalcitrant compounds in wastewater (Brito and Rangel, 2008; Comninellis, Kapalka, *et al.*, 2008; Klavarioti, Mantzavinos, *et al.*, 2009; Poyatos, Muñio, *et al.*, 2010; Ziylan, Ince, *et al.*, 2011; Babuponnusami and Muthukumar, 2012a; Adishkumar, Kanmani, *et al.*, 2014).

AOPs can be generally defined as oxidation methods based on the formation of highly reactive species such as the hydroxyl radical ($^{\bullet}OH$) and others, leading to the destruction of target pollutants (Poyatos, Muñio, *et al.*, 2010). These radicals are very powerful oxidizing agents and non-selective which can readily attack organic molecules by dehydrogenation reactions and/or hydroxylation leading to the digestion of pollutants, obtaining as final products carbon dioxide, water and some inorganic compounds (ammonia, nitrates, sulfates), or at least the conversion of organic compounds to preferably more highly oxidized and less harmful products.

These advanced technologies can be classified either as homogeneous or heterogeneous processes, the former being further divided into photochemical and non-photochemical processes (Figure 3.13). Most of these methods include Fenton reactions, ozonation, photocatalysis, sonolysis, combinations of UV irradiation and oxidizing chemical agents, etc. (Carvalho, Mestre, *et al.*, 2013).

The environmental applications of AOPs are quite numerous, including the treatment of domestic and industrial wastewater (i.e., removal of pollutants and organic and inorganic pathogens agents), reducing atmospheric pollution, and odor control and soil remediation. In the field of water treatment, the effectiveness of AOPs in destroying contaminants such as halogenated hydrocarbons, aromatic compounds (benzene, phenol, toluene), volatile organic compounds, detergents, dyes or pesticides, as well as inorganic contaminants has been demonstrated (Comninellis, Kapalka, *et al.*, 2008; Poyatos, Muñio, *et al.*, 2010; Sanz, Lombraña, *et al.*, 2013).

The range of application of these different technologies is wide, depending on the flow of wastewater and organic load flow to be purified. Many of these techniques can be used not only for purifying water, but also for disinfection, to kill or inactivate bacteria and viruses. They offer the advantage to destroy contaminants, as opposed to some conventional techniques

such as physical adsorption, or air stripping, in which the contaminants are only transferred from one phase to another. In contrast, the main problem of most AOPs is the high cost of the necessary reagents (for instance O_3, H_2O_2, and UV radiation).
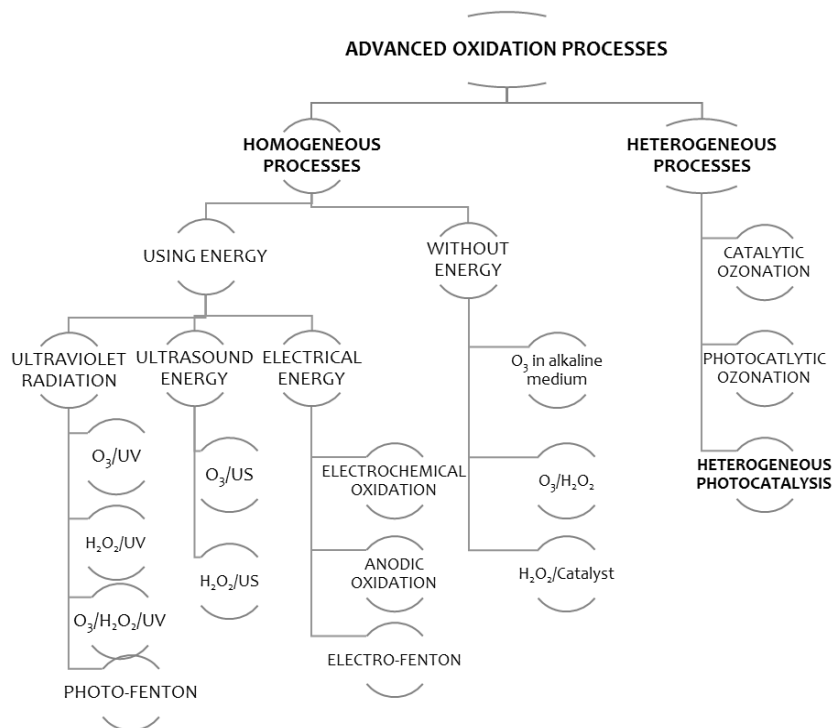
Figure 3.13- Advanced Oxidation Processes classification (adapted from Poyatos, Muñio, *et al.*, 2010).

The use of AOPs has been the subject of extensive research, being a central theme of studies covering various areas such as (Comninellis, Kapalka, *et al.*, 2008):

- Treatment of industrial influent including, among others, distillery waste, agrochemicals, kraft-bleaching, pulp and paper, textile dyeing, oil field and coating of metals;

- Treatment of hazardous urban waste including hospital and slaughterhouses influents;

- Removal of persistent pathogenic agents, pharmaceutical residues of endocrine disruptors from municipal WWTP effluent (i.e., after the secondary treatment);

- Removal of organic micropollutants from aqueous phase, such as pesticides and heavy metals (e.g. arsenic and chromium);

- Conditioning and stabilization of biological sludge from WWTPs.

These processes can provide technological solutions for water treatment that are vital to support and enhance the competitiveness of several industrial sectors -including water technology sector- in the global market. Furthermore, the use of solar energy in these technologies is gaining interest, as it could represent an effective and economically competitive solution to several environmental problems.

In the following sections a brief description of the most representative AOPs for the removal and/or degradation of water pollutants is presented.

3.4.1 Photolysis

Direct photolysis is the simplest process for the oxidation of pollutants involving the interaction of Ultraviolet-visible (UV-vis) radiation with the polluted water, in the absence of a catalyst. Irradiation with ultraviolet light has been used for the disinfection of drinking water, as an alternative to chlorination, avoiding the formation of harmful by-products (Pereira, Weinberg, *et al.*, 2007). This technique is usually combined with other methods due to its low efficiency.

3.4.2 Ozonation

Ozone is a strong oxidant that can easily react with organic molecules -eventually causing their decomposition- in water through the formation of superoxide and hydroxyl radicals (stronger oxidizing agents than ozone) or the selective attack of certain functional groups in the organic molecules through an electrophilic mechanism (Carvalho, Mestre, *et al.*, 2013). The reaction between ozone and superoxide radical gives rise to the formation of ozonide radical anions ($^\bullet O_3^-$), which also decomposes generating $^\bullet OH$ radicals.

Although it is widely used in wastewater disinfection (Ternes, Stüber, *et al.*, 2003), and drinking water treatment for odors and taste control, this technology presents some drawbacks. Its main disadvantages are the high energy costs for ozone generation and the low pollutant mineralization degree usually obtained for wastewater containing organic compounds. Very often complete oxidation can only be achieved by coupling the O_3 oxidation with, for instance, UV irradiation or H_2O_2 (O_3/UV and/or O_3/H_2O_2/UV processes), which considerably increases operating costs (Skoumal, Cabot, *et al.*, 2006).

Alternative ozonation processes catalysed by transition metals have been investigated for degradation of organic compounds in drinking water and wastewater, with an increasing number of data demonstrating the efficiency of this process (Legube, Leitner, *et al.*, 1999; Kasprzyk-Hordern, Ziółek, *et al.*, 2003). Catalytic ozonation can be considered firstly as homogeneous catalytic ozonation, which is based on ozone activation by metal ions present in aqueous solution, and secondly as heterogeneous catalytic ozonation in the presence of metal oxides or metals/metal oxides on supports.

3.4.3 Fenton and photo-Fenton

Fenton reaction was described over one hundred years ago (Fenton, 1884), and the oxidative power of Fenton's reagent (H_2O_2/Fe^{2+}) based on the generation of hydroxyl radicals was shown about forty years later (Haber and Weiss, 1934). Since then, the Fenton process has become one of the most studied catalytic processes for the remediation of polluted water. Mixtures of Fe^{3+}/H_2O_2 (Fenton's systems) may also be used to promote the oxidation of the pollutants. Although the reaction mechanism is not completely elucidated yet, the generation of hydroxyl radicals in the presence of Fenton's reagent can be described very briefly by the following reactions:

$$Fe^{2+} + H_2O_2 \rightarrow Fe^{3+} + \,^\bullet OH + \,^\bullet OH^- \qquad \text{reaction 3.9}$$

$$Fe^{3+} + H_2O_2 \rightarrow Fe^{2+} + \,^\bullet OOH + H^+ \qquad \text{reaction 3.10}$$
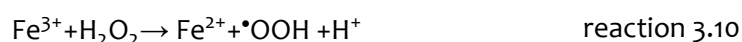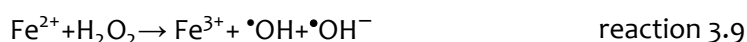
The rate constant of reaction 3.9 is very high and since it forms the ferric ion, the excess hydrogen peroxide is decomposed, generating more hydroxyl radicals according to reaction

presented in reaction 3.10. The Fenton reaction is quite sensitive to solution pH, with an optimum pH of about 2.8-3.0, at which it is spread by the pair of catalytic behaviour Fe^{3+}/Fe^{2+}. However, secondary reactions based on consumption of $^{\bullet}OH$ by Fenton reagent may also occur, contributing to the reduction of the oxidizing potential of Fenton systems. Fenton reaction efficiency can be increased under UV or solar irradiation, designated as photo-Fenton reaction, since it increases the production of hydroxyl radicals. This reaction is of particular interest, as the use of solar light with wavelengths below 580 nm, can reduce the cost of the process (the main drawback of most AOPs).

Fenton's systems are usually applied in the tertiary stage of water treatment, although in the case of effluents with a high pollution load -for example, hospital waste or pharmaceutical industries-, this technology can be applied in an early stage of the process, since it can mineralize a substantial fraction of the polluting species, increasing the efficiency of the subsequent biological treatment (Méndez, Melián, *et al.*, 2015). Satisfactory results have been obtained by Fenton processes in real wastewater samples (both domestic and industrial, covering for instance carpet dyeing wastewater, cork processing wastewater, textile secondary effluents, dye wastewater) (Mandal, Maity, *et al.*, 2010; Kavitha, Palanivelu, *et al.*, 2004, Li, Nanaboina, *et al.*, 2012); even solar photo-Fenton has proven to be an effective process, achieving removal rates of around 90 % (Méndez-Arriaga, Esplugas, *et al.*, 2010; Klamerth, Malato, *et al.*, 2011; Nogueira, Nascimento, *et al.*, 2012; Klamerth, Malato, *et al.*, 2013; Ioannou, Michael, *et al.*, 2014; Freire, da Fonseca, *et al.*, 2014).

The main disadvantages of this technology are related to the quite narrow operational range of pH and the need of introducing an additional stage for recovery of iron ions after treatment. The treated effluent will also have to be neutralized prior to reuse, increasing the salt content, which would be negative for certain purposes, such as irrigation. However, the high efficiency of photo-Fenton reaction natural pH was demonstrated using UV radiation at 254 nm, highlighting the possibility of its use in actual large-scale applications (De la Cruz, Giménez, *et al.*, 2012).

3.4.4 Electro-assisted degradation

The use of electricity for water treatment was first proposed in 1889 (Chen, 2004), and although its application to environmental processes is still quite recent, it is expanding rapidly. Extensive research has been done over the last decade on direct or integrated electrochemical processes applied to environmental remediation processes. Compared to the classical techniques of wastewater remediation, this technology offer many advantages, such as environmental compatibility (the electrons are cleaned reagents alone), energy efficiency, versatility (freedom of choice in setting potential and electrode material, ability to handle a wide range of pollutants), low cost and easy automation (Comninellis and Pulgarin, 1993; Sirés and Brillas, 2012; Martinez-Huitle and Ferro, 2006).

This technology still presents some challenges, especially related to the stability, cost and erosion of electrodes, reduction of energy costs by coupling with solar or renewable energy sources and increasing the mineralization efficiency in order to prevent the formation of oxidation intermediates, potentially more toxic than the original compound. Electrochemical techniques can be classified into separation and oxidation technologies. In separation techniques (membrane technologies, internal electrocoagulation, and internal

microelectrolysis) the pollutant is isolated, unlike the electrochemical oxidation techniques (direct and indirect anodic oxidation, electrooxidation, electro-Fenton, photoelectron-Fenton and photoelectrocatalysis) in which the pollutant is decomposed.

Indirect electrooxidation methods with H_2O_2 electrogeneration, such as electro-Fenton and photoelectron-Fenton, have also been recently applied to wastewater treatment (Babuponnusami and Muthukumar, 2012b), as well as in tandem with sunlight as powerful and economical source of UV radiation (Salazar, Brillas, *et al.*, 2012).

Despite the excellent performance obtained for the electrochemical technologies based on Fenton's reaction at laboratory scale for synthetic solutions, these processes have not yet been applied to real wastewaters. The complexity of real matrices prevents the study of the electrochemical oxidation process, since the parasitic uncontrolled reactions can be easily produced, thereby decreasing the electrode degradation performance and/or generating potentially toxic side products. Moreover, much research is being done in order to improve the performance of existing noble metals oxides based electrode devices, without disregarding new possible electrode materials.

3.4.5 Sonolysis

Sonolysis or ultrasonic irradiation is based on the application of high intensity acoustic radiation (typically in the range of 20-1000 kHz), to the aqueous medium to generate cavitation (i.e., bubbles), immediately followed by the implosion of these bubbles, leading to the release of hydroxyl radicals. The sonochemical reactions may occur in the cavitation bubble, at the interface or within the solution.

The application of ultrasounds to wastewater treatment is an area of increasing interest and promising results. In fact, over the past few years, sonochemistry was considered one of the successful degradation techniques of persistent organic pollutants (Méndez-Arriaga, Torres-Palma, *et al.*, 2008; Isariebel, Carine, *et al.*, 2009). Sonolysis efficiency can be improved by combination with other techniques (Méndez-Arriaga, Torres-Palma, *et al.*, 2009; Wang and Yu, 2013; Wu, Zhang, *et al.*, 2014). For example, for the application of Fenton, sono-Fenton, and sonophoto-Fenton processes for the oxidation of phenol in aqueous solution, the mineralization efficiency was 50.5, 55.8 and 71.0 %, respectively. The overall results suggest an additive or synergistic effect of the tested hybrid processes (Babuponnusami and Muthukumar, 2011).

3.4.6 Heterogeneous Photocatalysis

Photocatalysis originated from different catalysis laboratories in England and Germany, with the pioneering studies on the photocatalytic oxidation of CO in ZnO (Barry and Stone, 1960; Romero-Rossi and Stone, 1960; Doerfler and Hauffe, 1964a; Doerfler and Hauffe, 1964b), with the latter including the term "photocatalysis" for the first time in its title. The re-publication in English of a previous work by Fujishima and Honda (Fujishima, Honda, *et al.*, 1969) on the photo-water electrolysis using a titanium dioxide anode irradiated with UV in "Nature" (Fujishima and Honda, 1972) constituted the initial event for a globalization of photocatalysis, which had a preferential development in Japan.

Photocatalysis became a major discipline owing to the mutual enrichment of scientists arising from different fields, as illustrated in Figure 3.14. The interest in heterogeneous photocatalysis

semiconductors has rapidly expanded in many fields, with an exponential number of publications globally appearing in the literature, turning this process into one of the most popular and promising AOPs in the environmental remediation area (Pelizzetti and Serpone, 1989; Legrini, Oliveros, *et al.,* 1993; Ollis and Al-Ekabi, 1993; Oppenlander, 2003; Fujishima, Zhang, *et al.*, 2008; Comninellis, Kapalka, *et al.*, 2008).
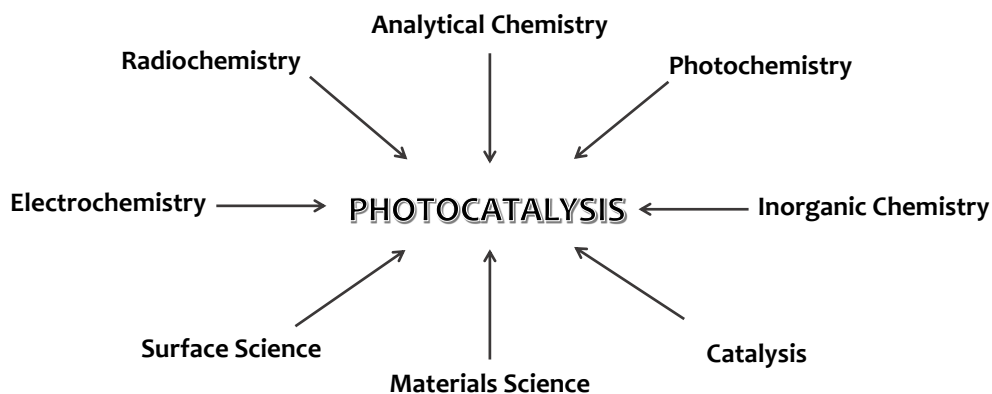
Figure 3. 14- Contributions to photocatalysis from various sub-disciplines of chemistry (adapted from Herrmann, 2010).

Efficient photocatalytic processes have the potential to tackle some of society's greatest challenges; most prominently in meeting clean energy demand and controlling environmental pollution. Photocatalysis applications of far-reaching importance include water splitting for hydrogen generation, degradation of environmental pollutants in aqueous medium, carbon dioxide remediation, self-cleaning activity and air purification (Leary and Westwood, 2011; Grabowska, Reszczyńska, *et al.*, 2012).

Despite the large gaps still existing concerning the knowledge of the chemistry involved in most photocatalytic processes, its use for wastewater and drinking water treatment has attracted increasing interest in recent years, specially for the degradation of organic compounds in aqueous medium (Ollis and Al-Ekabi, 1993; Parsons, 2004; Thu, Karkmaz, *et al.*, 2005; Martins, Vasconcelos, *et al.*, 2008; Faria and Wang, 2009; Ahmed, 2012).

The success of heterogeneous photocatalysis as an effective tool in environmental remediation relates mainly to the choice of titanium dioxide (TiO_2) as a photoactive layer. The use of TiO_2 in photocatalysis presents several advantages, since it is non-toxic, photo stable, cheap and very efficient under UV irradiation. It also requires a low operation temperature, low energy consumption, being insoluble under most environmental conditions, thus preventing the formation of undesirable by-products.

Other semiconductors based on oxides and sulfides of transition metals (such as ZnO, MgO, WO_3, Fe_2O_3, CdS), mixed oxides (Bi_2MoO_6, $BiVO_4$) or metal-doped semiconductors (Ag/TiO_2, Ag-AgBr and $Cu_2O/BiVO_4$) are also being used as photocatalysts; some of them show remarkakble photoactivity under visible light and quite high mineralization rates for the degradation of various pollutants have been reported (Klavarioti, Mantzavinos, *et al.* 2009; Zhang, Wang, *et al.*, 2012; Wang, Tang, *et al.*, 2012; Wang, Huang, *et al.*, 2013; Nalbandian, Zhang, *et al.*, 2015).

Triggered by the low photonic efficiency of most photocatalysts (particularly under visible light), new approaches are being explored. Among them, strategies based on the

immobilization of active phases in porous supports (silicas, glass fibers, carbonaceous supports), the synthesis of porous semiconductors with high surface areas (Choi, Stathatos, *et al.*, 2006;. Fernández, Lassaletta, *et al.*, 1995; Hsien, Chang, *et al.*, 2011; Velasco, Parra, *et al.*, 2010a; Velasco, Parra, *et al.*, 2010b), and the development of photocatalysts with improved light absorption, seem interesting alternatives to be explored to attain a more efficient use of solar energy (Méndez-Arriaga, Esplugas, *et al.*, 2008; Méndez-Arriaga, Maldonado, *et al.*, 2009; Miranda-García, Suárez, *et al.*, 2011; Klamerth, Miranda, *et al.*, 2009; Spasiano, Marotta, *et al.*, 2015).

The results found from solar photocatalytic technologies employed in different markets encourage further research in the use of solar photochemistry to advance in the field of commercial and industrial processes. In particular, application of heterogeneous solar photocatalysis with TiO_2 should have a future beneficial impact on the environment, public health and a greener economy, and thereby, on the quality of life. Regardless the good results obtained for the degradation of organic pollutants present in wastewaters, there are only a few examples of medium and large-scale application of solar photocatalytic chemical processes (Spasiano, Marotta, *et al.*, 2014). Solar photocatalysis it is still far for commercialization and implementation in the industry sector, despite its significant interest in the research community.

3.4.6.1 Fundamentals of heterogeneous photocatalysis

According to the IUPAC, photocatalysis is defined as a change in the rate of a chemical reaction or its initiation under the action of ultraviolet, visible, or infrared radiation in the presence of a substance -the photocatalyst- that absorbs light and is involved in the chemical transformation of the reaction partners (Braslavsky, 2007). Heterogeneous photocatalysis takes place at the interfacial boundary between two phases (solid/liquid, solid/gas, liquid/ gas) (Braslavsky, Braun, *et al.*, 2011). Compared to photolysis, the presence of a catalyst typically accelerates the rate of degradation reactions, increasing the efficiency of the process (Fujishima, Rao, *et al.*, 2000). As in heterogeneous catalysis, the overall kinetics of heterogeneous photocatalysis follows the 5 step process of chemical engineering, with the only difference that in photocatalysis, in step 3, instead of thermal activation, it implies the activation of the solid by photons (Herrmann, 2010):

1. Transfer of the reactants in the fluid phase;
2. Adsorption of the reactants at the surface of the catalyst;
3. Reaction in the adsorbed phase:
   a. Absorption of photons by the solid;
   b. Generation of excitons (namely pairs electron/ hole) and their separation;
   c. Electron transfer reactions (ionosorption, charge neutralization, radical formation, surface reactions,…).
4. Desorption of the final products;
5. Removal of the final products in the fluid phase.

Solids have different energy levels or delocalized orbitals that are spread throughout the three-dimensional network of the materials, being the result of the combination of discrete atomic orbitals of similar energy of the individual atoms of the solid. These electronic levels are grouped into two energy bands: the higher energy band occupied by electrons, called valence

band (VB) and the lowest free energy, known as conduction band (CB). The energy gap between the two bands is called forbidden energy band or bandgap (E_{bg}), and its magnitude will define the behaviour of the solid as conductor, insulator or semiconductor (ranging from 1-4 eV for semiconductors) (Figure 3.15A).

The photocatalytic reaction on a semiconductor (Figure 3.15B) is initiated by the absorption of a photon of energy equal or higher than the E_{bg} of the semiconductor (3.2 eV for TiO_2), causing the excitation of an electron (e^-) from the valence band to the conduction band; simultaneously a vacancy of electron or hole (h^+) is created in the valence band of the semiconductor, according to equation 3.11:

$$h\nu + semiconductor = h^+ + e^- \qquad \text{reaction 3.11}$$

The photo-generated charge carriers (electron-hole pairs, e^-/h^+) may recombine (radiatively or non-radiatively) or migrate to the surface of the photoactive material where they can react with electron donors or acceptors adsorbed on the surface of the photocatalyst. The competition between these processes determines the efficiency of the photocatalytic process. Spectroscopic studies have also demonstrated that the electron–hole trapping or recombination rates are extremely fast (of the order of 10^{-6}–10^{-15} s) (Colombo and Bowman, 1996) and therefore can largely affect the photocatalytic efficiency of the catalyst.

The photo-generated hole is a strong oxidant (redox potential of +2.53 eV vs standard hydrogen electrode - SHE), that can react with the pollutant (photo-oxidation, if the redox potential is less negative than that of the valence band of the semiconductor), or react with water molecules to produce hydroxyl radicals (+2.81 eV vs SHE), which leads to the oxidation of the pollutant by means of radical chain reactions (reaction 3.12).
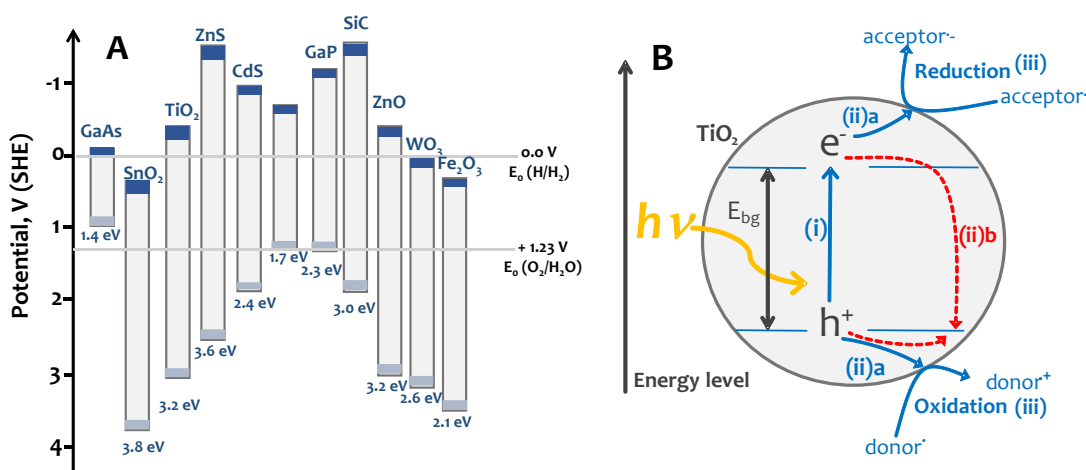
Figure 3.15- A) Location of the conduction band and valence of different semiconductors. (SHE- Standard Hydrogen Electrode). B) Major processes in semiconductor photocatalysis. (i) Photon absorption and electron–hole pair generation. (ii)a Charge separation and migration to surface reaction sites or (ii)b to recombination sites. (iii) Surface chemical reaction at active sites (adapted from Leary and Westwood, 2011).

Similarly, the electron in the conduction band is a strong reducing agent ($-$ 0.52 eV vs SHE) that may react with electron acceptors such as dissolved oxygen creating superoxide radicals $^{\bullet}O_2^-$ (+0.89 eV vs SHE) (reaction 3.13) or hydrogen peroxide, H_2O_2 (+1.78 eV vs SHE) (reactions 3.14 e 3.15), or other species, with a more positive redox potential than the conduction band of the

photocatalyst (photorreduction). These reactions avoid the recombination of the e^-/h^+ pairs, thereby contributing to the increased photo-oxidation of the target pollutants.

$$H_2O + h^+ \rightarrow {}^\bullet OH + H^+ \qquad\qquad \text{reaction 3.12}$$

$$O_2 + e^- \rightarrow {}^\bullet O_2^- \qquad\qquad \text{reaction 3.13}$$

$${}^\bullet O_2^- + H^+ \rightarrow HO_2^\bullet \qquad\qquad \text{reaction 3.14}$$

$$2\, HO_2^\bullet \rightarrow O_2 + H_2O_2 \qquad\qquad \text{reaction 3.15}$$
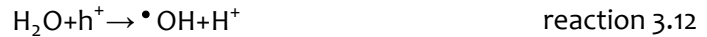
These oxidizing and reducing agents are able to promote the degradation of contaminants (inorganic and organic) through the solid/fluid interface, and in the case of organic pollutants can achieve complete mineralization (reaction 3.16):

$$\text{Organic pollutant} + h\nu\,(TiO_2) \rightarrow \text{Intermediates} \rightarrow CO_2 + H_2O \qquad \text{reaction 3.16}$$

The principle governing the efficiency of the photocatalytic oxidative degradation is to minimize the recombination of the photo-generated e^-/h^+ pairs and to enhance their separation through the solid/liquid interface, being its driving force the difference between the redox potential of the adsorbed species and the corresponding energy levels where the generated e^-/h^+ pairs in the semiconductor are located.

The overall reaction mechanism usually involves the formation of intermediate species resulting from the partial conversion of the pollutant, whose complexity and number depend on the nature of the molecule to degrade.

3.4.6.2 Operational parameters of the photocatalytic process

Understanding the impact that certain parameters have on the photocatalytic degradation efficiency and identifying the role that they play is of paramount importance -from the design and the application point of view-, to ensure an optimal performance of the photocatalytic system, as well as a sustainable and efficient operation in wastewater treatment (Chiou, Wu, *et al.*, 2008; Ahmed, 2012). These parameters influence both qualitatively and quantitatively the photocatalytic reaction being decisive in the overall efficiency of the process. Some of the most important parameters are discussed below.

***Photocatalyst composition and load*-** The photocatalytic activity depends on the characteristics of the semiconductor such as crystal composition, surface area, particle size distribution, porosity, band gap and surface hydroxyl density. Particle size is of primary importance in heterogeneous catalysis, because it is directly related to the efficiency of a catalyst through the definition of its specific surface area. The photocatalyst titanium dioxide Degussa (Evonik) P25 has been widely used in most of the experimental conditions; P25 contains 75 % anatase and 25 % rutile with a specific surface area of 50 $m^2\,g^{-1}$ and a primary particle size of 20 nm (Fujishima, Zhang, *et al.*, 2008).

Crystalline properties have an influence mainly on the generation of the e^-/h^+ pairs and availability of surface redox reactions. In this context, the degree of crystallinity, the crystalline phases and their ratio, and the crystal size must be taken into account (Tanaka, Capule, *et al.*, 1991) since, for instance, the presence of defects in the crystal structure may promote recombination processes. On the other hand, textural properties will affect the contact

between the catalyst and the reacting species. Generally, the process efficiency increases for photocatalysts with high surface area and uniform particle size and spherical shape (Herrmann, 2010).

The photocatalytic degradation rate increases with the increase in the catalyst loading and the number of active sites in solution, up to a point where the light penetration is compromised due to excessive particle concentration; then the rate decreases at high values due to light scattering and screening effects (Herrmann, 2010). Also, the tendency towards agglomeration of fine catalyst powders results in a reduction in the catalyst surface area available for light absorption and hence in a decrease of the photocatalytic degradation rate. The optimal concentration of photocatalyst will correspond to the least amount thereof, for which the maximum reaction rate is obtained. In the case of titanium oxides with specific surface areas between 50-200 m^2 g^{-1}, the optimal concentration lies in the range of 0.5-3.0 g L^{-1}, depending on the chemical and technical characteristics of the system (Kisch, 2010).

Pollutant type and concentration- The successful application of the photocatalytic oxidation system requires the investigation of the dependence of the degradation rate on the pollutant concentration (C_o). It has been indicated in several studies that as the concentration of the target pollutant increases, more and more molecules of the compound are adsorbed on the surface of the photocatalyst. Therefore, the reactive species required for the degradation of the pollutant also increases. However, the formation of these species remains constant for a given light intensity, catalyst amount and duration of irradiation. Hence, the available $^{\bullet}$OH radicals are inadequate for the degradation of pollutant at higher concentrations, with a decrease of the degradation rate.

An increase in the pollutant concentration also leads to the generation of more intermediates, which may adsorb on the surface of the catalyst. Slow diffusion of these intermediates can also result in the deactivation of active sites of the photocatalyst, and thus a drop in the degradation rate. In contrast, at low concentrations, the number of catalytic sites will not be the limiting factor and the rate of degradation is proportional to the concentration following an apparent first-order kinetics (Herrmann, 2010), with most photocatalytic reactions obeying the Langmuir–Hinshelwood rate form (Annex B.4).

Light intensity and wavelength- Light intensity determines the extent of light absorption by the semiconductor catalyst at a given wavelength. The variations of the reaction rate as a function of the wavelength follow the absorption spectrum of the catalyst, with a threshold corresponding to its band gap energy. Additionally, the rate of initiation of photocatalysis, and the photogeneration of e^-/h^+ pairs is strongly dependent on the light intensity. Light intensity distribution within the reactor invariably determines the overall pollutant conversion and degradation efficiency.

Radiant power- For all types of photocatalytic reactions, the reaction rate r is reported to be proportional to the radiant power, P (power emitted, transferred or received as radiation), for $P < 25$ mW cm^{-2}. Above this value, the reaction rate was shown to vary as $P^{1/2}$, indicating an increase of the electron-hole recombination rate. At higher intensity, the reaction rate is independent of light intensity (Herrmann, 2010). This is likely due to predominant low intensity reactions involving electron-hole formation, so that electron-hole recombination is

insignificant. The optimal light power utilization corresponds to the domain where the reaction rate is proportional to *P*.

Quantum yield- In photochemistry, the efficiency in substrate conversion, number of molecules converted per quantum absorbed by the medium, is characterized by the quantum yield, which according to its definition assumes knowledge of the number of photons of a particular wavelength absorbed by the system. While in homogeneous photochemistry this quantity can be measured with great accuracy, in heterogeneous photocatalysis the situation is more complex, and one can only easily know the number of photons incident onto the surface of the photocatalyst (Braslavsky, Braun, *et al.*, 2011). This corresponds to an upper limit for the actual number of absorbed photons, because due to scattering phenomena, in general the number of active photons are reduced, being able to be determined exactly only in a few cases.

For the above reasons, in addition to the quantum yield, the term photonic yield is convenient in photocatalysis. In this context, the term photonic is thus defined in terms of the incident amount of photons arriving at the internal surface of the irradiation window, rather than in terms of the absorbed. In addition, the use of efficiency was also adopted when irradiation within a wavelength range is used, whereas the term yield is reserved for excitation with monochromatic photons (i.e., photons of energy in the wavelength range λ and $\lambda + \delta\lambda$).

The notion of instantaneous quantum yield (QY), is closer to the kinetic reality and can be defined as a dimensionless, "doubly kinetic" magnitude equal to the ratio of two rates: the reaction rate, *r* (in molecules converted per second), divided by the efficient photonic flux, q_p (in UV photons per second) actually absorbed by the solid (Herrmann, 2010). The photon flux, q_p, the number of photons per time interval (s^{-1}) can be used on a chemical amount basis by dividing the photon flux, number basis, q_p, by the Avogadro constant, the symbol then being $q_{n,p}$, photon flux, amount basis (SI unit mol s^{-1} and common unit is Einstein s^{-1}).

The maximum values of QY are obtained at maximum coverage of reactants. On the contrary, for trace pollutant eliminations, QY mathematically decreases to less than 1 %, because of very low coverages resulting from the Langmuir-Hinshelwood equation. High quantum yields are indicative of the facility of the photocatalytic reactions performed. For low QY, it is not necessary to use over-powered electrical lamps.

Oxygen- Generally, O_2 is assumed to be adsorbed on the catalyst surface from the liquid phase, where its concentration according to Henry's law, is proportional to the gas phase. Acting as an electron acceptor, the presence of oxygen minimizes the recombination of the e^-/h^+ pairs, and it does not compete with the contaminant for the adsorption centers. However, some authors have found that too high concentrations of oxygen slow down the degradation rate; this has been attributed to a high hydroxylation of the semiconductor surface, which inhibits the adsorption of the compounds on the catalyst surface (Albini and Germani, 2009).

Solution pH- The pH is an important parameter in wastewater treatment since it may significantly influence the characteristics of the pollutants, particularly their ionization state, solubility and hydrophobicity. While some compounds are uncharged at common pH conditions typical of natural water or wastewater, others exhibit different surface charges depending on their dissociation constant (pKa). For instance for a given compound (HA) dissociating as a Bronsted acid (A- + H+), at pH below the pKa value, the neutral state is the predominant form

in solution; above the pKa value, the compound is negatively charged. Hence, some compounds can exist in positive, neutral, and negative forms in aqueous solutions.

Wastewater pH varies significantly and can play an important role in the photocatalytic degradation of organic contaminants since it does not only control the ionization state of the pollutant, but it also determines the surface charge of the photocatalyst and thus the size of the eventual particle aggregates formed. As a result, the electrostatic interactions between a semiconductor surface, the solvent molecules, the pollutant and other charged species (i.e., radicals) formed during the photocatalytic reaction strongly depend on the solution pH. In addition, protonation and deprotonation of the pollutants can occur depending on the solution pH. Sometimes protonated products are more stable under UV radiation than its main structures (Saien and Khezrianjoo, 2008).

Temperature- Since the photocatalyst activation occurs through the absorption of radiant energy, the temperature of the reaction medium is not expected to play an important role in the photocatalytic reaction (Albini and Germani, 2009). However other parameters such as the solubility and volatility of the contaminants and other participants species (O_2, additives, etc.), or the adsorption-desorption kinetics, must be taken into consideration if the working temperature changes during the process.

Photocatalytic reactor- The design of the photoreactors is subjected to two inherent difficulties in heterogeneous photocatalysis: it must ensure perfect contact between two different phases (solid/fluid) and allow uniform illumination of all the catalyst particles. Different configurations have been developed, based on aspects such as the location of the radiation source (external or internal), the required range of wavelengths, continuous operation or batch, liquid or gas phase, etc. The two more important factors to optimize in reactor design are the efficiency of energy use and the disposal of the catalyst. Different types of photocatalytic reactors used in the literature are classified and described in Table 3.6 (Zangeneh, Zinatizadeh, *et al.*, 2015, and references therein). The classification is based on batch or continuous processes operating with suspended and immobilized systems as well as slurry configurations.

Slurry reactors have been widely used due to their simplicity and enhanced degradation efficiency. Whereas, in the catalyst immobilized systems, the photocatalyst powders are immobilized on a support transparent to photoradiation, which facilitates the recovery and reuse in successive cycles in the case of working with powdered materials. Nevertheless, the use of supports also presents a number of disadvantages such as reduced useful semiconductor surface, and in the case of continuous operation, also limitations in mass transfer at low flow rates and increased pressure drop, thereby increasing energy costs.
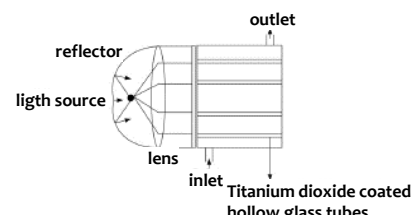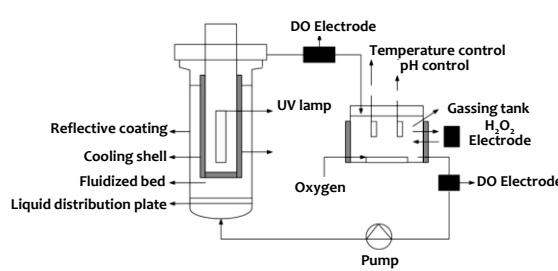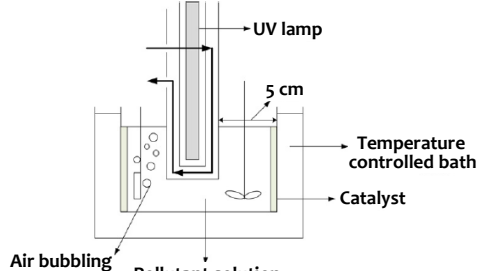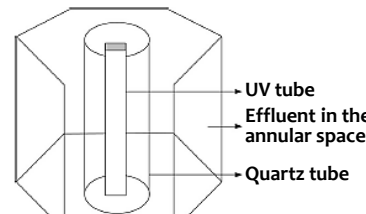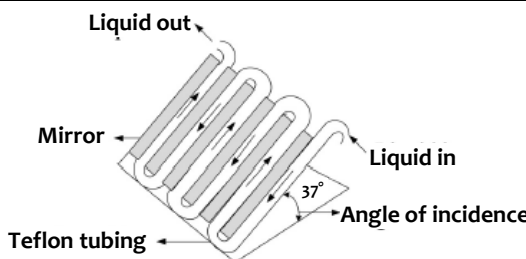
In contrast, when working with a suspended material and in order to prevent sedimentation, it is important to design the system so as to guarantee a turbulent flow. As for energy efficiency, better results are obtained for designs in which the power supply is in the center of an annular reactor, and in fact, commercial prototypes are based on this principle. However, the way radiation reaches the reactor and the optical path length of the inside are fundamental to determine the optimal concentration of catalyst and avoid shielding effects.

From a fundamental point of view, the analysis of the heterogeneous photocatalytic process in such systems requires the determination of all physical parameters governing the kinetics: the

mass of catalyst, the wavelength and radiant flux of the irradiating source, the quantum yields or turnover numbers of the photocatalytic process, the initial concentration of reactants, and the influence of oxygen pressure and temperature (Faria and Wang, 2009).

The optimization of the degradation parameters is crucial from the perspective of efficient design and the application of a photocatalytic oxidation process to ensure sustainable operation. The potential of this technique using industrial effluent needs further attention to yield stable pollutant removal through the optimization of process parameters.

Table 3. 6- Different types of photocatalytic reactors (adapted from Zangeneh, Zinatizadeh, *et al.*, 2015).

Reactor features	Schematic of reactor setup
Multiple tube reactor This set-up consists of hollow glass tubes that irradiated from the outside by light source and TiO$_2$ coated on hollow glass tubes.	
Fluidized bed photoreactor This photoreactor consists of small particles of TiO$_2$ coated on different supports. This configuration meets the requirements of higher surface area-to-volume ratio, makes better use of light, and shows improvement in mass transfer conditions and thus efficient reactant-catalyst contact. Other advantages include a low pressure drop, and high throughput.	
Batch reactor A cylindrical reactor placed in a thermostatic tank at certain temperature and photocatalytic media is immobilized on the inner wall of the photoreactor. The solution is mixed in the reactor by means of an impeller. Atmospheric dried air was introduced through a bubbler.	
Hexagonal annular photoreactor In this type of photocatalytic reactor, the outer configuration is in hexagonal shape. Photocatalyst can be in suspended form or immobilized on the quartz tube.	
Solar photocatalytic reactor The design depends on the type of sunlight provided, concentrated or non-concentrated, and also on the photocatalyst form (suspended or supported). Its main advantage is that it requires a smaller reactor volume for the same light-harvest area. It can also be operated at much higher flow rates.	

3.4.6.2 Operational parameters of the photocatalytic process

Table 3.6 (continued).

Photocatalytic membrane reactor

The catalyst is used in the suspended form. Membrane filtration may be used as a single step for the complete recovery of catalyst particles from solution. The major disadvantages of such configuration are deterioration of the permeate flux and membrane fouling. Different reactors have been tested including light source irradiation of the membrane module, the feed tank, catalyst supported in/on the membrane and the light source positioned above the membrane module or inside the membrane module and feed tank.
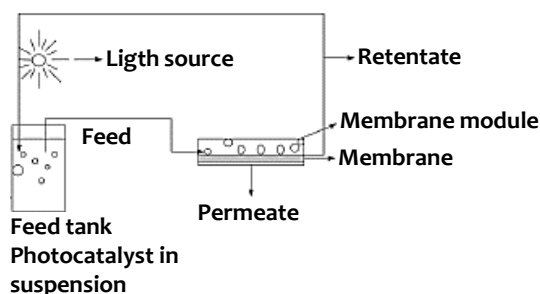
Rayonet multi-lamp photocatalytic reactor

A cylindrical vessel with a multi- lamp arrangement in which the cylinders are fabricated from quartz to allow for maximum UV transmission into the reaction zone from the inside and outside. The bottom portion of the reactor is conical to allow water to enter and then be distributed through the distributor. The photocatalyst particles are retained by a 425 m Nylon mesh screen held between steel plates with 58 holes of 5 mm diameter.
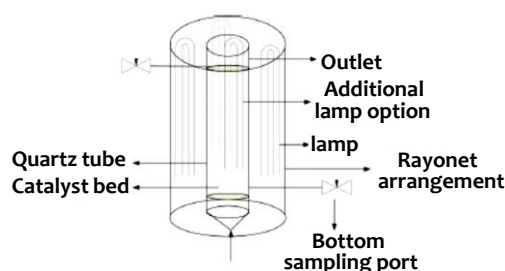
Photocatalytic reactor

This reactor consists of a quartz tube, with an inlet tube for oxygen purging during photocatalysis and another outlet for the collection of samples from the reactor. After being sampled, the suspension is centrifuged and the centrifugate is subjected to further analysis.
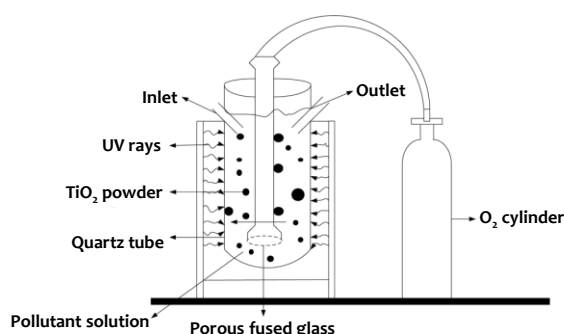
Despite extensive studies on photocatalysis, the commercial exploitation of this technique has been hindered by the lack of efficient and low-cost visible light-harvesting catalyst, a relatively poor understanding of the reactor design, and inadequate scale-up strategies.Despite numerous reported approaches to the synthesis and fabrication of various photocatalyst materials with demonstrated application potentials, a generalized and cost-effective method must be addressed before a photocatalyst can be practically used.

In addition, more work is required on the modeling of photoreactor to optimize its design for pollutant degradation. Because most of the presented data on photocatalytic system were collected at bench scale, performance and stability of the whole photocatalytic system at a pilot scale should be substantiated to utilize this process on a commercial basis (Ghatak, 2014).

3.4.6.3 Enhancement of TiO_2 photocatalysis

As it was already mentioned, TiO_2 is the most broadly used semiconductor in environmental applications (Pelizzeti and Serpone, 1989; Kwon, Fan, *et al.*, 2003; Choi, 2006; Ochiai and Fujishima, 2012; Park, Park, *et al.*, 2013), due to several reasons: many organic compounds have

an oxidation potential above the titanium oxide valence band, being for this reason photocatalytically oxidized by this material. Secondly, the redox potential of the pair $H_2O/{}^{\bullet}OH$ is located within the domain of the band gap of the material. Furthermore, the high resistance of TiO_2 to light-induced corrosion, along with its low cost and safety, makes this material the most suitable for application in heterogeneous catalysis based AOPs. Nevertheless its widespread application, the use of TiO_2 in heterogeneous photocatalysis presents some drawbacks.

The major disadvantage is related to its E_{bg} (3.2 eV), which requires irradiation with UV light below 380 nm, to obtain its total capacity as a photocatalyst. Thus, TiO_2 can use only 3-4 % of the solar energy that reaches the Earth, since its band gap limits the use of visible light. Moreover, the quantum efficiency of the photocatalytic process with TiO_2 is low, as a result of the rapid recombination of e^-/h^+ pairs photo-generated.

In this sense, three fundamental approaches for the enhancement of photocatalytic activity are currently being investigated (Kudo and Miseki, 2009; Hu, Li, *et al.*, 2010; Daghrir, Drogui, *et al.*, 2013):

- Photocatalyst band gap tuning via chemical modification;
- Minimizing charge carrier recombination;
- Promotion of the forward reaction and adsorption of reactants through provision of adequate quality and quantity of active sites.

Moreover, as the degradation rate is connected to the surface contact between the active sites in the photocatalyst and the compounds in solution, most research efforts on this field focus on incorporating porous catalysts, either via synthesis of porous semiconductors or immobilization on porous supports (Pelizzetti and Serpone, 1989, Faria and Wang, 2009, Leary and Westwood, 2011; Dozzi and Selli, 2013).

Modification of TiO_2 with non-metals has been suggested as an efficient approach to tuning the band gap energy for visible light. However, the overall photocatalytic performance still does not meet the requirements for industrial application and remains an important area for further investigation. On this matter, the development of a stable and reliable photocatalyst using visible or solar light irradiation is of great relevance to enable the commercial viability of photocatalysis.

Another clear disadvantage of TiO_2 photocatalysis, which in most cases is used as a suspension of fine powders, is related to the difficult recovery and further reuse of the catalyst after water treatment. This issue remains as the major obstacle towards large-scale implementation in the industry. This limitation can be overcome by semiconductor immobilization on different substrates, such as glass spheres and ceramics, polymers, thereby facilitating the need for a post-removal treatment. This strategy may allow the reuse of the photocatalyst in several sequential cycles while maintaining its activity, although slightly longer times may be needed for the completion of treatment (Miranda-García, Suárez, *et al.*, 2011).

A combined process comprising photocatalysis and membrane separation, can alternatively be used, wherein the membrane retains the catalyst, the unreacted pollutant and its by-products, and may then be recycled to the photoreactor (Mozia and Morawski, 2012, Benotti, Stanford,

et al., 2009). However, it should be noted that the immobilization of the catalyst inevitably leads to a decrease in surface area available for the reaction compared to suspension systems, slightly lowering the efficiency of the degradation.

In the following section, the role of carbon materials in heterogeneous photocatalysis will be discussed, whether as part of composites or as photocatalysts on their own.

3.4.6.4 Role of carbon materials in heterogeneous photocatalysis

Triggered by the rising interest in heterogeneous photocatalysis for environmental remediation, numerous efforts have been made in the last decades to improve the photocatalytic activity of semiconductors. Aside from tuning their nanostructure and chemical composition, novel hybrid materials prepared by immobilization of the photoactive semiconductor on appropriate substrates have been explored.

Despite carbons are strong light absorbing materials, extensive work has been carried out on the improvement of the catalytic activity of photo-active materials upon immobilization on different carbon supports (Hu, Wang, *et al.*, 2002; Inagaki, Park, *et al.*, 2010; Leary and Westwood, 2011). Indeed, many studies have shown that adding a carbonaceous phase to the catalyst provides superior performance in a number of photocatalytic degradation reactions, both in liquid and gaseous phase (Leary and Westwood, 2011; Faria and Wang, 2009; Ania, Velasco, *et al.*, 2012). The enhancement on the photocatalytic response of carbon/semiconductor composites has been attributed to either single or collective factors traditionally associated to visible light absorption, textural features (i.e. surface area) and strong interfacial electronic effects.

Most recently, the visible-light photochemical activity of certain carbon materials has been demonstrated in the absence of conventional semiconductors under monochromatic light (Velasco, Maurino, *et al.*, 2013a; Velasco, Maurino, *et al.*, 2013b; Velasco, Lima, *et al.*, 2014). An overview of the photochemical response of carbon-containing photocatalysts and their efficiency for the degradation of different pollutants will be presented in the next sections.

Carbon/TiO₂ Photocatalysts- The majority of the studies in the literature deal with the use of TiO$_2$ as photocatalyst, due to its low cost, high photoactivity and stability. As it was already mentioned, TiO$_2$ doping is nowadays considered a promising route to tune its band gap, allowing a more efficient use of sunlight in photocatalytic processes. Most of the approaches on TiO$_2$ photoactivity enhancement have been focused on the use of metallic (Fe, Cr, Ag, and Ce) and non-metallic (N, C, S, B, and F) doping (Asahi, Morikawa, *et al.*, 2001; Sakthivel and Kisch, 2003; Choi, Umebayashi, *et al.*, 2004). Non-metallic TiO$_2$ doping is considered to be more effective than transition metal doping due to their high photostability and lack of photocorrosion of the resulting catalyst. In this sense, nitrogen and most recently carbon have been widely investigated and were considered to be more effective than other non-metal heteroatoms for the degradation of organic pollutants (Asahi, Morikawa, *et al.*, 2001; Nie, Zhuo, *et al.*, 2009). **Carbon doping** seems to have a more beneficial effect, compared to nitrogen doping, despite the synthesis, structural and electronic control of carbon-doped TiO$_2$ are usually more complex (Di Valentin, Pacchioni, *et al.*, 2005).

Although still uncertain, the origin of the improved photocatalytic performance of carbon-doped TiO_2 is explained by most authors in terms of the shift in the absorption properties towards the visible region and the modifications in the electronic band structure of titanium oxide associated to band gap narrowing (Ania, Velasco, *et al.*, 2012).

Photocatalytic techniques based on carbon-containing catalysts have been employed for water splitting into H_2 and O_2, and in the gas-phase and liquid-phase degradation of a vast number of pollutants, being phenol and related aromatic compounds, dyes, pesticides, and herbicides, among the most representative classes of compounds studied in this context (Pelizzetti and Serpone, 1989; Oppenlander, 2003; Silva, Wang, *et al.*, 2006; Chong, Jin, *et al.*, 2010; Ahmed, 2012; Adishkumar, Kanmani, *et al.*, 2014;).

Besides semiconductor doping, the incorporation of porous supports in **carbon/TiO₂ composites** is another promising approach for the preparation of more efficient photocatalysts, overcoming the operational cornerstones usually associated to limited recovery and reuse of the catalyst. Extensive work has been carried out upon immobilization of photo-active materials on different carbon supports (Leary and Westwood, 2011; Faria and Wang, 2009; Ania, Velasco, *et al.*, 2012), and carbon/TiO₂ composites have shown quite high efficiencies for the photodegradation of a variety of pollutants (Leary and Westwood, 2011; Faria and Wang, 2009; Tryba, Morawski, *et al.*, 2003; Puma, Bono, *et al.*, 2008; Matos, Laine, *et al.*, 1998; Araña, Doña-Rodríguez, *et al.*, 2003a; Silva, Wang, *et al.*, 2006; Velasco, Parra, *et al.*, 2010; Velasco, Fonseca, *et al.*, 2012).

The photocatalytic performance of carbon/TiO₂ composites has been reported over a variety of carbon sources, forms, and morphologies, using different synthetic routes for the preparation of the hybrid catalyst (mechanical mixture, coating by liquid impregnation, hydrothermal process, chemical vapor deposition) (Leary and Westwood, 2011; Faria and Wang, 2009; Puma, Bono, *et al.*, 2008).

The superior response of the carbon/TiO₂ photocatalysts has been usually attributed to single or collective factors traditionally associated with to the nature of the carbon matrix itself, the increase in visible light absorption by the composite, synergistic effects based on the target pollutant confinement in the activated carbon porosity, and strong interfacial electronic effects in the carbon support (Leary and Westwood, 2011; Ania, Velasco, *et al.*, 2012). Furthermore, it seems generally accepted that the role of carbon on the overall photocatalytic enhancement differs greatly for porous carbons compared to other forms of nanostructured carbons (such as carbon nanotubes, fullerenes and graphene).

Beyond the above-mentioned synergistic effect, the presence of a carbon matrix in the catalyst composition has been reported to change the catalytic behaviour of TiO_2 (Araña, Doña-Rodríguez, *et al*, 2003a; Velasco, Parra, *et al.*, 2010; Velasco, Fonseca, *et al.*, 2012; Araña, Doña-Rodríguez, *et al*, 2003b). Different degradation intermediates have been detected using activated carbon/TiO₂ photocatalysts, compared to bare titania, confirming the outstanding role of the carbon matrix on the photodegradation mechanism of a target pollutant (Velasco, Parra, *et al.*, 2010a; Velasco, Parra, *et al.*, 2010b; Araña, Doña-Rodríguez, *et al.*, 2003b; Tryba, 2008). The modification of the photo-oxidation pathway observed for the organic pollutants can also be explained by some changes in the interactions occurring between the pollutant and

the photocatalyst surface in the presence of the carbon, as revealed by Infrared Spectrometry studies (Araña, Doña-Rodríguez, *et al.*, 2003b).

Carbon as Photocatalyst- Heretofore, knowledge on carbon/semiconductor photocatalysis is based mainly on the role of carbons as non-photoactive additives and supports (Matos, Laine, *et al.*, 1998; Matos, Chovelon, *et al.*, 2009) (see above sections). Research carried out in our group has demonstrated the photochemical activity of semiconductor-free nanoporous carbons under different irradiation conditions, demonstrating their ability to photogenerate radical oxygen species in aqueous environments (Velasco, Parra, *et al.*, 2010; Velasco, Fonseca, *et al.*, 2012). This has opened new perspectives in the field of applied photochemistry based on carbon materials covering environmental remediation, water splitting, enhanced adsorption/oxidation, or photoluminescence.

Beyond the synergistic effect observed for carbon/TiO$_2$ composites, these results have shown that the nanoporous carbon alone was capable of a significant level of self-photoactivity under different illumination conditions, resulting in improved photochemical conversions for several reactions (i.e., photo-oxidation of phenol and water splitting) (Velasco, Gomis-Berenguer, *et al.*, 2015). To shed light on the origin and mechanisms of the photoinduced reactions initiated upon illumination of carbon materials, spin trapping electron spin resonance data of activated carbons have confirmed their ability to generate a similar or even higher quantity of hydroxyl radicals than commercial P25, when exposed to UV irradiation in an aqueous system (Haro, Velasco, *et al.*, 2012; Velasco, Maurino, *et al.*, 2013a; Velasco, Maurino, *et al.*, 2013b).

The visible light photochemical activity of nanoporous carbons under monochromatic light was also demonstrated, showing the ability of semiconductor-free nanoporous carbons to convert the low-energy photons from the visible spectrum into chemical reactions (i.e. phenol photo-oxidation and photoelectrochemical water splitting) (Velasco, Lima, *et al.*, 2014; Velasco, Gomis-Berenguer, *et al.*, 2015; Gomis-Berenguer, Iniesta, *et al.*, 2016).

In spite of the growing interest in this discussion, the exact role of carbon materials in the sharp response of the photocatalytic composites TiO$_2$/carbon is not yet completely understood. Even though the relative abundance of the degradation intermediates detected in solution seems to be highly dependent on the characteristics (composition and structure) of the carbonaceous material itself, this singular photocatalytic behaviour does not apply for all types of carbon adsorbents.

The interesting results obtained so far in this field will definitely stand as a starting point for further studies in this area. The possibility of coupling the photocatalytic degradation of refractory pollutants with classic and highly skilled adsorption technologies based on carbon materials is very attractive and will certainly be a topic of intensive research of the scientific community in years to come.

3.5 Phenolic compounds in the aquatic environment

Phenol is a fairly important molecule in the area of environmental research, being often chosen as a model molecule of an aromatic organic pollutant, due to the following reasons (Mayani, Vishal, *et al.*, 2011):

•   It is refractory to the biologic process;

•   It is involved as an intermediate in the oxidation path of many aromatic molecules;

- • Its presence in water in very low concentrations (in the order of ppb), is sufficient to generate disagreeable odor and taste;
- • It is extremely toxic to humans.

3.5.1 Physical and chemical properties

Phenols are a very heterogeneous group of compounds with different physical and chemical properties. Phenol (Chemical Abstracts Service -CAS- number 108-95-2), a monosubstituted aromatic hydrocarbon, is the simplest member of this family of products. It is also known as carbolic acid, benzenol, phenylic acid, hydroxybenzene and phenic acid. Pure phenol is a colorless or white crystalline solid with a powerful antiseptic sweet odor, detectable to most people at 40 ppb in air and at about 1-8 ppm in water (Rappoport, 2003; Fiege, Voges, *et al.*, 2012). When exposed to air and light, the white crystals of phenol turn pink or red. This compound is moderately soluble in water, being commercially sold as a liquid product. Some physical properties of phenol are reported in Table 3.7.

Table 3. 7- Physical properties of phenol (Weber, Weber, *et al.*, 2004).

Molecular formula	C_6H_5OH
Molecular weight	$94.1\ g\ mol^{-1}$
Appearance	White crystalline solid
Density	$1.071\ g\ cm^{-3}$ (20 °C)
Melting point	40.9 °C
Boiling point	181.8 °C
Water solubility	8.36 g/100 mL (20 °C)
Acidity (pKa)	9.95

Phenols are widely distributed in nature, being produced by plants and animals, including humans. Naturally occurring phenols are responsible for the flavor and color of certain foods. They are also used by plants to produce lignin, the main natural polymer in timber.

3.5.2 Phenol production

By the late nineteenth century, phenol was obtained mainly from coal tar, but currently, only a small amount of phenol is still obtained in this way. In the early twentieth century, synthetic routes have been developed, in order to meet a growing demand of this compound caused by the marketing of phenolic resins (Weber and Weber, 2010). The first synthetic method for the production of phenol, which is no longer in use, involved chlorination and sulfonation of benzene.

After the end of World War II, the cumene-to-phenol process (Hock Process) was developed and marketed. This process, that generates acetone as a by-product, remains until today as the predominant route for the production of phenol, responsible for about 95 % of the phenol used in the world. However, it presents some disadvantages such as a high environmental impact, formation of explosive intermediates (cumene hydroperoxide), multiple steps, which makes it difficult to obtain a high conversion of the overall process, decreasing its cost-effectiveness. In the 1960's, phenol production process from toluene was also explored, although currently there is no commercial production of phenol by this process.

Over the last two decades, several attempts have been explored in order to develop new routes for obtaining phenol by the direct oxidation of benzene, in a single step. However, none of these alternative processes have yet been commercialized, since it is still necessary to improve process selectivity (Molinari and Lavorato, 2012; Fiege, Voges, *et al.*, 2012). Currently, phenol is produced at a rate of about 6 million ton/year worldwide, with a significant increasing trend (Busca, Berardinelli, *et al.*, 2008), particularly as an intermediate in the production of other chemicals.

3.5.3 Phenol industrial applications

Phenolic compounds are used in diverse industries, such as in the production of resins, nylon, plasticizers, antioxidants, oil additives, pesticides, dyes, explosives, disinfectants, etc. (Fiege, Voges, *et al.*, 2012; Weber and Weber, 2010). Phenol is generally used as a disinfectant, as a reactant in chemical analysis and in the manufacture of artificial resins, drugs, pharmaceuticals, organic compounds, fertilizers, explosives, industrial dyes and coke.

The largest application of phenol (35 %) is as an intermediate in the production of phenolic resins, like phenol-formaldehyde resins (Bakelite), which are low-cost thermosetting resins used in plywood adhesive, construction, automotive and appliances industries. It may also be converted in bisphenol-A, a monomer used in the manufacture of epoxy and other resins (28 %) by reaction with acetone, and also used for the production of caprolactam (16 %),which is used in the manufacture of Nylon 6 and other synthetic fibers.

3.5.4 Phenolic compounds in industrial wastewater

The wide-ranging use of phenols, combined with their toxicity and unavoidable discharge of considerable amounts into the environment, has promoted extensive research on phenolic compounds and their fate in the environment. These compounds are some of the key organic contaminants in industrial wastewater, considered as harmful pollutants because they are toxic and harmful for the life of organisms even when present in low concentrations. The detection, identification and quantification of phenol compounds in water and their subsequent monitoring is of great importance for the control and protection of the environment and for emission control.

Phenols present in wastewater discharged into water courses can be transported over great distances because of their stability and water solubility. The presence of phenols in surface water or groundwater can lead to the generation of more toxic chlorinated phenols during water disinfection processes. Chlorophenols can also be formed from different industrial activities or degradation of other pollutants like pesticides. Due to their broad spectrum of antimicrobial properties, chlorophenols are widely used as fungicides, herbicides, insecticides, being also widely used as intermediates in chemical syntheses. These compounds tend to be much more persistent, ecotoxic and susceptible to bioaccumulation. For example, pentachlorophenol that is used as a wood preservative and general biocide is widespread in the environment, being found in 80 % of human urine specimens, in an EPA study (Glezer, 2003).

Alkyl-substituted phenols are also very widely used phenol derivatives. The alkylation of phenols is a very important industrial reaction, and alkylphenols are used in a variety of applications, such as antioxidants, herbicides, insecticides, or polymers. The transformation and biodegradation of alkylphenol polyethoxylates, present in detergents as non-ionic surfactants,

leads to the formation of free alkylphenol, such as nonyl- and octylphenols that adsorb readily onto suspended soils and are known to exhibit estrogen-like properties, possibly linked to carcinogenic effects. In Figure 3.16, some of the most frequently detected phenolic compounds in aqueous medium are shown. The presence of phenolic compounds in the aquatic environment causes serious problems, such as unpleasant taste and odor at very low concentrations (approximately 5 ppb), being extremely toxic at concentrations higher than 2 mg L^{-1} and exhibiting a high BOD (2.4 mg O$_2$ mg^{-1} phenol), generating a wide variety of problems to aquatic life (De Luis, Lombraña, *et al.*, 2011).
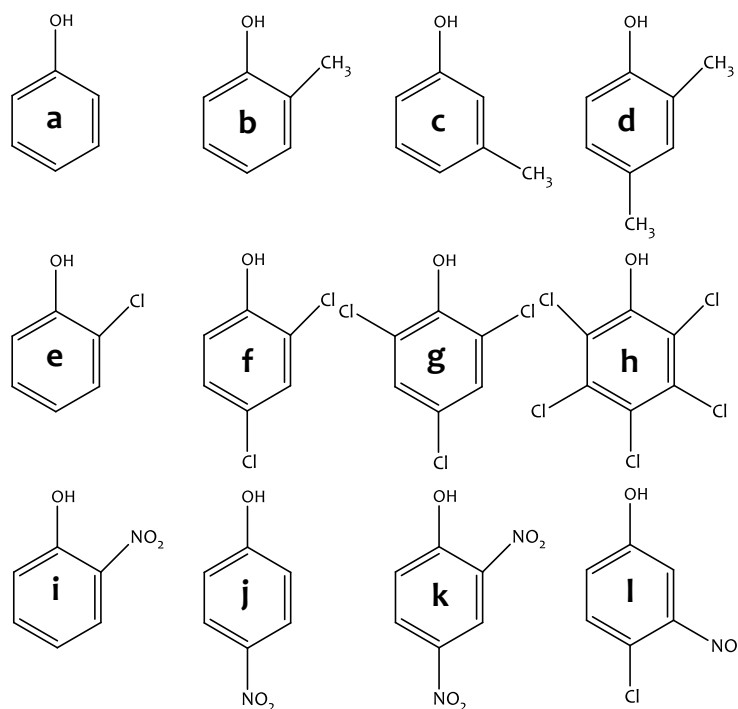
Figure 3.16- Chemical structure of some the most frequently phenolic compounds detected in wastewater- **a)** phenol; **b)** 2-methylphenol; **c)** 3-methylphenol; **d)** 2,4-dimethylphenol; **e)** 2-chlorophenol; **f)** 2,4-dichlorophenol; **g)** 2,4,6-trichlorophenol; **h)** pentachlorophenol; **i)** 2-nitrophenol; **j)** 4-nitrophenol; **k)** 2,4-dinitrophenol; **l)** 4-chloro-3-methylphenol.

The Ec$_{50}$ values for phenol and some of its oxidation intermediates are presented in Table 3.8. From the analysis of the data, it is possible to conclude that some of the species generated during the oxidation process, namely hydroquinone, catechol and 4-methylphenol, present higher ecotoxicity than phenol itself, given their lower EC$_{50}$ values. Phenol oxidation mechanism will be discussed further in this dissertation, in section 3.5.5.4.

Table 3. 8- Ecotoxicity of phenolic compounds according to the Microtox test on luminescent bacteria for an exposure of 15 minutes (De Luis, Lombraña, *et al.*, 2011).

Compound	EC$_{50}$ (% v/v)
Phenol	13.87
Hydroquinone	0.55
Cathecol	12.70
3-methylphenol	19.18
2-methylphenol	18.53
4-methylphenol	0.08

3.5.4 Phenolic compounds in industrial wastewater

Phenol causes local and systemic ecotoxic effects when entering the body through ingestion or by inhalation. Locally, phenol can cause irritation, skin burns, acute poisoning and death, as the result of respiratory failure. Chronic exposure to phenol is characterized by systemic problems and the long term effects of phenol exposure include a lifespan decrease, reproductive disorders, and changes in appearance or behaviour.

Due to its toxicity, phenolic compounds are subject to regulation as water environmental pollutants. The European Union (EU) specifies a level of legal tolerance of 0.5 µg L^{-1} of each phenolic compound in water for human consumption. The EU has also classified several phenolic compounds, such as nonylphenols, octylphenols and pentachlorophenol, as priority contaminants, being part of a list of 45 priority substances in the field of water policy (Directive 2013/39/EU). In Table 3.9, the environmental quality standards regarding the phenolic compounds classified as priority substances are summarized.

Table 3. 9- Environmental quality standards for EU phenolic priority substances (Directive 2013/39/EU).

Name	CAS number	AA- Inland surface waters (µg L^{-1})	AA- Other surface waters (µg L^{-1})	MAC- Inland surface waters (µg L^{-1})	MAC- Other surface waters (µg L^{-1})
Nonylphenol	84852-15-3	0.3	0.3	2.0	2.0
Octylphenol	140-66-9	0.1	0.1	n.a.	n.a.
Pentachlorophenol	87-86-5	0.4	0.4	1.0	1.0

AA- Annual Average; MAC- Maximum Allowable Concentration.

In Portugal, the recommended quality standards for different types of water, and also for WWTP discharges, regarding the presence of phenols, are presented in Table 3.10.

Table 3. 10- Portuguese water quality standards regarding phenolic compounds (Decreto-Lei nº 236, 1998).

	RMV	PMV	ELV
Surface waters for the production of water for human consumption (mg L^{-1})	-[a]/0.001[b]/0.100[c]	0.001[a]/0.005[b]/0.100[c]	n.a.
Water for human consumption (µg L^{-1})	-	0.5	n.a.
Bathing water quality (mg L^{-1})	0.005	0.05	n.a.
Wastewater discharges (mg L^{-1})	n.a.	n.a.	0.5

RMV- Recommended Maximum Value; PMV- Permissible Maximum Value; ELV- Emission Limit Value; a- Physical treatment and disinfection; b- Physical and chemical treatment and disinfection; c- Physical and chemical, advanced treatment and disinfection; n.a.- not applicable.

The United States Environmental Protection Agency, USEPA has set a water purification standard of less than 1 ppb of phenol in surface water and a maximum concentration of 0.5 µg L^{-1} for total phenols in drinking water. The limits for wastewater emissions are 0.5 mg L^{-1} for surface water and 1 mg L^{-1} for the sewerage system. Eleven phenolic compounds, among the different classes of these group of chemicals, have also been classified as priority pollutants by this entity, being listed in Table 3.11.

Table 3.11- Phenolic compounds classified as priority pollutants by USEPA (USEPA, 2015).

Compound	CAS number
Phenol	108-95-2
2-chlorophenol	95-57-8
2-metilphenol	95-48-7
2-nitrophenol	88-75-5
2,4-dimetilphenol	105-67-9
2,4-dichlorophenol	120-83-2
4-chloro-3-metilphenol	59-50-7
2,4,6-trichlorophenol	88-06-2
2,4-dinitrophenol	51-28-5
4-nitrophenol	93951-79-2
Pentachlorophenol	87-86-5

Phenols are present in wastewater of diverse industries, such as refineries, coking operations, coal processing, and petrochemicals manufacture, being also the main organic constituents of condensate streams in coal gasification and liquefaction processes. Other sources of wastewater containing phenols are pharmaceutical, plastics, polymeric resins, tanneries, food products preservatives, wood products, paints, pulp and paper, and herbicides and fungicides production industries. Reported levels of phenols in diverse industrial wastewater are presented in Table 3.12.

Table 3.12- Reported levels of phenol in industrial wastewater (Busca, Berardineli, *et al.*, 2008; Zangeneh, Zinatizadeh, *et al.*, 2015).

Industry	Phenol concentration (mg L^{-1})
Petroleum refineries	40 - 500
Petrochemical	200 - 1220
Textile	100 - 150
Leather	4.4 - 5.5
Coke ovens	600 - 3900
Coal conversion	1700 - 7000
Ferrous industry	5.6 – 9.1
Rubber industry	3 – 10
Pulp and paper industry	22
Wood preserving industry	50 – 953
Phenolic resin	1270 - 1345
Fiberglass manufacturing	40 – 2564

The occurrence of phenol and phenolic compounds in the year 2013, in European waters is documented by the European Pollutant Emission Transfer and Register of the European Environment Agency (EEA, 2013), and in Portuguese waters in the corresponding Registo de

Emissões e Transferências de Poluentes of Agência Portuguesa do Ambiente (APA, 2013), which is presented in Table 3.13.

Table 3.13- Portugal and Europe emission of phenolic compounds into water by sector in tonnes and correspondent number of facilities (in brackets) for the year of 2013.

Sector	Portugal	Europe
Energy sector	0.0531 (2)	459 (333)
Metal production and processing	-	32.5 (23)
Mining industry	-	0.675 (6)
Chemical industry	-	53.1 (49)
Residues and wastewater management	2.16 (3)	147 (158)
Paper production industry	1.09 (2)	20.4 (20)
Intensive livestock production and aquaculture	-	0.115 (2)
Animal and vegetable products of the food and beverages sector	-	0.0381 (1)
Other activities	-	0.294 (3)

According to the data available, relating to the year of 2013, the emission of phenolic compounds from the European Community countries was of 713 tonnes (corresponding to 395 manufacturing facilities). With respect to emissions in Portuguese waters, 3.31 tonnes were ascertained, accounting for only about 0.5 % of the European total. The largest contribution to these emissions is from the energy sector, from oil and gas refineries, gasification and liquefaction processes, power plants and other combustion plants and coke ovens. In Portugal, phenolic compounds emissions are attributed to the energy sector, wastewater treatment and processing of paper and wood.

3.5.5 Treatment of wastewater contaminated with phenolic compounds

Phenolic compounds are a particular class of organic molecules that raises great concern in the field of industrial wastewater treatment. Often chosen to be representative of a dangerous pollutant, a large amount of data is available on phenol, especially as regards its removal or destruction through wastewater treatment technologies.

3.5.5.1 Conventional treatments

In the last decade, the treatment of wastewater contaminated with phenol and phenolic species has attracted much attention due to the ecotoxicity and low biodegradability of these organic compounds. A number of technologies, both destructive and non-destructive, are available for the removal of phenolics from industrial wastewater. Conventional technologies for phenolic wastewater treatments include as secondary treatment physicochemical and/or biological methods (Busca, Berardinelli, *et al.*, 2008; Ranade and Bhandari, 2014).

Biodegradation processes are applied to phenolic effluents when low phenol concentrations are present, due to the ecotoxicity of these compounds towards most of the microorganisms. Phenol may be converted into less toxic compounds by microorganisms under aerobic or anaerobic conditions (Zangeneh, Zinatizadeh, *et al.*, 2015). Although the treatment of industrial

effluents by microorganisms units is difficult due to the high phenol concentration in batch systems, total phenol degradation of solutions with initial concentrations of 300 and 500 mg L^{-1} can be achieved (Busca, Berardinelli, *et al.*, 2008). Nevertheless, biological treatment is incapable of obtaining satisfactory phenol removal with current conventional biodegradation processes, which are severely affected by the large amounts of phenolic compounds usually found, for example, in olive oil mills effluents, coal chemistry, or solvents (De Luis, Lombraña, *et al.*, 2011). Furthermore, phenol accumulation on concentrated sludge creates also a disposal problem.

Biological treatment may be combined with a subsequent photocatalytic treatment, when lower concentrations of phenol are achieved. For example, an initial phenol concentration of 50 mg L^{-1} can be can be biologically degraded to 6.8 mg L^{-1}, and then subjected to a photocatalytic treatment (Suryaman, Hasegawa, *et al.*, 2006). This combination provides some advantages, namely a shorter mineralization time and the decomposition of non-biodegradable intermediate compounds, although requiring a higher energetic cost than the biological treatment alone.

Chemical methods include several processes, like coagulation or flocculation combined with flotation and filtration, precipitation–flocculation with Fe(II)/Ca(OH)$_2$, electroflotation, conventional oxidation methods by oxidizing agents, irradiation or electrochemical processes. These chemical techniques are often expensive, and although phenols can be successfully removed, the excessive use of chemicals may originate a secondary pollution problem.

Different physical methods are also widely used, such as membrane-filtration processes (NF, RO, electrodialysis, etc.) and adsorption techniques. The major disadvantage of the membrane processes is that they have a limited lifetime before membrane fouling occurs and the cost of periodic replacement must thus be included in any analysis of their economic viability. In the next section, phenol adsorption by activated carbons will be the subject of a more detailed discussion.

3.5.5.2 *Phenol adsorption on activated carbons*

Adsorption is a well-known equilibrium separation process and an effective method for water decontamination applications. The use of activated carbons in water treatment is probably one of the oldest chemical technologies, and a vast literature has accumulated on this subject (Faust and Aly, 1987; Derbyshire, Jagtoyen, *et al.*, 2001; Cheremisinoff, 2002; Bansal and Goyal, 2005; Le Cloirec and Faur, 2006; Marsh and Rodríguez-Reinoso, 2006; Rúa-Gómez, Guedez, *et al.*, 2012; Przepiórski, 2006; Ranade and Bhandari, 2014; Sorokhaibam and Ahmaruzzaman, 2014).

Adsorption on activated carbons has been found to be superior, when compared to other techniques, for water treatment in terms of initial cost, flexibility and simplicity of design, ease of operation and insensitivity to toxic pollutants. Activated carbons are the most common adsorbents used for the removal of pollutants from wastewater, due to their excellent adsorption abilities for organic pollutants (Derbyshire, Jagtoyen, *et al.*, 2001; Radovic, Moreno-Castilla, *et al.*, 2000; Moreno-Castilla, 2004; Nakagawa, Namba, *et al.*, 2004; Ahmaruzzaman, 2008; Mayani, Vishal, *et al.*, 20011).

Adsorption of phenolic compounds from aqueous solutions is one of the most investigated of all liquid-phase applications of carbon adsorbents. This technology is suggested for high

concentration and low volume of phenolic wastewater in wastewater (Ahmaruzzaman and Sharma, 2005; Dąbrowski, Podkościelny, *et al.*, 2005; Zangeneh, Zinatizadeh, *et al.*, 2015).

As for the liquid adsorption of aromatic compounds, phenol adsorption is a complex process governed by numerous factors that exert an important influence on this phenomenon (Moreno-Castilla, 2004; Dąbrowski, Podkościelny, *et al.*, 2005):

- The nature of the adsorbent, its pore structure, functional groups, ash content;

- The nature of the adsorbate, its pKa, functional groups present, polarity, aqueous solubility, molecular size and weight;

- The solution conditions, such as pH, ionic strength;

- The adsorbate concentration.

Other factors as the type of precursor of the carbon, and the oxygen availability in the solution, i.e., "oxic or anoxic conditions of adsorption" are also important.

The mechanism of phenol adsorption is still not well understood and has been the subject of several investigations. Especially, the more contentious issue is the role of surface-oxygen functionalities in the adsorption process. Several literature studies have contributed to a comprehensive knowledge of the adsorption mechanism and identification of the adsorption sites on the carbon surface (Salame and Bandosz, 2003; Terzyk, 2003; Velasco and Ania, 2011). According to these studies, phenol uptake is dependent on both the textural characteristics and surface chemistry of the activated carbons.

Both physi- and chemisorption sites for phenol were identified on activated carbons (Castillejos-López, Nevskaia, *et al.*, 2008; Velasco and Ania, 2011). It has been demonstrated that phenol physisorption depends strictly on the porosity, regardless the oxidation state of the carbon surface, as a result of dispersive interactions between the aromatic part of the phenol and the carbon's basal planes. On the other hand, phenol molecules interact with the edges of the basal planes in the carbons, showing various chemisorption sites desorbing at temperatures above 400°C (likely due to different orientations of phenol molecules). Consequently, carbon oxidation treatments, that promote the incorporation of surface functionalities on the edges of the basal planes suppresses the fraction of chemisorbed phenol (Velasco and Ania, 2011).

The adsorption of phenolic compounds is also well known to be pH dependent. Phenol adsorption from solution on carbons with acidic pH depends on the porosity, but more importantly, on the surface chemistry of the carbons, showing a strong dependence on the number of carboxylic groups. Phenol adsorption for pH < 10 is independent of the solution pH. On the other hand, for pH values higher than 10 an accentuated decrease in the phenol removal is observed. A favourable mechanism of adsorption observed when the carbon materials presented basic characteristics and the pH of the adsorptive-adsorbent system is lower than the point of zero charge.

Phenol adsorption occurs via two possible mechanisms being the first one attributed to the adsorption by means of dispersive interactions between the phenol aromatic ring and the activated carbon aromatic structure. In this case the electrostatic interactions do not have a significant role on the adsorption. The second mechanism based on the dispersive attractive

forces and the electrostatic repulsion interactions, occurs when phenol is predominantly in the phenolate form and the activated carbon surface is negatively charged.

In an attempt to clarify the role of the surface chemistry of activated carbons in the adsorption process, the nature of the surface functional groups of the adsorbents has been modified by thermal and chemical treatments. (Ania, Parra, *et al.*, 2002; Yin, Aroua, *et al.*, 2007; Stavropoulos, Samaras, *et al.*, 2008; Mourão, Laginhas, *et al.*, 2011). In the light of the reported results, the treatment with HNO_3 seems to affect the adsorption of phenol, decreasing the amount adsorbed and changing the isotherm shape. This last fact can be interpreted as a specific interaction of the water molecules with the oxygen surface groups, which act by inhibiting the adsorption of phenol at lower equilibrium concentrations.

Although commercial activated carbon is a preferred adsorbent for phenol removal, its widespread use is restricted due to the high cost. As such, alternative non-conventional adsorbents have been investigated over the last decade to overcome this drawback. Natural materials, industry and agriculture waste materials and bioadsorbents might be promising materials for environmental and purification purposes, as interesting alternatives to replace activated carbons for the adsorption of phenolic compounds (Sorokhaibam and Ahmaruzzaman, 2014).

Low-cost adsorbents have demonstrated high removal capabilities for certain phenolic compounds. Some promising results were found in the case of biomass, bentonite, starch, fly ash, petroleum coke, coal, charred sawdust, cyclodextrin, silica beads and sludge materials (Ioannidou and Zabaniotou, 2007; Ahmaruzzaman, 2008; Singh, Malik, *et al.*, 2008; Nabais, Gomes, *et al.*, 2009; Gupta, Nayak, *et al.*, 2014). However, despite the number of published laboratory data, non-conventional low-cost adsorbents have not yet been applied at an industrial scale.

The adsorption technique in the treatment of effluents, particularly using new adsorbent materials, provides a promising alternative for the treatment of industrial effluents in general and phenolic effluents, in particular. There are still some issues and drawbacks concerning the adsorption of phenolic compounds, such as the need of regeneration of the adsorbent materials and a post-treatment of the solid wastes, which are expensive operations. Activated carbon adsorption is a commercialized process but the spent carbon needs to be disposed safely.

3.5.5.3 Advanced oxidation processes for phenolic wastewater treatment

The limitations of conventional wastewater treatment methods previously discussed have prompted researchers to develop more efficient and environmentally friendly systems for wastewater treatment. Advanced oxidation technologies are emerging as the most effective option for the treatment of persistent organic pollutants, such as phenolic compounds. As it was discussed in the previous section, the use of advanced treatments for phenolic wastewater is critical to achieve high removal efficiencies of these compounds.

Different AOPs have already been applied as wastewater treatment technologies for phenol degradation in aqueous solution (ozonation, photolysis and UV/H_2O_2, Fenton and photo Fenton and photocatalysis). These techniques were used both in real and simulated effluents, achieving

in the majority of cases, high mineralization rates (Esplugas, Giménez, *et al.*, 2002; Sanz, Lombraña, *et al.*, 2013; Suzuki, Araki, *et al.*, 2015; Mohammadi, Kargari, *et al.*, 2015).

Typical effluents used in these studies are wastewater originated from olive mills, paper mills, petroleum refineries, textile and pharmaceutical industries, and also biologically pretreated wastewater. These technologies may be used alone, in combination with other physical, chemical and biological processes, or in hybrid processes, in order to improve the removal efficiency of target molecules. Table 3.14 gathers information on published data reporting phenol degradation by AOPs throughout the last decade.

According to the literature, the most effective AOPs for phenolic wastewater remediation are semiconductor heterogeneous photocatalysis, ozonation and Fenton reactions. Among these, heterogeneous photocatalysis is pointed out as one of the most promising approaches for the treatment of wastewater contaminated with phenolic compounds. In fact, phenol and phenol derivatives have been some of the most investigated compounds on this topic (Matos, Laine, *et al.*, 2001; Wang, Serp, *et al.*, 2005; Kubo, Fukuda, *et al.*, 2007; Tryba, Morawski, *et al.*, 2003; Tryba, Morawski, *et al.*, 2006a; Tryba, Morawski, *et al.*, 2006b; Velasco, Parra, *et al.*, 2010).

The increasing number of publications on this research topic in peer-reviewed journals is an indicator of the important potential of the photocatalytic degradation of phenol and substituted phenols in wastewater (Sobczyński, Duczmal, et al., 2004; Busca, Berardinelli, *et al.*, 2008; Liotta, Gruttadauria, *et al.*, 2009; Ahmed, Rasul, *et al.*, 2010; Chong, Jin, *et al.*, 2010; Zangeneh, Zinatizadeh, *et al.*, 2015).

The photocatalytic degradation process presents several advantages, such as a high mineralization efficiency, and mild temperature and pressure conditions. The use of solar light could also be an excellent alternative in heterogeneous photocatalysis since this natural and clean energy source could help to overcome the economical drawbacks associated with photochemical methods, reducing the costs of the treatment. The obtained results using solar photocatalysis process, mostly from preliminary tests at a pilot scale, suggest that this is a feasible technique for phenol degradation.

Several authors have also reported the beneficial effect of hybrid processes, through the combination of photocatalysis with other processes, conventional or advanced, for phenol degradation, highlighting the better results obtained in comparison when the individual treatment methods are applied (Malato, Fernández-Ibañez, *et al.*, 2009; Adishkumar, Kanmani, *et al.*, 2010). Recent findings suggested that the following operating parameters can play an important role on the photocatalytic degradation of phenolic compounds in wastewater (Ahmed, Rasul, *et al.*, 2010; Saratale, Noh, *et al.*, 2014; Zangeneh, Zinatizadeh, *et al.*, 2015):

- Photocatalyst type and composition
- Light intensity
- Pollutant type and initial concentration
- Catalyst loading
- Initial pH of the reaction medium
- Catalyst application mode
- Oxidizing agents/electron acceptors
- Presence of ionic components in solution

Table 3.14- Examples of the application of AOPs in the treatment of phenolic effluents.

Effluent characteristics	Operation conditions and results	Other considerations	Reference
Fenton Process			
Industrial effluents (chemistry, steel), Tamla River (Bengala, India). COD=2700-4000 mg L^{-1}, BOD= 900-1100 mg L^{-1}, phenols= 4-12 mg L^{-1}.	60 % COD reduction with 6 mg L^{-1} of Fe^{2+} and 44.40 g L^{-1} of H$_2$O$_2$. 95 % of COD reduction with 220 g L^{-1} of H$_2$O$_2$ and equal Fe^{2+} concentration.	Coupling to a biological system that reduces the COD by 97 %, compared with only 60 % reduction Fenton or just 17 % as biological oxidation, showing a synergistic effect.	Mandal, Maity, et al., 2010
Photo-Fenton Process			
Simulated and industrial wastewater. Phenolic effluent (1215 mg L^{-1}) from resins production, COD=2904 mg L^{-1}.	Solar facility of 400 W m^{-2}. Mineralization efficiency with Fenton, solar and UV-Fenton processes: 41%, 96 % and 97 %, respectively; the largest part of the degradation occurs in the first 10 minutes.	Solar photo-Fenton system yield is superior to Fenton; to achieve 82 % oxidation, twice the amount of iron is needed [Fe^{2+}]/[H$_2$O$_2$]= 0.026.	Kavitha, Palanivelu, et al., 2004
Solar photo-Fenton process			
Olive mill wastewater collected from one Portuguese and two Spanish mills. COD between 20 and 89 g L^{-1}.	Two solar photocatalytic reactors were used; one of conventional Compound Parabolic Collector type and an open non-concentrating Falling Film Reactor. Removal of up to 85 % COD and up to 100% of phenol index with different initial concentrations and sources.	Application of a flocculation pre-treatment to remove suspended solids led to a considerable increase of degradation rates and decrease of hydrogen peroxide consumption.	Gernjak, Maldonado, et al., 2004
UV/H$_2$O$_2$ process			
Simulated wastewater with phenol derivatives: 2,4-dichlorophenol (2,4-DCP) and the nonionic industrial surfactant nonylphenol decaethoxylate (NP-10).	H$_2$O$_2$/UVC oxidation and UVC photolysis with a low pressure 40 W lamp, radiation flux of 1.6 10^{-5} Einstein L^{-1} s^{-1}. After 90 min of H$_2$O$_2$/UV treatment, 95 % and 78 % TOC removals for 2,4-DCP and NP-10, respectively, could be achieved.	A very fast reduction in acute toxicity during H$_2$O$_2$/UVC oxidation of 2,4-DCP as compared to UVC photolysis; prolonged treatment resulted in the re-appearance of acute toxicity. H$_2$O$_2$/UVC process was less ecotoxic than UVC photolysis for the removal of aqueous NP-10.	Karci, Arslan-Alaton, et al., 2013

3.5.5.3 Advanced oxidation processes for phenolic wastewater treatment

Table 3.14- (continued).

Effluent characteristics	Operation conditions and results	Other considerations	Reference
Ozonation process			
Cork industry effluent, high content of phenolic, gallic, protocatechuic and ellagic acids, among others. pH=4.7, COD = 4.40 g L⁻¹, BOD = 1.75 g L⁻¹ content in tannins = 0.897 g L⁻¹, total suspended solids =0.28 g L⁻¹.	Experiments performed with and without UV radiation and H_2O_2. $V_{reactor}$=700 cm³, 0.05 mg of ozone mg TOC⁻¹, flow rate of 40 L h⁻¹, reaction time: 6 hours. All parameters are almost completely reduced (COD, color, absorbance at 254 nm and tannins).	Two operation schemes are proposed, integration of ozone with ultrafiltration and filtration followed by advanced oxidation (O_3/UV and O_3 /H_2O_2). The second option is the most effective.	Benítez, Acero, et al., 2008
Simulated phenolic wastewater with six phenolic acids typically found in olive mill wastewater with a concentration of 100 mg L⁻¹ of each.	Ozonation, single and catalytic over the several commercial and laboratory catalysts was performed. Best result obtained: 80 % TOC removal after 120 min of oxidation for catalyst Mn-Ce-O (70/30).	Single and catalytic ozonation over Ag-Ce-O led to a less biodegradable effluent, whereas the rest of the catalytic systems truly enhanced the biodegradability of the simulated wastewater.	Martins and Quinta-Ferreira, 2011
Heterogeneous photocatalysis			
Phenol solutions with an initial concentration of 50 mg L⁻¹.	Three commercial catalysts Degussa P25 (20 nm), TiO2-A1 (160 nm) and TiO2-A2 (330 nm) available in anatase form, and ZnO were tested. After 5 h of reaction, the order of the efficiency was: ZnO>P25>TiO₂-A1>TiO₂-A2. 92 % of phenol degradation was achieved in 6 h.	The observed variation in the efficiency is related to the structure, diameter of particles and electrical properties of the photocatalyst.	Salah, Bouhelassa, et al., 2004
Petroleum refinery wastewater, Rio de Janeiro, Brazil.	TiO₂ (Aldrich), ZnO (Aldrich), and TiO₂ (P25, Degussa) were tested. Optimized conditions: 3.0 g L⁻¹TiO₂ and pH 6.3. 93 % phenol removal, 63 % of dissolved organic carbon, and more than 50% of oil and grease.	P25 was the most active. The use of H_2O_2 showed no beneficial effect. Photocatalytic activity decreased as pH value tends to neutrality.	Santos, Azevedo, et al., 2006
Textile industry effluent, including biocide elements (chlorophenols), etc. Experiments with 200 and 1500 mg L⁻¹ of COD.	125 W black light bulb lamp, incident photon flux of 2.8 x 10⁻⁵ Einstein L⁻¹ s⁻¹, TiO₂/UVA and TiO₂/H_2O_2/UVA. [TiO₂]=1 g L⁻¹. 68 % COD elimination in 60 minutes (pH 3) with addition of 1 mM of H_2O_2.	COD removal indicates a strong dependence on reaction solution pH. Effective acute toxicity removal was also obtained after the treatment.	Arslan-Alaton, 2007

Table 3.14- (continued).

Effluent characteristics	Operation conditions and results	Other considerations	Reference
Phenol solutions with an initial concentration of 0.21 and 1 mM for kinetic study and intermediate product identification, respectively.	Experiments performed with N,C-doped TiO_2 under visible light and P-25 under UV irradiation. Similar efficiency of phenol degradation for doped TiO_2 excited by visible light to P-25 irradiated by UV light (69 and 76 % in 60 min, respectively).	Photoactivity under visible light of N,C-TiO_2 was four times higher than P-25 TiO_2. Different degradation pathways were observed. A lack of hydroxyl by-products after irradiation of phenol in the presence of N,C-TiO_2 and visible light was observed.	Górska, Zaleska, et al., 2009
Solar photocatalysis			
Simulated phenolic effluent.	Experiments with TiO_2 suspensions; phenol removal efficiency was 48, 46, 30 and 15 % for chloride concentration of 50, 100, 150 and 200 mg L^{-1}, respectively, and 79 % in the absence of chloride. Phenol removal efficiency was 30, 85 and 77 % for pre-aeration, with and without aeration.	The phenol removal efficiency reached its maximum of 95 % at maximum UV light intensity of 32 W/m² and the minimum of 59 % at minimum UV light intensity of 20 W/m². The results suggest that photocatalytic process with solar light irradiation is a feasible technique for phenol removal.	Adishkumar, Kanmani, et al., 2014.
Pharmaceutical industry wastewater (Chennai, India), phenol =360±40 mg L^{-1} COD=1080 mg L^{-1}, BOD=162 mg L^{-1} BOD/COD ratio = 0.15.	Phenol removal efficiency was 45% for [phenol]= 500 mg L^{-1}. In solar/TiO_2/H_2O_2 system, the addition of H_2O_2 from 0.15 to 0.3 g L^{-1} increases the degradation from 75 % to 99 %. When the H_2O_2 concentration is higher than 0.3 g L^{-1} the degradation rate decreases.	The solar/TiO_2/H_2O_2 process is two to three times faster than the solar/TiO_2 process. For 400 mg L^{-1} of phenol concentration, the BOD/COD ratio is 0, while solar photocatalytic treatment of 4 hours enhanced the biodegradability values.	Adishkumar and Kanmani, 2010
Photocatalysis and sonolysis			
Model solution containing 13 compounds typically found in olive mill wastewater, at a concentration of 50 mg L^{-1} each.	Experiments performed with 0.75 g L^{-1} Degussa TiO_2 suspensions, ultrasound frequency and intensity of 80 kHz and 120 W, respectively, ultraviolet power of 9, 250 and 400W, with or without the addition of H_2O_2. In 2 h, 97.5, 98.9 and 97.1 % reduction in COD, phenol and TOC, respectively.	The combined process was considerably more effective than the respective individual treatments, i.e. sonolysis and photocatalysis. Process efficiency was further enhanced in the presence of H_2O_2 acting as hydroxyl radical source.	Silva, Nouli, et al., 2007

Table 3.14- (continued).

Effluent characteristics	Operation conditions and results	Other considerations	Reference
Phenol solution with an initial concentration of 100 mg L^{-1}.	ZnFe$_2$O$_4$/TiO$_2$–GAC used as photocatalyst under visible light irradiation and combined with sonolysis. Phenol degradation rates were affected by the initial pH value, salt addition, gas supplying and the recycling of the recovered photocatalyst.	Phenol removal in the continuous system is better than that in adsorption process and photocatalytic reaction.	Wang and Yu, 2013
Photocatalysis and activated carbons			
Biologically treated and diluted olive mill wastewater with COD at the range of 80-200000 mg L^{-1} and a concentration of phenolic compounds of about 9 g L^{-1}.	Experiments performed with 3 g L^{-1} of TiO$_2$ and 0.45 g L^{-1} of PAC. After 24 h of irradiation under 365 nm UV light (7.6 W m^{-2}) in the presence of TiO$_2$-PAC, 87 % of the initial total polyphenols were removed, compared to only 58 % COD removal.	The results emphasize the potential of combining TiO$_2$ photocatalysis and adsorption as a physicochemical process employed for pre- or post-biological wastewater treatment.	Baransi, Dubowski, et al., 2012
Phenol solution (initial concentration: 100 mg L^{-1}).	TiO$_2$/carbon composite, prepared by infiltration of a suspension of TiO$_2$ on a commercial activated carbon (physical activation of bituminous coal). The removal efficiency was 98 % after 6 h of exposure to UV light.	The carbon support affects the phenol degradation mechanism. Photocatalytic decomposition rate over the carbon support outperformed that attained in the composite, suggesting an important self-photoactivity of the carbon support.	Velasco, Parra, et al, 2010
Combination of biological treatments and advanced oxidation techniques			
Water contaminated with phenol, formaldehyde and phenol/ formaldehyde mixtures.	TiO$_2$-photocatalysis, biological aerated filter and wetlands were efficient only for low concentrations. For concentrations between 100 and 500 mg L^{-1} the optimum system was TiO$_2$ photocatalysis + biological aerated filter and a wetland for final detoxification. Fenton reaction could degrade concentrations > 1000 mg L^{-1}.	Best combination of techniques: Fenton +biological aerated filter, able to detoxify concentrations of 1000 mg L^{-1} of phenol-formaldehyde. Fenton and photo-Fenton were more proficient for high concentrations, but mineralization and detoxification were low. Toxicity increased at higher concentrations due to the generated intermediates.	Méndez, Melián, et al., 2015

Table 3.14- (continued).

Effluent characteristics	Operation conditions and results	Other considerations	Reference
Combined heterogeneous photocatalysis oxidation and moving bed biofilm reactor process			
Biologically pretreated coal gasification wastewater: CDO=150-200 mg L^{-1}, BOD/COD ratio=0.05-0.08, total phenol=80-120 mg L^{-1}, TOC=90-140 mg L^{-1}, total nitrogen= 50-70 mg L^{-1}. The pH ranged between 6.5 and 8.0.	UV irradiation source: UV lamp with a nominal power of 8 W, emitting radiation at 325 nm. TiO$_2$/sludge based activated carbon was used as catalyst. All parameters were significantly reduced in the integrated system that was more effective than the individual processes.	The system integrating TiO$_2$ photocatalysis oxidation and the moving bed biofilm reactor process was successfully applied in advanced treatment of real biologically pre-treated wastewater.	Xu, Han, et al., 2015

Abbreviations: COD-Chemical Oxygen Demand; BOD- Biological Oxygen Demand, PAC- Powdered Activated Carbon; GAC- Granular Activated Carbon; TOC- Total Organic Carbon

The optimization of these parameters is therefore, crucial from the perspective of an efficient design and the application of the photocatalytic oxidation process to ensure a sustainable operation. The application of this technique for real wastewater treatment calls for further investigation through the optimization of these parameters. This would make a significant impact on the potential commercial application of this technique to industrial systems.

However, the major disadvantages presented by this technology are still low quantum efficiency, the design of the photoreactor, the recovery and reuse of titanium dioxide, the generation of toxic intermediates, and catalyst deactivation.

3.5.5.4 The mechanism of phenol photocatalytic degradation

Phenol photocatalytic oxidation mechanism has been the subject of plenty of studies, and it is now known with enough reliability (Santos, Yustos, *et al.*, 2002; Guo and Ma, 2006; Grabowska, Reszczyńska, *et al.*, 2012). According to the literature, in the presence of titanium dioxide and irradiation, phenol can be degraded by $^\bullet$OH radicals or directly via photo-generated carriers, depending on the used photocatalyst and irradiation source. However, some differences between identified by-products have been observed, and probably resulted not only from various reaction conditions but also from different analytical techniques applied for enrichment step and final detection of samples.

For pure TiO_2 (in the form of anatase or a mixture of anatase and rutile) excited by UV irradiation, $^\bullet$OH radicals are a primary oxidation species responsible for phenol degradation or mineralization. Phenol is thereby photocatalytically degraded through the attack of free hydroxyl radicals to the aromatic ring, resulting in various oxidation intermediates. As depicted in Figure 3.17, among the detected intermediates there is a predominantly aromatic nature of the compounds: catechol, hydroquinone, *p*-benzoquinone, and short chain organic acids (e.g., maleic acid, acetic acid, malonic acid and oxalic acid), the latter being more resistant to full oxidation to CO_2 and H_2O (mineralization).
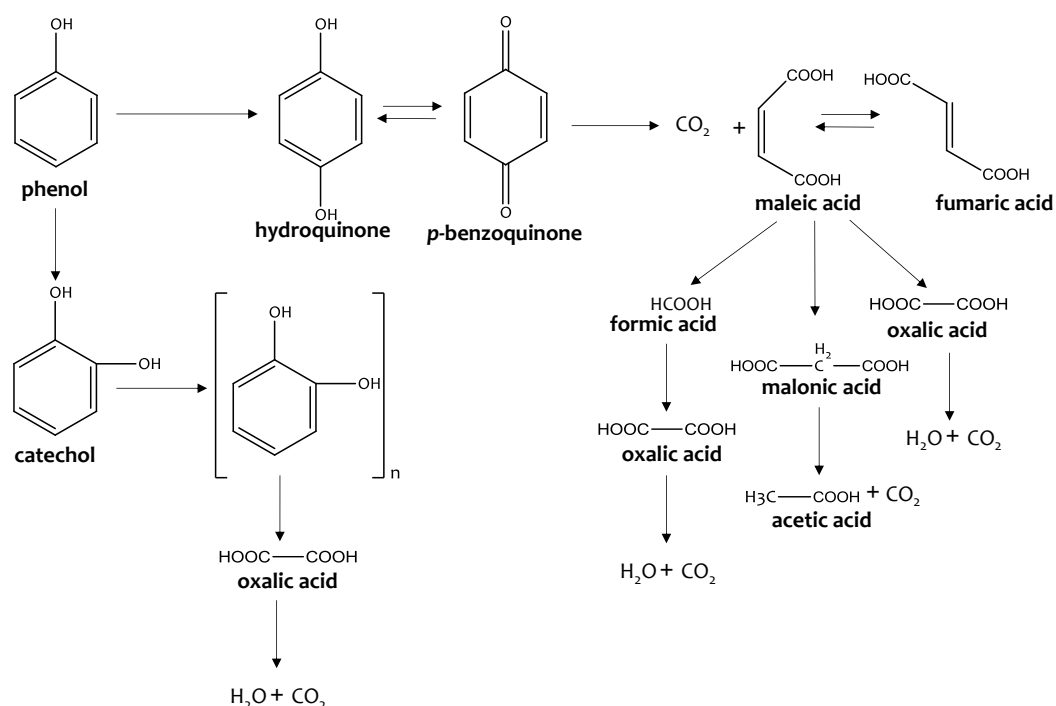
Figure 3.17- Phenol oxidation mechanism (Santos, Yustos, *et al.*, 2002).

In the case of metal doped-TiO_2 excited by visible light, both $^\bullet OH$ radicals and direct oxidation could be employed. However, $^\bullet OH$ radicals are not involved in phenol degradation during visible light excitation of non-metal-doped TiO_2. The analysis of intermediates also revealed the lack of hydroxyl by-products after irradiation of phenol in the presence of non-metal doped-TiO_2 and visible light, while they are found in P25/UV system.

The most probable degradation pathway using non-metal doped-TiO_2 irradiated by visible light is via the formation of electrons via carbonaceous species sensitizing and electron transfer to oxygen or direct charge transfer to the adsorbed compounds.

Hydroquinone and catechol, formed through hydroxyl radical's attack of the phenol ring at the first step of reaction, were observed in most investigated systems. Although, for some systems, formation of benzoquinone, hydroquinone, 1,2,3- benzenetriol and even salicylic acid were confirmed. Further irradiation leads to phenol ring cleavage and formation of low molar mass compounds such as 2-hydroxy-propaldehyde, glycerol, 3-hydroxypropyl acid, hydroxy-acetic acid, maleic acid and oxalic acid.

Phenol oxidation pathway via the initial formation of catechol originates less intermediates, so total mineralization occurs more rapidly. Furthermore, degradation through the formation of hydroquinone/benzoquinone pair is a much more complex process which results in the appearance of several of intermediates, which makes phenol mineralization much more difficult. It would therefore be desirable to enhance phenol degradation through the formation of catechol through the development of selective catalysts.

3.6 Conclusions

Phenolic compounds are currently considered, among other chemicals, a major threat to watercourses due of its long persistence, and continuous discharge into the environment, driven by its high consumption at industrial level. It is widely known that conventional wastewater treatment systems have serious shortcomings that can be addressed by the implementation of advanced treatments, such as activated carbon adsorption and advanced oxidation processes.

The well-established adsorption technologies for the removal of phenolic compounds from aqueous medium allows to achieve high removal efficiencies, that may be coupled to conventional water treatment or other advanced treatments. Activated carbons can be prepared from virtually any carbon rich material, allowing the use of several industrial and agricultural residues, thus also enabling the valorization of these wastes. The main disadvantage of the adsorption technologies relates to the fact that these are non-destructive processes, involving the regeneration of the spent adsorbent.

Different AOPs can be applied simultaneously to promote the oxidation rate of organic compounds or sequentially to increase selectivity; of a separation treatment can be applied before treatment by AOPs, so as to transfer the pollutant from the liquid phase to another phase, so that they can be handled more easily or AOPs can be applied as a pre-treatment to increase the biodegradability and lower toxicity, followed by a biological after-treatment.

In the light of the basic and applied researches reported in the literature, photocatalytic degradation of phenolic compounds appears to be a promising route for the treatment of wastewater contaminated with phenolic compounds. In most cases, high levels of phenolic

compounds degradation and almost total removal were obtained. Nevertheless, the extent of mineralization (complete conversion to CO_2 and H_2O) is still a major drawback.

Despite the great advances that have been made in the most recent decades, the low quantum efficiency due to inefficient visible light-harvesting catalysts, the design of the photoreactor, the recovery and reuse of titanium dioxide, the generation of toxic intermediates, and the concern over catalyst deactivation have been reported to be the major drawbacks toward the development of this technology. In this context, the interest in carbon materials for photocatalysis has been increasing in recent years, given their reported potential on the enhancement of semiconductor photoactivity enhancement, due to factors associated with to visible light absorption, the porosity of the carbon support, strong interfacial electronic effects, and to the intrinsic photochemical activity of certain carbons.

The coupling of a semiconductor oxide and carbon additive appears as an interesting strategy for the semiconductor photocatalytic activity enhancement, leading to better efficiencies in environmental remediation processes. Novel TiO_2/carbon combinations offer opportunities for the design of new photocatalytic systems, even though the understanding of the underlying mechanisms of the photocatalytic enhancement is still a great challenge.

CHAPTER 4

VALORIZATION OF SISAL WASTE

Environmental and economic concerns are stimulating research towards the development of new materials for construction, furniture, packaging and automotive industries. New materials derived from natural renewable resources are particularly attractive, since their use can prevent further stress on the environment. Examples of such raw material sources are native crops, plants and fibres that are abundantly available in tropical regions. If new uses of fast growing native plants can be developed for high value, non-timber based materials, they could reduce the use of traditional materials such as wood, minerals and plastics in some major applications.

4.1 The potential of natural fibres

Natural fibres have been used in human clothing and in the construction of housing since early 4000 BC in Europe, 3000 BC in Egypt and 6000 BC in China (FAO, 2012). Natural fibers of some kind are produced in almost all countries: in tropical countries, such as Brazil (several crop fibres), Colombia (fique), Ecuador and Philippines (abaca), India (coir and jute), Pakistan and Bangladesh (jute and coir), China (ramie), there exist a large variety of natural fibres with different mechanical, physical and chemical characteristics. Natural fibres are generally of lignocellulosic nature, containing mainly, lignin and cellulose, and consisting of helically-wound cellulose microfibrils in a matrix of lignin and hemicellulose (Mohanty, Misra, *et al.*, 2005). The sources of these substances include agricultural and agro-industrial residues, agricultural fibres, aquatic, grassy plants and other vegetal substances. The chemical composition of the main commercial fibres is given in Table 4.1. The purest one is cotton with ca. 90 % of cellulose, while the rest range between 70-75 % of cellulose, depending on the processing method used.

Table 4. 1- Chemical composition (% relative abundance) of the most important commercial fibres (Cherian, Leão, *et al.*, 2011).

Fibres	Cellulose	Hemicellulose	Pectins	Lignin	Extractive
Flax	71.2	18.6	2.0	2.2	6.0
Hemp	74.9	17.9	0.9	3.7	3.1
Jute	71.5	13.4	0.2	13.1	1.8
Kenaf	63.0	18.0	2.1	17.0	2.0
Ramie	76.2	14.6	0.6	0.7	6.4
Abaca	70.1	21.8	0.9	5.7	1.8
Sisal	73.1	13.3	2.6	11.0	1.6
Cotton	92.9	2.6	2.6	-	1.9
Curaua	70.7	10.7	4.5	11.1	3.0

Another important factor that influences the final properties of natural fibres is the presence of extractives (pectins, hemicellulose and lignin), which are of variable quality and amount (Cherian, Leão, *et al.*, 2011). The dimensions of natural fibres are also an important aspect. The physical properties vary sufficiently in function of the specific variety, place of growth, time of harvest, localization in the plant, methods of processing, and so forth.

4.2 Sisal fibre

Sisal fibre is one of the most widely used natural fibres and is very easily cultivated. It is extracted from the leaves of the sisal plant (*Agave sisalana*). Though native to tropical and sub-tropical North and South America, sisal plant is now widely grown in tropical countries of Africa, the West Indies and the Far East (Li, Mai, *et al.*, 2000). A sisal plant produces about 200-250 leaves and each leaf contains 1000-1200 fibre bundles which are composed of 4 % fibre, 0.75 % cuticle, 8 % dry matter and 87.25 % water. Normally, a leaf weighing about 600 g will yield about 3 % by weight of fibre.

Despite sisal is one of the most widely used natural fibres worldwide, a large quantity of this economic and renewable resource is still under-utilised. Until recently, sisal fibre was mainly used as ropes for the marine industry and agriculture. Other applications of sisal include twines, cords, upholstery, padding and mat making, fishing nets, fancy articles such as purses, wall hangings, table mats, etc. However, over the past decades, a pronounced downtrend in sisal production reflected the drop in demand for the fibre in traditional uses.

It was only recently that significant research has started to be conducted on the technological and economic implications of using sisal in various innovative applications, in particular as a component in industrial products (Li, Mai, *et al.*, 2000). Among the new potential applications which attracted early interest was the possible use of sisal for the production of paper and pulp. With regard to building materials, the use of renewable resources has also been recognized as contributing to sustainability by slowing the rate of deforestation for wood construction products. Thus, fibres were seen as offering potential in such uses as fibreboard, insulation, reinforcement or filler in lightweight concrete, bricks and building blocks and as a substitute for asbestos cement. The replacement of asbestos in cement by sisal is a particular aspect of the market of construction materials that has gained ground as the prohibition of asbestos has gained momentum, particularly in some large populous countries, and is expected to continue to do so.

Lignocellulosic resources have low densities, are low in cost, renewable, non-abrasive, have excellent specific mechanical properties, and are potentially outstanding reinforcing fillers in thermoplastic composites. These new advanced composite materials, that take advantage of the properties of agro-fibres (lignocellulosics) and other types of resources, are finding innovative applications and fresh markets never before envisioned by the agro-industrial sector anywhere (Leão, Sartor, *et al.*, 2006). The main advantages of composite materials based on natural fibres are the following (FAO, 2012):

•   Replacement of man-made fibres (glass and asbestos) with lower costs;

•   Reduction of the demand for petroleum-based products (carbon-based).

•   Substitution of solid wood by plastics reinforced with wood or other natural polymers.

•   Enhancement of fibre quality in end-use applications.

- Renewability, recyclability.

- Resistance, good mechanical properties.

- Release into the environment of only harmless residues when incinerated for energy recovery or final disposal.

- Absorption of renewable carbon (green carbon) contributes to a reduction of climate change.

- Low-energy consumption when processed.

- Possible applications with higher levels of reinforcement with new technologies such as extrusion and injection moulding.

- Enhancement of fibre quality in end-use applications through the use of better hybrids or varieties.

To a certain degree, the transformation of research results into a commercial reality has already taken place, for example in Brazil, where Ford is using sisal in various automobile parts. Among these potential new uses of sisal, the utilization of sisal waste to generate biogas, in Tanzania, has been demonstrated to be technically feasible. Other applications of natural fibres are in geotextiles, biocomposites, aerospace applications and nanocomposite applications (electronic Industry, pharmaceutical and biomedical applications) (FAO, 2012). There is, however, a need to provide greater information regarding the multitude of innovative applications of natural fibres that exist and which go beyond their traditional uses.

4.3 Sisal waste valorization

4.3.1 Sisal waste as precursor of activated carbons

Activated carbons are the prefered adsorbents for the removal of micropollutants from the aqueous phase. The major drawbacks associated with the use of activated carbons, already discussed in section 3.3, are a poor economic feasibility, and a short lifetime, often due to low and expensive regeneration capacities, that can be overcome by the use of low-cost adsorbents.

In this context, the production of low-cost activated carbons is an important research subject due to its vital importance for the water treatment process. Any cheap material, with a relatively high carbon content can be used as a raw material for the production of activated carbons. It is clear that conventional (from agriculture and wood industry) and non-conventional (from municipal and industrial activities) wastes can be used to prepare activated carbons (Dias, Alvim-Ferraz, *et al.*, 2007). Moreover, high surface areas can be obtained using either physical or chemical activation. Activated carbons prepared from both conventional and non-conventional wastes might effectively compete with the commercial ones.

Agricultural by-products and wastes are highly recommendable sources because they are readily available, low-cost, regularly produced with renewable feed stocks. They can be used for the production of activated carbons with a high adsorption capacity, considerable mechanical strength, and low ash content (Ioannidou and Zabaniotou, 2007). There have been many attempts to obtain adsorbents from agricultural wastes using the most diverse waste materials. In this sense, the use of largely available residues, as is the case of sisal waste, as precursors is an interesting strategy since it enables to deal with the problem of waste disposal

and recycling (Ioannidou and Zabaniotou, 2007; Michailof, Stavropoulos, *et al.*, 2008; Cabrita, Ruiz, *et al.*, 2010; Mestre, Bexiga, *et al.*, 2011; Delgado and Mendez, 2014).

Sisal residues, discarded from the rope manufacture industry, were already used in our research group as precursors for the preparation of activated carbons by chemical activation. Sisal-based activated carbons prepared with K_2CO_3 presented high apparent surface areas (A_{BET} up to 1038 m^2 g^{-1}) and pore volumes (ca. 0.49 cm^3 g^{-1}) (Mestre, Bexiga, *et al.*, 2011). Furthermore, the obtained materials proved to have suitable properties for the removal of pharmaceutical compounds from liquid phase.

4.3.2 Pyrolityc degradation of sisal waste

The thermal treatment of wastes, by gasification or pyrolysis, is considered an excellent approach for their valorization as energy resources and raw materials for chemical processes. It is also a viable alternative to the traditional strategies for solid waste transformation and disposal that include landfilling or incineration, minimizing its discharge into the environment.

Conventional pyrolysis consists on the slow, irreversible thermal decomposition of the organic components of biomass, most of which are lignocellulosic polymers. Gasification and pyrolysis enable the production of gaseous and/or liquid fuels from the waste materials thus recovering (at least partially) the energetic and organic value of these wastes. Wastes are subjected to high temperatures in the absence of air or in an oxygen-deficient atmosphere, producing a hydrocarbon mixture (vapour and liquid fractions) that can be used as fuel or as feedstock in chemistry industries, and a carbon-rich solid by-product (char) that can be directly used or, alternatively, upgraded to activated carbon (Buekens and Huang, 1998; Yaman, 2004). The carbonaceous residue is mostly constituted of carbon, but also contains the mineral matter initially present in the wastes and a significant amount of condensed by-products with high molecular weight, formed during the pyrolysis process. Generally, the pyrolytic char does not possess properties of sufficiently high quality to be further used as raw material, thus, unless an upgrade step is performed, its final destination is landfilling (Helleur, Popovic, *et al.*, 2001).

Biomass pyrolysis has a long history and a considerable future potential, driven by the increased interest in renewable energy, following the growing environmental commitments and the recently increased market prices for fossil fuels. The pyrolysis method has been used for commercial production of a wide range of fuels, solvents, chemicals and other products from biomass feedstocks. In comparison with coal, biomass pyrolysis starts earlier and the volatile matter content is higher. The fractional heat contribution by volatile matter is of the order of 70 %, compared with 36 % for coal; however, biomass char has more oxygen and its fractional heat contribution is of the order of 30 %, compared with 7 % for coal (Vamvuka, 2011).

The terms pyrolysis and carbonization are often used without any kind of distinction, and although they are in fact almost identical processes, there are some differences between the two. The aim of the pyrolysis process is the collection of gases and volatile compounds released from the solid, in which all of the process conditions (temperature, residence time, etc.) are focused on the production of gaseous compounds, regardless of the final carbonized residue. On the other hand, the heat treatment of the carbonization process focuses on the properties of the obtained carbonized (porous texture, hardness, density, etc.), disregarding the volatiles released.

The investigation of the pyrolytic behaviour of sisal fibres discarded from the rope industry, by analyzing the composition of the different fractions obtained allows to explore its potential applications in different fields.

In this sense, the objective of the work developed and reported in **Article I** (Andrade, M.; Parra, J. B.; Haro, M.; Mestre, A. S.; Carvalho, A. P. and Ania, C. O., 2012. Characterization of the different fractions obtained from the pyrolysis of rope industry waste. *Journal of Analytical and Applied Pyrolysis* 95, 31-37), was to study the possible valorization of sisal wastes discarded from the rope industry through pyrolysis. The different fractions (gas, tars, solid) originated by the pyrolysis process of this lignocellulosic residue were thoroughly characterized; this allowed to investigate potential applications of these materials.

ARTICLE I

Characterization of the different fractions obtained from the pyrolysis of rope industry waste

Marta Andrade[a], José B. Parra[b], Marta Haro[b], Ana S. Mestre[a], Ana P. Carvalho[a,*], Conchi O. Ania[b,**]

[a] Departamento de Química e Bioquímica and CQB, Faculdade de Ciências da Universidade de Lisboa, Ed. C8, Campo Grande, 1740-16 Lisboa, Portugal
[b] Instituto Nacional del Carbón (INCAR, CSIC), 33011 Oviedo, Spain

ARTICLE INFO

ABSTRACT

A study of the possibilities of pyrolysis for recovering wastes of the rope's industry has been carried out. The pyrolysis of this lignocellulosic residue started at 250 °C, with the main region of decomposition occurring at temperatures between 300 and 350 °C. As the reaction temperature increased, the yields of pyrolyzed gas and oil increased, yielding 22 wt.% of a carbonaceous residue, 50 wt.% tars and a gas fraction at 800 °C. The chemical composition and textural characterization of the chars obtained at various temperatures confirmed that even if most decomposition occurs at 400 °C, there are some pyrolytic reactions still going on above 550 °C. The different pyrolysis fractions were analyzed by GC–MS; the produced oil was rich in hydrocarbons and alcohols. On the other hand, the gas fraction is mainly composed of CO_2, CO and CH_4. Finally, the carbonaceous solid residue (char) displayed porous features, with a more developed porous structure as the pyrolysis temperature increased.

© 2012 Elsevier B.V. All rights reserved.

1. Introduction

Sisal fiber is one of the most widely used natural fibers. It is obtained from the leaves of sisal (*Agave sisalana*), an autoctone plant from Mexico, which is now also widely grown in tropical countries in Africa, the West Indies and the Far East [1].

A. sisalana belongs to the group of hard fibers which also includes flax, abaca, jute, coir and some others. Its annual production accounts for 2% of the overall worldwide production of natural fibers, which represents *ca.* 65% of the world's fibers. In 2008, the production of sisal fiber was around 250 thousands of tons, with Brazil, Tanzania and Kenya being currently the world's largest producers [2].

As for other lignocellulosic fibers, the major chemical constituents of sisal are cellulose and lignin, although large variations in the chemical composition can be found in the literature. As an example, Barreto et al. [3] reported the composition of natural sisal fibers from Brazil as 65.8% of cellulose, 12% of hemicelluloses, 9.9% of lignin, 0.8% of pectin and 0.3% of wax and water soluble compounds.

Sisal is one of the most widely used natural fibers, due to its outstanding characteristics related to its low cost and density, high specific resistance, good mechanical properties, and non-toxicity

[1]. Recently, increasing interest has arisen towards exploring novel applications for sisal, namely as reinforcement of polymers, rubber, gypsum and cement matrices, creating a large range of technological applications. However, as it was for centuries, its main use nowadays is still as raw material for the rope industry.

The rope manufacture process produces quite a large amount of residues that are frequently either recycled for the production of low quality ropes or used as fuel. In this regard, the potential of this waste to be transformed in an added-value product beyond the fabrication of low quality ropes has been explored in different fields, covering for instance the pyrolytic degradation of the residues and the synthesis of adsorbents, namely carbon fibers [4–6] and activated carbons [7,8] that proved to be efficient adsorbents for the removal of pharmaceutical compounds from water. Moreover, rising worldwide concerns on environmental pollution have urged the development of new strategies as alternatives for the disposal of wastes complying with current environmental regulations. In this regard, pyrolysis has proven to be an effective technology for the valorisation of several types of residues. Thus the purpose of this study was to investigate the pyrolysis behavior of sisal fibers discarded from the rope industry, by analyzing the composition of the different fractions obtained as well as their potential applications in different fields.

2. Experimental

2.1. Sample

Sisal fibers discards were provided by a rope manufacturer in Portugal (Cordex). The as-received residue was cut into small pieces

* Corresponding author. Tel.: +351 217500897; fax: +351 217500088.
** Corresponding author. Tel.: +34 985119090; fax: +34 985297662.
E-mail addresses: ana.carvalho@fc.ul.pt (A.P. Carvalho),
conchi.ania@incar.csic.es (C.O. Ania).

(ca. 1–2 cm) before any analysis, still preserving the characteristic morphology of sisal fibers.

2.2. Pyrolysis

The pyrolysis of the rope waste (ca. 20 g in each run) was carried out in a quartz reactor placed in a tubular horizontal furnace. In order to ensure an inert environment during the experiments a $100\,mL\,min^{-1}$ flow rate of nitrogen was continuously fluxed through the reactor. Different pyrolysis temperatures (400, 550, 700 and 800 °C) were investigated at constant heating rates ($10\,°C\,min^{-1}$). The volatiles evolved during the pyrolysis passed through various consecutive glass condensers immersed in an ice salt cooling mixture (ca. −20 °C) where the condensable liquid fraction was collected. The non-condensable gases were collected in 3 L Tedlar® bags (with a polypropylene fitting for sampling). Gas samples were collected at the following temperatures: 300, 400, 550, 700, 800 and 850 °C. Once the pyrolysis was over, the solid carbonaceous residue was recovered from inside the quartz reactor for subsequent characterizations. Carbonaceous residues were named C-T, where T stands for the final pyrolysis temperature. The solid and oil fraction yields were calculated from the weight of each fraction, while the gas yield was evaluated by difference.

The aqueous fraction recovered in the condensers (mostly water) accounted for ca. 10–15 wt.%, regardless the pyrolysis temperature. It was separated from the organic fraction by centrifugation and it was further discarded (not analyzed as it was outside the scope of this paper).

2.3. Analysis

The organic fraction obtained upon pyrolysis was dried, using anhydrous sodium sulfate, filtered and dissolved in dichloromethane for further analysis by GC–MS, using an Agilent 7890A gas chromatograph coupled to an Agilent 5975C quadrupole detector. The gas chromatograph was equipped with a 30 m × 0.25 mm capillary column coated with a 0.25 mm thick film of 5% phenylmethylpolysiloxane (HP-5). Helium of 99.999% purity was employed as a carrier gas at a constant flow rate of $1.8\,mL\,min^{-1}$. The initial oven temperature of 40 °C was held for 10 min. The oven was programmed from 40 to 300 °C at $8\,°C\,min^{-1}$ and the maximum temperature was maintained for 30 min, and a splitting ratio of 1:50 was used. The detector and injector temperatures were 350 and 300 °C, respectively, and the volume of sample injected was 1 μL. Data were collected in the full-scan mode between m/z 33 and 533. The compounds in the oil fraction were identified by comparison with those reported in the literature [9–12] and in the Wiley and NIST computer libraries. Although quantification of the components in the oil fraction was not possible due to the large number of compounds and functionalities present in the chromatographed fraction, a semiquantitive analysis was performed. The relative amount of the detected compounds was evaluated by calculating the area (%) from the total chromatographed area.

The gases were analyzed in a Hewlett-Packard HP 6890 gas chromatograph fitted to a thermal conductivity detector (TCD) and two packed columns (HP 10FT Porapak N, 80/100 and HP 3FT Molecular Sieve 13×, 45/60). The oven temperature was set at 50 °C and the carrier gas flow rate (He) was $20\,mL\,min^{-1}$. The injector and detector temperatures were 80 and 220 °C, respectively. The TCD was calibrated with a standard gas mixture at periodic intervals.

Chemical characterization of the solid fraction included: proximate analysis and elemental analysis (using a LECO CHN-2000 apparatus for the determination of the C, H and N contents, a LECO S-144DR for the S content, and a LECO VTF-900 for the oxygen content).

Table 1
Main characteristics of the rope waste and the chars obtained at different pyrolysis temperatures.

	Raw residue	C-400	C-550	C-700	C-800
Elemental analysis (wt.%, dry ash free basis)					
C	45.7	83.8	91.0	92.8	94.0
H	5.9	4.4	2.5	1.3	0.9
N	0.4	0.7	0.8	1.0	1.0
S	n.d.	n.d.	n.d.	n.d.	n.d.
O	48.1	11.1	5.7	4.9	4.1
Proximate analysis (wt.%)					
Moisture	9.8	1.56	0.98	0.37	0.68
Ash	1.2	5.3	6.3	6.9	5.7
Volatile matter	85.9	27.2	12.8	7.8	7.1

n.d. not detected.

The solid fraction was further characterized by gas adsorption of CO_2 at 0 °C, using an automatic Tristar 3020 apparatus from Micromeritics. Before the experiments, the samples were outgassed under vacuum at 120 °C overnight. The isotherms were used to calculate the specific surface area S_{BET}, total pore volume V_T, and pore size distribution using the density functional theory (DFT) method [13].

The as-received rope waste and the solid carbonaceous residue after pyrolysis were also characterized by thermal analysis. The thermal analyzer (Labsys, Setaram) was set to operate at a heating rate $15\,°C\,min^{-1}$ under a nitrogen flow rate of $100\,mL\,min^{-1}$. For each measurement about 25 mg of sample was used.

3. Results and discussion

3.1. Characterization and thermal behavior of the as-received waste in a thermobalance

Table 1 shows some bulk characteristics of the as-received rope residues. The lignocellulosic character of this material was confirmed by the large oxygen content determined by elemental analysis and the X-ray diffraction patterns (Fig. 1A). The diffractograms showed the typical diffraction peaks of the crystal polymorph of cellulose I (characteristic peaks at 2θ – 16.3 and 22.5°) associated to the (1 0 1) and (0 0 2) planes of the native crystal structure of cellulose [14,15]. This crystal form arises from the hydrogen bonds between cellulose molecules arranged in a regular and ordered system. This is in good agreement with the fact that sisal is a cellulose-rich fiber as above-mentioned.

Investigating the thermal stability of natural fibers is important to evaluate their potential use in the processing of biomaterials [16]. For this reason, the thermal degradation of sisal was initially studied by thermal analysis at different heating rates (Fig. 1B). The thermograms showed that the decomposition takes place in a narrow temperature range, with a first weight loss occurring at approximately 100 °C (ca. 6–7%) and a main devolatization step detected at temperatures between 250 and 350 °C. The first peak was attributed to the loss of moisture, which is a common feature observed for lignocellulose fibers [17,18]. The values of water loss obtained by thermal analysis are in agreement with the moisture content evaluated from ultimate analysis.

The pyrolytic reaction started at temperatures above 250 °C, and the rate of decomposition (DTG) curves showed two distinct peaks at 300 and 350 °C, indicating that the decomposition of the rope wastes occurs in two steps. The weight loss at about 300 °C is a shoulder in the main peak, due to depolymerization of hemicelluloses and the cleavage of glucosidic linkages of cellulose [19]. The mass loss occurring at 350 °C is assigned to the decomposition of cellulose oligomers into tars (levoglucosan and low molecular mass volatile compounds like aldehydes, ketones or furans [20]). The rupture of α- and β-aryl-alkyl-ether linkages originated from the
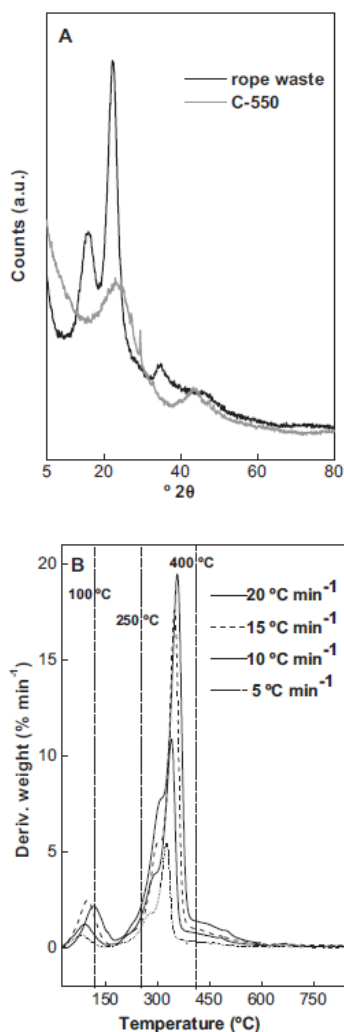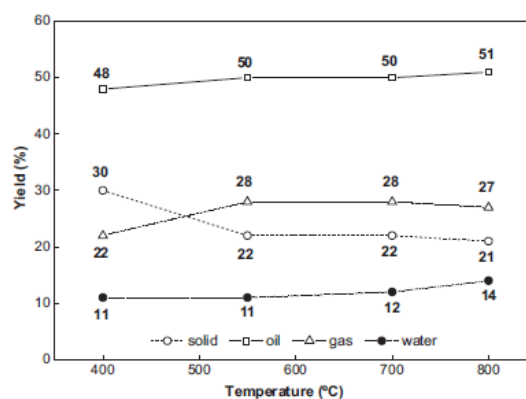
Fig. 2. Pyrolysis yields corresponding to the different fractions obtained during the pyrolysis of the rope wastes at various temperatures (lines are a guide for the eye).

thermal breakdown of lignin might also contribute to the mass loss behavior of these fibers [18]. In general terms, the thermal degradation of the rope wastes followed a similar trend than that of raw sisal fibers [21]. A gradual thermal degradation of the fibers was still observed at higher temperatures (*ca.* above 400 °C), which is attributed to the decomposition of cyclic rings and/or further carbonization of the formed tars [18]. Indeed, the char residue varied from 30 to 21 wt.% at 400 and 800 °C, respectively.

From the thermal profiles under inert atmosphere at different heating rates, the activation energies of the two decomposition processes detected during pyrolysis were calculated. The obtained values were 88 and 137 kJ mol^{-1}, which are slightly lower than the values reported for pure sisal fibers [22], but correlate very well with those of other lignocellulosic materials [18].

3.2. Pyrolysis yields

After investigating the thermal behavior of the sisal-based residues in a thermobalance, pyrolysis experiments were carried out at several temperatures: 400, 550, 700 and 800 °C. The solid, liquid and gas yields (wt.%) obtained in these pyrolysis experiments are presented in Fig. 2. The results correspond to the mean value of two pyrolysis runs, and the deviations were in all cases lower than 0.5%.

It can be observed that an increase in the pyrolysis temperature gives rise to a decrease in the solid fraction and to an increase in the gas fraction. The liquid fraction increases slightly when the temperature is increased from 400 to 550 °C, but remains more or less constant above this temperature. This behavior is in good agreement with the thermal behavior of the rope waste observed in the thermobalance, where the main decomposition of the residue

Fig. 1. (A) XRD patterns of the as-received rope waste and the solid fraction (char) obtained after pyrolysis at 550 °C and (B) thermal stability of the rope waste at different heating rates.

Table 2
Pyrolysis yield for lignocellulosic wastes and biomass samples.

Reference	Gas	Oil	Solid	Remarks
This work	28	43	22	Sample C-550
This work	27	41	21	Sample C-800
[18]	n.a	n.a	26–31	Temperature range 100–600 °C; various lignocellulose fibers
[21]	n.a	n.a	19.5	Sisal fiber degradation up to 600 °C
[22]	n.a	n.a	22	Sisal fiber degradation and polymer/sisal composites. Up to 500 °C
[23]	n.a	n.a	26–30	Temperature range 120–850 °C; various heating rates
[24]	20–42	30–72	1–47	Temperature range 430–700 °C; cellulose decomposition
[25]	22.6–27.2	50.6–56.2	10.1–22.8	Lignocellulosic biomass; temperature 450–470 °C; fluidized bed reactor
[26]	52.2–99.6	n.a.	0.4–40	Horse manure, straw, chicken litter (not lignocellulosic)

n.a. not available.
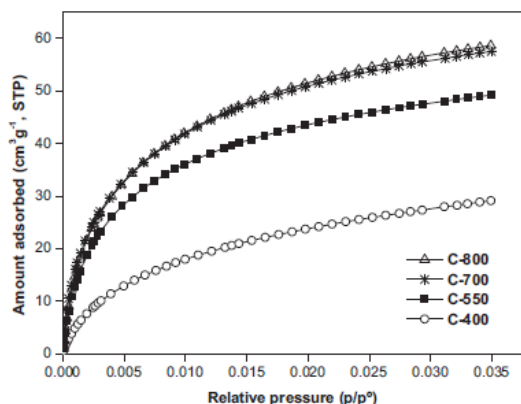
Fig. 3. CO_2 adsorption isotherms at 0 °C of the chars obtained at different temperatures.

Fig. 4. GC–MS chromatogram of the rope waste. Identification of main peaks with relative molar area > 1%: (a) 2-methoxytetrahydrofuran, (b) toluene, (c) 1-hydroxyl-2-butanone, (d) pentanoic acid, 2-methyl, (e) 1-penten-3-ol, (f) 2-cyclopenten-1-one, (g) 2-furanmethanol, (h) 2-propanone, 1-(acetyloxy), (i) furan, tetrahydro-2,5-dimethoxy-, (j) 2-cyclopenten-1-one, 2-methyl, (k) ethanone, 1-(2-furanyl), (l) 1,2-cyclopentanedione, (m), 2-furancarboxaldehyde, (n) 1-penten-3-ol, 2-methyl-, (o) 1,2-cyclopentanedione, 3-methyl, (p) guaiacol, (q) 2-cyclopenten-1-one, 3-ethyl-2-hydroxy-, (r) methylguaicol, (s) vinyl guiacaol, (t) syringol, (u) p-propylguaiacol, (v) vanillic acid, (w) o-hydroxybiphenyl, (x) 3-furancarboxylic acid, 5-ethyl-2,4-dimethyl-, (y) homovanillic acid, (z) syringaldehyde, (za) 4-allylsyringol, (zb) 2-pentanone, 1-(2,4,6-trihydroxyphenyl).

was observed to occur below 500 °C. Similar findings have been reported by other authors working with lignocellulosic wastes (see Table 2).

3.3. The solid carbonaceous residue

The char residue varied from 30 to 21% at 400 and 800 °C, respectively. The relatively low yield obtained for the char was somewhat expected for lignocellulosic precursor with a low content of lignin and high content of carbohydrates (high cellulose content). Moreover, these values are also characteristic of lignocellulosic materials containing high methoxyl group contents (hardwood or syringyl lignins) [23].

Some of the chemical properties of the chars obtained at different temperatures are summarized in Table 1. Data suggests that despite the thermal decomposition of the residue seemed to occur

mostly below 500 °C, the pyrolysis reaction does not seem to be complete as the corresponding char (sample C-550) still presents some volatile matter in its carbonaceous structure (i.e., 12.8 wt.%). In fact, the volatile matter decreased gradually when the pyrolysis temperature was raised (carbon content increased), indicating that devolatilization continues (although slowed down) at higher temperatures. Similar findings have been reported for the carbonization of coal and other biomass-derived wastes [23,27,28].

Pyrolysis of the rope waste rendered a carbonaceous material with low ash content. As the pyrolysis temperature favours the
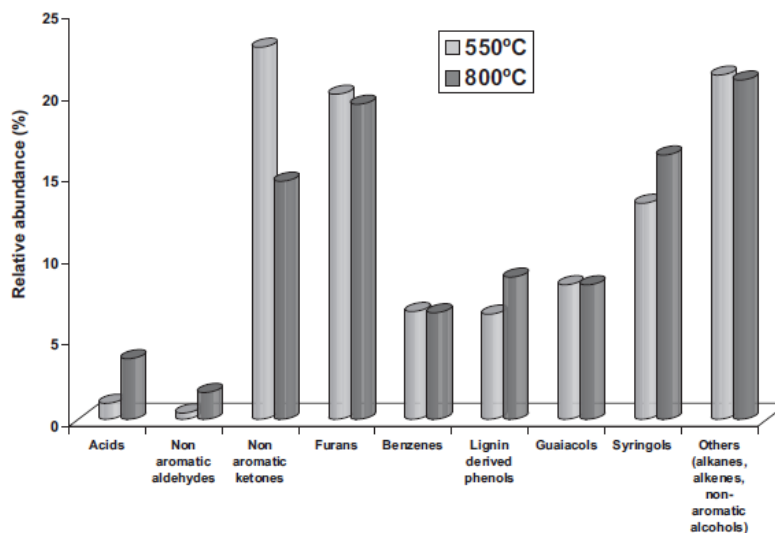
Fig. 5. Relative abundance (%) of the compounds detected by GC–MS in the pyrolysis oils of the rope waste.

devolatilization of the sample, as it was discussed in Section 3.1 (thermal profiles) and evidenced by elemental analysis, the overall composition of the solid residue (carbonaceous and inorganic matter) varies with temperature due to the modification in the volatiles content which is evolved at different temperatures. Consequently the weight ratio of both the carbon and inorganic matter increases with the pyrolysis temperature. The relatively high amount of heteroatoms, particularly oxygen, in the low temperature samples (C-400 and C-550) indicates that the solid carbonaceous char has abundant functionalities, and confirms that the char still undergoes some pyrolytic reactions when treated above 550 °C. The textural characterization of the chars obtained at different temperatures (Fig. 3) also showed that there is a certain development of microporosity during pyrolysis, being more important as the pyrolysis temperature was raised. Consequently, the solid residue obtained from the pyrolytic degradation of rope wastes could be a potential precursor to be used in the synthesis of low cost adsorbents. Indeed, previous results carried out in our research group have reported the synthesis of high surface carbon adsorbents from this char [7]. The resulting porous carbon also presented outstanding properties as support of metallic species with catalytic applications; the obtained metal-doped carbon supports showing good dispersion of the metal species on the carbon matrix.

The char treated at 400 °C showed a poor porous development compared to the rest of the samples; this suggests that this temperature is too low for a complete degradation of the rope waste, thus inhibiting the evolution of volatiles and the creation of porosity. The porosity of the chars obtained at higher temperatures is more developed, as it can be seen in the CO_2 adsorption isotherms (Fig. 3), particularly for the samples prepared at 700 and 800 °C. This confirms that even if the main degradation occurs at 550 °C, there is still a fraction of volatiles decomposing at higher temperatures and creating pores. Moreover, the XRD pattern of the char (Fig. 1A) demonstrates that the crystal structure of cellulose is deteriorated during pyrolysis, as the characteristic broad bands of carbon materials due to reflection of (1 0 1) and (0 0 2) planes are evident at 25 and 44 $2\theta°$, respectively, after the pyrolysis.

3.4. The liquid fraction

The liquid fraction corresponding to condensable vapors obtained during the pyrolysis was recovered and analyzed by GC–MS after separation from the aqueous fraction (mostly water). The chromatogram corresponding to the soluble fraction in dichloromethane from the oil obtained by pyrolysis at 550 °C of the studied waste is shown in Fig. 4, as an example. The pyrograms of the tars obtained at different pyrolysis temperatures rendered similar composition (not shown) with slight variation in the relative abundance of the pyrolysis components.

The pyrolysis products identified in the oil fraction are a complex mixture of carbohydrates and methoxylated phenols that correspond to the different lignin monomers (p-hydroxylphenylpropanoid, guaiacylpropanoid and syringylpropanoid lignin units). The main lignin-derived compounds detected were guaiacol, syringol, vanillic acid, eugenol and propenylsyringol. Some products arising from pyrolysis of carbohydrates can be also identified, including: furfural, cyclopentadienone, 2-furaldehyde, and 2-furanmethanol. The complete list of identified products has been included in Table 3. The relative abundance of the individual compounds is shown in Fig. 5, and corresponds to the identification of ca. 80% of the chromatographed material (total area). In all cases a predominance of hydrocarbons over phenolic compounds was obtained, which is in good agreement with other studies reported in the literature for lignocellulosic materials.

Table 3
List of main GC–MS detectable compounds in the pyrolysis oils of the rope waste at 550 and 800 °C (area %).

	C-550	C-800
Acids		
Propionic acid	0.25	
Pentanoic acid, 2-methyl-	0.39	
2-Propenoic acid, 3-(2-furanyl)-, ethyl ester	0.34	
Heptadecanoic acid, heptadecyl ester		3.23
Propargylacetic acid		0.49
Non aromatic aldehydes		
2-Butenal, 2-methyl-, dimethylhydrazone	0.16	
Hexanal, 4,4-dimethyl-	0.22	
Propionaldehyde		1.21
3-Pentenal, 4-methyl		0.43
Non aromatic ketones		
1-Hydroxy-2- butanone	1.20	1.19
Cyclopentanone	0.44	0.00
2-Cyclopenten-1-one	0.92	0.84
2-Propanone, 1-(acetyloxy)-	0.53	0.75
2-Cyclopenten-1-one, 2-methyl-	0.77	1.82
1,2-Cyclopentanedione		
γ-Butyrolactone	0.54	
2(5H)-Furanone	1.26	
1,2-Cyclopentanedione	2.58	0.81
2,3-Dimethylcyclopent-2-en-1-one	0.26	
3-Hexanone	0.44	
2-Butanone, 1-(acetyloxy)	0.48	0.50
3-Methylcyclopentanone	0.56	
3-hexen-2-one, 3-methyl	0.64	
1,2-Cyclopentanedione, 3-methyl	3.62	3.24
2-Cyclopenten-1-one, 2,3-dimethyl-	0.71	
2,4-Dimethylcyclopent-4-ene-1,2 dione	0.96	
2-Cyclopenten-1-one, 3-ethyl-2-hydroxy	2.64	2.56
2-Butanone, 4-hydroxy-3,3-dimethyl	0.63	
2-(2,2-Dimethylpropylidene)cyclopentane-1,3-dione	0.87	
2-Cyclopenten-1-one, 3-ethyl-2-hydroxy	2.81	
2-Butanone, 4-hydroxy-3,3-dimethyl		1.19
2-(2,2-Dimethylpropylidene)cyclopentane-1,3-dione		1.12
7,7-Dimethylbicyclo[3.3.0]octan-2-one		0.60
2-Butanone, 1-hydroxy-	1.20	1.19
1,3-Cyclopentanedione, 2-(2,2-dimethylpropylidene)-	0.44	0.00
2-Butanone, 3,3-dimethyl-	0.92	0.84
Furans		
2-Methoxytetrahydrofuran	0.74	0.58
Furfural	6.63	5.71
2,5-Dimethoxytetrahydrofuran		0.56
2-Furanmethanol		5.43
Furan, tetrahydro-2,5-dimethoxy-	0.74	0.60
Ethanone, 1-(2-furanyl)-	1.31	1.60
2-Furancarboxaldehyde, 5-methyl	2.37	1.46
2(3H)-Furanone, 5-methyl-		0.92
2-Furanmethanol, acetate	0.48	0.33
4,7-Methanoisobenzofuran, octahydro-3a,7a-dimethyl-	2.57	
2(5H)-Furanone		1.34
5-Acetoxymethyl-2-furaldehyde	0.79	0.81
3-Furancarboxylic acid	4.33	
Benzenes		
Toluene	1.02	0.60
Benzene, 1,3-dimethyl-	0.37	0.00
O-Hydroxybiphenyl	5.23	4.09
Benzenemethanol, 3-fluoro-		1.85
Lignin derived phenols		
Phenol	0.34	0.88
Phenol, 2-methyl-	0.34	0.40
1,2-Benzenediol, 3-methoxy-	0.81	
2,6-Dimethyl-3-(methoxymethyl)-p-benzoquinone		1.42
Phenol, 4-(3-hydroxy-1-propenyl)- (p-Coumaryl alcohol)		0.55

Table 3 (*Continued*)

	C-550	C-800
Phenol, 2-butyl-	1.85	1.60
Benzoic acid, 2,3-dihydroxy-		0.38
Phenol, 4-(2-methylpropyl)-	0.73	0.58
2-Pentanone, 1-(2,4,6-trihydroxyphenyl)	2.39	2.92
Guaiacols (methoxy-phenols)		
Phenol, 2-methoxy- (guaiacol)	2.12	1.99
2-Methoxy-4-vinylphenol (vinyl guaiacol)	0.76	0.63
Phenol, 2-methoxy-4-methyl- (methyl guaiacol)	0.73	0.47
Phenol, 2-methoxy-4-(2-propenyl)- (eugenol)	0.17	1.58
Phenol, 2-methoxy-4-propyl- (5-propyl guaiacol)	0.40	
Benzoic acid, 4-hydroxy-3-methoxy- (vanillic acid)	3.01	2.16
Benzeneacetic acid, 4-hydroxy-3-methoxy-(Homovanillic acid)	0.67	0.97
Ethyl vanillin		0.47
Phenol, 5-methoxy-2,3,4-trimethyl-	0.41	1.99
Syringols (dimethoxy phenol)		
Phenol, 2,6-dimethoxy-(SYRINGOL)	6.82	7.63
Phenol, 2,6-dimethoxy-4-(2-propenyl)- (propenil SYRINGOL)	5.22	4.72
Benzaldehyde, 4-hydroxy-3,5-dimethoxy- (Syringaldehyde)	0.48	0.25
Ethanone, 1-(4-hydroxy-3,5-dimethoxyphenyl)-	0.75	0.31
1-(3,4-Dimethoxyphenyl)-1-ethanol		3.31
Others (alkanes, alkenes, non aromatic ketones)	21.14	20.51

It is interesting to remark that the liquid fraction is rich in flavoring compounds commonly used in food preparation industry. For instance, syringol is the main chemical responsible for the smoky aroma; guaiacol contributes mainly to taste and it is also used as antipyretic [26]; vanillic acid used as food blending agent, fragrance for perfumes and in pharmaceuticals. Also large quantities of furfural and furfuryl alcohol are obtained, which are known valuable chemicals with industrial applications in synthetic chemistry, refining of lubricating oils, purification of hydrocarbons, or reactive solvents. The acidity of the pyrolysis oil fraction was low (low content of propionic, pentanoic acids), which makes it suitable for further processing for chemical production.

The results show that when pyrolysis is carried out at lower temperatures, the oil fraction was richer in volatile compounds comprising non-aromatic alcohols and ketones, and furans. Moreover, the lignin to hydrocarbons ratio (L/HC) slightly increased as the pyrolysis temperature was raised from 550 to 800 °C (ratio 0.53 and 0.66, respectively), thus confirming the occurrence of secondary reactions of hydrocarbons at high temperatures. This is also in good agreement with previous observations based on the thermogravimetric analysis. Indeed, although degradation of the rope waste mostly occurred at low temperature, further heating seems to provoke the evolution of medium and high molecular mass volatile compounds arising from the thermal breakdown of the lignin units.

3.5. The gas fraction

Analyses of the composition of the gas fraction obtained from the pyrolysis at various temperatures have shown that CO_2, CO, H_2, O_2, and C_xH_y are the main components released. The histograms in Fig. 6 show that CO and CO_2 are the dominant species at all temperatures, followed by methane and H_2. As expected, increasing the pyrolysis temperature lead to a decrease in the amount of
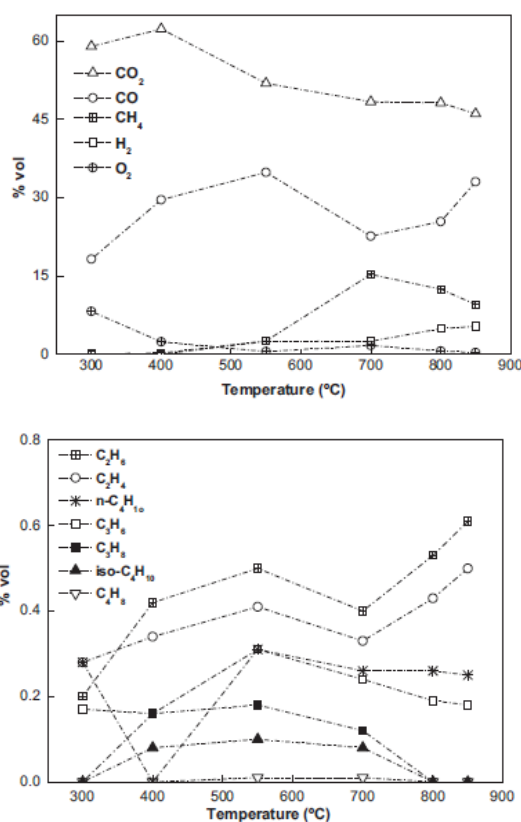
Fig. 6. Evolution of the gas fraction composition with the pyrolysis temperature (lines are a guide for the eye).

CO_2, along with an increase in CO, and H_2 over the whole range of temperatures studied. The concentration of combustible gases changed with the pyrolysis temperature, with a maximum in the yield of the hydrocarbons usually at temperatures higher than 700 °C. This is the case, for instance of methane, which originates from the methoxy groups in the side chains of the lignin units of the ropes, reaching a maximum yield of *ca.* 16 wt.% in the gas fraction when the pyrolysis is carried out at 700 °C. Traces of benzene, cathecol and phenols were also detected in the gas phase, which are typical products from lignin thermal degradation [29,30].

4. Conclusions

This work described the characterization of the different fractions obtained from the pyrolysis of lignocellulosic wastes from the rope industry. The pyrolytic reaction of the rope waste started from 250 °C, showing two decomposition peaks between 300 and 350 °C assigned to the depolymerization of hemicelluloses and the decomposition of cellulose oligomers into tars. Above 400 °C, some degradation still takes place to a small extent, due to the decomposition of cyclic rings and further carbonization of the formed tars.

The oil fraction was the most abundant during the pyrolysis of the rope waste, regardless the temperature, with solid and gas yields varying between 20 and 30 wt.%. The pyrolysis gases are

mainly composed of CO and CO_2, with significant proportions of CH_4 when the pyrolysis is carried out above 600 °C. A low content of hydrocarbons C_2–C_4 was also detected.

The GC–MS analysis of the degradation products in the liquid fraction revealed that the bio-oil fraction was rich in flavoring compounds and other valuable chemicals such as furfural, which have large applications in synthetic chemistry, food industry, and pharmaceuticals. The possibility of the recovery of these valuable chemicals, along with the reduced acidity of the pyrolysis oil fraction makes it suitable for further processing in chemical production.

The solid carbonaceous char also displayed interesting features to be used as precursor in the synthesis of low cost high performance porous adsorbents and catalysts supports. The yield of the solid fraction can be modulated by the pyrolysis temperature, which also defines the surface chemistry of the final char residue, and therefore its reactivity. The great potentiality of the solid fraction for the preparation of high surface area carbon adsorbents and supports of metallic particles has been demonstrated in previous works.

Acknowledgements

References

[1] Y. Li, Y.W. Mai, L. Ye, Sisal fiber and its composites: a review of recent developments, Compos. Sci. Technol. 60 (2000) 2037–2055.
[2] FAO, Jute, Kenaf, Sisal, Abaca, Coir and Allied Fibres, Statistics, Food and Agricultural Organization of The United Nations, Rome, 2009, June, pp. 34–38 http://www.fao.org/es/esc/common/ecg/323/en/STAT_BULL_2009.pdf (accessed 07.10.11).
[3] A.C.H. Barreto, D.S. Rosa, P.B.A. Fechine, S.E. Mazzeto, Properties of sisal fibers treated by alkali solution and their application into cardanol-based biocomposties, Composites: Part A 42 (2011) 492–500.
[4] S. Chen, J. Liu, H. Zeng, Structure, antibacterial activity of silver-supporting activated carbon fibers, J. Mater. Sci. 40 (2005) 6223–6231.
[5] R. Fu, L. Liu, W. Huang, P. Sun, Studies on the structure of activated carbon fibers activated by phosphoric acid, J. Appl. Polym. Sci. 87 (2003) 2253–2261.
[6] R. Fu, H. Zeng, Y. Lu, S.Y. Lai, W.H. Chan, C.F. Ng, The reduction of Pt (IV) with activated carbon fibers – an XPS study, Carbon 33 (1995) 657–661.
[7] M. Haro, V. Ruiz, M. Andrade, A.S. Mestre, J.B. Parra, A.P. Carvalho, C.O. Ania, Dual role of copper on the reactivity of activated carbons from coal and lignocellulosic precursors, Micropor. Mesopor. Mater. (2011), doi:10.1016/j.micromeso.2011.07.005.
[8] A.S. Mestre, A.S. Bexiga, M. Proença, M. Andrade, M.L. Pinto, I. Matos, I.M. Fonseca, A.P. Carvalho, Activated carbons from sisal waste by chemical activation

[9] with K_2CO_3: kinetics of paracetamol and ibuprofen removal from aqueous solution, Bioresour. Technol. 102 (2011) 8253–8260.
[9] O. Faix, D. Meier, I. Fortman, Studies on isolated lignins and lignins in woody materials by pyrolysis–gas chromatography–mass spectrometry and off-line pyrolysis–gas chromatography with flame ionization detection, J. Anal. Appl. Pyrolysis 11 (1987) 403–416.
[10] J. Ralph, R.D. Hatfield, Pyrolysis–GC–MS characterization of forage materials, J. Agric. Food Chem. 39 (1991) 1426–1437.
[11] J.C. del Rio, A. Gutierrez, A.T. Martinez, Identifying acetylated lignin units in non-wood fibers using pyrolysis–gas chromatography/mass spectrometry, Rapid Commun. Mass Spectrom. 18 (2004) 1181–1185.
[12] J.C. del Rio, A. Speranza, M.J. Gutierrez, A.T. Martinez, Lignin attack during eucalypt wood decay by selected basidiomycetes: a Py–GC/MS study, J. Anal. Appl. Pyrolysis 64 (2002) 421–431.
[13] F. Rouquerol, J. Rouquerol, K. Sing, Adsorption by Powders & Porous Solids, Academic Press, London, 1999.
[14] P. Langan, Y. Nishiyama, H. Chanzy, A revised structure and hydrogen-bonding system in cellulose II from a neutron fiber diffraction an alysis, J. Am. Chem. Soc. 121 (1999) 9940–9946.
[15] R. Teeaar, R. Serlmaa, T. Paakkari, Crystallinity of cellulose, as determined by CP/MAS NMR and XRD methods, Polym. Bull. 17 (1987) 231–237.
[16] A. Alemdar, M. Sain, Biocomposites from wheat straw nanofibers: morphology, thermal and mechanical properties Compos. Sci. Technol. 68 (2008) 557–565.
[17] A. Bismarck, A.K. Mohanty, I. Aranberri-Askargorta, S. Czapla, M. Misra, G. Hinrichsen, J. Springer, Surface characterization of natural fibers; surface properties and water up-take behavior of modified sisal and coir fibers, Green Chem. 3 (2001) 100–107.
[18] A.L.F.S. d'Almeida, D.W. Barreto, V. Calado, J.R.M. d'Almeida, Thermal analysis of less common lignocellulose fibers, J. Therm. Anal. Calorim. 91 (2) (2008) 405–408.
[19] D. Areseneau, Competitive reactions in the thermal decomposition of cellulose, Can. J. Chem. 49 (1971) 632–639.
[20] K.C.M. Nair, R.P. Kumar, S.C. Schit, K. Ramamurthy, S. Thomas, Rheological behavior of short sisal fiber-reinforced polystyrene composites, Composites Part A 31 (2000) 1231–1240.
[21] A.R. Martin, M.A. Martins, O.R.R.F. da Silva, L.H.C. Mattoso, Studies on the thermal properties of Sisal fibers and its constituents, Thermochim. Acta 506 (2010) 14–19.
[22] C. Albano, J. González, M. Ichazo, D. Kaisera, Thermal stability of blends of polyolefins and sisal fiber, Polym. Degrad. Stab. 66 (1999) 179–190.
[23] E. Jaka, O. Faix, F. Tilla, Thermal decomposition of milled wood lignins studied by thermogravimetry/mass spectrometry, J. Anal. Appl. Pyrolysis 40–41 (1997) 171–186.
[24] D.K. Shen, S. Gu, The mechanism for thermal decomposition of cellulose and its main products, Bioresour. Technol. 100 (2009) 6496–6504.
[25] A.M. Azeez, D. Meier, J. Odermatt, T. Willner, Fast pyrolysis of African and European lignocellulosic biomasses using Py–GC/MS and fluidized bed reactor, Energy Fuels 24 (2010) 2078–2085.
[26] C.S. Avenell, I. Sainz-Diaz, A.J. Griffiths, Solid waste pyrolysis in a pilot scale batch pyrolyser, Fuel 75 (1996) 1167–1174.
[27] M. Inguanzo, A. Dominguez, J.A. Menendez, C.G. Blanco, J.J. Pis, On the pyrolysis of sewage sludge: the influence of pyrolysis conditions on solid, liquid and gas fractions, J. Anal. Appl. Pyrolysis 63 (2002) 209–222.
[28] S.S. Alves, J.L. Figueiredo, Pyrolysis kinetics of lignocellulosic materials by multistage isothermal thermogravimetry, J. Anal. Appl. Pyrolysis 13 (1988) 123–134.
[29] S.N. Naik, V.V. Goud, P.K. Rout, A.K. Dalai, Production of first and second generation biofuels: a comprehensive review, Renew. Sustain. Energy Rev. 14 (2010) 578–597.
[30] A.H. Carter, Antipyretic effects of external applications of guaiacol, Br. Med. J. 7 (1894).

CHAPTER 5

COPPER-DOPED ACTIVATED CARBONS

Porous carbon materials constitute a very flexible set of supports for the preparation of heterogeneous catalysts. Besides providing high-energy adsorption sites for physical or specific adsorption, nanoporous carbons, which consist of both small pores and functional groups, are able to catalyse surface reactions (Leon y Leon and Radovic, 1990; Radovic and Rodríguez-Reinoso, 1996).

A large variety of carbon materials can and have been widely applied in catalysis (either as supports or as catalysts on their own) due to their superior structural, mechanical, chemical, thermal, and unique electrical transporting properties (Rodríguez-Reinoso and Sepúlveda-Escribano, 2009; Figueiredo and Pereira, 2009). The most investigated carbon materials in catalytic applications are carbon blacks and granular and powdered activated carbons, but there is increasing interest in related materials, such as activated carbon fibers and cloths, nanotubes, and nanofibres.

The physical and chemical surface properties of activated carbons can easily be tailored to: i) develop a large surface area to disperse the active phases; ii) adjust a proper pore size distribution to facilitate the diffusion of reactants and products to and from the surface; and iii) define the adequate acid-base character needed for obtaining the best performance. These properties can be exploited in a great number of catalytic reactions, as indicated in Table 5.1.

Table 5.1- Main reactions catalysed by carbons as catalysts and catalysts support (Rodríguez-Reinoso and Sepúlveda-Escribano, 2009; Figueiredo and Pereira, 2009, and references therein).

Carbon as catalyst	Carbon as catalyst support
Oxidative dehydrogenation of hydrocarbons	Hydroprocessing of petroleum feedstocks
Dehydration and dehydrogenation of alcohols	Ammonia synthesis
NO_x reduction	Hydrodesulfurization
NO, SO_x and H_2S oxidation	Hydrodenitrogenation
Ozonation	Hydrogenation of carbon oxides
Catalytic wet oxidation	

The factors affecting the performance of a carbon catalyst are the nature of surface groups, its concentration and accessibility, while the properties affecting carbon's role as catalyst support include its surface area and porosity, surface chemical properties and inertness.

Regarding the surface chemistry of an activated carbon (usually originating from the precursor or activation agent), the specific adsorbate–adsorbent interactions or the catalytic properties of the carbon surfaces may be enhanced by post-synthesis modifications of their surfaces, via the incorporation of the desired heteroatoms. The incorporation of metallic species with catalytic activity (e.g., Pt, Co, Ni, Cu) into the carbon matrix is known to improve the stability, efficiency, and dispersion of the catalyst. Several approaches have been explored for the immobilization of transition metals in carbon materials, including:

- Incorporation in the precursor of the activated carbon (Hines, D., Bagreev, *et al.*, 2004; Ania and Bandosz, 2006a; Liou and Chen, 2009; de Castro, Martínez-Escandell, *et al.*, 2010);
- Incorporation directly in the activated carbon, by means of oxidation treatments (Qiu, Han, *et al.*, 2011);
- Impregnation with metal oxides or metal chlorides (Ma, Rodriguez, *et al.*, 2000; Petit, Karwacki, *et al.*, 2007; Bian, Wei, *et al.*, 2010; Hermans, Deffernez, *et al.*, 2010; Álvarez-Montero,
  Gómez-Sainero, *et al.*, 2011);
- Carbonization of polymers of organic salts with metals on its composition, and so forth (Ania and Bandosz, 2006b).

Most common synthetic methods for the preparation of metal-doped carbons is usually performed by impregnation (wet and incipient wetness) or ion-exchange methods, often followed by calcination and reduction treatments (Ania, 2013). The role of oxygen groups and basic sites on the dispersion of metals on carbon supports is widely documented in the literature, and as a general rule, oxidation leads to better dispersion and strong anchoring of the metallic species (Sepúlveda-Escribano, Coloma, *et al.*, 1998; Moreno-Castilla, López-Ramón, *et al.*, 2000; Fraga, Jordão, *et al.*, 2002; Bandosz, 2009; Ania, 2013). However, basic groups are more beneficial than acidic ones, and owing to the low thermal stability of acidic groups (i.e., carboxylic), sintering of the metallic particles might occur if high temperature reduction treatments are applied.

Despite the fact that impregnation is the most common method used to deposit metal and semi-metal compounds on the surface of an activated carbon, an attractive alternative method to this post-treatment consists in the preparation of activated carbon using a mixture of a chemical compound and the carbon precursor. This method is particularly interesting if the metal/semi-metal compound can be dissolved in the carbon precursor, since a homogeneous distribution and a higher dispersion in the activated carbon is expected, although aggregation may occur during the thermal treatment inherent to the activation process. In all cases it is crucial to obtain a high dispersion and distribution of the metal in the carbon, while developing or maintaining the porosity of the support (Rodríguez-Reinoso and Sepúlveda-Escribano, 2009; Figueiredo and Pereira, 2009).

The transition metals present in an organic precursor can also influence the porosity of the final product and therefore its performance as adsorbent and/or catalyst. Moreover, thermal treatments (i.e., carbonization) in the presence of catalytic metals can create new forms of carbon. For instance, at high temperature the organic matter vaporizes, dehydrogenation occurs, and carbon particles can be deposited back on the surface of an inorganic support,

typically with formation of carbon nanotubes or filaments. The resulting carbons show high porosity and highly dispersed catalytically active metals (Ania and Bandosz, 2006a).

An important aspect of the preparation procedure is that the surface properties can be tailored using various contents of the metals and different ligands. Moreover, the exposure of the active surface formed during carbonization to various gases reacting with metals present can result in expansion of graphene layers and formation of additional porosity (Hines, Bagreev, *et al.*, 2004). This may open the door for engineering the texture of the materials toward desired applications. Besides the unique porous nature of these materials, metal-doped carbons may find applications as catalysts due to the high dispersion of catalytic metals on the surface and high micropore volumes.

In **Article II** (Haro, M.; Ruiz, B., Andrade, M.; Mestre, A. S.; Parra, J. B., Carvalho, A. P. and Ania, C. O., 2012. Dual role of copper on the air reactivity of carbons from different precursors, Microporous and Mesoporous Materials 154, 68-73), the synthesis of copper-doped activated carbons from different origins (i.e., lignocellulosic and bituminous coal) by a wet impregnation and low temperature calcination procedure was explored, as well as the role of copper particles on the physical, chemical and structural features of the resulting materials. The choice of cooper in this study is related to the fact that many oxidative reactions are catalysed by different complexes and oxides of this metal, namely water oxidation, hydrodechlorination, of dichloromethane, desulfurization, N_2O decomposition, ammonia adsorption (Chen and Meyer, 2013; Chen, Zhang, *et al.*, 2013; Ania, Bandosz, 2006b, Ma, Rodriguez, *et al.*, 2000; Petit, C., Karwacki, *et al.*, 2007; Seredych and Bandosz, 2010). Furthermore, copper-doped carbons were used as additives to TiO_2 powders in the preparation of hybrid semiconductor/carbon photocatalysts; this issue will be discussed in Chapter 6 (Article III).
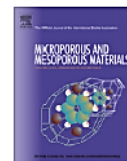
ARTICLE II

Dual role of copper on the reactivity of activated carbons from coal and lignocellulosic precursors

M. Haro [a], B. Ruiz [a], M. Andrade [b], A.S. Mestre [b], J.B. Parra [a], A.P. Carvalho [b,*], C.O. Ania [a,*]

[a] Instituto Nacional del Carbón, INCAR-CSIC, Apdo. 73, 33080 Oviedo, Spain
[b] Departamento de Química e Bioquímica and CQB, Faculdade de Ciências da Universidade de Lisboa, Ed. C8, Campo Grande, 1740-16 Lisboa, Portugal

ARTICLE INFO

ABSTRACT

The synthesis of copper-doped activated carbons from different origin (i.e., lignocellulosic and bituminous coal) by a wet impregnation and low temperature calcination procedure has been explored, as well as the role of copper particles on the physicochemical and structural features of the resulting materials. The textural characterization and isothermal reactivity analysis of the pristine and doped activated carbons have shown that the role of copper during the calcination step strongly depended on the nature of the carbon matrix. Copper impregnation of a coal-derived activated carbon catalyzed the air gasification of the material at a very low temperature (i.e., 325 °C), bringing about the development of microporosity on the doped carbon. In contrast, when copper was immobilized on a lignocellulose-derived activated carbon, the metallic species act as combustion retardant during the calcination step, protecting the carbon matrix during the catalytic gasification. In both cases, the resulting materials displayed a homogenous distribution of copper within the carbon matrix, while preserving large textural properties.

1. Introduction

Activated carbons are extensively used in a large number of industrial applications, mainly covering adsorption (both in gas and aqueous phase) and catalytic processes [1–3]. This is due to their low cost, wide availability and high performance, owing to their flexible coordination chemistry that allows an infinite possibility of three-dimensional structures with expanded pore network, and to their ability to react with other heteroatoms on the surface or within the structural framework.

In many applications, knowledge of the surface chemistry of carbons is of paramount importance as it determines the chemical stability and the reactivity in adsorptive and catalytic processes [4,5]. A high number of activated carbon applications have arisen because of the existence of a superficial layer of chemically bonded elements. Very often, the natural chemistry of an activated carbon surface (usually coming from the precursor or activation agent) is not potent enough to promote specific adsorbate–adsorbent interactions or catalytic properties of the carbon surfaces. Thus, the possibility of enhancing the physicochemical properties of carbons via modification of their surface by the incorporation of the desired heteroatoms is among current research interests in carbon science.

In this regard, various methods have been described in the literature to modify carbon surface chemistry [6–9]. Particularly, the incorporation of transition metals of catalytic activity on porous solids (including zeolites, pillared clays and carbonaceous materials) has attracted widespread interest for some decades due to the potential applications of such materials in catalytic and adsorption processes [1,3,10,11]. This is the result of the demand for highly functionalized materials in emergent areas, where besides tailoring the porosity (efforts are concentrated in the synthesis of carbons with tailorable pore sizes, controlled pore shapes and large surface areas), the surface chemistry of the obtained materials plays a crucial role to develop selective adsorbents and more efficient catalysts.

To meet such demands many approaches have been explored; the incorporation of the metal has been made in the precursor of the activated carbon, directly in the activated carbon, by means of oxidation treatments, impregnation with metal oxides or metal chlorides, carbonization of polymers of organic salts with metals on its composition, and so forth [12–18]. In all cases it is crucial to obtain a high dispersion and distribution of the metal in the carbon, while developing or maintaining the porosity of the support.

The objective of this work was to explore the dual role of copper as activating and protective agent of activated carbons of different nature (i.e., lignocellulosic and coal precursors). The presence of the metal in the carbon materials may enhance their catalytic [19], redox [20,21], or adsorptive properties [14,22,23]. We have focused on the study of the porous structure and the metal content and dispersion of doped carbon materials. In a typical procedure,

* Corresponding authors. Tel.: +351 217500897 (A.P. Carvalho), +34 985 118846 (C.O. Ania).
E-mail addresses: apcarvalho@fc.ul.pt (A.P. Carvalho), conchi.ania@incar.csic.es (C.O. Ania).

the carbon material was impregnated with the inorganic salt containing the selected metal (i.e., copper nitrate) and calcined. The effect of the carbon precursor on the dispersion of the metallic species and the porosity of the resulting metal doped carbons has been investigated; these features of paramount interest to prepare copper-doped carbons with a homogenous distribution of the metallic species on the carbon matrix and large surface areas.

2. Experimental methods

2.1. Materials

Two activated carbons obtained from different precursors were selected: a lignocellulosic-derived activated carbon obtained from CO_2 activation (800 °C, 1 h) of sisal (*Agave Sis alana*) fibers (S), and a commercially available activated carbon obtained from steam activation of a bituminous coal precursor (Q). Copper nitrate (Sigma Aldrich, 99% purity) was used as inorganic salt precursor. The metal-loaded carbons were prepared by a wet impregnation technique using an aqueous solution of the copper salt. About 20 mL of this solution were put in contact with 1 g of activated carbon and stirring for 24 h. The solution concentration was adjusted to attain 1 wt.% copper in the activated carbons. Impregnated samples were dried overnight at 100 °C in an air recirculation oven and then calcined at 325 °C for 3 h in air atmosphere (2 °C/min). The calcination step allowed the removal of the counter-ion of the metallic cation and thus to fix the metallic species on the carbon matrix. The calcined copper-loaded samples will be referred to as SCu and QCu. Blanks of the raw non-impregnated activated carbons calcined at the same temperature were also prepared (labeled as Scal and Qcal).

2.2. Characterization of the carbon materials

Textural characterization of the carbon materials was carried out by N_2 and CO_2 adsorption–desorption isotherms at −196 and 0 °C, respectively. Before the experiments, the samples were outgassed under secondary vacuum at 120 °C overnight. The isotherms were used to calculate the specific surface area, S_{BET}, total pore volume, V_T (evaluated at p/p^0 0.95), and pore size distributions using the density functional theory (DFT) approach [24]. The volume of narrow micropores was evaluated from the DR formulism applied to the CO_2 adsorption data, using 1.023 g/cm³ as the density of adsorbed CO_2 and 0.36 as the value of the β parameter. Elemental analysis of the raw carbons was carried out in LECO automatic analyzers (LECO CHNS-932 and LECO VTF-900 for the oxygen content).

The samples were further characterized by thermogravimetric analysis (Setaram Labsys) employing the following instrument settings: heating rate of 15 °C min⁻¹; nitrogen and air atmosphere at a flow rate of 50 mL min⁻¹. X-ray diffraction (XRD) patterns were recorded on a Bruker D8 Advance instrument operating at 40 kV and 40 mA, and using Cu Kα (λ = 0.15406 nm) radiation. Dispersion of the metallic particles incorporated to the carbon matrices was characterized using a Ziess DSM 942 scanning electron microscope; particles were dispersed on a graphite adhesive tab placed on an aluminum stub. The images were generated in the back scattered electron signal mode, which yielded better quality pictures.

Reactivity measurements of the impregnated carbons before calcination were carried out in dry air at 325 °C in a thermobalance. The sample (ca. 10–15 mg) was initially heated under N_2 up to 325 °C (50 mL min⁻¹), and then the nitrogen flow was changed to dry air and maintained during 3 h. The flow was changed again to nitrogen during the cooling down experiments. The

reactivity tendency in air was corrected versus the corresponding blank experiments in inert atmosphere.

3. Results and discussion

3.1. Characterization and reactivity of the raw activated carbons

Nitrogen adsorption isotherms presented in Fig. 1 illustrate the evolution of porosity from the pristine (samples S and Q) to the copper-loaded final activated carbons (samples SCu and QCu). Additionally, the corresponding textural parameters evaluated are presented in Table 1. As it can be observed in Fig. 1, the pristine carbons before copper impregnation exhibit a hybrid I/IV isotherm according to the IUPAC classification, which is characteristic of microporous materials with an important contribution of mesoporosity [25]. Both raw activated carbons show a broad knee at relative pressures p/p^0~0.2, suggesting the presence of wide micropores. The N_2 adsorption isotherms also show a hysteresis loop (type H4) at relative pressures about 0.5 where the adsorption and desorption branches are parallel, that indicates the presence of small slit-shaped pores and a well developed mesoporosity for both carbons [25]. An exhaustive analysis of the distribution of pore sizes was carried out combining the information of N_2 and CO_2 adsorption isotherms (Fig. 2). In the case of sample Q, the micropore volume obtained by the DR equation applied to N_2 was larger than that obtained from CO_2 adsorption, indicating the presence of wide micropores (disregarding kinetic restrictions) [26]. The opposite trend was obtained for sample S, showing the contribution of the narrow micropores for this material.

It can be observed that the calcination at 325 °C brought about quite a different response of both activated carbons, with important modifications in the textural properties for the sisal-derived sample. In the case of the coal-derived activated carbon (Qcal), a slight increase in the oxygen content was observed (Table 2) after calcination, which indicates that oxidation of the carbonaceous matrix was the dominant reaction taking place during the calcination of this activated carbon [27]. This behavior was somewhat expected based on the low temperature chosen for the calcination treatment, which aimed at decomposing the counter-anion of the copper salts while preventing the gasification reaction under air atmosphere (which did not seem to occur at 325 °C). Indeed, both the thermal analysis of the inorganic salt used in the impregnation and the DTG profiles of the raw carbon Q in air (Fig. 3 and inset) confirmed both observations: the complete decomposition of copper nitrate below 325 °C and the inertness of carbon Q at these conditions. Consequently, minor changes in the textural properties of carbon Q were detected upon calcination (sample Qcal). The slight decrease in the surface area and pore volumes (accounting for ca. 10%), can be attributed to the slight oxidation of the matrix (Table 2). Although some works in the literature report that air gasification of carbon materials at moderate temperatures (between 300–500 °C) leads to an increase in the mesopore volume of activated carbons [28], our results show that this was not the case of sample Q, at least for the non-catalytic gasification. The study of the reactivity of carbon Q in air in a thermobalance (isothermal gasification) also confirmed that this carbon does not react with air under these conditions, even when long times (ca. 3 h) are applied (Fig. 4).

In contrast, calcination brought about a severe modification of the sisal-derived activated carbon. This sample (Scal) was almost completely burnt-out when exposed to air at 325 °C during 3 h (mass loss 23%), and the resulting material had a negligible porosity (Figs. 1 and 2) and a grayish color (see inset in Fig. 2). This structural collapse suggests that a strong gasification of this lignocellulose-derived activated carbon takes place at 325 °C, as
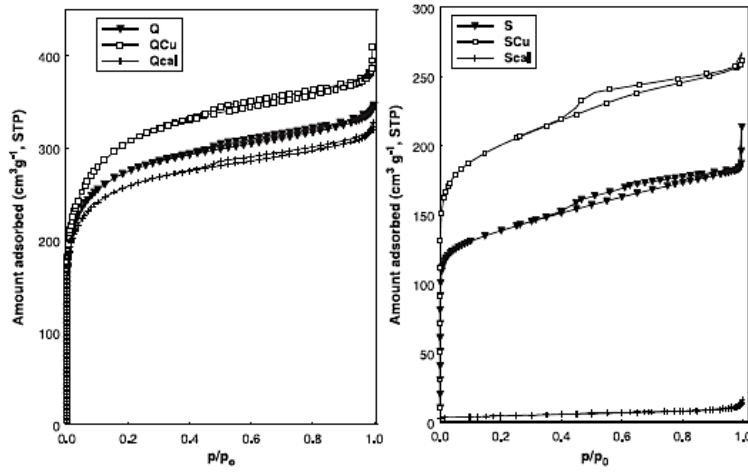
Fig. 1. N_2 adsorption isotherms at $-196\,^\circ\text{C}$ of the pristine, calcined and copper-loaded activated carbons.

Table 1
Main textural parameters of the activated carbons obtained from gas adsorption data.

	S_{BET} [m^2 g^{-1}]	V_{TOTAL}[a] [cm^3 g^{-1}]	V_{MICRO}[b] [cm^3 g^{-1}]	V_{MESO}[b] [cm^3 g^{-1}]	Wo, N_2 (DR)[c] [cm^3 g^{-1}]	Wo, CO_2 (DR)[c] [cm^3 g^{-1}]
Q	1030	0.51	0.32	0.09	0.31	0.21
Qcal	976	0.48	0.301	0.08	0.36	0.21
QCu	1140	0.57	0.34	0.12	0.42	0.20
S	525	0.27	0.16	0.08	0.20	0.25
Scal	16	0.02	–	–	–	0.02
SCu	760	0.39	0.23	0.10	0.29	0.27

[a] Evaluated at $p/p^o \sim 0.95$.
[b] Evaluated from DFT applied to N_2 adsorption data.
[c] Evaluated from DR equation.
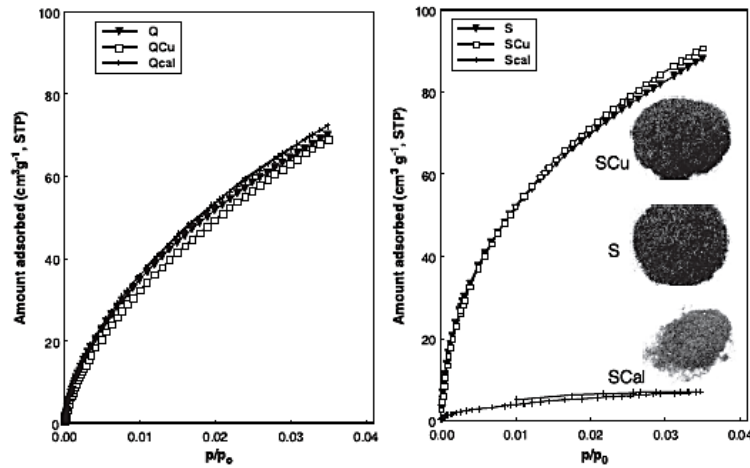
Fig. 2. CO_2 adsorption isotherms at $0\,^\circ\text{C}$ of the studied activated carbons. Inset: images of the sisal-derived materials.

opposed to what was observed for carbon Q. In fact, the fast calcination of the sisal-derived activated carbon was confirmed by the reactivity studies in the thermobalance). It can be observed in Fig. 3 that mass loss of the lignocellulosic-derived activated carbon in air becomes to be important at temperatures above 280 °C, below the temperature chosen for the calcination treatment in this study. Moreover, the isothermal gasification tests at 325 °C (Fig. 4) confirmed an overall mass loss close to 25 wt.% after 3 h, as opposed to 0.5 wt.% for the coal-derived carbon.

Table 2
Elemental analysis [wt.%, DAF basis] of the pristine, copper-loaded and calcined activated carbons.

	C [wt.%]	H [wt.%]	N [wt.%]	O [wt.%]	S [wt.%]
Q	96.3	0.6	0.7	2.1	0.3
Qcal	95.7	0.6	0.4	3.1	0.3
QCu	92.3	0.7	0.4	6.4	0.2
S	94.3	0.3	0.4	5.0	n.d.
Scal	–	–	–	–	–
SCu	90.9	0.5	0.5	8.1	n.d.

Although the non-catalytic gasification of biomass-derived chars at low temperatures has been reported in the literature [29], an important difference here is that in our study the air gasification has been carried out in an activated carbon (not on the solid residue after pyrolysis of the biomass, this is a 'char'). Sample S, being an activated carbon, has already been exposed to high temperatures during the activation step and consequently the amount of volatiles resulting from the thermal cracking of the carbon matrix is not very high (ca. below 7 wt.%, and similar to that of carbon Q). Thus, the high reactivity towards air exposure of this carbon can be associated to the presence of highly reactive sites in this material, likely as a result of the rich surface chemistry (Table 2) characteristic of lignocellulose-derived carbons.

3.2. Characterization and reactivity of the copper-doped activated carbons

When copper was incorporated to the carbon matrix, outstanding differences were obtained for both materials, particularly if one bears in mind the low amount of metal (ca. 1%) immobilized. It can be observed from the gas adsorption isotherms that the impregnation of copper brought about an important porosity development (Figs. 1 and 2) in both cases. This effect was undoubtedly more pronounced for the lignocellulose-derived activated carbon, where copper impregnation appeared not only to promote the air gasification but to prevent the complete calcination and further structural collapse of the pristine activated carbon. Since this effect was not observed for the corresponding non-impregnated calcined carbons, it has to be attributed to the copper incorporated to the carbon matrix.
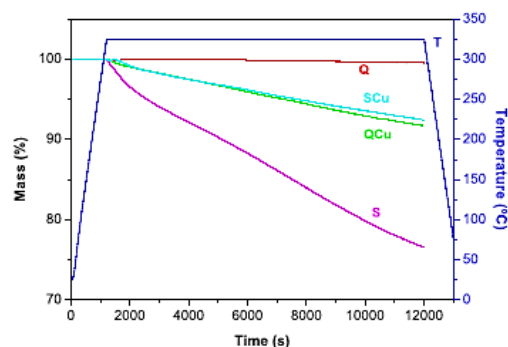
Fig. 4. Reactivity profiles of the isothermal air gasification at 325 °C for 3 h of the pristine and copper-loaded samples.

In the case of sample Q, the catalytic effect of copper for the air gasification was evident on the textural parameters of the resulting carbon (Table 1). It was also corroborated by the reactivity studies in the thermobalance. The DTG profiles under air (Fig. 3) of the impregnated copper–carbon (sample QCu before calcination) showed that the onset of the calcination reaction of the copper-doped carbon Q occurred at about 200 °C lower than that of the pristine activated carbon Q. The isothermal gasification at 325 °C during 3 h also confirmed the higher mass loss (ca. 7 wt.%) of the copper impregnated activated carbon (Fig. 4).

The catalytic activity of copper as well as other transition metals on the gasification of carbons is rather well known, due to their ability to undergo oxidation–reduction reactions at the carbon–metal interface [30–33]. However, most studies have reported this behavior in chars obtained from various precursors and at higher temperatures than those herein used. This is an important advantage, since reducing the activation temperature might limit the sintering of copper particles, thus enabling a better distribution of the metallic species on the resulting carbon material.

Moreover, we have observed that the gasification causes mainly an enlargement of the microporous structure of Q carbon (N_2 adsorption isotherms are parallel from relative pressures above 0.3). Analysis of the gas adsorption data revealed that the narrow microporosity – determined by the CO_2 adsorption isotherms –
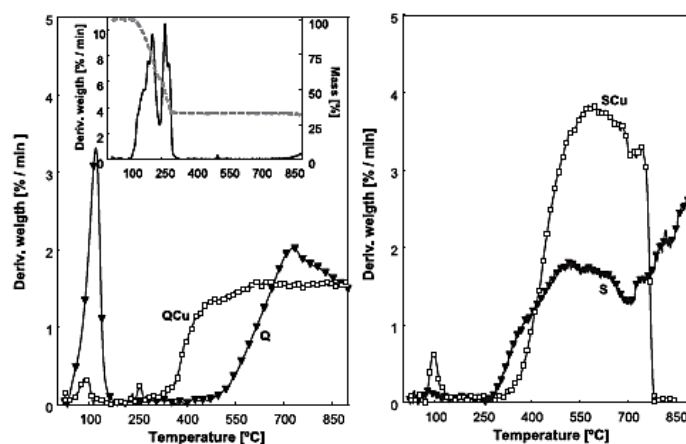
Fig. 3. DTG profiles in air of the as-received and copper-doped samples.
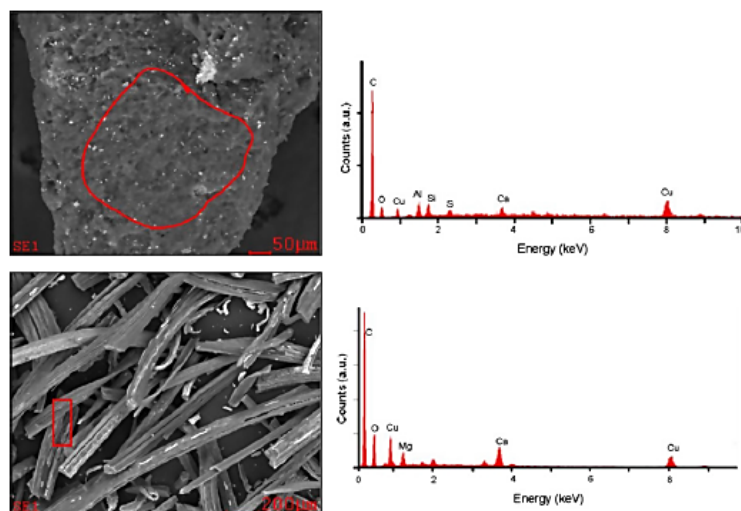
Fig. 5. SEM micrographs of the copper-loaded activated carbons and EDX analysis (qualitative) of the marked patch showing the distribution of heteroatoms on the carbon surface.

of the pristine carbon remained rather unchanged, and that the modifications in the pore volume and surface area are associated to an enlargement of the micropores of wider sizes. It is also interesting to remark that the incorporation of copper to activated carbons has been reported to provoke a collapse in the porosity of the metal-loaded carbons [34,35].

In the case of the lignocellulose-derived activated carbon (sample SCu), the effect of copper is more striking, as it seems to provoke the opposite effect. Calcination of the non-impregnated sample (Scal) at 325 °C was very strong, which caused a remarkable damage in the carbon structure and porosity. In contrast, the mass loss after 3 h of calcination decreased from 23 to 7 wt.% when copper was incorporated to this material (Fig. 4). Indeed, the DTG profiles in air show that the onset temperature of the calcination is delayed ca. 60 °C, compared to the pristine sisal-derived activated carbon (Fig. 3). As a result of this, a slight pore development in the copper-doped material was obtained, rather than its burning-out (Table 1). Thus, although it is evident that the gasification reaction occurs (similarly to carbon Q), it would seem that copper plays another role here, behaving as gasification retardant as opposed to what has been reported so far for the role of copper in the gasification of coal and lignocellulosic chars [30,36,37].

The SEM images and XRD analysis of the copper-loaded carbon materials (QCu and SCu) were used to further investigate the distribution of the copper species on the surface of the doped carbons. The SEM micrographs (Fig. 5) show no visual signs of the impregnation (no arrays of copper clustering); according to EDX analysis, the white particles observed in the micrographs correspond to the mineral matter of the carbons. Moreover, the EDX screening of bigger areas (see red[1] mark in Fig. 5) of the carbon particles (in both cases) show copper distributed within the carbon matrix. This confirms that copper is homogeneously distributed on the carbon, rather than forming large copper clusters. The low amount of copper incorporated to the carbon matrix (ca. 1 wt.%) compared to other studies might be responsible for the even distribution of the copper species, preventing the formation of large particle aggregates [14].

---

[1] For interpretation of color in Fig. 5, the reader is referred to the web version of this article.

XRD of these samples confirmed the co-existence of copper oxides and metallic Cu on the carbon matrix. These results also indicate the good dispersion of the metallic salt before calcination, and thus a relatively strong Cu-carbon interaction in both activated carbons. The elemental analysis data of the studied carbons indicated that along with copper, quantities of oxygen were also incorporated to the carbon matrix during the calcination treatment (Table 2). The SEM image of SCu also shows that the calcination did not destroy the fibrous structure of the sisal-derived material, as it was the case for calcination in the absence of copper.

The catalytic gasification of copper on carbons (graphites and chars) has been explained by the mobility of confined Cu/CuO nanoparticles [37–39] at temperatures close to the Tamman value (i.e. temperature at which sintering starts). This mobility is valid for particles below a critical size (below 100 nm), and facilitates the diffusion of oxygen to the copper-carbon interface when the material is exposed to air, thereby favoring oxidation–reduction reactions according to:

$$Cu + O_2 = CuO$$
$$CuO + C = Cu + CO$$
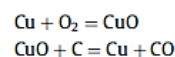
The SEM images (Fig. 5) confirmed the small size of the copper particles in both materials, for which migration of the metallic species is not restricted. However, 325 °C is far below the Tamman temperature reported for Cu and CuO (405 and 527 °C, respectively [36]), although mobility of copper particles could still be possible by an extra heat arisen from other redox reactions occurring at the carbon surface [36]. This could be the case for the gasification of sample Q, in which the extra-heat may come from the thermal decomposition of the nitrate ion (inset in Fig. 3).

In the case of sisal-derived activated carbon, the situation seems more complex. As mentioned above, the rich surface chemistry (Table 2) of this activated carbon could explain the easier gasification in air and in the absence of a metallic catalyst. The impregnation with copper somehow protects this material from the fast oxidation, as if the copper species would create an inert film on the carbon surface that would prevent the reactions when this is exposed to air. A somewhat similar role of copper salts as flame retardants of thermoplastic polymers has been reported in the

literature [40]. However its effect on the delay of the combustion of an activated carbon (protection) had not been previously reported. Moreover, the good dispersion of the copper particles within the carbon matrix (no large aggregates are observed) along with the preservation of the porous structure and the increased oxidation resistance make theses copper-loaded carbons excellent candidates to be used as catalysts in advanced oxidation processes for the degradation of refractory pollutants.

4. Conclusions

This work describes the dual role of copper as both catalyst and chemical protector (i.e., combustion retardant) during the calcination of activated carbon materials from different origins (i.e., ligno-cellulose and coal-derived). In the case of a coal-derived activated carbon, the immobilization of copper on the carbon matrix catalyzes the air gasification, by lowering the calcination temperature by 100 °C. As a result of the low temperature, the sintering of metallic species is avoided and the resulting material presented a homogenous dispersion of metallic particles within the carbon matrix, while displaying an enlargement of the existing microporous network (to mesopores). On the other hand, the copper immobilized on a highly reactive lignocellulosic activated carbon prevented the structural collapse of the materials during calcination, while promoting the porosity development. In this case, a dual role of copper particles was observed, acting as a protective layer of the carbon (to avoid its burning-out), and enlarging the microporosity to create mesopores. These materials showing a good dispersion of nanosized copper particles and large textural development are promising candidates as highly selective adsorbents and catalysts to be used in advanced remediation techniques.

Acknowledgments

References

[1] J.L. Figueriedo, Carbon Materials for Catalysis, Serp Ph, John Wiley and Sons, New Jersey, 2009.
[2] H. Marsh, F. Rodriguez-Reinoso, Activated Carbon, Elsevier, Oxford, 2006.
[3] D. Nguyen-Tahnh, T.J. Bandosz, Microporous Mesoporous Mat. 92 (2006) 47–55.
[4] C.O. Ania, T.J. Bandosz, Energy & Fuels 20 (2006) 1076–1080.
[5] L.R. Radovic, C. Moreno-Castilla, J. Rivera-Utrilla, in: L.R. Radovic (Ed.), Chemistry and Physics of Carbon, Marcel Dekker Inc., New York, 2001.
[6] H. Oka, M. Inagaki, Y. Kaburagi, Y. Hishiyama, Solid State Ion 121 (1999) 157–163.
[7] F. Goutfer-Wurmser, H. Konno, Y. Kaburagi, K. Oshida, M. Inagaki, Synthetic Metals 118 (2001) 33–38.
[8] M. Inagaki, Y. Okada, H. Miura, H. Konno, Carbon 37 (1999) 329–334.
[9] C.W. Zhou, J. Kong, E. Yenilmez, H.J. Dai, Science 290 (2000) 1552–1555.
[10] R. Szosta, Molecular Sieves Principles of Synthesis and Identification, Van Nostrand Reinhold, New York, 1983.
[11] C.O. Ania, T.J. Bandosz, Microporous Mesoporous Mat. 89 (2005) 315–324.
[12] C. Petit, C. Karwacki, G. Peterson, T.J. Bandosz, Journal of Physical Chemistry C 111 (2007) 12705–12714.
[13] D. Hines, A. Bagreev, T.J. Bandosz, Langmuir 20 (2004) 3388–3397.
[14] C.O. Ania, T.J. Bandosz, Carbon 44 (2006) 2404–2412.
[15] C.O. Ania, T.J. Bandosz, Studies in Surface Science and Catalysis 160 (2006) 559–566.
[16] S. Hermans, A. Deffernez, M. Devillers, Catalysis Today 157 (2010) 77–82.
[17] M.A. Alvarez-Montero, L.M. Gomez-Sainero, A. Mayoral, I. Diaz, R.T. Baker, J.J. Rodriguez, Journal of Catalysis 279 (2011) 389–396.
[18] B.A. Qiu, L.N. Han, J.C. Wang, L.P. Chang, W.R. Bao, Energy & Fuels 25 (2011) 591–595.
[19] J.H. Choy, H. Jung, Y.S. Han, J.B. Yoon, Y.G. Shul, H.J. Kim, Chemistry of Materials 14 (2002) 3823–3828.
[20] A. Sayari, Chemistry of Materials 8 (1996) 1840–1852.
[21] Q.H. Meng, L. Ling, H.H. Song, Journal of Applied Electrochemistry 36 (2006) 63–67.
[22] G.X. Yu, J. Sun, X.M. Hou, X.L. Zhou, C.L. Li, L.F. Chen, J.A. Wang, in: J.A. Wang, G.Z. Cao, J.M. Dominguez (Eds.), Advances in New Catalytic Materials, Trans Tech Publications Ltd, Stafa-Zurich, 2010, pp. 133–140.
[23] Z.J. Mei, Z.M. Shen, Q.J. Zhao, W.H. Wang, Y.J. Zhang, Journal of Hazardous Materials 152 (2008) 721–729.
[24] F. Rouquerol, J. Rouquerol, K. Sing, Adsorption by Powders and Porous Solids, Academic Press, London, 1999.
[25] K.S.W. Sing, D.H. Everett, R.A.W. Haul, L. Moscou, R.A. Pierotti, J. Rouquerol, T. Siemieniewska, Pure and Applied Chemistry 57 (1985) 603–619.
[26] J.M. Juarez-Galan, A. Silvestre-Albero, J. Silvestre-Albero, F. Rodriguez-Reinoso, Microporous Mesoporous Mat. 117 (2009) 519–521.
[27] H. Ogawa, K. Saito, Carbon. 33 (1995) 783–788.
[28] A.R. Sánchez, A.A. Elguézabal, L. de La Torre Saenz, Carbon. 39 (2001) 1367–1377.
[29] J. Gañan, J.F. Gonzalez, C.M. Gonzalez-Garcia, A. Ramiro, E. Sabio, S. Roman, Applied Surface Science 252 (2006) 5988–5992.
[30] C. Moreno-Castilla, J. Rivera-Utrilla, A. López-Peinado, I. Fernández-Morales, F.J. López-Garzón, Fuel 64 (1985) 1220–1223.
[31] C. Moreno-Castilla, A. López-Peinado, J. Rivera-Utrilla, I. Fernández-Morales, F.J. López-Garzón, Fuel 66 (1987) 113–118.
[32] H. Marsh, B. Rand, Carbon. 9 (1971) 63–72, IN67–IN10, 73–77.
[33] J.S.J. Vandeventer, M.A. Reuter, Thermochimica Acta 137 (1989) 383–386.
[34] D.J. Kim, J.E. Yie, J. Colloid, Interface Science 283 (2005) 311–315.
[35] S.J. Park, B.J. Kim, J. Colloid, Interface Science 292 (2005) 493–497.
[36] T.G. Devi, M.P. Kannan, G.N. Richards, Fuel 69 (1990) 1440–1447.
[37] R.T.K. Baker, J.J. Chludzinski Jr, Carbon. 19 (1981) 75–82.
[38] D.W. McKee, Carbon. 8 (1970) 131–136, IN133–IN138, 137–139.
[39] D.W. McKee, Carbon. 8 (1970) 623–626, IN625–IN627, 627–635.
[40] G. Fontaine, T. Turf, S. Bourbigot, Fire and Polymers V, Chapter 20, ACS Symposium Series, 2009.

CHAPTER 6

PHOTOCATALYTIC DEGRADATION OF PHENOL BY HYBRID TiO₂/CARBON CATALYSTS

As discussed in previous sections, the minimum wavelength required to promote the excited state of a semiconductor depends on the band-gap energy. For TiO_2, only photons with energy correspondent to $\lambda < 400$ nm can be absorbed to induce the excitation of electrons from the valence to the conduction band and to enable the charge separation that would eventually lead to the degradation reaction, of for instance, a target pollutant. Many organic compounds present a strong absorption of light at $\lambda < 400$ nm, that could lead to direct degradation in the absence of a catalyst (photolytic reaction). Given its limitations, the photocatalytic enhancement of TiO_2 has been the subject of extensive research, as previously discussed in section 3.4.6.3, with great efforts being made to extend the useful response of this material to the visible region, in order to improve the solar conversion efficiency. So as to enhance TiO_2 photocatalysis, as well as the response to visible light, different approaches have been investigated, and TiO_2 has been doped with certain transition metals, non-metals and ionic components.

TiO_2 doping with transition metals has been widely employed with reported improved photoactivities, being clearly related to the efficiencies of the doping centers in trapping charge carriers and interceding in the interfacial transfer (Colón, Maicu, *et al.*, 2006, Rashad, Elsayed, *et al.*, 2013). Metal ions also serve as charge trapping sites and thus reduce electron-hole recombination rate. The doping of metal/metal oxides enables the formation of a hybrid O 2p conduction band with a lower band gap energy, favouring absorption over the whole visible spectrum.

Numerous metal ions have been investigated as potential dopants, including iron, chromium, manganese, cobalt, copper, etc. The effect of metal doping on the photoactivity depends on many factors, e.g. the method of doping, and the type and concentration of the dopant. Among these, copper has been used as an effective dopant for electron trapping in the conduction band of TiO_2, improving the photocatalytic performance (Choi, Termin, *et al.*, 1994; Inturi, Boningari, *et al.*, 2014; Colón, Maicu, *et al.*, 2006). The introduction of copper (II) into the TiO_2 matrix results in a composite catalyst with an enhanced absorption ability for visible light, fast charge transfer rates and better charge separation efficiency (Zhang, 2010).

Despite these many enhancement attempts, efficient and commercially viable photocatalysts for important processes such as water splitting and degradation of various pollutants are yet to be realized. In this sense, given the known deactivation of metal-doped semiconductors, due to aggregation of the metallic dopants, a different approach can be entailed, through the incorporation of transition metals in the surface of carbonaceous materials. This procedure,

already addressed in Chapter 5, however in a different context, envisages the preparation of more efficient photocatalysts, allowing a good dispersion of metallic species on the carbonaceous matrix. These metal doped carbons can be used with TiO_2 in hybrid photocatalysts in the photodegradation of organic compounds.

In **Article III** (Andrade, M.; Mestre, A. S.; Matos, J.; Carvalho, A. P. and Ania, C. O., 2014. Visible light driven photo-oxidation of phenol on TiO_2/Cu-loaded carbon catalysts. Carbon 76, 183-196), the aim was precisely to explore the role of copper on the photocatalytic activity of a hybrid TiO_2/copper containing carbon photocatalyst towards phenol degradation in liquid phase under visible light irradiation.

Hybrid TiO_2/carbon photocatalysts have shown so far a good performance with increased photo-oxidation conversions under sunlight and certain semiconductor-free carbons have even demonstrated the ability to convert photons from the visible spectrum in chemical reactions. Despite these facts, the origin and dependence of the carbon/light interactions with the irradiation source is not so straightforward, and in the case of hybrid carbon/semiconductor catalysts it becomes more complex (Ania, Velasco, *et al.*, 2012). Additionally, in photocatalytic reactions involving hybrid catalysts with porous materials, several reactions occur simultaneously upon irradiation of the catalysts (namely adsorption, direct photolysis and photocatalysis) that have to be considered when comparing the performance of different systems.

The irradiation wavelength will have an influence on the degradation mechanism, and consequently on the amount and distribution of degradation intermediates. In the case of the photocatalytic degradation of phenol, a regioselectivity towards the formation of catechol over quinones has already been reported for nanoporous carbons under UV illumination (Velasco, Fonseca, *et al.*, 2012). This is quite an important fact since catechol has a higher reactivity over quinones, which would account for the improved conversion of phenol upon UV radiation, as discussed in section 3.4.6.4. Given the growing interest of the use of carbon materials in photocatalytic applications, to clarify the role played by these materials upon irradiation under different wavelengths would be an interesting contribution to this research area.

The focus of **Article IV** (Andrade, M. A.; Carmona, R. J.; Mestre, A. S.; Carvalho, A. P. and Ania, C. O., Effect of the irradiation wavelength on the performance of nanoporous carbon as an additive to TiO_2. Applied Catalysis A: General 507, 91-98) was the study of the effect of the irradiation wavelength on the performance of nanoporous carbon as an additive to TiO_2 on the photocatalytic degradation of phenol.

ARTICLE III

Visible light driven photooxidation of phenol on TiO₂/Cu-loaded carbon catalysts

CrossMark

Marta A. Andrade [a,b], Rocio J. Carmona [b], Ana S. Mestre [a], Juan Matos [c], Ana P. Carvalho [a,*], Conchi O. Ania [b,*]

[a] Centro de Química e Bioquímica, Faculdade de Ciências, Universidade de Lisboa, 1749-016 Lisboa, Portugal
[b] Adsorption and Environmental Remediation On Porous Solids (ADPOR), Dpt. Chemical Processes for Energy and Environment, Instituto Nacional del Carbón, INCAR-CSIC, Apdo. 73, 33080 Oviedo, Spain
[c] Dpt. Photocatalysis and Alternative Energies, Venezuelan Institute for Scientific Research (IVIC), 20632, Caracas 1020-A, Venezuela

ARTICLE INFO

ABSTRACT

The photocatalytic performance of titania/Cu-carbon composites was investigated towards phenol degradation under visible light. The approach consisted on the incorporation of the transition metal on the carbon component of the hybrid composite via impregnation of the carbon precursor with a metal salt followed by activation. Data showed a homogeneous dispersion of copper particles within the carbonaceous matrix, predominantly as copper (II) species. The synthesized carbons displayed a well developed nanoporous texture, although comparatively the impregnation of copper caused a marked inhibition of the textural development of the carbon precursor. The phenol photooxidation tests carried out on 1:1 titania/carbon composites showed the outstanding role of copper under visible light, with an increased efficiency in terms of phenol conversion, mineralization degree and degradation rate. This is important, since similar overall conversions were obtained with half of the amount of the photoactive semiconductor (1:1 composites). The beneficial effect of copper loading was also observed in the marked regioselectivity towards the preferential formation of catechol. Furthermore, the copper-loaded photocatalyst was found to be stable with no lixiviation or photoreduction of the copper species after illumination.

© 2014 Elsevier Ltd. All rights reserved.

1. Introduction

In the last few years, a considerable amount of research has been carried out in the field of advanced oxidation processes (AOPs) to be applied in the removal and degradation of emergent contaminants from wastewater [1–3]. Heterogeneous photocatalysis is widely recognized as an effective AOP for the degradation and mineralization of recalcitrant organic compounds [4–6]. Compared to other semiconductors, titanium dioxide plays a leading role as photocatalyst due to its cost effectiveness, low toxicity and high chemical photostability. As many other materials, titania powders suffer from several drawbacks mainly related to the low surface area, low activity under visible light, high recombination rate of photogenerated electron-hole pairs, and recovery and reutilization issues [7,8]. Hence, many research efforts are being made to overcome these limitations. The incorporation of a carbon component as additive to semiconductors seems to be an adequate strategy to improve the efficiency of the photocatalyst; the enhanced performance of carbon/TiO₂

composites has been reported for the photodegradation of a variety of pollutants, and being attributed to several factors associated to visible light absorption, the porosity of the carbon support, strong interfacial electronic effects, and the intrinsic photochemical activity of certain carbons [9–12].

The incorporation of transition metals to improve the photocatalytic activity of TiO_2 has also been extensively investigated, with reported visible light activation of the doped photocatalyst due to the effective electronic interaction between the semiconductor and the metal [13–16]. Among transition metals, copper is a relatively available and effective dopant for trapping the electrons in the conduction band of TiO_2 [17–20]; additionally, many oxidative reactions are catalyzed by different copper complexes and oxides [21–23]. However, metal-doped semiconductors suffer from deactivation due to aggregation of the metallic dopants [24]. On the other hand, the incorporation of transition metals in the surface of carbonaceous materials appears as a powerful alternative offering great possibilities for the preparation of more efficient photocatalysts [25–27], since the dispersion of metallic species on a carbonaceous matrix can be easily accomplished (by the choice of the precursor, and impregnation with metal oxides or salts) [28–33].

Knowing this, we aimed at exploring the photooxidative activity of copper-based materials by producing a hybrid titania/carbon photocatalyst incorporating copper on the carbon component during the carbon preparation step. The objective of this work is to study the photocatalytic activity of a Cu-loaded carbon/TiO_2 composite towards phenol degradation under visible light irradiation. As carbon component in the composite we have selected a nanoporous carbon prepared by chemical activation of a lignocellulosic precursor (sisal fibers, discarded from the rope industry), in line with a current interest of our research group on the valorization of several types of residues for the production of low-cost adsorbents [34,35]. Phenol was selected as model refractory contaminant, since it is a priority pollutant frequently found in wastewater, representing a high environmental risk according to the European and American Environmental Protection Agencies.

2. Experimental

2.1. Materials synthesis

A copper-loaded nanoporous carbon was synthesized by chemical activation of a lignocellulosic industrial residue – discarded sisal ropes – supplied by a rope industry. Briefly, 1 cm long sisal pieces were impregnated with an aqueous solution of $Cu(NO_3)_2.3H_2O$ (Sigma–Aldrich, 99%), with a concentration adjusted to attain 5 wt.% of copper in the final material, stirred overnight and dried. The material was then impregnated with a K_2CO_3 solution (Aldrich, 99%), according to the weight ratio sisal: K_2CO_3 of 2:1, and activated in a horizontal furnace (Thermolyne Model 21100) at 700 °C, for 1 h under N_2 flow (5 cm^3 s^{-1}). After the activation, the sample was thoroughly washed with distilled water until pH 7 and dried at 100 °C. This material will be referred to as SCu5. A blank sample was also prepared by activation with K_2CO_3

in the absence of copper (sample S). The titania/carbon photocatalysts with a 1:1 weight ratio composition were prepared by physical mixture of the individual components.

2.2. Characterization of the catalysts

The porosity of the samples was characterized by measuring the N_2 and CO_2 adsorption isotherms at −196 and 0 °C, respectively (ASAP 2010 and Tristar 3020, Micromeritics). Before the experiments, the samples were outgassed under vacuum (ca. 10^{-3} torr) at 120 °C overnight. The isotherms were used to calculate the specific surface area, A_{BET}, total pore volume, V_{total}, while the micropore volumes were analyzed using the Dubinin–Radushkevich formulism to the N_2 and CO_2 adsorption data ($W_{0,N2}$, $W_{0,CO2}$) [36]. Elemental analysis was carried out in LECO CHNS-932 and LECO VTF-900 automatic analyzers. The surface chemistry was characterized by the determination of the pH at the point of zero charge (pH$_{PZC}$) using the mass-titration procedure, according to the experimental procedure described elsewhere [37]. The morphology of the samples and the dispersion of the metallic particles were observed by Field Emission Gun Scanning Electron Microscopy (FEG-SEM) with an X-ray Energy-Dispersive System (EDS) and Transmission Electron Microscopy (TEM), in a JEOL JSM-7001F (using an accelerating voltage of 25 kV) and a Hitachi H-8100 (operating at 200 kV) equipments, respectively.

The actual copper content of sample SCu5 was determined by Inductively Coupled Plasma-Optical Emission Spectrometry (ICP-OES, Perkin Elmer Optima 2000 DV). The chemical state of the copper species was also investigated by X-ray Photoelectron Spectroscopy (XPS), and Temperature Programmed Reduction (TPR). X-ray photoelectron spectra were recorded on a SPECS spectrometer with a Phoibos 100 hemispherical analyzer with a multichannel detector. The base pressure in the ultra high vacuum chamber was below 10^{-7} kPa. The X-ray radiation source was monochromatic AlKα (1486.74 eV) at 100 W X-ray power and anode voltage of 14 kV. The photo-excited electrons were analyzed in constant pass energy mode, using pass energy of 50 eV for the survey spectra and 10 eV for the high resolution core level spectra. During data processing of the XPS spectra, binding energy values were referenced to the C 1s peak at 284.6 eV [38]. The CasaXPS software package was used for acquisition and data analysis. A Shirley-type background was subtracted from the signals. Recorded spectra were always fitted using Gauss–Lorentz curves, in order to determine the binding energy of the different element core levels more accurately. The error in binding energy was estimated to be ca. 0.1 eV. Photorreduction of Cu(II) species was avoided as much as possible by using short irradiation times (first acquisition was performed within 8 min), although reduction in high vacuum during the analysis cannot be excluded [39]. TPR analyses were performed in a chemisorption analyzer (Autochem 2920, Micromeritics) equipped with a TCD reactor and a mass spectrometer (OmniStar 3000). For each analysis approximately 40 mg of sample was treated with a 50 cm^3 min^{-1} stream of 10% H_2 in Argon from 100 to 600 °C at 5 °C min^{-1}. X-ray diffraction (XRD) patterns were obtained at room temperature on a Philips PX-1730 with automatic data acquisition (APD

Phillips (v3.6B) software), using CuKα radiation as incident beam.

2.3. Photodegradation runs

Phenol photodegradation experiments using commercially available titania (P25, Evonik) and titania/carbon composites – using a 1:1 weight ratio – as catalysts were carried out at room temperature using a photo-reactor of 500 cm³ capacity, a loading catalyst ratio of 0.5 g L⁻¹ and 85 ppm as initial phenol concentration in solution. The irradiation source was provided by a high pressure mercury lamp (Helios Italquartz, 125 W, emitting at 313, 360, 404, 436, 546, 577 and 579 nm; see spectrum in Supp. Information, Fig. S1), vertically suspended in a cylindrical, double-walled Pyrex jacket cooled by flowing water, immersed in the solution. The Pyrex jacket acts as a cut-off filter of the UV irradiation lower than 360 nm, minimizing the photolytic reaction in all the catalytic runs. The water cell was used to control the temperature during the experiments, preventing any overheating of the suspension due to the irradiation. The reactor was open to air in all the experiments to ensure that enough oxygen was present in the reaction solution. In each run, 250 mg of the catalysts were added to 500 cm³ of phenol solution under vigorous stirring (900 rpm). As we are studying porous photocatalysts, to maintain the same phenol concentration in solution (ca. 85 ppm) at the beginning of the irradiation, a pre-equilibration step at dark conditions was carried out to account for the amount adsorbed. Hence phenol adsorption kinetics of the materials was initially evaluated at dark conditions to establish the time required for the equilibrium (ca. 30 min in all cases) and the amount adsorbed. Consequently, before the irradiation was applied the composites were allowed to pre-equilibrate with phenol solutions of 104 and 96 ppm concentration, respectively, for TiO₂/S and TiO₂/SCu5. After the equilibration step, the suspension was irradiated for 360 min. All the experiments were done in duplicate with deviations below 5% in all cases; reported data represent the average values.

During the irradiation, small aliquots of the solution (~1 cm³) were taken out at predetermined time intervals and analyzed by reverse-phase HPLC (Spherisorb C18 column 125 × 4 mm, methanol to water 5:95, 30 °C, 0.7 cm³ min⁻¹ flow rate, photodiode array detector). The samples were previously filtered using cellulose filters with a mean pore size of 0.45 μm. Total organic carbon (TOC) of the solution at the end of each run was also measured in a TOC-V analyzer.

Assays in the same experimental conditions, but in the absence of irradiation, were performed (series *dark*) for further comparison with the experiments upon irradiation (series *irrad*) of the catalysts, so as to detect any modifications upon illumination. The spent catalysts were recovered by filtration, dried overnight at 60 °C and characterized. An aqueous suspension of the Cu-loaded carbon was also irradiated to investigate the possible photo-induced degradation of the carbonaceous matrix. The concentration of copper ions potentially released to the solution during the photocatalytic experiments was monitored by ICP-MS (Agilent).

3. Results and discussion

3.1. Characterization of the materials

A detailed textural characterization of the nanoporous carbons and the TiO₂/carbon composites as well as that of P25 is summarized in Fig. 1(a–c) and Table 1. The carbon samples
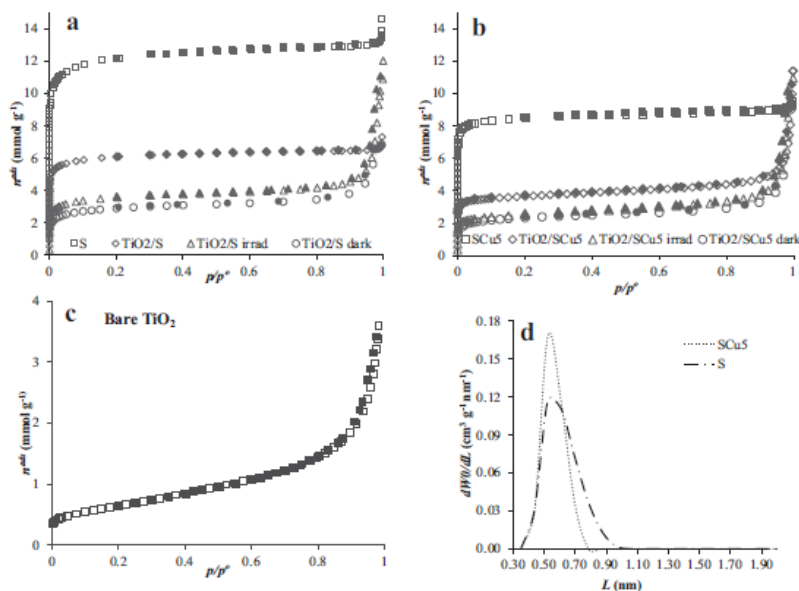

Fig. 1 – (a–c) Nitrogen adsorption–desorption isotherms at −196 °C (closed symbols are desorption points); (d) micropore size distributions obtained from the CO₂ adsorption data according to the method described in Pinto et al. [41].

prepared by chemical activation of the sisal waste resulted to be essentially microporous materials. Comparatively, the impregnation of the carbon precursor with copper resulted in the inhibition of the textural development, as revealed by the pronounced drop in the apparent surface area (larger than 30%), that goes beyond the mass effect of copper (ca. 5 wt.%). Furthermore, for the copper-loaded samples (both SCu5 and TiO$_2$/SCu5), $W_{0,N2} < W_{0,CO2}$, which is indicative of a narrow microporous distribution as opposed to the non-loaded materials (with $W_{0,N2} > W_{0,CO2}$) [40]. This micropore distribution is attributed to the porosity of the carbon component, since TiO$_2$ is non-porous. The evaluation of the micropore size distribution from the CO$_2$ adsorption isotherms at 0 °C (Fig. 1(d)) [41] confirmed the broader distribution of micropores in the raw activated carbon, with a maximum centered at the same value (ca. 0.5 nm) for both carbons but extended to micropores of larger size for the non copper loaded carbon.

For the TiO$_2$/carbon composites, the nitrogen adsorption isotherms changed towards a hybrid I/IV shape, confirming that they inherited the textural properties of both precursors according to expectations. A large decrease in the apparent surface area and microporosity (roughly 50%) was also observed for the composites. This result was rather expected for 1:1 composites, due to the non-porous nature of P25, with a low specific surface area and a type II nitrogen adsorption isotherm, Fig. 1(c).

As for the nature of the carbons, the elemental analysis and their pH$_{PZC}$ values are displayed on Table 2. Both carbons present rather large oxygen contents, an usual characteristic of lignocellulosic materials [42], which is also in agreement with the slightly acidic nature of both materials, as evaluated by the pH$_{PZC}$ values.

The analysis of the composition of sample SCu5 revealed 4.8 wt.% of copper content, as expected based on the synthesis procedure followed. The SEM and TEM images (Fig. 2) showed a good dispersion of the metallic particles of different sizes along the carbon matrix, with no visual signs of copper clustering in large metallic aggregates; the homogeneous distribution of small copper particles was also supported by the EDX mapping (Fig. 2(d)).

The chemical state and distribution of copper species in the carbon matrix was investigated by XRD and XPS (Figs. 3 and 4(a)). The XRD patterns of SCu5 were analyzed according

Table 2 – Elemental analysis and pH of the point of zero charge of the studied carbon materials. For a better comparison of the samples, the composition is shown on a dry basis.

Elemental analysis (wt.%)							pH$_{PZC}$
	C	H	N	S	O	ash	
S	80.3	1.2	0.3	0	15.1	3.1	5.3
SCu5	75.0	1.0	0.5	0	15.0	8.5	6.0

to the International Center for Diffraction Data (ICDD) and revealed the presence of Cu^0 (ICDD 4-836), Cu$_2$O (ICDD 5-0667) and CuO (ICDD 5-0661) species. Regarding the XPS analysis, the Cu 2p core level spectra of SCu5 showed the main Cu p$_{3/2}$ signal, composed of two contributions at 932.5 and 934.5 eV that are assigned to surface Cu(I) and Cu(II), with fractions of 14 and 85%, respectively. The high ratio of the areas of the satellite region (938–945 eV) and the area of the main Cu 2p$_{3/2}$ signal indicates that oxidized copper species are predominant (value Cu 2p$_{3/2}$sat/Cu 2p$_{3/2}$mp of 0.46, whereas when only Cu(II) species are present this ratio is 0.55). The small signal at 932.9 eV (accounting for only 0.7%) suggests that the surface contribution of reduced copper is almost negligible despite it was detected by XRD. This suggests that Cu^0 is located in the inner surface of the carbon, rather than in the external area.

TPR data shown in Fig. 4(b) also point out to a large contribution of Cu(II) and Cu(I) species. The profiles show two clearly distinguished areas, with decomposition peaks due to the reduction of copper in the range of 150–400 °C; the humps at higher temperatures (above 400 °C) are attributed to the reduction of oxygen species of the carbon, as they also appear in the unmodified carbon [43]. Deconvolution of TPR plots was performed using Gaussian curves to facilitate data interpretation. Three reduction peaks are presented at 190, 245 and 360 °C, that are assigned to the stepwise reduction of copper oxide (Cu^{2+} → Cu$^+$ → Cu^0), [44,45]. The reduction of bulk CuO is considered as one-step process at about 230 °C [46], while multistep patterns have been reported for supported CuO. The lower temperature of the reduction profile of SCu5 implies that the metallic species are small and highly dispersed in the carbon matrix [47,48].

Table 1 – Main textural parameters of the investigated materials obtained from gas adsorption data.

Sample	A_{BET} (m^2 g^{-1})	V_{total}[a] (cm^3 g^{-1})	V_{meso}[b] (cm^3 g^{-1})	$W_{0,N2}$ (cm^3 g^{-1})	$W_{0,CO2}$ (cm^3 g^{-1})
TiO$_2$	57	0.14	–	0.02	–
S	968	0.45	0.04	0.41	0.37
TiO$_2$/S	484	0.23	0.02	0.21	0.15
TiO$_2$/S dark	236	0.13	0.02	0.11	–
TiO$_2$/S irrad	288	0.16	0.04	0.12	0.14
SCu5	674	0.31	0.01	0.30	0.34
TiO$_2$/SCu5	292	0.17	0.04	0.13	0.23
TiO$_2$/SCu5 dark	190	0.12	0.03	0.09	–
TiO$_2$/SCu5 irrad	201	0.13	0.04	0.09	0.12

[a] Evaluated at p/p^0 = 0.9, to avoid the contribution of the inter particular voids in P25 and in the composites.
[b] Difference between V_{total} and $W_{0,N2}$.
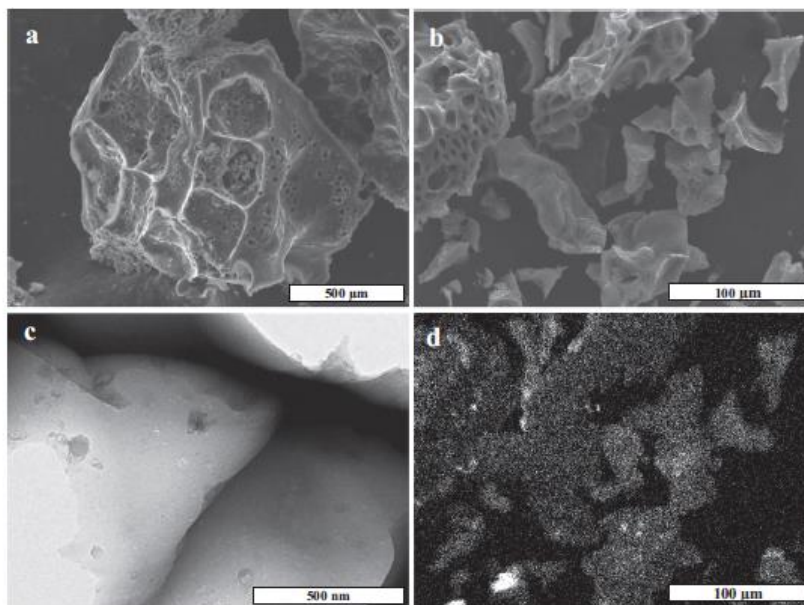
Fig. 2 – SEM images of the unloaded (a) and copper loaded (b) carbons; (c) TEM image and (d) EDX mapping of Cu for SCu5.
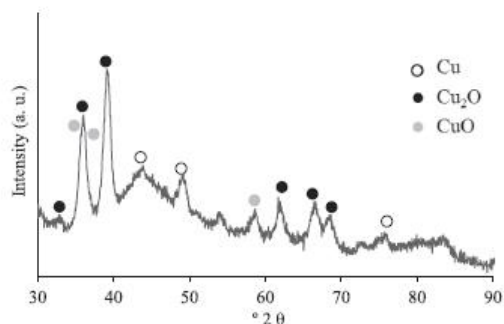
Fig. 3 – X-ray diffraction pattern of the copper-loaded carbon (sample SCu5).

3.2. Photocatalytic experiments

Due to the porous nature of the carbon materials a pre-equilibration step at dark conditions was carried out before the photocatalytic runs, to assure the same phenol concentration in solution at the beginning of the illumination for all three studied materials. This approach allowed the discrimination of the fraction of degraded pollutant in the photocatalytic reaction from that removed by adsorption – an important issue in porous catalysts. Furthermore, the use of a Pyrex filter to cut-off the UV contribution of the irradiation source also allowed to neglect the effect of direct photolysis (Fig. 5), whose contribution can be expected due to the changes in the solution concentration [49].
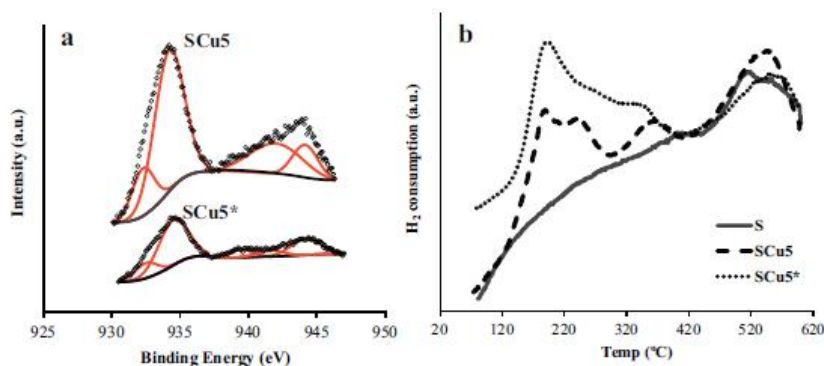
Fig. 4 – (a) Cu 2p₃/₂ XPS spectrum for sample SCu5 and the sample obtained after illumination in aqueous solution, SCu5*; (b) TPR for samples S and SCu5 and the sample obtained after illumination in aqueous solution, SCu5*. (A color version of this figure can be viewed online.)
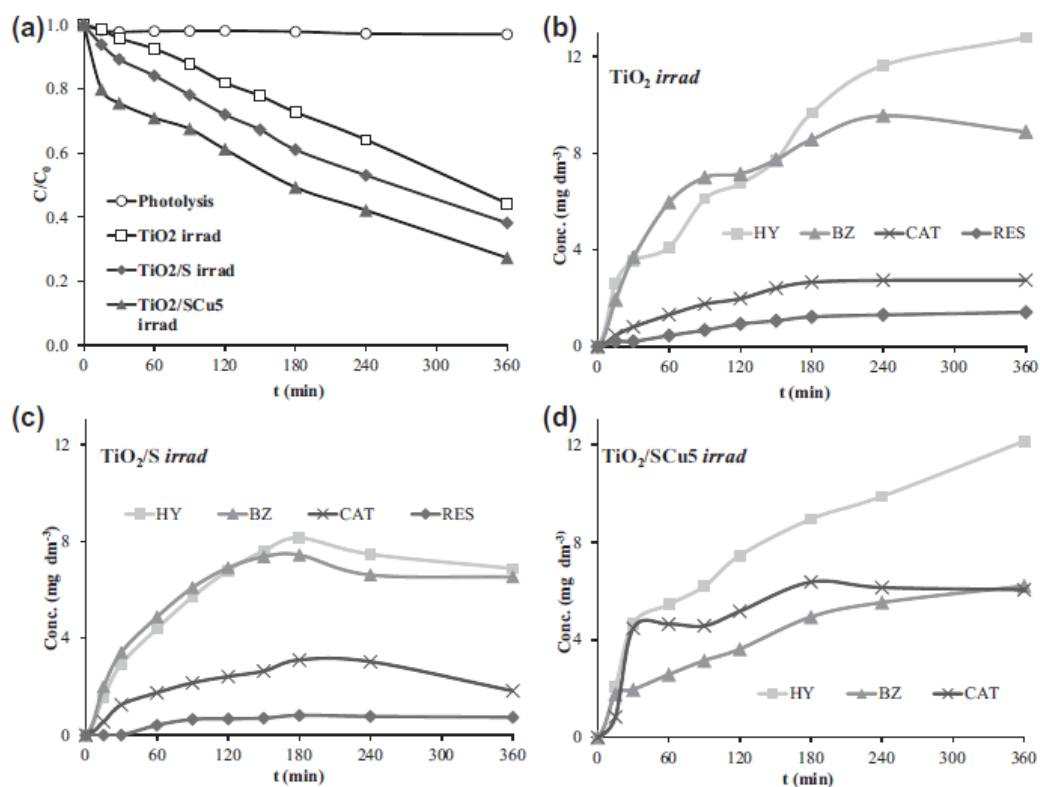
Fig. 5 – (a) Phenol concentration decay curves of the investigated materials under irradiation. (b–d) Evolution of phenol degradation intermediates detected upon irradiation of the materials investigated (HY- hydroquinone; BZ- benzoquinone; CAT-catechol, RES- resorcinol).

Hence, phenol adsorption kinetics and capacity of both S and SCu5 carbons were previously evaluated at dark conditions. The initial rate of phenol adsorption was very fast for both cases with the equilibrium uptake attained after 30 min. This is consistent with their well developed porosity, as shown in Table 1. For bare titania, the amount of phenol adsorbed at dark conditions is almost negligible (~3%), as expected given its non-porous nature. Consequently the initial phenol concentration in solution was adjusted for TiO_2/S and $TiO_2/SCu5$ (104 and 96 ppm, respectively), to achieve 85 ppm after the preequilibration step (see Fig. S2 in Supplementary Information). Additionally, irradiation of aqueous suspensions of the carbon materials confirmed their stability under our illumination conditions, as neither the carbonaceous matrix nor copper species on the metal-loaded carbon lixiviated. The lack of copper ions release to the solution is reasonable considering that the solution pH did not significantly change during the photocatalytic runs (ranging from 6.5 to 5.6).

The photocatalytic behavior of the studied catalysts under visible light is presented in Fig. 5. As stated before, under our experimental conditions the effect of direct photolysis can be neglected (phenol conversion after 6 h of irradiation was below 3% with no noticeable mineralization), while adsorption is suppressed in the pre-equilibration step; thus conversion can be exclusively ascribed to the photocatalytic efficiency of the studied materials. Several differences become clear when comparing the performance of the TiO_2/carbon composites to that of bare titania. First of all, phenol removal efficiency was slightly better for the composites, with values of 57, 62 and 73% after 6 h of irradiation, for TiO_2, TiO_2/S and $TiO_2/SCu5$, respectively. Although the conversion values may seem somewhat low for titania-based photocatalysts, it should be recalled that only visible light is used in this work (see experimental section). What is interesting to note is that phenol photooxidation efficiency was significantly enhanced for the TiO_2/carbon composites, when compared to that of TiO_2 alone. This is particularly observed for the copper-loaded carbon, which also rendered a better photocatalytic response than the composite based on the unmodified carbon.

To compare the photocatalytic activity of the studied materials, the kinetic curves in Fig. 5(a) were fitted to the Langmuir–Hinshelwood model using the simplified apparent first-order equation (Table 3). The first-order apparent rate constants followed the trend: $TiO_2 < TiO_2/S < TiO_2/SCu5$, with the latter presenting a rate constant 1.6 and 1.2 times higher than TiO_2 and composite TiO_2/S, respectively. This data shows the cooperative effect between the carbon and the inorganic component of the catalysts, as well as the copper effect on accelerating the photooxidation reaction under visible light.

189

Table 3 – Apparent first-order rate constants (k_{app}), half reaction time ($t^{1/2}$) and correlation coefficient (R^2) obtained from fitting experimental data to the Langmuir–Hinshelwood model (ln (C_0/C) = k_{app} t).

Sample	$k_{app} \times 10^{-3}$ (min⁻¹)	$t_{1/2}$ (min)	R^2
TiO₂ irrad	1.9	365	0.994
TiO₂/S irrad	2.6	267	0.999
TiO₂/SCu5 irrad	3.1	224	0.993

Secondly, although the detected intermediate products were the same for all three studied catalysts, their amount and distribution was different (Fig. 5(b–d)), with slightly higher values for bare titania than for TiO₂/carbon composites. Phenol degradation pathway using TiO₂ and TiO₂/S was similar, with quinones (hydroquinone and benzoquinone) as predominant intermediates and concentrations reaching a maximum after ca. 3 h of irradiation. In the case of TiO₂/SCu5, a marked regioselectivity is noticed towards the preferential oxidation in ortho position to form catechol. Such regioselective formation of catechol over quinones has been reported for other carbon materials under UV illumination [12] and copper catalysts in wet oxidation reactions [50] and it is considered more advantageous for the overall reaction yield, due to the higher reactivity of catechol over quinones [51,52]. Given the less energetic irradiation source used in this work, we attribute this characteristic to the copper loading, although the contribution of the carbon matrix cannot be completely ruled out.

The mineralization degree was estimated from the total organic carbon values determined in solution after 6 h of irradiation (Table 4) and considering an initial TOC value of 65 mg C L⁻¹, that corresponds to the concentration of phenol in solution after the pre-equilibration step. The highest mineralization degree after 6 h of irradiation was obtained for the copper-loaded carbon composite (ca. 42%), twice as larger than that of titania and the unmodified carbon composite. This demonstrates that the effect of copper does not only enhance the photooxidation rate (Table 3) and modifies the degradation pathway (Fig. 5) but also shows a superior photocatalytic activity under visible light.

On the other hand, similar mineralization values were obtained for bare titania and TiO₂/S composite. These are interesting results bearing in mind that, as the experiments were carried out with a constant total solid loading of

Table 4 – Total organic carbon (TOC, mg C L⁻¹) values and mineralization degree after 6 h irradiation of the catalysts. Initial TOC value was 65 mg C L⁻¹ for all the samples.

Sample	TOC (t = 360 min)	TOC$_{HPLC}$ (phenol + TQ + CAT + RES)	Mineralization (%)
TiO₂ irrad	51.3	39.2	21
TiO₂/S irrad	50.4	40.3	22
TiO₂/SCu5 irrad	37.5	32.3	42

0.5 g L⁻¹, the amount of semiconductor on the composites (ratio 1:1) is half of the amount used in the experiments with titania powders. Furthermore, the conversion obtained using titania with a total solid loading of 0.25 g L⁻¹ (the same as in the composites) was below 40%.

The difference between the values of TOC and the TOC$_{HPLC}$, computed considering the aromatic intermediates detected by HPLC (Table 4) can give us an indication of the amount of short-chain alkyl acids present in solution at the end of the reaction. In fact, the smaller difference between these values, that is, the lesser amount of acids, is observed for composite TiO₂/SCu5, which is in good agreement with the high mineralization value obtained, and points out the positive effect of copper towards an efficient photooxidation of phenol itself and its degradation products.

According to the literature, copper catalysts may suffer deactivation during oxidation reactions caused by the leaching of the copper cation under specific conditions (temperature, pH), with important consequences on the toxicity of the effluents due to the change from heterogeneous to homogeneous catalysis [53]. Hence, the spent catalysts were analyzed to detect any likely modifications in the course of the photocatalytic runs. XPS data in Fig. 4(a) shows that the chemical status of the copper species in SCu5 was not modified after irradiation in aqueous solution (SCu5*). The patterns showed the negligible contribution of Cu(0) at 932.9 eV and a similar ratio of the areas of the main peaks and the satellite regions (ratio Cu 2p₃/₂sat/Cu 2p₃/₂mp of 0.49). However, some changes appeared on the TPR profiles of sample SCu5*, Fig. 4(b). Although the patterns exhibit a similar stepwise reduction fingerprint of copper oxide, the deconvolution of the peaks showed a slight decrease (ca. 20 %) in the contribution of the peak at 190 °C – assigned to the presence of oxocations (Cu-O-Cu)²⁺, at expenses of the contribution at 245 °C, ascribed to copper oxide particles of larger sizes or to copper oxide species with lower oxidation states [44,45]. This suggests a slight photorreduction of the copper (II) species, or an agglomeration of the dispersed metallic particles. Anyhow, this is not observed on the surface of the catalysts (XPS data) nor in solution (no lixiviation of copper), indicating that the changes occur in the bulk of the catalysts.

The analysis of the textural properties of the composites after irradiation (series *irrad*) and after adsorption in the absence of irradiation (series *dark*) provides an interesting insight on the photooxidation process on porous catalysts. As seen in Table 1, the porosity of the series *irrad* and *dark* was similar, indicating a similar fraction of species adsorbed for both cases and hence suggesting that further adsorption of phenol and/or degradation intermediates in the course of the photooxidation experiments can be discarded. Also, although the porosity of the carbon is partially clogged in both cases, the composites still present relatively large pore volumes and surface areas (a significant fraction of the porosity remains unoccupied).

Summarizing, our data shows the positive effect of copper loading of the carbon component on phenol photooxidation reaction, in terms of phenol conversion, regioselectivity in the formation of intermediates, superior mineralization degree and enhanced degradation rate. To analyze the effect of copper, several aspects have to be considered.

First of all, based on the synthesis procedure of the copper-loaded carbons, we do not expect any modification of the crystalline structure of the semiconductor as the metallic species are dispersed in the carbon matrix. Indeed, the optical properties of the TiO_2/carbon composites (Fig. S3 in Supplementary Information) showed the characteristic absorption sharp edge of the anatase form of TiO_2 (predominant phase) in the UV region lying above 400 nm, and the broader background absorption in the visible light region due to the presence of the carbon component. The absorption onset was about the same for all three studied catalysts, with no differences for the Cu-loaded and unmodified carbon composites, as expected considering the low copper loading (i.e., 5 wt.%).

On the other hand, copper could act as an oxygen activator. The carbonaceous phase with well dispersed copper species is expected to create a specific fast electron transfer environment (which would minimize the recombination of the excited electron/hole pairs created upon illumination of the semiconductor), as well as specific hydrophobic sites on which molecular oxygen dissolved in water is easily adsorbed (the higher hydrophobicity of the Cu-loaded carbon is confirmed by the pH_{PZC} and water adsorption experiments, see SI). This would also favor the formation of O-radical species – promoted by the reaction with the photogenerated charge carriers – that would contribute to the enhanced photooxidation reaction. In this regard, several studies in the literature have reported that some copper-organic complex (porphyrins, phthalocyanines) have strong absorption in the visible light region and can activate O_2 or H_2O_2 to oxidize toxic organic pollutants [54–56], mimicking the activity of peroxidases [57]. Our material could follow a similar mechanism as that proposed for copper catalysts in wet oxidation reactions [58–60], initiated by the light absorption of the semiconductor. The photoexcitation of the semiconductor near the Cu(II) species can lead to the subsequent formation of O-radicals under visible light irradiation, to produce Cu^+ intermediates. The reduced metal species have high electronegativity, and thus interact with dissolved O_2 (retained in the nanoporosity of the carbon component), to regenerate the Cu(II) and further radical species responsible for the improved phenol photooxidation.

Further studies with spectroscopic tools are currently ongoing to provide experimental evidences on the formation of the radicals, expected based on the quantification of the degradation intermediates and the superior performance of the Cu-loaded carbon/TiO_2 composite in the overall phenol conversion and mineralization extent.

4.   Conclusions

This work investigated the photocatalytic performance of a copper-containing photocatalyst composite towards phenol degradation using visible light. The incorporation of the transition metal was carried out on the carbon component of the hybrid composite, by impregnation of the carbon precursor with a copper salt and subsequent chemical activation. The copper-loaded carbon displayed a well developed porosity and a good dispersion of metallic particles within the carbonaceous matrix. The analysis of the chemical status of the metal showed that oxidized copper species are dominant in the prepared material, as expected by the oxidizing atmosphere during the activation.

The performance of the synthesized titania/carbon composites for the photodegradation of phenol under visible light has been evaluated and compared to that of commercial TiO_2 under similar experimental conditions. The enhanced overall efficiency in terms of phenol conversion, mineralization degree and degradation rate found for the copper-loaded hybrid composite, showed the outstanding role of copper incorporated on the carbon matrix. This is important since the amount of semiconductor in the composites (ratio 1:1) is half of the amount used in the experiments with titania powders. The analysis of the textural properties of the composites after irradiation showed an interesting insight on the photo-oxidation process. A similar clogging of the porosity of the photocatalysts was found in dark and irradiation conditions, demonstrating that the higher conversion values cannot be solely attributed to the adsorption.

The beneficial effect of copper loading was also observed in the marked regioselectivity towards the preferential formation of catechol over quinones, which is considered to be more effective for a complete mineralization. Furthermore, the copper-loaded photocatalyst was found to be stable with no lixiviation or photorreduction of the copper species after illumination. As the optical properties of the photoactive semiconductor were not modified upon the incorporation of the copper species on the carbon component, the effect of copper is attributed to several factors including its role as oxygen activator and/or the fast electron transfer environment, which would minimize the recombination of the excited electron/hole pairs created upon illumination of the semiconductor.

Although further studies with spectroscopic tools are needed to confirm the role of copper on the superior performance of the TiO_2/Cu-carbon composite, several hypotheses may be postulated. The photooxidation reaction would be initiated by the light absorption of the semiconductor near the Cu(II) species, and leading to the formation of O-radicals under visible light irradiation. The reduced metal species would interact with dissolved O_2 adsorbed in the hydrophobic sites of the carbon component, thereby regenerating the Cu(II) and further radical species responsible for the improved phenol photooxidation.

Acknowledgments

Appendix A. Supplementary data

Supplementary data associated with this article can be found, in the online version, at http://dx.doi.org/10.1016/j.carbon.2014.04.066.

REFERENCES

[1] Oppenlander T. Photochemical Purification of Water and Air: Advanced Oxidation Processes (AOPs): Principles, Reaction Mechanisms, Reactor Concepts. Wiley-VHC; 2003.

[2] Comninellis C, Kapalka A, Malato S, Parsons SA, Poulios L, Mantzavinos D. Advanced oxidation processes for water treatment: advances and trends for R&D. J Chem Technol Biotechnol 2008;83(6):769–76.

[3] Gogate PR, Pandit AB. A review of imperative technologies for wastewater treatment I: oxidation technologies at ambient conditions. Adv Environ Res 2004;8(3–4):501–51.

[4] Ollis DF, Al-Ekabi H. Photocatalytic purification and treatment of water and air. Amsterdam: Elsevier; 1993.

[5] Pelizzetti E, Serpone N. Photocatalysis: Fundamentals and Applications. New York: Wiley; 1989.

[6] Legrini O, Oliveros E, Braun AM. Photochemical processes for water treatment. Chem Rev 1993;93(2):671–98.

[7] Fujishima A, Zhang XT, Tryk DA. TiO₂ photocatalysis and related surface phenomena. Surf Sci Rep 2008;63(12):515–82.

[8] Hashimoto K, Irie H, Fujishima A. TiO2 photocatalysis: a historical overview and future prospects. Jpn J Appl Phys 1 2005;44(12):8269–85.

[9] Leary R, Westwood A. Carbonaceous nanomaterials for the enhancement of TiO₂ photocatalysis. Carbon 2011;49(3):741–72.

[10] Matos J, Garcia A, Zhao L, Titirici MM. Solvothermal carbon-doped TiO₂ photocatalyst for the enhanced methylene blue degradation under visible light. Appl Catal A: Gen 2010;390(1–2):175–82.

[11] Bandosz TJ, Matos J, Seredych M, Islam MSZ, Alfano R. Photoactivity of S-doped nanoporous activated carbons: a new perspective for harvesting solar energy on carbon-based semiconductors. Appl Catal A: Gen 2012;445:159–65.

[12] Velasco LF, Fonseca IM, Parra JB, Lima JC, Ania CO. Photochemical behaviour of activated carbons under UV irradiation. Carbon 2012;50(1):249–58.

[13] Choi WY, Termin A, Hoffmann MR. The role of metal-ion dopants in quantum-sized TiO₂ – correlation between photoreactivity and charge-carrier recombination dynamics. J Phys Chem-Us 1994;98(51):13669–79.

[14] Inturi SNR, Boningari T, Suidan M, Smirniotis PG. Visible-light-induced photodegradation of gas phase acetonitrile using aerosol-made transition metal (V, Cr, Fe Co, Mn, Mo, Ni, Cu, Y, Ce, and Zr) doped TiO2. Appl Catal B: Environ 2014;144:333–42.

[15] Rashad MM, Elsayed EM, Al-Kotb MS, Shalan AE. The structural, optical, magnetic and photocatalytic properties of transition metal ions doped TiO₂ nanoparticles. J Alloy Compd 2013;581:71–8.

[16] Maicu M, Hidalgo MC, Colon G, Navio JA. Comparative study of the photodeposition of Pt, Au and Pd on pre-sulphated TiO₂ for the photocatalytic decomposition of phenol. J Photochem Photobiol A 2011;217(2–3):275–83.

[17] Colon G, Maicu M, Hidalgo MC, Navio JA. Cu-doped TiO₂ systems with improved photocatalytic activity. Appl Catal B: Environ 2006;67(1–2):41–51.

[18] Xin BF, Wang P, Ding DD, Liu J, Ren ZY, Fu HG. Effect of surface species on Cu-TiO₂ photocatalytic activity. Appl Surf Sci 2008;254(9):2569–74.

[19] Irie H, Kamiya K, Shibanuma T, Miura S, Tryk DA, Yokoyama T, et al. Visible light-sensitive Cu(II)-grafted TiO₂ photocatalysts: activities and X-ray absorption fine structure analyses. J Phys Chem C 2009;113(24):10761–6.

[20] Zhang YX, Huang M, Li F, Zhao H, Wen ZQ. Decoration of Cu nanowires with chemically modified TiO₂ nanoparticles for their improved photocatalytic performance. J Mater Sci 2013;48(19):6728–36.

[21] Kang P, Bobyr E, Dustman J, Hodgson KO, Hedman B, Solomon EI, et al. Bis(mu-oxo) dicopper(III) species of the simplest peralkylated diamine: enhanced reactivity toward exogenous substrates. Inorg Chem 2010;49(23):11030–8.

[22] Chen ZF, Meyer TJ. Copper(II) catalysis of water oxidation. Angew Chem Int Ed 2013;52(2):700–3.

[23] Chen ZF, Kang P, Zhang MT, Stoner BR, Meyer TJ. Cu(II)/Cu(0) electrocatalyzed CO₂ and H₂O splitting. Energy Environ Sci 2013;6(3):813–7.

[24] Nishikiori H, Sato T, Kubota S, Tanaka N, Shimizu Y, Fujii T. Preparation of Cu-doped TiO₂ via refluxing of alkoxide solution and its photocatalytic properties. Res Chem Intermed 2012;38(2):595–613.

[25] Nguyen-Thanh D, Bandosz TJ. Metal-loaded carbonaceous adsorbents templated from porous clay heterostructures. Microporous Mesoporous Mater 2006;92(1–3):47–55.

[26] Ania CO, Bandosz TJ. Highly mesoporous carbons obtained using a dynamic template method. Microporous Mesoporous Mater 2006;89(1–3):315–24.

[27] Jiang GH, Wang RJ, Jin H, Wang Y, Sun XK, Wang S, et al. Preparation of Cu₂O/TiO₂ composite porous carbon microspheres as efficient visible light-responsive photocatalysts. Powder Technol 2011;212(1):284–8.

[28] Ania CO, Bandosz TJ. Metal-loaded polystyrene-based activated carbons as dibenzothiophene removal media via reactive adsorption. Carbon 2006;44(12):2404–12.

[29] Petit C, Karwacki C, Peterson G, Bandosz TJ. Interactions of ammonia with the surface of microporous carbon impregnated with transition metal chlorides. J Phys Chem C 2007;111(34):12705–14.

[30] Hines D, Bagreev A, Bandosz TJ. Surface properties of porous carbon obtained from polystyrene sulfonic acid-based organic salts. Langmuir 2004;20(8):3388–97.

[31] Hermans S, Deffernez A, Devillers M. Preparation of Au-Pd/C catalysts by adsorption of metallic species in aqueous phase for selective oxidation. Catal Today 2010;157(1–4):77–82.

[32] Alvarez-Montero MA, Gomez-Sainero LM, Mayoral A, Diaz I, Baker RT, Rodriguez JJ. Hydrodechlorination of chloromethanes with a highly stable Pt on activated carbon catalyst. J Catal 2011;279(2):389–96.

[33] Qiu BA, Han LN, Wang JC, Chang LP, Bao WR. Preparation of sorbents loaded on activated carbon to remove H₂S from hot coal gas by supercritical water impregnation. Energy Fuel 2011;25:591–5.

[34] Mestre AS, Bexiga AS, Proenca M, Andrade M, Pinto ML, Matos I, et al. Activated carbons from sisal waste by chemical activation with K₂CO₃: kinetics of paracetamol and ibuprofen removal from aqueous solution. Bioresour Technol 2011;102(17):8253–60.

[35] Cabrita I, Ruiz B, Mestre AS, Fonseca IM, Carvalho AP, Ania CO. Removal of an analgesic using activated carbons prepared from urban and industrial residues. Chem Eng J 2010;163(3):249–55.

[36] Gregg SJ, Sing KSW. Adsorption, Surface Area and Porosity. second ed. London: Academic Press Inc.; 1982.

[37] Noh JS, Schwarz JA. Estimation of the point of zero charge of simple oxides by mass titration. J Colloid Interface Sci 1989;130(1):157–64.

[38] Moulder JF, Stickle WF, Sobol PE, Bomben KD. Standard Spectra for Identification and Interpretation of XPS Data. Eden Prairie, MN: Perkin Elmer; 1992.

[39] Poulston S, Parlett PM, Stone P, Bowker M. Surface oxidation and reduction of CuO and Cu_2O studied using XPS and XAES. Surf Interface Anal 1996;24(12):811–20.

[40] Rodríguez-Reinoso F, Sepúlveda-Escribano A. Porous carbons in adsorption and catalysis. In: Nalwa HS, editor. Handbook of Surfaces and Interfaces of Materials. London: Academic Press; 2001. p. 309–55.

[41] Pinto ML, Mestre AS, Carvalho AP, Pires J. Comparison of methods to obtain micropore size distributions of carbonaceous materials from CO_2 adsorption based on the Dubinin–Radushkevich isotherm. Ind Eng Chem Res 2010;49(10):4726–30.

[42] Andrade M, Parra JB, Haro M, Mestre AS, Carvalho AP, Ania CO. Characterization of the different fractions obtained from the pyrolysis of rope industry waste. J Anal Appl Pyrolysis 2012;95:31–7.

[43] Barrabes N, Just J, Dafinov A, Medina F, Fierro JLG, Sueiras JE, et al. Catalytic reduction of nitrate on Pt-Cu and Pd-Cu on active carbon using continuous reactor – the effect of copper nanoparticles. Appl Catal B: Environ 2006;62(1–2):77–85.

[44] Chen LY, Horiuchi T, Osaki T, Mori T. Catalytic selective reduction of NO with propylene over $Cu-Al_2O_3$ catalysts: influence of catalyst preparation method. Appl Catal B: Environ 1999;23(4):259–69.

[45] Tsoncheva T, Linden A, Areva S, Minchev C. Copper oxide modified large pore ordered mesoporous silicas for ethyl acetate combustion. Catal Commun 2006;7(6):357–61.

[46] Hartmann M, Racouchot S, Bischof C. Characterization of copper and zinc containing MCM-41 and MCM-48 mesoporous molecular sieves by temperature programmed reduction and carbon monoxide adsorption. Microporous Mesoporous Mater 1999;27(2–3):309–20.

[47] Subbaramaiah V, Srivastava VC, Mall ID. Catalytic activity of Cu/SBA-15 for peroxidation of pyridine bearing wastewater at atmospheric condition. Aiche J 2013;59(7):2577–86.

[48] Bian J, Xiao M, Wang SJ, Lu YX, Meng YZ. Carbon nanotubes supported Cu-Ni bimetallic catalysts and their properties for the direct synthesis of dimethyl carbonate from methanol and carbon dioxide. Appl Surf Sci 2009;255(16):7188–96.

[49] Priya SS, Premalatha M, Subramanian P. Elucidation of kinetics of photolysis of phenol. J Inst Eng Chem Eng 2009;90:10–6.

[50] Santos A, Yustos P, Quintanilla A, Garcia-Ochoa F. Kinetic model of wet oxidation of phenol at basic pH using a copper catalyst. Chem Eng Sci 2005;60(17):4866–78.

[51] Santos A, Yustos P, Quintanilla A, Rodriguez S, Garcia-Ochoa F. Route of the catalytic oxidation of phenol in aqueous phase. Appl Catal B Environ 2002;39(2):97–113.

[52] Ross LBC, Vinqvist MR. Phenols as antioxidants. In: Rappoport Z, editor. The Chemistry of Phenols. England: John Wiley & Sons; 2003. p. 839–909.

[53] Santos A, Yustos P, Quintanilla A, Garcia-Ochoa F, Casas JA, Rodriguez JJ. Evolution of toxicity upon wet catalytic oxidation of phenol. Environ Sci Technol 2004;38(1):133–8.

[54] Mohamed RM, Mohamed MM. Copper (II) phthalocyanines immobilized on alumina and encapsulated inside zeolite-X and their applications in photocatalytic degradation of cyanide: a comparative study. Appl Catal A: Gen 2008;340(1):16–24.

[55] Islam SM, Roy AS, Mondal P, Mubarak M, Mondal S, Hossain D, et al. Synthesis, catalytic oxidation and antimicrobial activity of copper(II) Schiff base complex. J Mol Catal A: Chem 2011;336(1–2):106–14.

[56] Cao TT, Zou CQ, Luo GF, Chen DX, Zhao XR, Li RP, et al. Heterogeneous degradation of toxic organic pollutants by hydrophobic iron(III) schiff base complex under visible irradiation. Chem J Chin U 2011;32(1):105–12.

[57] Riva S. Laccases: blue enzymes for green chemistry. Trends Biotechnol 2006;24(5):219–26.

[58] Suarez-Ojeda ME, Stuber F, Fortuny A, Fabregat A, Carrera J, Font J. Catalytic wet air oxidation of substituted phenols using activated carbon as catalyst. Appl Catal B: Environ 2005;58(1–2):105–14.

[59] Louloudi M, Mitopoulou K, Evaggelou E, Deligiannakis Y, Hadjiliadis N. Homogeneous and heterogenized copper(II) complexes as catechol oxidation catalysts. J Mol Catal A: Chem 2003;198(1–2):231–40.

[60] Santos A, Yustos P, Quintanilla A, Ruiz G, Garcia-Ochoa F. Study of the copper leaching in the wet oxidation of phenol with CuO-based catalysts: causes and effects. Appl Catal B: Environ 2005;61(3–4):323–33.

Article III- Supplementary Information

Visible light driven photooxidation of phenol on TiO₂/Cu-loaded carbon catalysts

Marta A. Andrade[1,2], Rocio J. Carmona[2], Ana S. Mestre[1], Juan Matos[3], Ana P. Carvalho[1*], Conchi O. Ania[2]*

[1] Dpt. Química e Bioquímica and CQB, Faculdade de Ciências da Universidade de Lisboa, Ed. C8, Campo Grande 1749-016 Lisboa, Portugal

[2] Adsorption and Environmental Remediation on Porous Solids (ADPOR), Dpt. Chemical Processes for Energy and Environment, Instituto Nacional del Carbón, INCAR-CSIC, Apdo. 73, 33080 Oviedo, Spain

[3] Dpt. Photocatalysis and Alternative Energies, Venezuelan Institute for Scientific Research (IVIC), 20632, Caracas 1020-A, Venezuela

*Corresponding author

apcarvalho@fc.ul.pt (AP Carvalho) conchi.ania@incar.csic.es (CO Ania)

Water Adsorption. The surface hydrophobicity of the nanoporous carbons was determined by their affinity to adsorb water. Predetermined amounts of dry samples were exposed either to water vapors in air-tight environments for 24 hours at room temperature. The amounts adsorbed were measured gravimetrically in a Setaram instrument thermal analyzer under inert atmosphere. The weight in nitrogen between 25 and 120 ºC was assumed as an equivalent to the quantity of water adsorbed on the surface. Data showed a 9.6 and 6.3 wt.% increased mass for S and SCu5 samples, respectively, confirming the more hydrophobic character of the copper-loaded carbons.
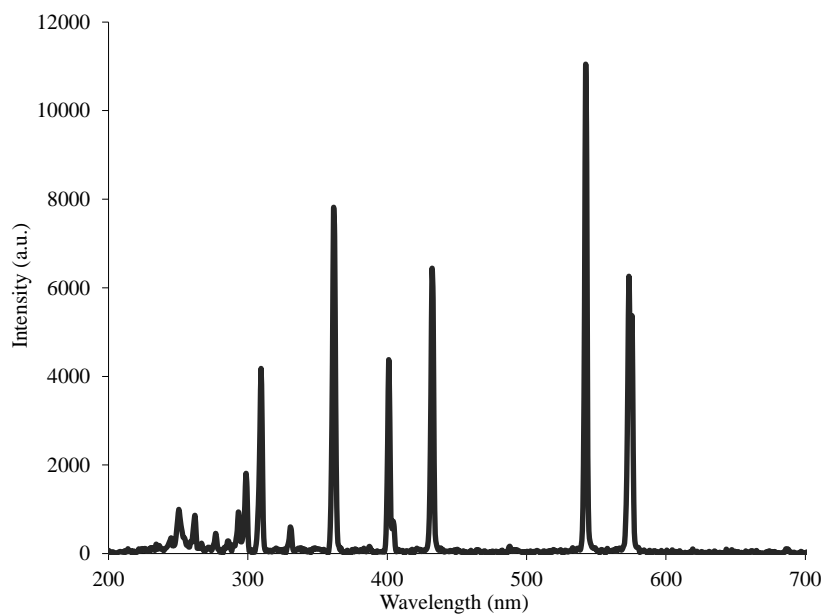
Figure S1. Emission spectrum of the high pressure mercury lamp (Helios Italquartz, 125 W) used as irradiation source for the photocatalytic experiments.
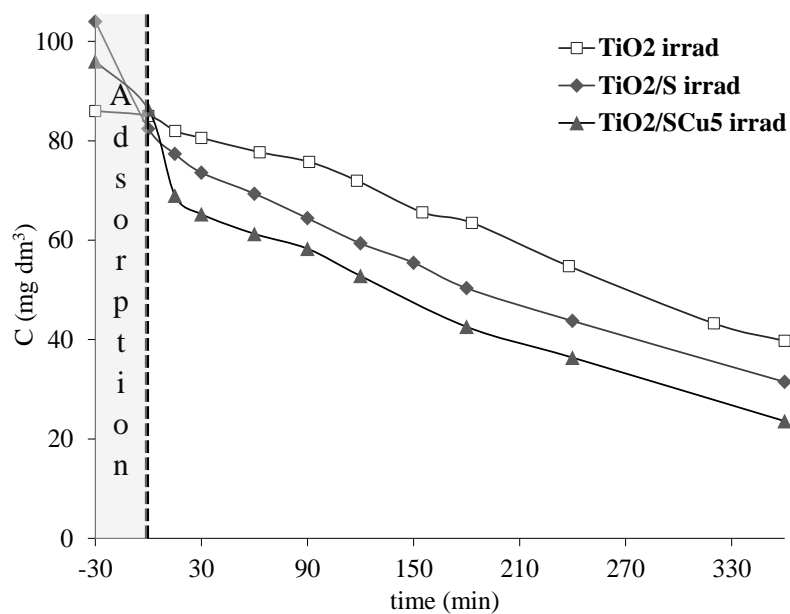
Figure S2. Phenol concentration decay curves of the investigated materials in the pre-adsorption step and under irradiation.
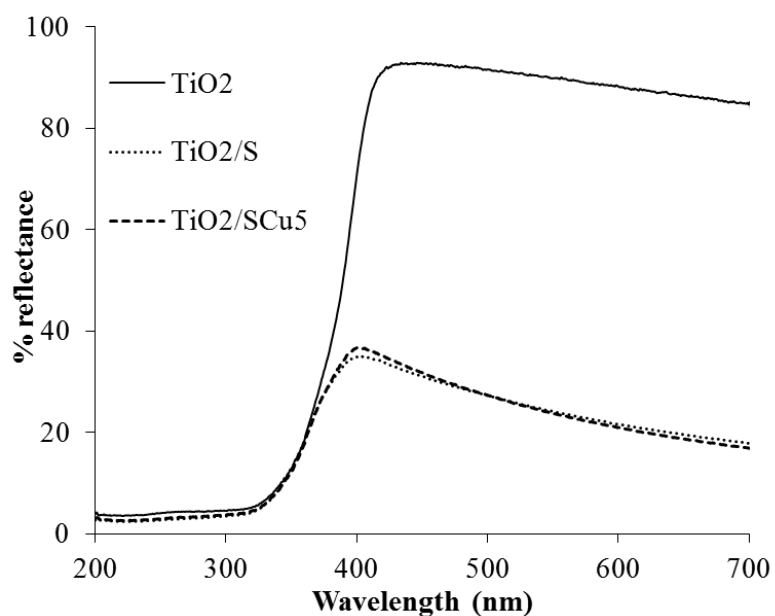
Figure S3. UV/Vis diffuse reflectance spectra of the TiO_2/carbon composites employed as photocatalysts. Spectra were recorded on a Shimadzu spectrometer (UV-2501) equipped with an integrating sphere and using $BaSO_4$ as a blank reference.

ARTICLE IV

Effect of the irradiation wavelength on the performance of nanoporous carbon as an additive to TiO₂

Marta A. Andrade [a,b], Ana S. Mestre [a], Rocío J. Carmona [b], A.P. Carvalho [a,*],
Conchi O. Ania [b,**]

[a] Centro de Química e Bioquímica, Faculdade de Ciências, Universidade de Lisboa, 1749-016 Lisboa, Portugal
[b] ADPOR Group, Department Chemical Processes for Energy and Environment, Instituto Nacional del Carbón, INCAR-CSIC, Apdo. 73, 33080 Oviedo, Spain

A B S T R A C T

We report the dependence of the photochemical activity of titania/carbon hybrid catalysts toward the degradation of phenol from solution using polychromatic light and filters. In all cases larger photooxidative efficiencies were obtained using light at 200 nm < λ < 600 nm. The incorporation of a carbon additive to TiO₂ increased the photocatalytic performance regardless the illumination conditions, although, the effect was more pronounced at λ > 200 nm. The photocatalytic runs carried out with the nonporous carbon alone confirmed a certain level of intrinsic photoactivity under both irradiation conditions. Nevertheless, a clear deactivation was evident after 60 min of irradiation suggesting that the photoactive sites in the carbon are either consumed or deactivated in the course of the reaction. The composition of the catalyst and the illumination conditions also have a strong effect on the nature of the degradation intermediates, with a marked regioselectivity toward *ortho*-substitution at high energy photons and when the carbon component is added to the catalyst composition.

1. Introduction

Heterogeneous photocatalysis has become a popular topic in environmental remediation and energy conversion [1], and the low photonic efficiency of common semiconductors is still a challenge that calls out for research to be conducted on exploring novel materials [2]. Despite carbons are strong light absorbing materials, they have been extensively investigated in a number of photo-assisted reactions [3–9 and references therein]. The incorporation of carbon materials either as additives or supports to semiconductors has been long explored and many studies have shown that adding a carbonaceous component can enhance the performance of the photoactive material in a number of photocatalytic reactions. Furthermore, the use of carbon/semiconductor catalysts overcomes the operational drawbacks associated to the use of nanosized semiconductor powders that hinder the application in continuous flow systems due to limited recovery and reuse of the catalyst [6].

The origin of the increased photoconversion yields of carbon/semiconductor catalysts has been long speculated and mostly discussed in terms of: (i) the enhanced visible light absorption of the carbon component, (ii) an enhanced mass transfer of the adsorbed pollutant from the bulk solution to the photoactive particles through the interface between the two catalyst components, and (iii) strong interfacial electronic effects between the substrate and the immobilized catalyst in the case of carbon nanostructures with high electronic mobility [3,4,10]. Also, it is considered that the photocatalytic response depends on the nature of the carbon; hence different mechanisms would apply for nanoporous carbons compared to nanostructured carbon nanotubes, fullerenes and graphene. Our recent investigations have also proved the photoactivity of semiconductor-free nanoporous carbons under UV and visible light [11–13] and their ability to photogenerate oxygen reactive species as the key aspect to achieve enhanced degradation yields of pollutants from solution.

The origin and dependence of the carbon/light interactions with the irradiation source still remains uncertain [14–16]. For instance, it is well known that only photons with λ < 400 nm can be absorbed by TiO₂ to induce the excitation of electrons from the valence to the conduction band, allowing the charge separation that would eventually lead to the desired pollutant's degradation reaction [1,2]. Simultaneously, many organic compounds present a strong absorption of light at λ < 400 nm, leading to direct degradation in the absence of a catalyst (photolytic reaction). When using

* Corresponding author. Fax: +351 217500088.
** Corresponding author. Fax +34 985 118846.
E-mail addresses: apcarvalho@fc.ul.pt (A.P. Carvalho), conchi.ania@incar.csic.es (C.O. Ania).

hybrid carbon/semiconductor catalysts, the situation is more complex due to the above-mentioned carbon/light interactions. Indeed, by using monochromatic light we have recently reported the ability of certain semiconductor-free carbons to convert photons from the visible spectrum in chemical reactions [13].

Knowing this, and since the use of carbon in photochemical applications has recently gained considerable attention, in this work we aimed at exploring the influence of the irradiation source on the photooxidative activity of a hybrid titania/carbon catalyst. Our approach consisted in exposing the catalysts to varied illumination conditions using filters to cut-off the light, while evaluating the effect on the photoconversion of phenol from aqueous solution and on the degradation mechanism. As additive to the semiconductor we have selected a nanoporous carbon prepared by chemical activation of a lignocellulosic precursor, in line with a current interest of our research group [17]. Furthermore, our previous studies have shown the good performance of this material as additive to titania with increased photooxidation conversions under sunlight [18]. We herein describe the performance of these materials under different illumination conditions, aiming at clarifying the role of the carbon matrix upon irradiation at high and low wavelengths. Thus the outcome of our previous studies is used only for data interpretation. Phenol was selected as model compound representing a toxic pollutant frequently found in wastewater and classified as a high environmental risk according to the European and American Environmental Protection Agencies.

2. Experimental

2.1. Materials synthesis

A nanoporous carbon prepared by chemical activation of a lignocellulosic industrial residue – discarded sisal ropes – was selected as carbon material for the preparation of the titania/carbon photocatalysts. Details on the synthesis of sisal-derived carbons have been reported elsewhere [18]. Briefly, 1 cm long sisal pieces were impregnated with a K_2CO_3 solution (weight ratio sisal: K_2CO_3 of 2:1) and activated in a horizontal furnace at 700 °C for 1 h under N_2 flow (5 cm^3 s^{-1}). After the activation, the sample was thoroughly washed with distilled water until pH 7 and dried at 100 °C. The sample will be labeled as S. Commercially available TiO_2 (P25 Degussa, Evonik) was used as a standard catalyst for the photocatalytic activity. The hybrid titania/carbon photocatalyst with a 1:1 weight ratio composition was prepared by physical mixture of TiO_2 and carbon powders in a mortar. The sample will be labeled as TiO_2/S.

2.2. Photodegradation runs

Phenol photodegradation experiments were carried out at room temperature using a photoreactor of 0.5 L capacity and a loading catalyst ratio of 0.5 g L^{-1}. The irradiation source was provided by a high pressure mercury lamp (Helios Italquartz, 125 W) emitting in the UV and visible light spectrum (between 200 and 600 nm, see Fig. S1 in the Electronic Supplementary information); the lamp was vertically suspended in a cylindrical, double-walled jacket cooled by flowing water, immersed in the solution. The water cell was used to control the temperature during the experiments, preventing any overheating of the suspension due to the irradiation. The reactor was open to air in all the experiments to ensure that enough oxygen was present in the reaction solution. The series of experiments were performed in the photoreactor with a quartz jacket (λ > 200 nm) or glass (pyrex) jacket (λ > 360 nm) that acts as a cut-off filter of the irradiation below 360 nm, and hence avoids the photolytic reaction in the catalytic runs (spectra in Fig. S1). The incident photon flux emitted by the lamp and transferred to

the photoreactor in both irradiation conditions was measured by chemical actinometry [19]. The values determined were 9.1×10^{-6} and 1.35×10^{-5} Einstein s^{-1} for the lamp with and without the pyrex filter, respectively.

In each run, the catalyst was added to the phenol solution under vigorous stirring (900 rpm) and allowed to equilibrate in dark conditions for 30 min. This step accounts for the adsorption on the porous catalysts and assures a similar phenol concentration in solution when the catalysts are illuminated (86 mg L^{-1}) [18]. After the equilibration step, the suspension was irradiated for 360 min. During the irradiation, small aliquots of the solution (~1 cm^3) were taken out at predetermined time intervals, and analyzed by reverse-phase HPLC (Spherisorb C18 column 125 mm × 4 mm, methanol to water 5:95, 30 °C, 0.7 cm^3 min^{-1} flow rate, photodiode array detector using the corresponding wavelengths) to determine the residual concentration of phenol (269 nm) and its aromatic degradation products, namely quinones (1,4-benzoquinone—245 nm and 1,4-dihydroxybenzene—288 nm), 1,2-dihydroxybenzene (o-catechol—275 nm), 1,3-dihydroxybenzene (resorcinol—273 nm), 1,3,5-trihydroxybenzene (264 nm) and 1,2,4-trihydroxybenzene (482 nm). All patterns were Aldrich 99% reagents. The samples were previously filtered using cellulose filters with mean pore size of 0.45 μm. All the experiments were done in duplicate with deviations below 5% in all cases; reported data represent the average values. Total organic carbon (TOC) of the solution at the end of each run was also measured in a TOC-V analyzer.

Experiments were also carried out in the absence of irradiation (series dark), for further comparison between the extent of phenol photodegradation and the uptake due to adsorption. The stability of the photocatalysts under irradiation was also explored upon illumination of the catalyst's suspensions in water in the absence of phenol.

2.3. Characterization of the catalysts

The physicochemical and textural characterization was carried out on the fresh and used catalysts (after the photocatalytic runs). The porosity of the samples was characterized by measuring the N_2 and CO_2 adsorption isotherms at −196 and 0 °C, respectively (ASAP 2020 and Tristar 3000, Micromeritics). Before the experiments, the samples were outgassed under vacuum (ca. 10^{-3} torr) at 120 °C overnight. The isotherms were used to calculate the specific surface area, A_{BET}, total pore volume, V_{total}, while the micropore volumes were analyzed using the Dubinin–Radushkevich formulism to the N_2 and CO_2 adsorption data ($W_{0,N2}$, $W_{0,CO2}$) [20]. For the characterization of the spent catalysts, the samples were recovered by filtration, dried overnight at 60 °C and then outgassed as detailed above. Elemental analysis was carried out in LECO CHNS-932 and LECO VTF-900 automatic analyzers. Fourier transformed infrared spectroscopy (FTIR) was carried out using a Nicolet Magna-IR 560 spectrometer with a high-sensitivity MCT/A detector. Spectra were obtained using the attenuated total reflectance method (ATR) on powdered samples, without KBr addition. Each spectrum was obtained by collecting 300 interferograms with 4 cm^{-1} resolution. The optical features of the catalysts were determined by UV–vis diffuse reflectance spectroscopy, recorded on a Shimadzu spectrometer (UV-2501) equipped with an integrating sphere and using $BaSO_4$ as a blank reference. Measurements were recorded in the diffuse reflectance mode (R) and transformed to a magnitude proportional to the extinction coefficient through the Kubelka–Munk function, F($R\infty$). The morphology of the samples was observed by Field Emission Gun Scanning Electron Microscopy (FEG-SEM) with an X-ray Energy-Dispersive System (EDS) in a JEOL JSM-7001F, and in a FE-SEM apparatus (QuantaSEM, FEI), using an accelerating voltage of 25 kV.

3. Results and discussion

Before the photocatalytic runs, the catalysts were thoroughly characterized by different techniques. A more elaborated discussion on the physicochemical properties of the nanoporous carbon used as additive was reported in a previous study [18], however selected properties are herein shown for data interpretation purposes. It should be pointed out that the carbon additive is a nanoporous material with high surface area and pore volume (Table 1), thus the hybrid carbon/titania photocatalysts also shows an outstanding porosity. The carbon material is also characterized by a slightly acidic character (surface pH of 6.3), in agreement with a quite large oxygen content (elemental analysis rendered 15.9, 82.2 and 1.2 wt.% of oxygen, carbon and hydrogen, respectively, Table S1). Additional characterization of the carbon component was carried out by infrared and diffuse reflectance spectroscopy (Fig. 1). The infrared spectra of the nanoporous carbon (Fig. 1(b)) showed the presence of the broad band between 3200 and 3600 cm^{-1} (representing the vibrations of OH moieties in water molecules and/or structural OH groups), a week band at 1000 cm^{-1}, representing C—O—vibrations, a more intense band at ca. 1400 cm^{-1}, representing C—OH groups and a sharper band at 1672 cm^{-1}, accounting for C=C from the aromatic ring mode conjugated carbonyl and carboxylate groups. A similar infrared pattern was obtained for the carbon/semiconductor photocatalysts, as expected since it was prepared by physical mixture of both components. For the same reason, no changes were detected in the optical features of the catalysts; as seen in Fig. 1(a), the reflectance spectrum of titania showed the characteristic absorption sharp edge of the anatase in the UV region lying above 400 nm; the incorporation of the carbon material results in a broader background absorption in the visible light region, while the absorption onset is the same.

In photocatalytic reactions involving porous materials, several reactions occur simultaneously upon irradiation of the catalysts (namely adsorption, direct photolysis and photocatalysis) and must be considered when comparing the performance of different systems. Due to the characteristics of our irradiation source (i.e., wavelength and incident flux, Fig. S1), the photolytic breakdown of phenol at λ > 200 nm was quite large in terms of phenol conversion, reaching similar values of those obtained when the catalysts are irradiated (Table 2). However, the mineralization extent of the photolysis – estimated from the TOC values in solution after 6 h of illumination – was very poor (ca. 5% for direct photolysis and 55% in the presence of the catalyst, Table 2). This is important as it shows the need of an appropriate catalyst to further degrade the intermediates, thus enabling the comparison of the efficiency of both irradiation set-ups. Similar mineralization values have been reported in the literature for direct photolysis of phenol aqueous solutions at λ > 200 nm using much powerful irradiation sources
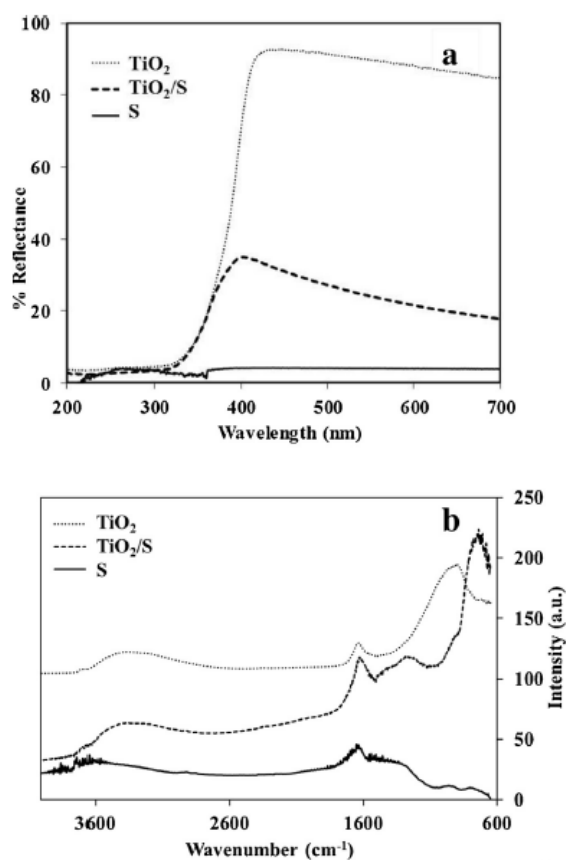
Fig. 1. Diffuse reflectance (a) and infrared (b) spectra of the catalysts.

(ca. 500 W) [21,22]. When the light below 360 nm was cut-off with the pyrex filter, the photolytic reaction was largely suppressed as inferred from the low phenol conversion after 6 h (i.e., 3%) with no noticeable mineralization. This finding was quite expected considering that the fraction of light absorbed by the aqueous phenol solution above 360 nm is negligible [13] and the dependence of the energy of the photons with the emission wavelength of the irradiation source [22].

Table 1
Main textural parameters obtained from gas adsorption data of the fresh and used catalysts (after the photocatalytic runs) at different illumination conditions. Data corresponding to the materials after the pre-equilibration in the dark (adsorption) is also included for comparison.

	S_{Bet} (m² g⁻¹)	V_{Total}[a] (cm³ g⁻¹)	$V_{Mesopores}$[b] (cm³ g⁻¹)	$W_{0,N2}$[c] (cm³ g⁻¹)	$W_{0,CO2}$[c] (cm³ g⁻¹)
TiO₂	57	0.4	–	0.02	–
S	968	0.45	0.04	0.41	0.37
TiO₂/S	484	0.23	0.02	0.21	0.16
S_{dark}	351	0.17	0.02	0.15	0.24
TiO₂/S_{dark}	236	0.13	0.02	0.11	–
$S_{λ>200nm}$	354	0.17	0.02	0.15	0.29
TiO₂/$S_{λ>200nm}$	288	0.16	0.04	0.12	0.14
$S_{λ>360nm}$	388	0.18	0.03	0.17	0.29
TiO₂/$S_{λ>360nm}$	288	0.16	0.04	0.12	0.14

[a] Evaluated at $p/p^0 \sim 0.9$ to avoid the contribution of interparticle voids.
[b] Difference between V_{Total} and $W_{0,N2}$.
[c] Evaluated from the Dubinin–Raduskevich approach.

Table 2
Phenol degradation, Total Organic Carbon values (TOC, in mg C L^{-1}) and mineralization degree after 6 h of irradiation of the catalysts under varied illumination conditions. Initial TOC values correspond to the phenol concentration in solution after the pre-adsorption step.

	Conversion (%)[a]	TOC (mg C L^{-1})	TOC$_{HPLC}$[b] (mg C L^{-1})	Mineralization (%)
Photolysis$_{\lambda>360nm}$	3	64.8	64.8	1
S$_{\lambda>360nm}$	21	61.5	61.5	5
TiO$_2{}_{\lambda>360nm}$	54	51.3	39.2	21
TiO$_2$/S$_{\lambda>360nm}$	62	50.4	40.3	22
Photolysis$_{\lambda>200nm}$	81	62.1	17.4	5
S$_{\lambda>200nm}$	85	30.6	12.6	53
TiO$_2{}_{\lambda>200nm}$	70	43.6	25.2	33
TiO$_2$/S$_{\lambda>200nm}$	84	29.3	11.4	55
2xTiO$_2$/S$_{\lambda>200nm}$	88	24.6	15.3	62

[a] Catalyst loading 0.5 g L^{-1}; 86 mg L^{-1} phenol in solution at the beginning of illumination.
[b] Values calculated considering the aromatic intermediates detected by HPLC.
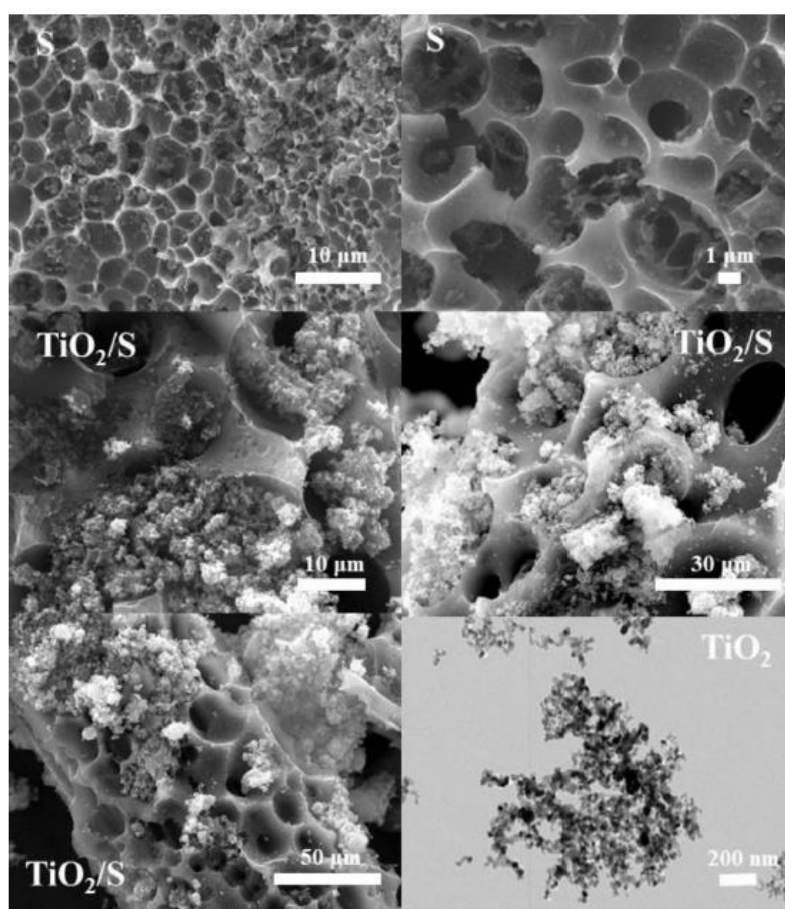
Fig. 2. SEM images of the catalysts.

As the yield of photolysis is highly dependent on the concentration of phenol in solution [23], controlling the extent of the non-catalyzed reaction is of paramount importance for comparing the performance of the catalysts. For this reason, the photocatalytic runs were carried out on catalysts previously exposed to phenol (pre-adsorption step), so as to allow the adsorption of the pollutant on the porosity at equilibrium conditions, and to maintain the same initial concentration of phenol in the solution at the beginning of the illumination period. This procedure also enables to discriminate between the adsorption and photooxidation reactions, as both may take place simultaneously in porous catalysts.

The first step then consisted on evaluating the adsorption capacity of the catalysts at dark conditions (series dark) and the time needed to reach equilibrium during the pre-loading step. Phenol

95
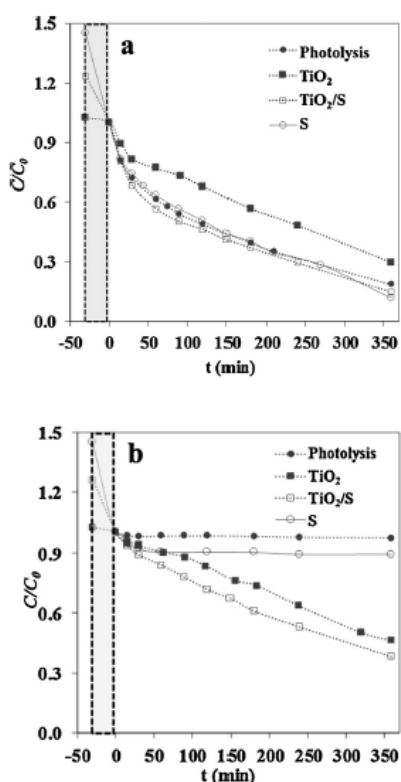
Fig. 3. Phenol concentration decay curves with the illumination time after irradiation at (a) $\lambda > 200$ nm and (b) $\lambda > 360$ nm. Negative times highlighted in shaded correspond to the pre-adsorption period of 30 min to equilibrate each system. Catalyst loading 0.5 g L^{-1}; 86 mg L^{-1} phenol in solution at the beginning of illumination.

adsorption kinetics was quite fast for all the catalysts, with the equilibrium being reached after 30 min (Fig. S2). The amount adsorbed by titania powders was negligible (below 3%), in agreement with the low porosity of the semiconductor (Table 1). In contrast, it was quite large for the carbon (ca. 145 mg g^{-1}) and the carbon/titania photocatalyst (ca. 70 mg g^{-1}), which is attributed to the open porosity of the catalyst provided by the carbon component (Table 1). Along with surface area and micropore volume, the open pore structure of the carbon matrix is also seen in the SEM images (Fig. 2) showing a globular structure with large cavities, characteristic of materials with high external area, hence favoring the adsorption kinetics. At converse, the uptake was almost negligible (below 3%) for bare titania, as expected based on its non-porous nature. Hence, the concentration of phenol in the solution was adjusted for each run considering the adsorption capacity of each catalyst, so as to obtain a constant value of 86 mg L^{-1} phenol in solution after the pre-equilibration step.

Figs. 3 and 4 show the evolution of phenol and its degradation intermediates in solution at different irradiation conditions. Several differences become clear; first, higher phenol conversions and mineralization were obtained when the catalysts are irradiated using light at >200 nm (lamp without filter); this is consistent given the higher energy of the photons and the higher photon flux of the arriving radiation at the system measured by chemical actinometry. Second, phenol photooxidation conversion after 6 h was higher for TiO₂/S compared to bare TiO₂ and regardless the illumination

conditions (Table 1), although, the effect was more pronounced at $\lambda > 200$ nm (Fig. 3(a)). This is most remarkable bearing in mind that the amount of semiconductor in the catalyst (weight ratio 1:1) is half of the amount used in the experiments with titania, since the photocatalytic runs were carried out using a constant total solid loading of 0.5 g L^{-1}.

The extent of mineralization followed a similar trend, being the beneficial effect of the carbon more significant when the catalysts are exposed to light at $\lambda > 200$ nm as seen in Table 1; while the values obtained for TiO₂ and TiO₂/S exposed to light at $\lambda > 360$ nm are rather similar, phenol mineralization increased by 1.5 times for the hybrid carbon/titania photocatalyst at $\lambda > 200$ nm, with half the amount of titania as mentioned before. The higher efficiency of the photooxidation when the catalysts were exposed to more energetic light (lower wavelength) is in agreement with the light absorption features of the semiconductors, since it is well known that for titania only photons with energy above 3.2 eV (corresponding to $\lambda < 400$ nm) are capable of promoting the electrons from the valence band.

For the carbon component, our previous studies using monochromatic light have shown that the intrinsic photochemical activity of nanoporous carbons (if any) is higher under UV light [13]. It is also interesting to note the distinct performance of the carbon material alone (in the absence of titania) with the irradiation source. When exposed to light at $\lambda > 200$ nm in the absence of the semiconductor, a relatively high photooxidation yield was obtained. In fact, similar results were obtained for the nanoporous carbon ($S_{\lambda > 200 \text{ nm}}$) and for carbon/titania (TiO₂/$S_{\lambda > 200 \text{ nm}}$) under the same illumination conditions, indicating that the carbon material presents a certain level of self-photochemical activity. The conversions however dropped significantly when the pyrex filter was used to cut-off the light (Table 1), particularly for the carbon alone.

To further explore the superior performance of the hybrid carbon/titania photocatalyst compared to bare titania, additional photocatalytic runs were carried out varying the total solids loading between 0.25 and 1 g L^{-1} (Fig. 5(a) and (b)). Data of photolysis corresponding to zero catalysts loading is also plotted for comparison. The beneficial effect of the carbon component in the catalyst is clearly seen; for the experiments performed using a titania loading of 0.25 g L^{-1}, phenol conversion was under 40%, far below the 84% obtained for the hybrid carbon/titania photocatalyst with a total solids loading of 0.5 g L^{-1}, thus using an identical amount of TiO₂. When the total loading of the photocatalyst is raised to 1 g L^{-1} (sample labeled as 2xTiO₂/S, see Fig. 5), for which the amount of semiconductor was doubled, a high and almost unchanged phenol conversion was observed, whereas the mineralization extent improved (Table 1). An enhanced performance of the yield with increasing the catalyst loading is rather common in heterogeneous photocatalysis [24]; in this case it also seems consistent as both individual components of TiO₂/S show some photoactivity (although very different) under adequate irradiation (Table 1).

The analysis of the porous features of the catalysts after the photocatalytic runs also revealed interesting information. First of all, it is worth noting that the accessible porosity of the nanoporous carbon after the pre-equilibration step in darkness (S_{dark}) was largely reduced, which was expected considering the phenol uptake of this carbon. Second, the textural features of the used catalysts (after the photocatalytic runs) are larger than those of their corresponding counterparts after dark adsorption (Table 1), which indicates a lower pore clogging of the used catalysts after the photocatalytic runs than after the adsorption in dark conditions. The effect is similar for both illumination conditions, although it was more pronounced when the catalysts were exposed to light at $\lambda > 200$ nm.

This is more clearly evidenced in the analysis of the narrow microporosity by means of the CO₂ adsorption isotherms at
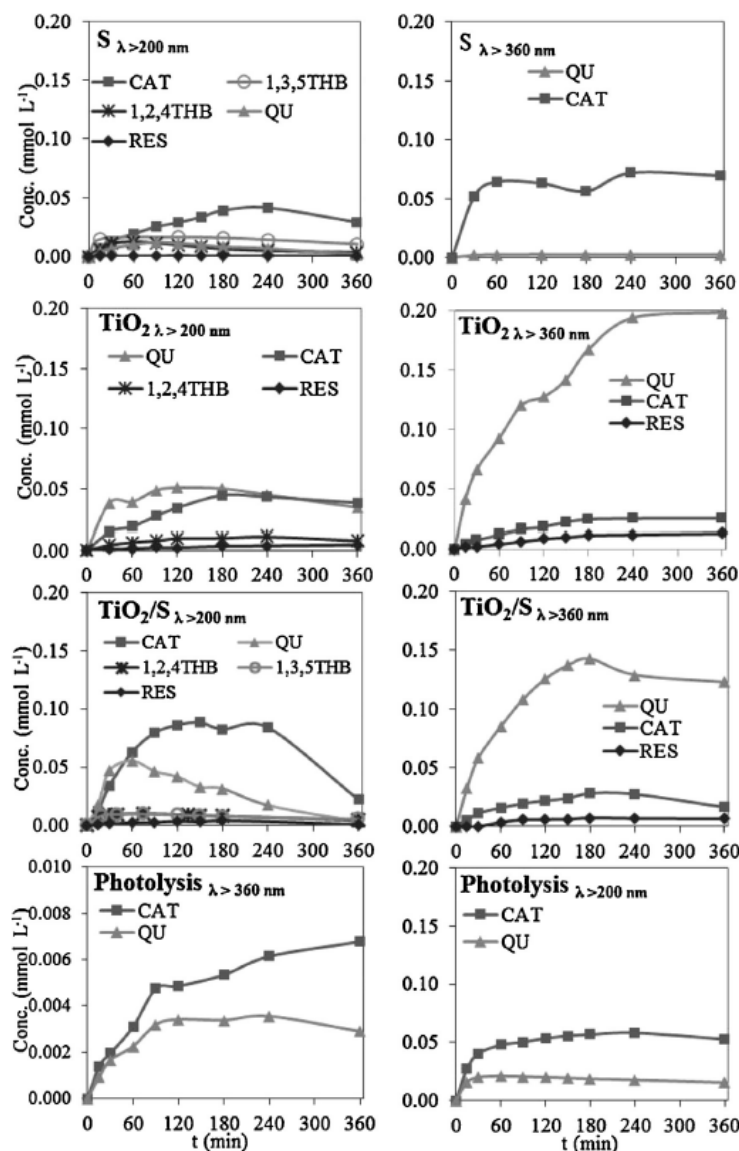
Fig. 4. Evolution of phenol degradation intermediates upon irradiation under different illumination conditions; QU-quinones; BZ-benzoquinone; CAT-catechol, RES-resorcinol; 124THB-1,2,4-trihydroxybenzene; 135THB-1,3,5-trihydroxybenzene. Catalyst loading 0.5 g L^{-1}; 86 mg L^{-1} phenol in solution at the beginning of illumination.

0 °C (Fig. 6). According to literature the adsorption of phenolic compounds on hydrophobic nanoporous carbons at low coverage occurs preferentially on the narrow micropores [25,26]. Since the microporosity of the hybrid carbon/titania photocatalyst is inherited from the carbon component, investigating the evolution of the volume of narrow micropores allows clarifying the fate of the fraction of phenol initially adsorbed on the porosity of the carbon material in the course of the photocatalytic reaction.

The higher micropore volume of the catalysts illuminated for 6 h compared to the accessible porosity after the pre-equilibration step in darkness (series dark) demonstrates that neither phenol nor its intermediates are accumulated (adsorbed) in the micropore network but rather decomposed due to the photocatalytic reaction. During the photocatalytic runs, a small fraction of the pollutants may be decomposed inside the carbon matrix, since the fraction retained in the porosity decreased compared to the starting of the illumination, and the concentration in solution does not rise. This is in agreement with our previous studies reporting the photodegradation of the adsorbed fraction for some nanoporous carbons [11,13].

Interestingly, the same trend was seen when the nanoporous carbon alone was exposed to light (Table 1), which points out to
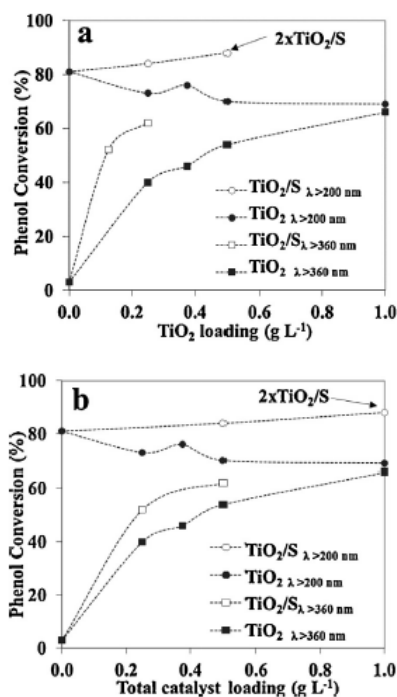
Fig. 5. Effect of the catalyst loading at different irradiation conditions: (a) effect of TiO₂ loading; (b) effect of the total catalyst loading (symbols represent experimental values while lines are guides for the eye). Catalyst loading 0.5 g L⁻¹; 86 mg L⁻¹ phenol in solution at the beginning of illumination.
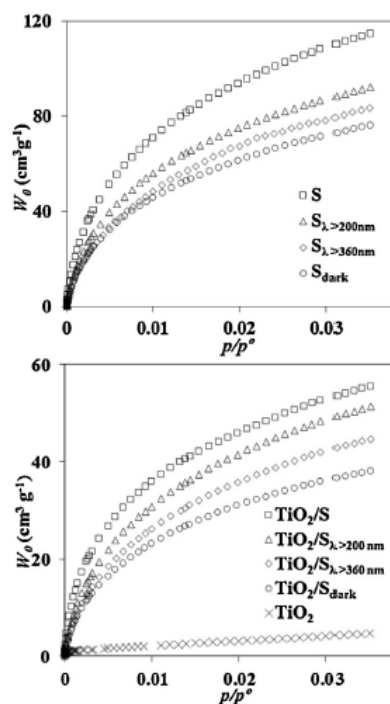
Fig. 6. CO₂ adsorption isotherms obtained at 0 °C on the as-received and exposed catalysts at different illumination conditions.

some level of photochemical activity for this carbon. Based on our previous studies [12], we attribute this to the ability of the carbon material to generate oxygen radicals when exposed to high energy light. The large amount of polyhydroxylated degradation intermediates also corroborates this. The concentration decay curves of phenol and intermediates upon irradiation of sample S showed an interesting pattern. When exposed to light at λ > 200 nm (high energy), the conversion of phenol is quite similar to that obtained from direct photolysis (Fig. 3), while the time evolution of intermediates detected in solution is markedly smaller (Fig. 4). This behavior is not accompanied by a clogging of the pore structure of the carbon (Fig. 6 and Table 1), which confirms that the disappearance of phenol (and intermediates) from the aqueous solution cannot be attributed to the accumulation in the porosity. Additionally, an outstanding mineralization was achieved (ca. 53% for $S_{λ > 200 nm}$), a value comparable to that of TiO₂/S and higher than that of direct photolysis and bare titania (Table 1).

When the filter is used (light at λ > 360 nm), the conversion of phenol obtained upon irradiation of the nanoporous carbon alone is quite small; the concentration decay curve displays an interesting shape with a sharp decrease at short irradiation times (Fig. 3) followed by a steady conversion above 60 min. As discussed above, the accessible microporosity of the carbon after the photocatalytic runs is still higher than that after dark adsorption, indicating some photoactivity. However, the plateau indicates that the photochemical reaction is stopped after 60 min of illumination; under these illumination conditions (λ > 360 nm) the contribution of direct photolysis of phenol can be neglected, thus data suggests that the photoactive sites of the carbon under visible light are consumed or deactivated in the course of the reaction.

In a previous study [18] we observed that the incorporation of the nanoporous carbon in the catalyst does not affect the degradation mechanism of phenol under visible light. Indeed, as seen in Fig. 4, similar intermediate patterns were obtained for TiO₂ and TiO₂/S when exposed to light at λ > 360 nm, with quinones (due to the pH dependence of hydroquinone and benzoquinone, these are discussed together as total quinones, QU) as predominant compounds. The concentration of intermediates steadily increases with time for titania; in contrast it reaches a maximum after ca. 3 h of irradiation for TiO₂/S, pointing out a faster degradation of phenol and its intermediates.

A different trend appeared when the samples were irradiated with light at λ > 200 nm. Overall, the intermediate products are the same as those detected when the filter is applied, although their amount and distribution is different. A marked regioselectivity is noticed towards the preferential oxidation in the *ortho* position to form catechol (over *meta* or *para* positions in resorcinol and hydroquinone) in the case of samples S and TiO₂/S and for the non-catalyzed reaction (photolysis λ > 200 nm). In the case of TiO₂, the amount of CAT increased although QU are still the major intermediates. Interestingly, a similar regioselectivity to the formation of CAT over QU has been reported for other nanoporous carbons under UV illumination [11]. This is important since CAT has a higher reactivity over QU [27], which would account for the improved conversion of phenol upon irradiation at λ > 200 nm. Additionally, trace concentrations of trihydroxylated benzenes (i.e., 1,2,4-trihydroxybenzene and 1,3,5-trihydroxybenzene) were detected for all three catalysts, not seen in the photolytic breakdown under the same illumination conditions nor upon irradiation with light at λ > 360 nm. The formation of polyhydroxylated subproducts suggests that more hydroxyl

radicals are involved when the reaction is carried out using light at $\lambda > 200$ nm and catalysts.

Doubling the amount of TiO$_2$ in the catalyst (sample 2xTiO$_2$/S) reversed the distribution of the intermediates (Fig. S3 in Supplementary Information), showing again the predominance of QU over CAT, following the same trend as TiO$_2$. Thus it seems that the distribution of the intermediates depends on the composition of the catalysts, with QU being favored over CAT at low energy photons and when titania is the major component of the photocatalyst (either TiO$_2$ alone or high loadings in the catalyst), and vice versa when the carbon component is added to the catalyst composition. Both cases indicate that the photooxidation of phenol proceeds through the *ortho*- and *para*-substitution, which are the preferred positions in electrophilic substitutions of aromatic rings [27]. The formation of polyhydroxylated compounds along with the accumulated amounts of intermediates – suggesting lower photooxidation reactivity than phenol itself – are also characteristics of electrophilic mediated pathways.

Another distinctive aspect of the photocatalytic runs under different illumination conditions is the variation of the solution pH observed for all the studied systems (photolysis and photocatalysis). The initial solution pH decreased between 1 and 3 pH units within the first 3 h of irradiation using light at $\lambda > 200$ nm, as opposed to a fall by 0.5 units when the filter was used (light at $\lambda > 360$ nm). Such pH variation is consistent with the difference between TOC and TOC$_{HPLC}$ values (Table 1), which account for the amount of short-chain alkyl acids present in solution at the end of the reaction. In fact, a smaller difference between these values, that is, a lesser amount of acids, is observed when a higher mineralization is obtained. This is also consistent with the above-mentioned mechanism based on electrophilic additions leading to the regioselective oxidation in the *ortho* position, which are more favored at acidic pH [27].

Additionally, the stability of the catalysts was confirmed upon irradiation of suspensions in water in the absence of phenol. Regardless the illumination conditions (lamp with and without filter), the carbon component was found to be stable when illuminated alone or in the hybrid TiO$_2$/carbon catalysts, as inferred from the elemental analysis of the samples (Table S1). On the other hand, according to the results previously obtained with TiO$_2$ powders and TiO$_2$/carbon composites [28] the slightly acidic characteristics of the sisal based allow us to anticipate the re-use of the catalysts in consecutive phenol photooxidation cycles.

4. Conclusions

We have investigated the dependence of the photochemical activity of hybrid titania/carbon photocatalysts with the wavelength of the irradiation source, by using polychromatic light and a pyrex filter to remove the contribution at $\lambda < 360$ nm. Phenol photooxidative efficiencies were larger at $200 < \lambda < 600$ nm for both the photolytic and catalyzed reactions. The use of a nanoporous carbon as additive increased both the photoconversion of phenol and the mineralization extent using half of the amount of the semiconductor. The effect was more pronounced at $\lambda < 200$ nm. Photocatalytic runs carried out with the carbon material alone (in the absence of titania) demonstrated a certain level of intrinsic photochemical activity of the nanoporous carbon additive under both irradiation conditions. When the light is filtered at $\lambda > 360$ nm, the conversion of phenol upon irradiation of the nanoporous carbon alone dropped significantly with a steady conversion above 60 min, suggesting that the photoactive sites of the carbon under visible light are consumed or deactivated in the course of the reaction.

In all the studied systems the photooxidation of phenol follows an electrophilic mediated pathway, with a marked regioselectivity

depending on the composition of the catalyst and the illumination conditions. Quinones are favored over catechol at low energy photons and when titania is the major component of the photocatalyst (either TiO$_2$ alone or high loadings in carbon/titania catalyst), and vice versa when the carbon component is added to the catalyst composition. At $\lambda > 200$ nm higher amounts of polyhydroxylated intermediates were detected, suggesting that more hydroxyl radicals are involved under these illumination conditions.

Appendix A. Supplementary data

Supplementary data associated with this article can be found, in the online version, at http://dx.doi.org/10.1016/j.apcata.2015.09.036.

References

[1] N. Serpone, E. Pelizzetti, Photocatalysis: Fundamental and Applications, Wiley Interscience, New York, 1989.
[2] M.A. Henderson, Surf. Sci. Rep. 66 (2011) 185–297.
[3] R. Leary, A. Westwood, Carbon 49 (2011) 41–72.
[4] J.L. Faria, W. Wang, Carbon Materials for Catalysis, in: P. Serp, J.L. Figueiredo (Eds.), John Wiley & Sons, New York, 2009, pp. 481–506.
[5] J. Matos, J. Laine, J.M. Herrmann, Appl. Catal. B: Environ. 91 (1998) 281–291.
[6] J. Araña, J.M. Doña-Rodríguez, E. Tello Rendón, C. Garriga i Cabo, O. González-Díaz, J.A. Herrera-Melián, J. Pérez-Peña, G. Colón, J.A. Navío, Appl. Catal. B: Environ. 44 (2003) 161–172.
[7] B. Tryba, A.W. Morwski, M. Inagaki, Appl. Catal. B: Environ. 41 (2003) 427–433.
[8] Y. Yu, J.C. Yu, J.-G. Yu, Y.-C. Kwok, Y.-K. Che, J.-C. Zhao, L. Ding, W.-K. Ge, P.-K. Wong, Appl. Catal. A: Gen. 289 (2005) 186–196.
[9] R.R. Ocampo-Pérez, M. Sánchez-Polo, J. Rivera-Utrilla, R. Leyva-Ramos, Appl. Catal. B: Environ. 104 (2011) 177–184.
[10] C.O. Ania, L.F. Velasco, T. Valdes-Solis, Novel Carbon Adsorbents, in: J.M.D. Tascon (Ed.), Elsevier, London, 2012, pp. 521–547.
[11] L.F. Velasco, I.M. Fonseca, J.B. Parra, J.C. Lima, C.O. Ania, Carbon 50 (2012) 249–258.
[12] L.F. Velasco, V. Maurino, E. Laurenti, C.O. Ania, Appl. Catal. A: Gen. 453 (2013) 310–315.
[13] L.F. Velasco, J.C. Lima, C.O. Ania, Angew. Chem. Int. Ed. 53 (2014) 4146–4148.
[14] M. Haro, L.F. Velasco, C.O. Ania, Catal. Sci. Tech. 2 (2012) 2264–2272.
[15] T.J. Bandosz, J. Matos, M. Seredych, M.S.Z. Islam, R. Alfano, Appl. Catal. A: Gen. 445 (2012) 159–165.
[16] Y. Luo, Y. Heng, X. Dai, W. Chen, J. Li, J. Solid State Chem. 182 (2009) 2521–2525.
[17] A.S. Mestre, A.S. Bexiga, M. Proença, M. Andrade, M.L. Pinto, I. Matos, I.M. Fonseca, A.P. Carvalho, Biores. Technol. 102 (2011) 8253–8260.
[18] M.A. Andrade, R.J. Carmona, A.S. Mestre, J. Matos, A.P. Carvalho, C.O. Ania, Carbon 76 (2014) 183–192.
[19] H.K. Kuhn, S.E. Braslavsky, R. Schmidt, Pure Appl. Chem. 76 (2004) 2105–2146.
[20] J. Rouquerol, F. Rouquerol, P. Llewellyn, G. Maurin, K.S.W. Sing, Adsorption by Powders and Porous Solids: Principles, Methodology and Applications, second ed., Academic Press, Amsterdam, 2014.
[21] H. Chun, W. Yizhong, T. Hongxiao, Chemosphere 41 (2000) 120–1209.
[22] B. Bayarri, M.N. Abellan, J. Gimenez, S. Esplugas, Catal. Today 129 (2007) 231–239.
[23] M. Shanmuga Priya, IE(J) Chem. Eng. 90 (2009) 10–16, Journal of The Institution of Engineers (Chemical Engineering Division), Vol: 90, September 2009, pp. 10–16.
[24] J.-M. Herrmann, Appl. Catal. B: Environ. 99 (2010) 461–468.
[25] L.F. Velasco, C.O. Ania, Adsorption 17 (2010) 247–254.
[26] C. Moreno-Castilla, Carbon 42 (2004) 83–94.
[27] V. Prakash Reddy, G.K. Surya-Prakash, The Chemistry of Phenols, in: Z. Rappoport (Ed.), John Wiley & Sons, England, 2003, pp. 600–660.
[28] L.F. Velasco, R.J. Carmona, J. Matos, C.O. Ania, Carbon 73 (2014) 206–215.

Article IV- Supplementary Information

Effect of the irradiation wavelength on the performance of nanoporous carbon as an additive to TiO₂

Marta A. Andrade[1,2], Rocío J. Carmona[2], Ana S. Mestre[1], Ana P. Carvalho[1]*, Conchi O. Ania[2]*

[1] Centro de Química e Bioquímica, Faculdade de Ciências, Universidade de Lisboa, 1749-016 Lisboa, Portugal

[2] ADPOR Group, Dpt. Chemical Processes for Energy and Environment, Instituto Nacional del Carbón, INCAR-CSIC, Apdo. 73, 33080 Oviedo, Spain
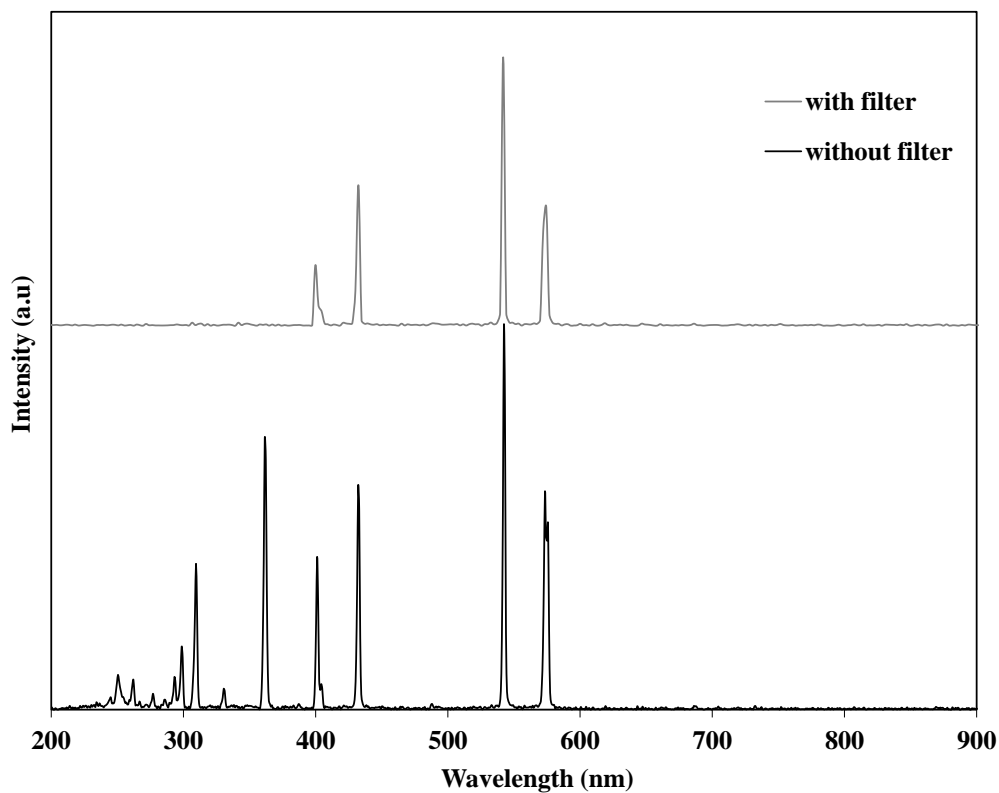
Figure S1. Emission spectra of the high pressure mercury lamp used (Helios Italquartz, 125 W) with and without pyrex filter.
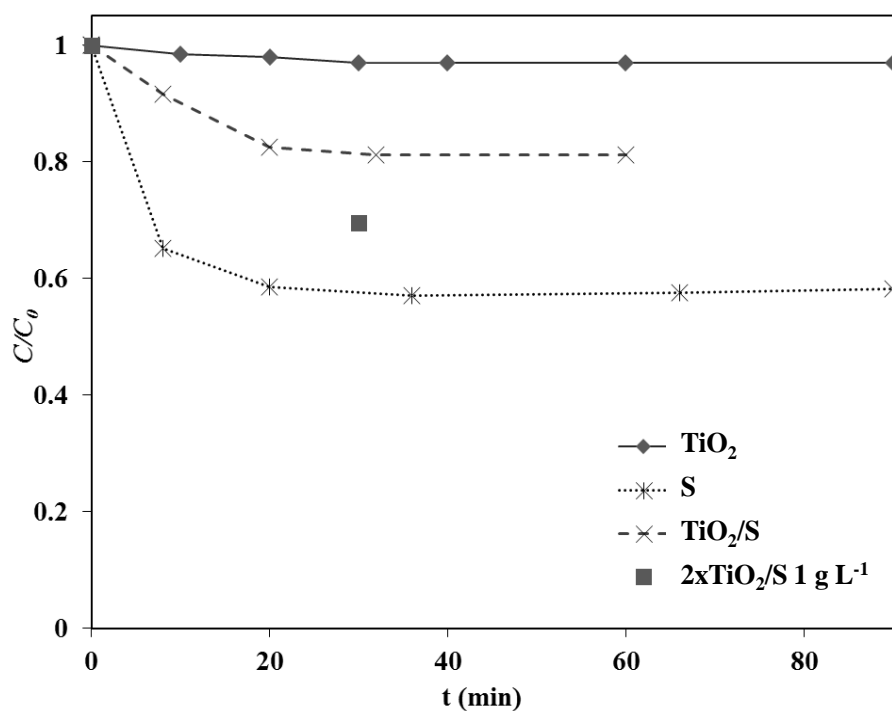
Figure S2. Phenol adsorption kinetics for the catalysts (in the same experimental conditions of the photocatalytic runs). For 2xTiO₂/S (catalyst loading 1 g L^{-1}) only the data corresponding the 30 min is shown, allowing the comparison of the amount adsorbed.
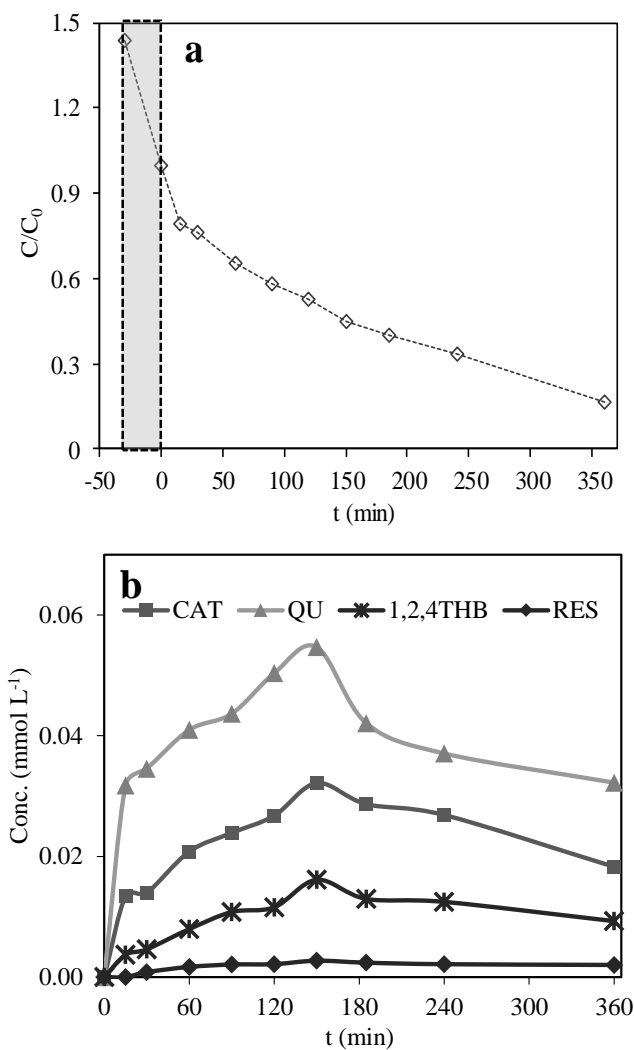
Figure S3. a) Phenol concentration decay curve, including the pre-adsorption step, for sample 2xTiO$_2$/S; b) Evolution of phenol degradation intermediates detected upon irradiation of sample 2xTiO$_2$/S: QU-quinones, CAT-catechol, RES- resorcinol; 124THB-1,2,4-trihydroxybenzene.

Table S1- Elemental analysis of carbon S and of the catalysts (after irradiation of the catalyst's suspensions in water in the absence of phenol).*-normalized per gram of carbon.

	C	**H**	**O**
S	82.8	1.2	16.0
S $_{\lambda>200nm}$	79.5	1.4	15.6
S $_{\lambda>360nm}$	81.0	1.1	15.4
***TiO₂/S $_{\lambda>200nm}$**	82.4	1.4	16.2
***TiO₂/S $_{\lambda>360nm}$**	82.9	1.2	15.9

Chapter 7

Conclusions

The main aim of this PhD thesis was the development of nanoporous adsorbents and catalysts using industrial by-products of low commercial value as precursors and to investigate their application in advanced remediation technologies for the removal and/or degradation of aromatic pollutants in aqueous solution.

The valorization of sisal residues was explored through thermochemical conversion reactions for the preparation of nanoporous carbons. These sisal-based carbon materials were further used in hybrid TiO_2/carbon materials for the photocatalytic degradation of phenol in aqueous medium. The most important concluding remarks that can be inferred from this work are as follows:

- The pyrolysis of the rope wastes showed two decomposition peaks between 300 and 350 °C assigned to the depolymerization of hemicelluloses and the decomposition of cellulose oligomers into tars, along with some degradation occurring to a small extent above 400 °C, due to the decomposition of cyclic rings and further carbonization of the formed tars.

- The different fractions (solid, tar, gas) obtained from the pyrolysis of lignocellulosic wastes from the rope industry were collected and characterized. The oil fraction was the most abundant during the pyrolysis of the rope waste, regardless the temperature, with solid and gas yields varying between 20 and 30 wt. %. The pyrolysis gases were mainly composed of CO and CO_2, with a significant amount of CH_4 when the pyrolysis was carried out above 600 °C.

- The analysis of the liquid fraction revealed that the bio-oil was rich in flavoring compounds and other valuable chemicals such as furfural, which have large applications in synthetic chemistry, food industry, and pharmaceuticals.

- The yield of the solid fraction can be modulated by the pyrolysis temperature, which also defines the surface chemistry of the final char residue, and therefore its reactivity. The solid carbonaceous char displayed interesting features to be used as precursor in the synthesis of low cost high performance porous adsorbents and catalysts supports.

- The immobilization of copper on the carbon matrix of activated carbon materials from different origins (coal-derived and lignocellulosic biomass), revealed the dual role played by the transition metal, as both catalyst and chemical protector.

- In the first case, copper catalyses the air gasification of the studied carbon, avoiding the sintering of metallic species, and thus enabling an homogenous dispersion of metallic particles within the carbon matrix, while displaying an enlargement of the existing microporous network (to mesopores).

- The copper immobilized on a highly reactive sisal derived activated carbon prevented the structural collapse of the materials during calcination, while promoting the porosity development. In this case, copper particles acted as a protective layer of the carbon (to avoid its burning-out), and also promoted the enlargement of the microporosity to create mesopores.

- These materials showing a good dispersion of nanosized copper particles and large textural development are promising candidates as highly selective adsorbents and catalysts to be used in advanced remediation techniques.

- A well-developed porosity and a good dispersion of metallic particles was also obtained with the incorporation of the transition metal on the carbon matrix, by impregnation of the carbon precursor with a copper salt and subsequent chemical activation. The analysis of the chemical status of the metal showed that oxidized copper species are dominant in the prepared material, as expected by the oxidizing atmosphere during the activation.

- The performance of the synthesized titania/carbon composites for the photodegradation of phenol under visible light was evaluated and compared to that of commercial TiO_2. An overall enhancement of the efficiency in terms of phenol conversion, mineralization degree and degradation rate using visible light was observed for the copper-loaded hybrid composites compared to titania powders even when using half of the amount of semiconductor

- The analysis of the textural properties of the composites after irradiation showed an interesting insight on the photo-oxidation process. A similar clogging of the porosity of the photocatalysts was found in dark and irradiation conditions, demonstrating that the higher conversion values cannot be attributed to the adsorption of the intermediates inside the pore structure of the carbons.

- The beneficial effect of copper is attributed to several factors, including its role as oxygen activator and/or the fast electron transfer environment, which would minimize the recombination of the excited electron/hole pairs.

- Regarding the dependence of the photochemical activity of hybrid titania/carbon photocatalysts with the wavelength of the irradiation source, phenol photooxidative efficiencies were found to be larger at $200 < \lambda < 600$ nm, for both the photolytic and catalysed reactions. The use of a nanoporous carbon as additive increased the photoconversion of phenol and the mineralization extent, with a more pronounced effect at $\lambda > 200$ nm.

- The carbon material alone also demonstrated a certain level of intrinsic photochemical activity under both irradiation conditions. However, the conversion of phenol upon irradiation of the nanoporous carbon alone dropped significantly for $\lambda > 360$ nm, with a

steady conversion above 60 min, suggesting that the photoactive sites of the carbon under visible light are consumed or deactivated in the course of the reaction.

- In all the studied systems the photo-oxidation of phenol follows an electrophilic mediated pathway, with a marked regioselectivity depending on the composition of the catalyst and the illumination conditions. Quinones are favoured over catechol at low energy photons and when titania is the major component of the photocatalyst, and *vice-versa* when the carbon component is added to the catalyst composition. At $\lambda > 200$ nm higher amounts of polyhydroxylated intermediates were detected, suggesting that more hydroxyl radicals are involved under these illumination conditions.

The results presented in this thesis are undoubtedly important findings to the valorization of sisal residues, by showing the potentialities of these lignocellulosic materials for other end-applications beyond their traditional use. The data obtained regarding the photocatalytic degradation of phenol in aqueous medium, where sisal-derived carbon materials proved to be efficient photocatalysts, are also a significant contribution to enlightenment of some questions related to the photocatalytic role of carbon materials, an increasingly growing research area.

CHAPTER 8

REFERENCES

Adinata, D.; Daud, W. M. A. W. and Aroua, M. K., 2007. Preparation and characterization of activated carbon from palm shell by chemical activation with K_2CO_3. *Bioresource Technology* 98, 145-149.

Adishkumar, S. and Kanmani, S., 2010. Treatment of phenolic wastewaters in single baffle reactor by Solar/TiO_2/H_2O_2 process. *Desalination and Water Treatment* 24, 67-73.

Adishkumar, S.; Kanmani, S. and Banu, J. R., 2014. Solar photocatalytic treatment of phenolic wastewaters: influence of chlorides, sulphates, aeration, liquid volume and solar light intensity. *Desalination and Water Treatment* 52, 7957-7963.

APA, 2013. Registo de Emissões e Transferências de Poluentes- Agência Portuguesa do Ambiente. Downloaded from http://www.apambiente.pt/ at 23rd October 2015.

Ahmaruzzaman, M. and Sharma, D. K., 2005. Adsorption of phenols from wastewater. *Journal of Colloid and Interface Science* 287, 14-24.

Ahmaruzzaman, M., 2008. Adsorption of phenolic compounds on low-cost adsorbents: A review. *Advances in Colloid and Interface Science* 143, 48-67.

Ahmed, S., 2012. Impact of Operating Conditions and Recent Developments in Heterogeneous Photocatalytic Water Purification Process. *Critical Reviews in Environmental Science and Technology* 42, 601-675.

Ahmed, S.; Rasul, M. G.; Martens, W. N.; Brown, R. and Hashib, M. A., 2010. Heterogeneous photocatalytic degradation of phenols in wastewater: A review on current status and developments. *Desalination* 261, 3-18.

Alapi, T. and Dombi, A., 2007. Comparative study of the UV and UV/VUV-induced photolysis of phenol in aqueous solution. *Journal of Photochemistry and Photobiology A: Chemistry* 188, 409-418.

Albini, A. and Germani, L., 2009. Photochemical Methods. In: *Handbook of Synthetic Photochemistry*, A. Albini, A. and M. Fagnoni (Eds.), Wiley-VCH Verlag GmbH & Co. KGaA: Weinheim; Chapter 1, 1-24.

Álvarez-Montero, M. A., Gomez-Sainero, L. M., Mayoral, A., Diaz, I., Baker, R. T., Rodriguez, J. J., 2011. Hydrodechlorination of chloromethanes with a highly stable Pt on activated carbon catalyst. *Journal of Catalysis* 279, 389-396.

Ania, C. O., 2013. Surface Chemistry of Green Carbons. In: *Green Carbon Materials: Advances and Applications*, Rufford, T. E.; Hulicova-Jurcakova, D. and Zhu, J. (Eds.), Pan Stanford Publishing; Chapter 1, 35-63.

Ania, C. O. and Bandosz, T. J., 2006a. Highly mesoporous carbons obtained using a dynamic template method. *Microporous and Mesoporous Materials* 89, 315-324.

Ania, C. O. and Bandosz, T. J. 2006b. Metal-loaded polystyrene-based activated carbons as dibenzothiophene removal media via reactive adsorption. *Carbon*, 44, 2404-2412.

Ania, C. O.; Parra, J. B. and Pis, J. J., 2002. Influence of oxygen-containing functional groups on active carbon adsorption of selected organic compounds. *Fuel Processing Technology* 79, 265-271.

Ania, C. O., Velasco, L. F. and Valdés-Solís, T., 2012. Photochemical Behavior of Carbon Adsorbents. In: *Novel Carbon Adsorbents*, Tascón, J. M. D. (Ed.), Elsevier; Chapter 17, 521-547.

Ania, C. O. and Béguin, F., 2008. Electrochemical regeneration of activated carbon cloths exhausted with bentazone. *Environmental Science and Technology* 42, 4500-4506.

Ania, C. O.; Menéndez, J. A.; Parra, J. B. and Pis, J. J., 2004. Microwave-induced regeneration of activated carbons polluted with phenol. A comparison with conventional thermal regeneration. *Carbon* 42, 1377-1381

Ania, C. O.; Parra, J. B.; Menéndez, J. A. and Pis, J. J., 2005. Effect of microwave and conventional regeneration on the microporous and mesoporous network and on the adsorptive capacity of activated carbons. *Microporous and Mesoporous Materials* 85, 7-15.

Ania, C. O.; Parra, J. B.; Menéndez, J. A. and Pis, J.J., 2007. Microwave-assisted regeneration of activated carbon loaded with pharmaceuticals. *Water Research* 41, 3399-3306.

Araña, J.; Doña-Rodríguez, J. M.; Tello–Rendón, E.; Garriga i Cabo, C.; González-Díaz, O.; Herrera-Melián, J. A.; Pérez-Peña, J.; Colón, G. and Navío, J. A., 2003a. TiO₂ activation by using activated carbon as a support. Part I. Surface characterisation and decantability study. *Applied Catalysis B: Environmental* 44, 161-172.

Araña, J.; Doña-Rodríguez, J. M.; Tello–Rendón, E.; Garriga i Cabo, C.; González-Díaz, O.; Herrera-Melián, J. A.; Pérez-Peña, J.; Colón, G. and Navío, J. A., 2003b. TiO₂ activation by using activated carbon as a support. Part II. Photoreactivity and FTIR study. *Applied Catalysis B: Environmental* 44, 153-160.

Arslan-Alaton, I., 2007. Degradation of a commercial textile biocide with advanced oxidation processes and ozone. *Journal of Environmental Management* 82, 145-154.

A/RES/65/154, 2011. Resolution adopted by the General Assembly of the United Nations, on 20 December 2010, International Year of Water Cooperation, 2013.

Asahi, R.; Morikawa, T.; Ohwaki, T.; Aoki, K. and Taga, Y., 2001. Visible-light photocatalysis in nitrogen doped titanium oxides, *Science* 293, 269-271.

Babuponnusami, A. and Muthukumar, K. 2011. Degradation of Phenol in Aqueous Solution by Fenton, Sono-Fenton and Sono-photo-Fenton Methods. *Clean-Soil Air Water* 39, 142-147.

Babuponnusami, A. and Muthukumar, K. 2012a. Advanced oxidation of phenol: A comparison between Fenton, electro-Fenton, sono-electro-Fenton and photo-electro-Fenton processes. *Chemical Engineering Journal* 183, 1-9.

Babuponnusami, A., Muthukumar, K., 2012b. Removal of phenol by heterogenous photo electro Fenton-like process using nano-zero valent iron. *Separation and Purification Technology*, 98, 130-135.

Baccar, R.; Sarrà, M.; Bouzid, J.; Feki, M. and Blánquez, P., 2012. Removal of pharmaceutical compounds by activated carbon prepared from agricultural by-product. *Chemical Engineering Journal* 211-212, 310-317.

Bandosz, T. J. and Ania, C. O., 2006. Surface chemistry of activated carbons and its characterization. In: *Activated Carbon Surfaces in Environmental Remediation*, Bandosz, T. J., (Ed.), Volume 7, Elsevier: New York; Chapter 4, 159-229.

Bandosz, T. J., 2009. Surface Chemistry of Carbon Materials. In: Carbon Materials for Catalysis, Serp, Ph and Figueiredo, J. L. (Eds.), John Wiley & Sons, Inc: New Jersey; Chapter 2, 45-92.

Bansal, R. C.; Donnet, J. -B. and Stoeckli, R., 1988. *Active Carbon*. Marcel Dekker: New York.

Bansal, R. C. and Goyal, M., 2005. *Activated Carbon Adsorption*. CRC Press Taylor & Francis Group: Boca Raton, USA.

Baransi, K.; Dubowski, Y. and Sabbah, I., 2012. Synergetic effect between photocatalytic degradation and adsorption processes on the removal of phenolic compounds from olive mill wastewater. *Water Research* 46, 789-798.

Barry, T. I. and Stone, F. S., 1960. The Reactions of Oxygen at Dark and Irradiated Zinc Oxide Surface. Proceedings of the Royal Society of London A 255, 124-144.

Benítez, F. J.; Acero, J. L.; Leal, A. I. and Real, F. J., 2008. Ozone and membrane filtration based strategies for the treatment of cork processing wastewaters. *Journal of Hazardous Materials* 152, 373-380.

Benotti, M. J.; Stanford, B. D.; Wert, E. C. and Snyder, S. A., 2009. Evaluation of a photocatalytic reactor membrane pilot system for the removal of pharmaceuticals and endocrine disrupting compounds from water. *Water Research* 43, 1513-1522.

Bian, J.; Wei, X. W.;. Jin, Y. R.; , L. Wang, L.; D.C. Luan, D. C. and Guan, Z. P., 2010. Direct synthesis of dimethyl carbonate over activated carbon supported Cu-based catalysts. *Chemical Engineering Journal* 165, 686-692.

Braslavsky, S. E., 2007. Glossary of terms used in photochemistry. *Pure and Applied Chemistry* 79, 293-465.

Braslavsky, S. E.; Braun, A. M.; Cassano, A. E.; Emeline, A. V.; Litter, M. I.; Palmisano, L.; Parmon, V. N. and Serpone, N., 2011. Glossary of terms used in photocatalysis and radiation catalysis. *Pure and Applied Chemistry* 83, 931-1014.

Britto, J. M. and Rangel, M. D., 2008. Advanced oxidation process of phenolic compounds in industrial wastewater. *Quimica Nova* 31, 114-122.

Buekens, A. G. and Huang, H., 1998. Catalytic plastics cracking for recovery of gasoline range hydrocarbons from municipal plastic wastes. *Resources Conservation and Recycling* 23, 163-181.

Bui, T. X. and Choi, H., 2010. Influence of ionic strength, anions, cations, and natural organic matter on the adsorption of pharmaceuticals to silica. *Chemosphere* 80, 681-686.

Busca, G.; Berardinelli, S.; Resini, C. and Arrigi, L., 2008. Technologies for the removal of phenol from fluid streams. A short review of recent developments. *Journal of Hazardous Materials* 160, 265-288.

Cabrita, I.; Ruiz, B.; Mestre, A. S.; Fonseca, I. M.; Carvalho, A. P. and Ania, C. O., 2010. Removal of an analgesic using activated carbons prepared from urban and industrial residues. *Chemical Engineering Journal* 163 249-255.

Carrott, P. J. M.; Carrott, M. M. L. R. and Mourão, P. A. M., 2006. Pore size control in activated carbons obtained by pyrolysis under different conditions of chemically impregnated cork. *Journal of Analytical and Applied Pyrolysis* 75, 120-127

Carvalho, A. P.; Gomes, M.; Mestre, A. S.; Pires, J. and Brotas de Carvalho, M., 2004. Activated carbons from cork waste by chemical activation with K_2CO_3: Application to adsorption of natural gas components. *Carbon* 42, 672-674.

Carvalho, A. P.; Mestre, A. S.; Pires, J.; Pinto, M. L. and Rosa, M. E., 2006. Granular activated carbons from powdered samples using clays as binders for the adsorption of organic vapours. *Microporous and Mesoporous Materials* 93, 226-231.

Carvalho, A. P.; Mestre, A. S.; Andrade, M. and Ania, C. O., 2013. Ibuprofen in the aquatic environment: occurrence, ecotoxicity and water remediation technologies. In: *Ibuprofen-Clinical Pharmacology, Medical uses and Adverse effects*. Carter, W. C. and Brown, B R., (Eds.) Nova Science Publishers, Inc; Chapter 1, 1-84.

Castillejos-López, E.; Nevskaia, D. M.; Munoz, V. and Guerrero-Ruiz, A., 2008. On the interactions of phenol, aniline and p-nitrophenol on activated carbon surfaces as detected by TPD. *Carbon* 46, 870-875.

de Castro, M. M., Martinez-Escandell, M., Molina-Sabio, M. and Rodríguez-Reinoso, F., 2010. Hydrogen adsorption on KOH activated carbons from mesophase pitch containing Si, B, Ti or Fe. *Carbon* 48, 636-644.

Cazetta, A. L., Junior, O. P.; Vargas, A. M. M.; Silva, A. P.; Zou, X.; Asefa, T. and Almeida, V. C., 2013. Thermal regeneration study of high surface area activated carbon obtained from coconut shell: Characterization and application of response surface methodology. *Journal of Analytical and Applied Pyrolysis* 101, 53-60.

Çalışkan, E.; Bermúdez, J. M.; Parra, J. B.; Menéndez, J. A.; Mahramanlıoğlu, M. and Ania, C. O., 2012. Microwave-assisted low temperature regeneration of activated carbon loaded with pharmaceuticals. *Journal of Environmental Management* 102, 134-140.

Chanan, A. P.; Vigneswaran, S.; Kandasamy, J. and Simmons, B., 2013. Wastewater Management Journey – From Indus Valley Civilization to the Twenty-First Century. In: *Wastewater Reuse and Management*, Sharma, S. J. and Sanghi, R. (Eds.), Springer Netherlands; Chapter 1, 3-18.

Chen, G., 2004. Electrochemical technologies in wastewater treatment. *Separation and Purification Technology* 38, 11-41.

Chen, Z. F. and Meyer, T. J., 2013. Copper(II) catalysis of water oxidation. *Angewandte Chemie-International Edition* 52, 700-703.

Chen, Z. F., Kang, P., Zhang, M. T., Stoner, B. R. and Meyer, T. J., 2013. Cu(II)/Cu(0) electrocatalyzed CO_2 and H_2O splitting. *Energy & Environmental Science* 6, 813-817.

Cheremisinoff, N. P., 2002. *Handbook of Water and Wastewater Treatment Technologies-*Butterworth-Heinemann: Woburn, MA, USA.

Chiou, C. H.; Wu, C. Y. and Juang, R. S., 2008. Influence of operating parameters on photocatalytic degradation of phenol in UV/TiO_2 process. *Chemical Engineering Journal* 139, 322–329.

Cho, H. H.; Huang, H. and Schwab, K., 2011. Effects of solution chemistry on the adsorption of ibuprofen and triclosan onto carbon nanotubes. *Langmuir* 27, 12960-12967.

Choi, W., 2006. Pure and modified TiO_2 photocatalysts and their environmental applications. *Catalysis Surveys from Asia* 10, 16-28.

Choi, H.; Stathatos, E. and Dionysiou, D., 2006. Sol-gel preparation of mesoporous photocatalytic TiO_2 films and TiO_2/Al_2O_3 composite membranes for environmental applications. *Applied Catalysis B: Environmental* 63, 60-67.

Choi, W. Y.; Termin, A. and Hoffmann, M. R., 1994. The role of metal-ion dopants in quantum-sized TiO_2 - Correlation between photoreactivity and charge-carrier recombination dynamics. *Journal of Physical Chemistry* 98, 13669-13679.

Choi, Y.; Umebayashi, T. and Yoshikawa, M. J., 2004. Fabrication and characterization of C-doped anatase TiO_2 photocatalysts. *Materials Science* 39, 1837-1839.

Choma, J. and Jaroniec, M., 2006. Characterization of Nanoporous Carbons by Using Gas Adsorption Isotherms. In: *Activated Carbon Surfaces in Environmental Remediation*, Bandosz, T. J. (Ed.), Volume 7, Elsevier: New York; Chapter 3, 107-158.

Chong, M. N.; Jin, B.; Chow, C. W. K. and Saint, C., 2010. Recent developments in photocatalytic water treatment technology: A review. *Water Research* 44, 2997-3027.

Colombo, D. P. and Bowman, R. M., 1996. Does interfacial charge transfer compete with charge carrier recombination? A femtosecond diffuse reflectance investigation of TiO_2 nanoparticles. *Journal of Physical Chemistry* 100, 18445-18449.

Colón, G.; Maicu, M.: Hidalgo, M. C. and Navío, J. A., 2006. Cu-doped TiO_2–systems with improved photocatalytic activity. *Applied Catalysis B: Environmental* 67, 41-51.

Comninellis, C. and Pulgarin, C., 1993. Electrochemical oxidation of phenol for wastewater treatment using SnO_2, anodes. *Journal of Applied Electrochemistry* 23, 108-112.

Comninellis, C.; Kapalka, A.; Malato, S.; Parsons, S. A.; Poulios, I. and Mantzavinos, D., 2008. Advanced oxidation processes for water treatment: advances and trends for R & D. *Journal of Chemical Technology and Biotechnology* 83, 769-776.

Corcoran, E.; Nellemann, C.; Baker, E.; Bos, R.; Osborn, D. and Savelli, H. (Eds.), 2010. *Sick Water? The central role of wastewater management in sustainable development. A Rapid Response Assessment.* United Nations Environment Programme.

De la Cruz, N.; Giménez, J.; Esplugas, S.; Grandjean, D.; de Alencastro, L. F. and Pulgarín, C., 2012. Degradation of 32 emergent contaminants by UV and neutral photo-Fenton in domestic wastewater effluent previously treated by activated sludge. Water Research 46, 1947-1957.

Dąbrowski, A.; Podkościelny, P.; Hubicki, Z. and Barczak, M., 2005. Adsorption of phenolic compounds by activated carbon - a critical review. *Chemosphere* 58, 1049–1070.

Daghrir, R.; Drogui, P. and Robert, D., 2013. Modified TiO_2 For Environmental Photocatalytic Applications: A Review. *Industrial & Engineering Chemistry Research* 52, 3581-3599.

Decreto-Lei nº 236, 1998.Diário da República- I Série-A Nº 176 - 1-8-1998, 3676-3722.

Delgado, L. F.; Charles, P.; Glucina, K. and Morlay, C., 2012. The removal of endocrine disrupting compounds, pharmaceutically activated compounds and cyanobacterial toxins during drinking water preparation using activated carbon-A review. *Science of the Total Environment* 435, 509-525.

Delgado, C. N. and Mendez, J. R. R., 2014. Preparation of Carbon Materials from Lignocellulosic Biomass. In: *Green Carbon Materials: Advances and Applications*, Rufford, T. E.; Hulicova-Jurcakova, D. and John Zhu, J. (Eds.), Pan Stanford Publishing; Chapter 2, 35-63.

Derbyshire, F.; Jagtoyen, M.; Andrews, R.; Rao, A.; Martin-Gullon, I. and Grulke, E., 2001. Carbon materials in environmental applications. In: *Chemistry and Physics of Carbon*, Radovic, L. R. (Ed.), Volume 27, Marcel Dekker: New York; Chapter 1, p. 1-66.

Dias, J. M.; Alvim-Ferraz, M. C. M.; Almeida, M. F., Rivera-Utrilla, J. and Sanchez-Polo, M., 2007. Waste materials for activated carbon preparation and its use in aqueous-phase treatment: A review. *Journal of Environmental Management* 85, 833-846.

Directive 2013/39/EU of the European parliament and of the council of 12 August 2013 amending Directives 2000/60/EC and 2008/105/EC as regards priority substances in the field of water policy.

Doerfler, W. and Hauffe, K., 1964a. Heterogeneous photocatalysis I. The influence of oxidizing and reducing gases on the electrical conductivity of dark and illuminated zinc oxide surfaces. *Journal of Catalysis* 3, 156-170.

Doerfler, W. and Hauffe, K., 1964b. Heterogeneous photocatalysis II. The mechanism of the carbon monoxide oxidation at dark and illuminated zinc oxide surfaces. *Journal of Catalysis* 3, 171-178.

Donnet, J. B. and Bansal, R. C., 1990. Carbon Fibers. Marcel Dekker: New York.

Dosoretz, C. G. and Böddeker, K. W., 2004. Removal of trace organics from water using a pumped bed-membrane bioreactor with powdered activated carbon. *Journal of Membrane Science* 239, 81-90.

Dozzi, M. V. and Selli, E., 2013. Doping TiO_2 with p-block elements: Effects on photocatalytic activity. *Journal of Photochemistry and Photobiology C: Photochemistry Reviews* 14, 13-28.

Dubey, S. P.; Dwivedi, A. D.; Sillanpää, M. and Gopal, K., 2010. Artemisia vulgaris-derived mesoporous honeycomb-shaped activated carbon for ibuprofen adsorption. *Chemical Engineering Journal* 165, 537-544.

El-Naas, M. H.; Al-Zuhair, S. and Abu Alhaija, M., 2010. Removal of phenol from petroleum refinery wastewater through adsorption on date-pit activated carbon. *Chemical Engineering Journal* 162, 997-1005.

EEA, 2013. The European Pollutant Release and Transfer Register-European Environment Agency. http:// prtr.ec.europa.eu. Last access on October 23 [rd] 2015.

Esplugas, S.; Giménez, J.; Contreras, S.; Pascual, E. and Rodríguez, M., 2002. Comparison of different advanced oxidation processes for phenol degradation. *Water Research* 36, 1034-1042.

FAO, 2012. Unlocking the Commercial Potential of Natural Fibres. Publication of the Market and Policy Analyses of the Non-Basic Food Agricultural Commodities Team, Trade and Markets Division. www.fao.org/economic/futurefibres/resources2/en/

Faria, J. L. and Wang, W., 2009. Carbon Materials in Photocatalysis In: *Carbon Materials for Catalysis*, Serp, Ph and Figueiredo, J. L. (Eds.), John Wiley & Sons, Inc: New Jersey; Chapter 13, 481-506.

Faust, S. and Aly, O., 1987. *Adsorption Processes for Water Treatment*, Butterworths: Boston.

Fenton, H. J., 1884. Oxidative properties of the H_2O_2/Fe^{2+} system and its application. *Journal of the Chemical Society* 65, 889-899.

Fernandes, S.; Andrade, M.; Ania, C. O.; Martins, A.; Pires, J. and Carvalho, A. P., 2012. Pt/carbon materials as bi-functional catalysts for n-decane hydroisomerization. *Microporous and Mesoporous Materials* 163, 21-28.

Fernández, A.; Lassaletta, G.; Jimenez, V. M.; Justo, A.; Gonzalez-Elipe, A. R. and Herrmann, J. M., 1995. Preparation and characterization of TiO_2 photocatalysts supported on various rigid supports (glass, quartz and stainless steel). Comparative studies of photocatalytic activity in water purification. *Applied Catalysis B: Environmental* 7, 49-63.

Fiege, H., Voges, H.W., Hamamoto, T., Umemura, S., Iwata, T., Miki, H., Fujita, Y., Buysch, H.J., Garbe, D. and Paulus, W., 2012. Phenol Derivatives. In: *Ullmann's Encyclopedia of Industrial Chemistry* (6th ed.), Wiley-VCH: Weinheim, Germany.

Figueiredo, J. L. and Pereira, M. F. R., 2009. Carbon as Catalyst. In: *Carbon Materials for Catalysis*, Serp, Ph and Figueiredo, J. L. (Eds.), John Wiley & Sons, Inc: New Jersey; Chapter 6, 177-217.

Foo, K. Y. and Hameed, B. H., 2012. Microwave-assisted regeneration of activated carbon. *Bioresource Technology* 119, 234-240.

Fraga, M. A.; Jordão, E.; Mendes, M. J.; Freitas, M. M. A.; Faria, J. L., and Figueiredo, J. L., 2002. Properties of carbon-supported platinum catalysts: role of carbon surface sites. *Journal of Catalysis* 209, 355-364.

Freire, L. F. A.; da Fonseca, F. V.; Yokoyama, L. and Teixeira, L. A. C., 2014. Study of solar photo-Fenton system applied to removal of phenol from water. *Water Science and Technology*, 70, 780-786.

Fujishima, A.; Honda, K., and Kikuchi, S., 1969. *Journal of the Chemical Society of Japan* (Kogyo Kagaku Zasshi) 72, 108-113 (in japanese).

Fujishima, A. and Honda, K., 1972. Electrochemical photolysis of water at a semiconductor electrode. *Nature* 238, 37-38.

Fujishima, A.; Rao, T. N. and Tryk, D. A., 2000. Titanium dioxide photocatalysis. *Journal of Photochemistry and Photobiology C: Photochemistry Reviews* 1, 1-21.

Fujishima, A.; Zhang, X. T. and Tryk, D. A., 2008. TiO_2 photocatalysis and related surface phenomena. *Surface Science Reports* 63, 515-582.

Galhetas, M.; Mestre, A. S.; Pinto, M. L.; Gulyurtlu, I.; Lopes, H. and Carvalho, A. P., 2014. Chars from gasification of coal and pine activated with K_2CO_3: Acetaminophen and caffeine adsorption from aqueous solutions. *Journal of Colloid and Interface Science* 433, 94-103.

Gernjak, W., Maldonado, M.I., Malato, S., Caceres, J., Krutzler, T., Glaser, A. and Bauer, R. 2004. Pilot-plant treatment of olive mill wastewater (OMW) by solar TiO_2 photocatalysis and solar photo-Fenton. *Solar Energy* 77, 567-572.

Ghatak, H. R., 2014. Advanced Oxidation Processes for the Treatment of Biorecalcitrant Organics in Wastewater. *Critical Reviews in Environmental Science and Technology* 44, 1167-1219.

Glezer, V., 2003. Environmental effects of substituted phenols. In: *The Chemistry of Phenols*. Rappoport, Z. (Ed.), John Wiley & Sons: England, Chapter 18, 1347-1368.

Gomis-Berenguer, A.; Iniesta, J.; Maurino, V.; Lima, J. C. and Ania, C. O., 2016. Nanoconfinement and wavelength dependence of the phochemistry of nanoporous carbons. *Carbon* 96, 98-104.

Górska, P.; Zaleska, A. and Hupka, J., 2009. Photodegradation of phenol by UV/TiO_2 and Vis/N,C-TiO_2 processes: Comparative mechanistic and kinetic studies. *Separation and Purification Technology* 68, 90-96.

Grabowska, E.; Reszczyńska, J. and Zaleska, A., 2012. Mechanism of phenol photodegradation in the presence of pure and modified-TiO_2: A review. *Water Research* 46, 5453-5471.

Guo, Y. and Du, E., 2012. *The effects of thermal regeneration conditions and inorganic compounds on the characteristics of activated carbon used in power plant*. International Conference on Future Electrical Power and Energy Systems, *Energy Procedia* 17 (Part A), 444-449.

Guo, Z. and Ma, R., 2006. Degradation of phenol by nanomaterial TiO_2 in wastewater. *Chemical Engineering Journal* 119, 55-59.

Gupta, V. K., Nayak, A., Agarwal, S., Tyagi, I. 2014. Potential of activated carbon from waste rubber tire for the adsorption of phenolics: Effect of pre-treatment conditions. *Journal of Colloid and Interface Science* 417, 420-430.

Gutterres, M. and de Aquim, P. M., 2013. Wastewater Reuse Focused on Industrial Applications. In: *Wastewater Reuse and Management*, Sharma, S. K. and Sanghi, R. (Eds.) Springer.

Haber, F. and Weiss, J., 1934. The catalytic decomposition of hydrogen peroxide by iron salts. *Proceedings of the Royal Society A* 147, 332-351.

Hancock, F. E., 1999. Catalytic strategies for industrial water re-use. *Catalysis Today* 53, 3-9.

Haro, M.; Velasco, L. F. and Ania, C. O., 2012. Carbon-mediated photoinduced reactions as a key factor in the photocatalytic performance of C/TiO$_2$. *Catalysis Science & Technology* 2, 2264-2272.

Henning, G. R., 1966. Electron Microscopy of Reactivity Changes near Lattice Defects in Graphite. In: *Chemistry and Physics of Carbon*, Volume 2, Walker, P. L., (Ed.), Marcel Dekker: New York, Chapter 1, pp. 1-49.

Hermans, S., Deffernez, A. and Devillers, M. 2010. Preparation of Au-Pd/C catalysts by adsorption of metallic species in aqueous phase for selective oxidation. *Catalysis Today* 157, 77-82.

Herrmann, J. M., 2010. Photocatalysis fundamentals revisited to avoid several misconceptions. *Applied Catalysis B: Environmental* 99, 461-468.

Helleur, R.; Popovic, N.; Ikura, M.; Stanciulescu, M. and Liu, D., 2001. Characterization and potential applications of pyrolytic char from ablative pyrolysis of used tyres. *Journal of Analytical and Applied Pyrolysis* 58-59, 813-824.

Hines, D., Bagreev, A. and Bandosz, T. J. 2004. Surface properties of porous carbon obtained from polystyrene sulfonic acid-based organic salts. *Langmuir* 20, 3388-3397.

Hsien, Y. H.; Chang, C. F.; Chen, Y. H. and Cheng, S., 2001. Photodegradation of aromatic pollutants in water over TiO$_2$ supported on molecular sieves. *Applied Catalysis B: Environmental* 31, 241-249.

Hu, X . L.; Li, G. S. and Yu, J. C., 2010. Design, Fabrication, and Modification of Nanostructured Semiconductor Materials for Environmental and Energy Applications. *Langmuir* 26, 3031-3039.

Hu, B., Wang, K., Wu, L. H.; Yu, S. H.; Antonietti, M. and Titirici, M. M., 2002. Engineering carbon materials from the hydrothermal carbonization process of biomass. *Advanced Materials* 2, 813-828.

Ikehata, K., 2013. Hazardous Agents in Wastewater: Public Health Impacts and Treatment Options for Safe Disposal and Reuse. In: *Wastewater Reuse and Management*. Sharma, S. K. and Sanghi, R., (Eds.), Springer Netherlands; Chapter 6, 165-191.

Inagaki, M.; Park, K. C. and Endo, M., 2010. Carbonization under pressure. *New Carbon Materials*, 409-420.

Inturi, S. N. R., Boningari, T., Suidan, M. and Smirniotis, P. G., 2014. Visible-light-induced photodegradation of gas phase acetonitrile using aerosol-made transition metal (V, Cr, Fe, Co, Mn, Mo, Ni, Cu, Y, Ce, and Zr) doped TiO_2. *Applied Catalysis B: Environmental* 144, 333-342.

Ioannou, L.; Michael, C.; Kyriakou, S. and Fatta-Kassinos, D., 2014. Solar Fenton: from pilot to industrial scale application for polishing winery wastewater pretreated by MBR. *Journal of Chemical Technology and Biotechnology* 89, 1067-1076.

Ioannidou, O. and Zabaniotou, A., 2007. Agricultural residues as precursors for activated carbon production- A review. *Renewable and Sustainable Energy Reviews* 11, 1966-2005.

Isariebel, Q. P.; Carine, J. L.; Ulises-Javier, J. H.; Anne-Marie, W. and Henri, D., 2009. Sonolysis of levodopa and paracetamol in aqueous solutions. *Ultrasonic Sonochemistry* 16, 610-616.

Karci, A.; Arslan-Alaton, I.; Olmez-Hanci, T. and Bekbolet, M., 2013. Degradation and detoxification of industrially important phenol derivatives in water by direct UV-C photolysis and H_2O_2/UV-C process: A comparative study. *Chemical Engineering Journal* 224, 4-9.

Kasprzyk-Hordern, B.; Ziółek, M. and Nawrocki, J., 2003. Catalytic ozonation and methods of enhancing molecular ozone reactions in water treatment. *Applied Catalysis B: Environmental* 46, 639-669.

Kavitha, V. and Palanivelu, K., 2004. The role of ferrous ion in Fenton and photo-Fenton processes for the degradation of phenol. *Chemosphere* 55, 1235-1243.

Kisch, H., 2010. On the problem of comparing rates or apparent quantum yields in heterogeneous photocatalysis. *Angewandte Chemie International Edition* 49, 9588-9589.

Klamerth, N.; Miranda, N.; Malato, S.; Aguera, A.; Fernandez-Alba, A. R.; Maldonado, M. I. and Coronado, J. M., 2009. Degradation of emerging contaminants at low concentrations in MWTPs effluents with mild solar photo-Fenton and TiO_2. *Catalysis Today* 144, 124-130.

Klamerth, N.; Malato, S.; Maldonado, M. I.; Agüera, A. and Fernández-Alba, A., 2011. Modified photo-Fenton for degradation of emerging contaminants in municipal wastewater effluents. *Catalysis Today* 161, 241-246.

Klamerth, N.; Malato, S.; Agüera, A. and Fernández-Alba, A., 2013. Photo-Fenton and modified photo-Fenton at neutral pH for the treatment of emerging contaminants in wastewater treatment plant effluents: A comparison. *Water Research* 47, 833-840.

Klavarioti, M.; Mantzavinos, D. and Kassinos, D., 2009. Removal of residual pharmaceuticals from aqueous systems by advanced oxidation processes. *Environment International* 35, 402-417.

Kolpin, D. W.; Furlong, E. T.; Meyer, M. T.; Thurman, E. M.; Zaugg, S. D.; Barber, L. B. and Buxton, H. T., 2002. Pharmaceuticals, hormones, and other organic wastewater contaminants in U.S. streams, 1999-2000: A national reconnaissance. *Environmental Science & Technology* 36, 1202-1211.

Kubo, M.; Fukuda, H.; Chua, X. J. and Yonemoto, T. 2007. Kinetics of ultrasonic degradation of phenol in the presence of composite particles of titanium dioxide and activated carbon. *Industrial & Engineering Chemistry Research* 46, 699-704.

Kudo, A. and Miseki, Y., 2009. Heterogeneous photocatalyst materials for water splitting. *Chemical Society Reviews* 38, 253-278.

Kwon, S.; Fan, M.; Cooper, A. T. and Yang, H. Q., 2008. Photocatalytic applications of micro- and Nano-TiO$_2$ in environmental engineering. *Critical Reviews in Environmental Science and Technology*, 38, 197-226.

Lafi, W. K. and Al-Qodah, Z., 2006. Combined advanced oxidation and biological treatment processes for the removal of pesticides from aqueous solutions. *Journal of Hazardous Materials* 137, 489-497.

Leão, A.; Sartor, S. M. and Caraschi, J. C., 2006. Natural fibers based composites - Technical and social issues. *Molecular Crystals and Liquid Crystals*, 448, 161-177.

Cherian, B. M.; Leão, A. L.; Souza, S. F., Thomas, S., Pothan, L. A. and Kottaisamy, M., 2011. Cellulose Nanocomposites for High Performance Application. In: *Cellulose Fibres: Bio and Nano-Polymer Composites - Green Chemistry and Technology*, Kalia, S.; Kaith, B. S. and Kaur, I. (Eds.), Springer-Verlag: New York, USA.

Leary, R. and Westwood, A., 2011. Carbon nanomaterials for the enhancement of TiO$_2$ photocatalysis. *Carbon* 49, 741-772.

Le Cloirec, P. and Faur, C., 2006. Adsorption of organic compounds onto activated carbon - applications in water and air treatments. In: *Activated Carbon Surfaces in Environmental Remediation*, Bandosz, T. J. (Ed.), Elsevier: New York; Chapter 375-419.

Legrini, O.; Oliveros, E. and Braun, A. M., 1993. Photochemical processes for water treatment. *Chemical Reviews* 93, 671-698.

Legube, N. and Leitner, N. K. V., 1999. Catalytic ozonation: a promising advanced oxidation technology for water treatment. *Catalysis Today* 53, 61-72.

Leon y Leon, C. A. and Radovic, L. R., 1990. Chemistry and Physics of Carbon, Thrower, P. A. (Ed.), Volume 24, Marcel Dekker: New York.

Li, X. Q.; Hai, F. I. and Nghiem, L. D., 2011. Simultaneous activated carbon adsorption within a membrane bioreactor for an enhanced micropollutant removal. *Bioresource Technology* 102, 5319-5324.

Li, Y.; Mai, Y. W. and Ye, L., 2000. Sisal fibre and its composites: a review of recent developments. *Composites Science and Technology* 60, 2037-2055.

Li, W.; Nanaboina, V.; Zhou, Q. X. and Korshin, G. V., 2012. Effects of Fenton treatment on the properties of effluent organic matter and their relationships with the degradation of pharmaceuticals and personal care products. *Water Research* 46, 403-412.

Lillo-Ródenas, M. A.; Cazorla-Amorós, D. and Linares-Solano, A., 2003. Understanding chemical reactions between carbons and NaOH and KOH: an insight into the chemical activation mechanism. *Carbon* 41, 267-275.

Linares-Solano, A.; Lozano-Castelló, D.; Lillo-Rodenas, M. A. and Cazorla-Amoros, D., 2008. Carbon activation by alkaline hydroxides preparation and reactions, porosity and performance. In: *Chemistry and Physics of Carbon* (Ed.), Volume 30, Crc Press-Taylor & Francis Group: Boca Raton, Chapter 1, 1-62.

Liotta, L.F.; Gruttadauria, M.; Di Carlo, G.; Perrini, G. and Librando, V., 2009. Heterogeneous catalytic degradation of phenolic substrates: catalysts activity, *Journal of Hazardous Materials* 162, 588-606.

Liou, R. M. and Chen, S.H., 2009. CuO impregnated activated carbon for catalytic wet peroxide oxidation of phenol. *Journal of Hazardous Materials* 172, 498-506.

De Luis, A. M.; Lombraña, J. I.; Menéndez, A. and Sanz, J., 2011. Analysis of the Toxicity of Phenol Solutions Treated with H_2O_2/UV and H_2O_2/Fe Oxidative Systems. *Industrial & Engineering Chemical Research* 50, 1928-1937.

Ma, J., Rodriguez, N. M., Vannice, M. A., Baker, R. T. K., 2000. Nitrous oxide decomposition and reduction over copper catalysts supported on various types of carbonaceous materials. *Topics in Catalysis* 10, 27-38.

Mailler, R.; Gasperi, J.; Coquet, Y.; Deshayes, S.; Zedek, S.; Cren-Olive, C.; Cartiser, N.; Eudes, V.; Bressy, A.; Caupos, E.; Moilleron, R.; Chebbo, G. and Rocher, V., 2015. Study of a large scale powdered activated carbon pilot: Removals of a wide range of emerging and priority micropollutants from wastewater treatment plant effluents. *Water Research* 72, 315-330.

Malato, S.; Fernández-Ibañez, P., Maldonado, M. I., Blanco, J. and Gernjak, W., 2009. Decontamination and disinfection of water by solar photocatalysis: recent overview and trends. *Catalysis Today* 147, 1-59.

Mandal, T.; Maity, S.; Dasgupta, D. and Datta, S., 2010. Advanced oxidation process and biotreatment: Their roles in combined industrial wastewater treatment. *Desalination*, 250, 87-94.

Mantzavinos, D. and Psillakis, E., 2004. Enhancement of biodegradability of industrial wastewaters by chemical oxidation pre-treatment. *Journal of Chemical Technology and Biotechnology* 79, 431-454.

Marsh, H. and Rodríguez-Reinoso, F., 2006. *Activated Carbon*, Elsevier: Oxford.

Martinez-Huitle, C. A. and Ferro, S., 2006. Electrochemical oxidation of organic pollutants for the wastewater treatment: Direct and indirect processes. *Chemical Society Reviews* 35, 1324-1340.

Martins, R. C. and Quinta-Ferreira, R. M., 2011. Remediation of phenolic wastewaters by advanced oxidation processes (AOPs) at ambient conditions: Comparative studies. *Chemical Engineering Science* 66, 3243–3250.

Martins, A. F.; Vasconcelos, T. G.; Henriques, D. M.; Frank, C. D.; Konig, A. and Kummerer, K., 2008. Concentration of ciprofloxacin in Brazilian hospital effluent and preliminary risk aassessment: A case study. *Clean-Soil Air Water* 36, 264-269.

Matos, J.;. Chovelon, J. M.; Cordero, T. and Ferronato, C., 2009. Influence of surface properties of activated carbon on photocatalytic activity of TiO_2 in 4-chlorophenol degradation, *The Open Environmental Engineering Journal* 2, 21-9.

Matos, J.; Laine, J., and Herrmann, J. M., 1998. Synergy effect in the photocatalytic degradation of phenol on a suspended mixture of titania and activated carbon. *Applied Catalysis B: Environmental* 18, 281-291.

Matos, J.; Laine, J., and M. Herrmann, J. M., 2001. Effect of the type of activated carbons on the photocatalytic degradation of aqueous organic pollutants by UV-irradiated titania. *Journal of Catalysis* 200, 10-20.

Matos, J., 2013. Environmental and Green Chemistry Applications of Nanoporous Carbons. In: *Green Carbon Materials: Advances and Applications,* Rufford, T. E.; Hulicova-Jurcakova, D. and Zhu, J. (Eds.), Pan Stanford Publishing; Chapter 6, 147-160.

Mayani, S. V.; Vishal, J.; Mayani, V. J.; Krishna, G. and Bhattacharyya, K. G., 2011. Phenol and its analogues in water: Sources, environmental fate, effects and treatment. In: *Chemistry of Phenolic Compounds: State of the Art,* Baruah, J. B., (Ed.), Nova Science Publishers, Inc.; Chapter 13, 181-202.

Méndez, J. A. O.; Melián, J. A. H.; Araña, J.; Rodríguez, J. M. D.; Díaz, O. G. and Peña, J. P., 2015. Detoxification of waters contaminated with phenol, formaldehyde and phenol–formaldehyde mixtures using a combination of biological treatments and advanced oxidation techniques. *Applied Catalysis B: Environmental* 163, 63–73.

Méndez-Arriaga, F.; Esplugas, S. and Giménez, J., 2008. Photocatalytic degradation of non-steroidal anti-inflammatory drugs with TiO_2 and simulated solar irradiation. *Water Research* 42, 585-594.

Méndez-Arriaga, F.; Esplugas, S. and Giménez, J., 2010. Degradation of the emerging contaminant ibuprofen in water by photo-Fenton. *Water Research* 44, 589-595.

Méndez-Arriaga, F.; Maldonado, M. I.; Giménez, J.; Esplugas, S. and Malato, S., 2009. Abatement of ibuprofen by solar photocatalysis process: Enhancement and scale up. *Catalysis Today* 144, 112-116.

Méndez-Arriaga, F.; Torres-Palma, R. A.; Pétrier, C.; Esplugas, S.; Giménez, J. and Pulgarin, C., 2008. Ultrasonic treatment of water contaminated with ibuprofen. *Water Research* 42, 4243-4248.

Menéndez-Diaz, J. Á. and Martín-Gullón, I., 2006. Types of carbon adsorbents and their production. In: *Activated Carbon Surfaces in Environmental Remediation,* Bandosz, T. J. (Ed.), Volume 7, Elsevier: New York; Chapter 1, 1-48.

Mestre, A. S.; Bexiga, A. S.; Proença, M.; Andrade, M.; Pinto, M. L.; Matos, I.; Fonseca, I. M., and Carvalho, A. P., 2011. Activated carbons from sisal waste by chemical activation with K_2CO_3: Kinetics of paracetamol and ibuprofen removal from aqueous solution. *Bioresource Technology* 102, 8253-8260.

Mestre, A. S.; Marques, S. C. R. and Carvalho, A. P., 2012. Effect of the alcohol cosolvent in the removal of caffeine by activated carbons. *Industrial & Engineering Chemistry Research* 51, 9850-9857.

Mestre, A. S.; Pires, J.; Nogueira, J. M. F. and Carvalho, A. P., 2007. Activated carbons for the adsorption of ibuprofen. *Carbon* 45, 1979-1988.

Mestre, A. S.; Pires, J.; Nogueira, J. M. F.; Parra, J. B.; Carvalho, A. P. and Ania, C. O., 2009. Waste-derived activated carbons for removal of ibuprofen from solution: role of surface chemistry and pore structure. *Bioresource Technology* 100, 1720-1726.

Mestre, A. S.; Tyszko, E.; Andrade, M. A.; Galhetas, M.; Freire, C. and Carvalho, A. P., 2015. Sustainable activated carbons prepared from a sucrose-derived hydrochar: remarkable adsorbents for pharmaceutical compounds. *Rsc Advances* 5, 19696-19707.

Michailof, C.; Stavropoulos, G. G. and Panayiotou, C., 2008. Enhanced adsorption of phenolic compounds, commonly encountered in olive mill wastewaters, on olive husk derived activated carbons. *Bioresource Technology* 99, 6400-6408.

Miranda-García, N.; Suárez, S.; Sánchez, B.; Coronado, J. M.; Malato, S. and Maldonado, M. I., 2011. Photocatalytic degradation of emerging contaminants in municipal wastewater treatment plant effluents using immobilized TiO_2 in a solar pilot plant. *Applied Catalysis B: Environmental* 103, 294-301.

Mohammadi, S.; Kargari, A.; Sanaeepur, H.; Abbassian, K.; Najafi, A. and Mofarrah, E., 2015. Phenol removal from industrial wastewaters: a short review. *Desalination and Water Treatment* 53, 2215-2234.

Molinari, R.; Lavorato, C. and Poerio, T., 2012. Performance of vanadium based catalyst in a membrane contactor for the benzene hydroxylation to phenol. *Applied Catalysis A: General*, 417-418, 87-92.

Mohanty, A. K.; Misra, M. and Drzal, L. T., 2005. *Natural Fibres, Biopolymers, and Bio-composites*, CRC Press.

Morales-Torres, S.; Carrasco-Marín , F.; Pérez-Cadenas, A. F. and Maldonado-Hódar, F. J., 2015. Coupling Noble Metals and Carbon Supports in the Development of Combustion Catalysts for the Abatement of BTX Compounds in Air Streams. *Catalysts* 5, 774-799.

Moreno-Castilla, C., López-Ramón, M. V., and Carrasco-Marín, F., 2000. Changes in surface chemistry of activated carbons by wet oxidation. *Carbon* 38, 1995-2001.

Moreno-Castilla, C., 2004. Adsorption of organic molecules from aqueous solutions on carbon materials. *Carbon* 42, 83-94.

Mourão, P. A. M.; Laginhas, C.; Custódio, F.; Nabais, J. M. V.; Carrott, P. J. M. and Carrott, M. M. L. R., 2011. Influence of oxidation, process on the adsorption capacity of activated carbons from lignocellulosic precursors. *Fuel Processing Technology* 92, 241-246.

Mozia, S. and Morawski, A. W., 2012. The performance of a hybrid photocatalysis-MD system for the treatment of tap water contaminated with ibuprofen. *Catalysis Today* 193, 213-220.

Nabais, J. M. V.; Gomes, J. A.; Suhas; Carrott, P. J. M., Laginhas, C. and Roman, S., 2009. Phenol removal onto novel activated carbons made from lignocellulosic precursors: Influence of surface properties. *Journal of Hazardous Materials*, 167, 904-910.

Nakagawa, K., Namba, A., Mukai, S.R., Tamon, H., Ariyadejwanich, P., Tanthapanichakoon, W. 2004. Adsorption of phenol and reactive dye from aqueous solution on activated carbons derived from solid wastes. *Water Research*, 38, 1791-1798.

Nalbandian, M. J.; Zhang, M. L.; Sanchez, J., Choa, Y. H., Cwiertny, D. M. and Myung, N. V., 2015. Synthesis and optimization of $BiVO_4$ and co-catalyzed $BiVO_4$ nanofibers for visible light-activated photocatalytic degradation of aquatic micropollutants. *Journal of Molecular Catalysis A: Chemical* 404, 18-26.

Nie, X.; Zhuo, S.; Maeng, G. and K. Sohlberg, K., 2009. Doping of TiO_2 polymorphs for altered optical and photocatalytic properties. *International Journal of Photoenergy* Article ID 294042.

Nogueira, K. R. B.; Nascimento, C. A. O.; Guardani, R. and Teixeira, A. C. S. C., 2012. Feasibility study of a solar reactor for phenol treatment by the photo-Fenton process in aqueous solution. *Chemical Engineering & Technology*, 35, 2125-2132.

Ochiai, T. and Fujishima, A., 2012. Photoelectrochemical properties of TiO_2 photocatalyst and its applications for environmental purification. *Journal of Photochemistry and Photobiology C: Photochemistry Reviews* 13, 247-262.

Oki, T. and Kanae, S., 2006. Global hydrological cycles and world water resources. *Science* 313, 1068-1072.

Ollis, D. F. and Al-Ekabi, H.,1993. *Photocatalytic purification and treatment of water and air*, Elsevier: Amsterdam.

Oppenlander, T., 2003. *Photochemical purification of water and air: advanced oxidation processes (AOPs): Principles, reaction mechanisms, reactor concepts*, Wiley-VCH Verlag GmbH & Co. KGaA: Weinheim, Germany.

Park, H.; Park, Y.; Kim, W. and Choi, W., 2013. Surface modification of TiO_2 photocatalyst for environmental applications. *Journal of Photochemistry and Photobiology C: Photochemistry Reviews* 15, 1-20.

Parsons, S., 2004. *Advanced Oxidation Processes for Water and Wastewater Treatment*, IWA Publishing.

Pastrana-Martinez, L. M., López-Ramón, M. V. and Moreno-Castilla, C. 2009. Adsorption and thermal desorption of the herbicide fluroxypyr on activated carbon fibers and cloth at different pH values. *Journal of Colloid and Interface Science*, 331, 2-7.

Pelizzetti, E. and Serpone, N., 1989. *Photocatalysis: fundamental and applications*. Wiley: New York.

Pereira, V. J.; Weinberg, H. S.; Linden, K. G. and Singer, P. C., 2007. UV degradation kinetics and modeling of pharmaceutical compounds in laboratory grade and surface water via direct and indirect photolysis at 254 nm. *Environmental Science & Technology* 41, 1682-1688.

Petit, C., Karwacki, C., Peterson, G. and Bandosz, T. J., 2007. Interactions of ammonia with the surface of microporous carbon impregnated with transition metal chlorides. *Journal of Physical Chemistry C* 111, 12705-12714.

Poyatos, J. M.; Muñio, M. M.; Almecija, M. C.; Torres, J. C.; Hontoria, E. and Osorio, F., 2010. Advanced Oxidation Processes for Wastewater Treatment: State of the Art. *Water Air Soil Pollution* 205, 187-204.

Przepiórski, J., 2006. Activated carbon filters and their industrial applications. In: *Activated Carbon Surfaces in Environmental Remediation*, Bandosz, T. J. (Ed.), Volume 7, Elsevier: New York; Chapter 9, 421-474.

Puma, G. L.; Bono, A.; Krishnaiah, D. and Collin, J. G., 2008. Preparation of titanium dioxide photocatalyst loaded onto activated carbon support using chemical vapor deposition: a review paper. *Journal of Hazardous Materials* 157, 209-219.

Qiu, B. A., Han, L. N., Wang, J. C., Chang, L. P. and Bao, W. R., 2011. Preparation of sorbents loaded on activated carbon to remove H_2S from hot coal gas by supercritical water impregnation. *Energy & Fuels* 25, 591-595.

Radovic, L. R.; Moreno-Castilla, C. and Rivera- Utrilla, J., 2000. Carbon materials as adsorbents in aqueous solutions. In: *Chemistry and Physics of Carbon- A Series of Advances*. Radovic, L. R. (Ed.), Volume 27, Marcel Dekker, Inc: New York; Chapter 4, 227-405.

Radovic, L. R. and Rodríguez-Reinoso, F., 1996, *Chemistry and Physics of Carbon*, Thrower, P. A. (Ed.), Volume 25, Marcel Dekker: New York.

Radovic, L. R. and Bockrath, B., 2005. On the Chemical Nature of Graphene Edges: Origin of Stability and Potential for Magnetism in Carbon Materials. *Journal of the American Chemical Society* 127, 5917-5927.

Radovic, L. R.; Silva-Villalobos, A. F.; Silva-Tapia, A. B. and Vallejos-Burgos, F., 2011. On the mechanism of nascent site deactivation in graphene. *Carbon* 49, 3471-3487.

Rashad, M. M., Elsayed, E. M., Al-Kotb, M. S. and Shalan, A. E., 2013. The structural, optical, magnetic and photocatalytic properties of transition metal ions doped TiO_2 nanoparticles. *Journal of Alloys and Compounds* 581, 71-78.

Ranade, V. V. and Bhandari, V. M., 2014. Industrial Wastewater Treatment, Recycling, and Reuse – Past, Present and Future. In: *Industrial Wastewater Treatment, Recycling, and Reuse.* Ranade, V. V. and Bhandari, V. M., (Eds.), Elsevier; Chapter 14, 521-535.

Rappoport, Z., 2003. *The Chemistry of Phenols,* Rappoport, Z. (Ed.), John Wiley & Sons: England.

Rodríguez-Reinoso, F. and Sepúlveda-Escribano, A., 2001. Porous carbons in adsorption and catalysis. In: *Handbook of Surfaces and Interfaces of Materials*. Volume 5, Nalwa, H. S. (Ed.), Academic Press; 309-355.

Rodríguez-Reinoso, F.; McEnaney, B.; Rouquerol, J. and Unger, K. K., 2002. *Characterization of Porous Solids VI. Studies in Surface Science and Catalysis*, Volume 144; Elsevier: Amsterdam.

Rodríguez-Reinoso, F. and Sepúlveda-Escribano, A., 2009. In: *Carbon Materials for Catalysis*, Serp, Ph and Figueiredo, J. L. (Eds.), John Wiley & Sons, Inc: New Jersey; Chapter 4, 131-217.

Romero-Rossi, F. and Stone, F. S., 1960. Actes 2° Congrès Internationale de Catalyse; Paris, Tome II; 1481.

Roskill Report, 1998. *The Economics of Activated Carbon*, 6th ed. Roskill Information Services Ltd; Claphham Road: London.

Rouquerol, J.; Avnir, D.; Fairbridge, C. W.; Everett, D. H.; Haynes, J. H.; Pernicone, N.; Ramsay, J. D. F.; Sing, K. W. and Unger, K. K., 1994. Recommendations for the characterization of porous solids. *Pure and Applied Chemistry* 66, 1739-1758.

Rúa-Gómez, P. C.; Guedez, A. A.; Ania, C. O. and Püttmann, W., 2012. Upgrading of Wastewater Treatment Plants Through the Use of Unconventional Treatment Technologies: Removal of Lidocaine, Tramadol, Venlafaxine and Their Metabolites. *Water* 4, 650-669.

Saien, J. and Khezrianjoo, S. 2008. Degradation of the fungicide carbendazim in aqueous solutions with UV/TiO_2 process: Optimization, kinetics and toxicity studies. *Journal of Hazardous Materials* 157, 269-276.

Sakthivel, S. and Kisch, H., 2003. Daylight photocatalysis by carbon-modified titanium dioxide, *Angewandte Chemie International Edition* 42, 4908-4911.

Salah, N. H.; Bouhelassa, M.; Bekkouche, S. and Boultif, A., 2004. Study of photocatalytic degradation of phenol. *Desalination* 166, 347-354.

Salame, I. I. and Bandosz, T. J., 2003. Role of surface chemistry in adsorption of phenol on activated carbons. *Journal of Colloid and Interface Science* 264, 307-312.

Salazar, R., Brillas, E. and Sirés, I. 2012. Finding the best Fe^{2+}/Cu^{2+} combination for the solar photoelectro-Fenton treatment of simulated wastewater containing the industrial textile dye Disperse Blue 3. *Applied Catalysis B: Environmental* 115, 107-116.

Santos, F. V.; Azevedo, E. B.; Sant'Anna Jr., G. L. and Dezotti, M., 2006. Photocatalysis as a tertiary treatment for petroleum refinery wastewaters. *Brazilian Journal of Chemical Engineering* 23, 450-460.

Santos, A.; Yustos, P.; Quintanilla, A.; Rodríguez, S. and Garcia-Ochoa, F., 2002. Route of the catalytic oxidation of phenol in aqueous phase. *Applied Catalysis B: Environmental* 39, 97-113.

Sanz, J.; Lombraña, J. I. and de Luis, A., 2013. State of art in advanced oxidation application to industrial effluents: new developments and future trends. *Afinidad LXX* 561, Enero-Marzo.

Saratale, R. G., Noh, H. S., Song, J. Y. and Kim, D. S., 2014. Influence of parameters on the photocatalytic degradation of phenolic contaminants in wastewater using TiO_2/UV system. *Journal of Environmental Science and Health Part A: Toxic/Hazardous Substances & Environmental Engineering* 49, 1542-1552.

Sepúlveda-Escribano, J. A.; Coloma, F., and Rodríguez-Reinoso, F., 1998. Platinum catalysts supported on carbon blacks with different surface chemical properties. *Applied Catalysis A: General* 173, 247-257.

Seredych, M. and Bandosz, T. J., 2010. Adsorption of dibenzothiophenes on activated carbons with copper and iron deposited on their surfaces. *Fuel Processing Technology* 91, 693-701.

Shiklomanov, I. A., 2000. Appraisal and Assessment of World Water Resources. *Water International* 25, 11-32.

Silva, A. M. T., Nouli, E., Carmo-Apolinario, A. C., Xekoukoulotakis, N. P. and Mantzavinos, D., 2007. Sonophotocatalytic/H_2O_2 degradation of phenolic compounds in agro-industrial effluents. *Catalysis Today* 124, 232-239.

Silva, C. G.; W. Wang, W. and Faria, J. L., 2006. Photocatalytic and photochemical degradation of mono-, di- and tri-azo dyes in aqueous solution under UV irradiation. *Journal of Photochemistry Photobiology A: Chemistry* 181, 314–324.

Singh, K. P., Malik, A., Sinha, S. and Ojha, P., 2008. Liquid-phase adsorption of phenols using activated carbons derived from agricultural waste material. *Journal of Hazardous Materials* 150, 626-641.

Sirés, I. and Brillas, E., 2012. Remediation of water pollution caused by pharmaceutical residues based on electrochemical separation and degradation technologies: A review. *Environmental International* 40, 212-229.

Skoumal, M.; Cabot, P. L.; Centellas, F.; Arias, C.; Rodriguez, R. M.; Garrido, J. A. and Brillas, E., 2006. Mineralization of paracetamol by ozonation catalyzed with Fe^{2+}, Cu^{2+} and UVA light. *Applied Catalysis B: Environmental* 66, 228-240.

Snyder, S. A.; Adham, S.; Redding, A. M.; Cannon, F. S.; DeCarolis, J.; Oppenheimer, J.; Wert, E. C. and Yoon, Y., 2007. Role of membranes and activated carbon in the removal of endocrine disruptors and pharmaceuticals. *Desalination* 202, 156-181.

Sorokhaibam, L. G. and Ahmaruzzaman, M., 2014. Phenolic Wastewater Treatment: Development and Applications of New Adsorbent Materials. In: *Industrial Wastewater Treatment, Recycling, and Reuse,* Ranade, V. V. and Bhandari, V. M., (Eds.), Elsevier; Chapter 8, 323-368.

Sobczyński, A.; Duczmal, Ł. and Zmudziński, W., 2004. Phenol destruction by photocatalysis on TiO_2: an attempt to solve the reaction mechanism, *Journal of Molecular Catalysis A: Chemical,* 213, 225–230.

Spasiano, D.; Marotta, R.; Malato, S., Fernandez-Ibanez, P. and Di Somma, I., 2015. Solar photocatalysis: Materials, reactors, some commercial, and pre-industrialized applications. A comprehensive approach. *Applied Catalysis B: Environmental* 170, 90-123.

Stavropoulos, G. G., Samaras, P. and Sakellaropoulos, G. P., 2008. Effect of activated carbons modification on porosity, surface structure and phenol adsorption. *Journal of Hazardous Materials* 151, 414-421.

Stoquart, C.; Servais, P.; Bérubé, P. R. and Barbeau, B., 2012. Hybrid Membrane Processes using activated carbon treatment for drinking water: A review. *Journal of Membrane Science* 411, 1-12.

Suhas; Carrott, P. J. M. and Carrott, M. M. L. R., 2007. Lignin - from natural adsorbent to activated carbon: A review. *Bioresource Technology,* 98, 2301-2312.

Suryaman, D.; Hasegawa, K. and Shigehiro, S., 2006. Combined biological and photocatalytic treatment for the mineralization of phenol in water. *Chemosphere* 65, 2502-2506.

Suzuki, H., Araki, S. and Yamamoto, H., 2015. Evaluation of advanced oxidation processes (AOP) using O_3, UV, and TiO_2 for the degradation of phenol in water. *Journal of Water Process Engineering* 7, 54–60.

Tanaka, K.; Capule, M. F. V. and Hisanaga, T., 1991. Effect of crystallinity of TiO_2 on its photocatalytic action. *Chemical Physics Letters* 187, 73-76.

Tay, T.; Ucar, S. and Karagöz, S., 2009. Preparation and characterization of activated carbon from waste biomass. *Journal of Hazardous Materials* 165, 481-485.

Ternes, T. A. and Joss, A., 2006. *Human pharmaceuticals, hormones and fragrances: the challenge of micropollutants in urban water management*. IWA: London.

Ternes, T. A.; Stüber, J.; Herrmann, N.; McDowell, D.; Ried, A.; Kampmann, M. and Teiser, B., 2003. Ozonation: A tool for removal of pharmaceuticals, contrast media and musk fragrances from wastewater? *Water Research* 37, 1976-1982.

Terzyk, A. P., 2003. Further insights into the role of carbon surface functionalities in the mechanism of phenol adsorption. *Journal of Colloid and Interface Science* 268, 301-329.

Thu, H. B.; Karkmaz, M.; Puzenat, E.; Guillard, C. and Herrmann, J. M., 2005. From the fundamentals of photocatalysis to its applications in environment protection and in solar purification of water in arid countries. *Research on Chemical Intermediates* 31, 449-461.

Tchobanoglous, G.; Burton, F. L. and Stensel, H. D., 2004a. Constituents in Wastewater. In: *Wastewater Engineering: Treatment and Reuse* (4th ed.), Metcalf & Eddy Inc. (Eds.), McGraw-Hill: New York; Chapter 2, 27-151.

Tchobanoglous, G.; Burton, F. L. and Stensel, H. D., 2004b. Advanced Wastewater Treatment. In: Wastewater Engineering: Treatment and Reuse (4th ed.), Metcalf & Eddy Inc. (Eds.), McGraw-Hill: New York; Chapter 11, 1138-1161.

Tryba, B., 2008. Increase of the photocatalytic activity of TiO_2 by carbon and iron modifications. *International Journal of Photoenergy*. ID 721824, 1-15.

Tryba, B.; Morwski, A. W. and Inagaki, M., 2003. Application of TiO_2-mounted activated carbon to the removal of phenol from water, *Applied Catalysis B: Environmental* 41, 427–433.

Tryba, B.; Morwski, A. W.; Inagaki, M. and Toyoda, M., 2006a. Effect of the carbon coating in Fe–C–TiO_2 photocatalyst on phenol decomposition under UV irradiation via photo-Fenton process. *Chemosphere* 64, 1225-32.

Tryba, B.; Morwski, A. W.; Inagaki, M. and Toyoda, M., 2006b. Mechanism of phenol decomposition on $FeCTiO_2$ and $FeTiO_2$ photocatalysts via photo-Fenton process. *Journal of Photochemistry and Photobiology A: Chemistry* 179, 224-8.

UN, 2009. The United Nations World Water Development Report 3- Water in a changing world - Facts and figures. World water assessment programme, UNESCO.

UN, 2012. The United Nations World Water Development Report 4- Managing Water under Uncertainty and Risk. World water assessment programme, UNESCO.

UN, 2014a. The United Nations World Water Development Report- Water and Energy. World water assessment programme, UNESCO.

UN, 2014b. The United Nations World Water Development Report- Water and Energy - Facts and figures. World water assessment programme, UNESCO.

USEPA, 2015. Update of Human Health Ambient Water Quality Criteria: Phenol 108-95-2

Di Valentin, C.; Pacchioni, G. and A. Selloni, A., 2005. Theory of carbon doping of titanium dioxide. Chemistry of Materials 17, 6656-6665.

Vamvuka, D., 2011. Bio-oil, solid and gaseous biofuels from biomass pyrolysis processes-An overview. *International Journal of Energy Research* 35, 835-862.

Velasco, L. F.; Parra, J. B. and Ania, C. O., 2010a. Phenol adsorption and photo-oxidation on porous C/Ti composites. *Adsorption Science & Technology* 17, 726-739.

Velasco, L. F.; Parra, J. B. and Ania, C. O., 2010b. Role of activated carbon features on photodegradation of phenol. Applied Surface Science 256, 5254- 5258.

Velasco, L. F. and Ania, C. O., 2011. Understanding phenol adsorption mechanisms on activated carbons. *Adsorption* 17, 247-254.

Velasco, L. F., Fonseca, I. M., Parra, J. B., Lima, J. C. and Ania, C. O., 2012. Photochemical behaviour of activated carbons under UV irradiation. *Carbon* 50, 249-258.

Velasco, L. F.; Maurino, V.; Laurenti, E.;. Fonseca, I. M.; Lima, J. C. and Ania, C. O., 2013a. Photoinduced reactions occurring on activated carbons. A combined photooxidation and ESR study. *Applied Catalysis A: General* 452, 1-8.

Velasco, L. F.; Maurino, V.; Laurenti, E. and Ania, C. O., 2013b. Light-induced generation of radicals on semiconductor-free carbon photocatalysts. *Applied Catalysis A: General* 453, 310-315.

Velasco, L. F.; Lima, J. C. and Ania, C., 2014. Visible-light photochemical activity of nanoporous carbons under monochromatic light. *Angewandte Chemie International Edition* 53, 4146-4148.

Velasco, L. F.; Gomis-Berenguer, A.; Lima, J. C. and Ania, C. O., 2015. Tuning the surface chemistry of nanoporous carbons for an enhanced nanoconfined photochemical activity, *ChemCatChem* 7, 3012-319.

Wang, W. Z.; Huang, X. W.; Wu, S., Zhou, Y. X.; Wang, L. J.; Shi, H. L.; Liang, Y. J. and Zou, B., 2013. Preparation of p-n junction $Cu_2O/BiVO_4$ heterogeneous nanostructures with enhanced visible-light photocatalytic activity. *Applied Catalysis B-Environmental* 134, 293-301.

Wang, W.; Serp, Ph; Kalck, P. and Faria, J. L., 2005. Visible light photodegradation of phenol on $MWNT-TiO_2$ composite catalysts prepared by a modified sol–gel method. *Journal of Molecular Catalysis A: Chemistry* 235, 194-199.

Wang, X.; Tang, Y.; Chen, Z. and Lim, T.-T., 2012. Highly stable heterostructured $Ag-AgBr/TiO_2$ composite: a bifunctional visible-light active photocatalyst for destruction of ibuprofen and bacteria. *Journal of Materials Chemistry* 22, 23149-23158.

Wang, R.-C. and Yu, C.-W., 2013. Phenol degradation under visible light irradiation in the continuous system of photocatalysis and sonolysis. *Ultrasonics Sonochemistry* 20, 553-564.

Weber, M. and Weber, M., 2010. Phenols. In: *Phenolic Resins: A Century of Progress*, Pilato, L. (Ed.), Springer-Verlag: Berlin Heidelberg; Chapter 2, 9-23.

Wu, C. D.; Zhang, J. Y.; Wu, Y. and Wu, G. Z., 2014. Degradation of phenol in water by the combination of sonolysis and photocatalysis. *Desalination and Water Treatment* 52, 1911-1918.

Xu, P.; Han, H. J.; Hou, B. L.; Zhuang, H. F.; Jia, S. Y.; Wang, D. X.; Li, K. and Zhao, Q., 2015. The feasibility of using combined TiO_2 photocatalysis oxidation and MBBR process for advanced treatment of biologically pretreated coal gasification wastewater. *Bioresource Technology* 189, 417-420.

Yaman, S., 2004. Pyrolysis of biomass to produce fuels and chemical feedstocks. *Energy Conversion and Management* 45, 651-671.

Yin, C. Y.; Aroua, M. K. and Daud, W. M. A. W., 2007. Review of modifications of activated carbon for enhancing contaminant uptakes from aqueous solutions. *Separation and Purification Technology* 52, 403-415.

Zangeneh, H.; Zinatizadeh, A. A. L.; Habibi, M.; Akia, M. and Isa, M. H., 2015. Photocatalytic oxidation of organic dyes and pollutants in wastewater using different modified titanium dioxides: A comparative review. *Journal of Industrial and Engineering Chemistry*, 26, 1-36.

Zhang, D. F., 2010. Enhanced photocatalytic activity for titanium dioxide by co-modification with copper and iron. *Transition Metal Chemistry* 35, 933-938.

Zhang, Z. J.; Wang, W. Z.; Ren, J. e Xu, J. H., 2012. Highly efficient photocatalyst Bi_2MoO_6 induced by blue light-emitting diode. *Applied Catalysis B: Environmental* 123, 89-93.

Ziylan, A. and Ince, N. H., 2011. The occurrence and fate of anti-inflammatory and analgesic pharmaceuticals in sewage and fresh water: Treatability by conventional and non-conventional processes. *Journal of Hazardous Materials* 187, 24-36.

ANNEXES

ANNEX A

EXPERIMENTAL

A.1 Pyrolysis of sisal wastes

The pyrolysis of sisal wastes was the topic of Article I (Chapter 4). In Figure A.1, some images of the pyrolysis equipment are presented for a clearer understanding of the experimental process. In each run, ca. 20 g of sisal was used, and experiments were carried out in a quartz reactor placed in a tubular horizontal furnace. To ensure an inert environment during the experiments a 100 mL min^{-1} flow rate of nitrogen was continuously fluxed through the reactor. The volatiles evolved during the pyrolysis passed through various consecutive glass condensers immersed in an ice salt cooling mixture (ca. –20 °C) where the condensable liquid fraction was collected. The non-condensable gases were collected in 3 L Tedlar® bags (with a polypropylene fitting for sampling). The aqueous fraction recovered in the condensers (mostly water) was separated from the organic fraction by centrifugation.
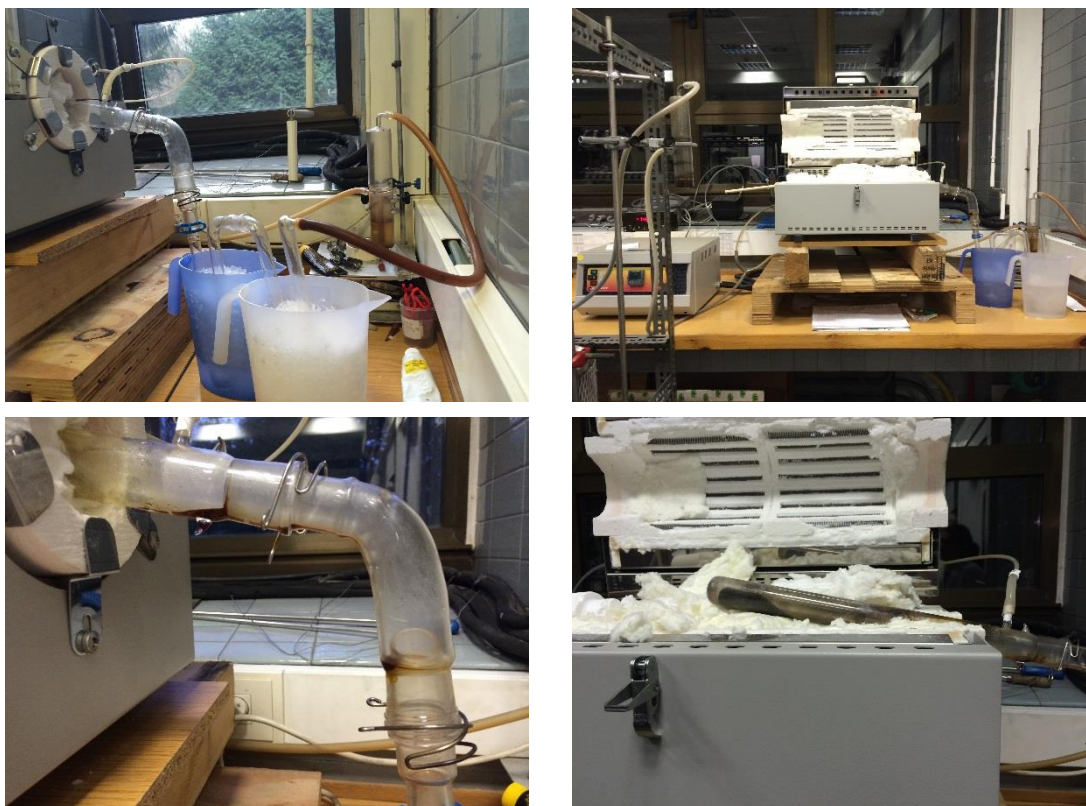

Figure A.1- Images of the experimental procedure of sisal waste pyrolysis.

The organic fraction obtained upon pyrolysis of the sisal wastes was analysed by gas chromatography coupled to mass spectrometry, using an Agilent 7890A gas chromatograph coupled to an Agilent 5975C quadrupole detector. The compounds in the oil fraction were identified by comparison with those reported in the literature and in the Wiley and NIST computer libraries. The gases were analysed in a Hewlett-Packard HP 6890 gas chromatograph fitted to a thermal conductivity detector and two packed columns.

A.2 Preparation of materials

The sisal samples used in this study for the preparation of activated carbons are from the industrial facilities of the CORDEX Group, in Esmoriz, Portugal. These materials are residues of the final stage of string or wire production. The experimental procedure of the preparation of the sisal-based and coper-doped sisal-based activated carbons by physical and chemical activation with carbon dioxide and K_2CO_3 is detailed in Article II and Article III (Chapters 5 and 6). Briefly, 1 cm long sisal pieces were impregnated with a K_2CO_3 solution (weight ratio sisal: K_2CO_3 of 2:1) and activated in a horizontal furnace at 700 °C for 1 h under N_2 flow (5 $cm^3 s^{-1}$). After the activation, the sample was thoroughly washed with distilled water until pH 7 and dried at 100 °C.

A.3 Characterization of materials

A.3.1 Textural characterization

The prepared carbons were characterized regarding their apparent specific surface area and pore volume properties, obtained from the respective N_2 and CO_2 adsorption isotherms at -196 and 0 °C, respectively, in automatic equipments (ASAP 2010 and 2020 and Tristar 3020, Micromeritics). All the analysed samples were previously outgassed under vacuum (ca. 10^{-3} torr) at 120 °C overnight. The apparent specific surface area, A_{BET} was assessed from the application of the BET equation to the experimental data obtained from the N_2 adsorption isotherms, in the range of relative pressures 0.05-0.15. To determine the total pore volume the amount adsorbed at $p/p°$=0.95 was considered. The microporosity evaluation was made using the Dubinin–Radushkevich formulism to the N_2 and CO_2 adsorption data, (W_{0,N_2}, W_{0,CO_2}). The mesoporous volume V_{meso} was obtained by the difference between the total pore volume V_{total} and micropore volume, W_{0,N_2}.

The characterization of the textural parameters of the several batches of carbons S and SCu5 prepared was made, to assure that the variations of these parameters was not significant, and is presented in Table A.1.

Table A.1- Textural parameters of the different batches of carbons S and SCu5 prepared in this study.

Sample	Batch	A_{BET} ($m^2 g^{-1}$)	V_{total} ($cm^3 g^{-1}$)	V_{meso} ($cm^3 g^{-1}$)	W_{0,N_2} ($cm^3 g^{-1}$)	W_{0,CO_2} ($cm^3 g^{-1}$)
S	A	968	0.45	0.04	0.41	0.37
	B	915	0.41	0.01	0.41	0.40
	C	932	0.43	0.02	0.42	-
	D	834	0.38	0.01	0.37	-
SCu5	A	674	0.31	0.01	0.30	0.34
	B	678	0.32	0.02	0.30	-
	C	787	0.36	0.01	0.35	-

A.3.2 Elemental Analysis

Elemental analysis was used for the chemical characterization of the solid fraction obtained after the pyrolysis of sisal waste. For the determination of carbon, hydrogen, nitrogen and sulfur content, the samples were burned at a very high temperature (~ 1200 °C) under oxygen flow. The solids were previously dried under vacuum at 120 °C for 17 hours. The measurements were carried out in LECO automatic analysers (LECO CHNS-932 and LECO VTF-900 for the oxygen content).

A.3.3 Thermal Analysis

The as-received rope waste and the solid carbonaceous residue obtained after pyrolysis were characterized by thermogravimetric analysis. The thermal analyser (Labsys, Setaram) was set to operate at a heating rate of 15 °C min^{-1} under a nitrogen flow rate of 100 mL min^{-1}; for each measurement about 25 mg of sample was used. The ash content of samples S and SCu5 was also determined by thermogravimetric analysis in air atmosphere.

The Temperature Programmed Reduction analysis was performed to determine the chemical state of the copper species in sample SCu5, in a chemisorption analyser (Autochem 2920, Micromeritics) equipped with a thermal conductivity reactor and a mass spectrometer (OmniStar 3000). For each analysis approximately 40 mg of sample was treated with a 50 cm^3 min^{-1} stream of 10 % H$_2$ in Argon from 100 to 600 °C at 5 °C min^{-1}.

A.3.4 X-ray Diffraction

X-ray Diffraction (XRD) patterns were obtained for the sisal waste and the solid fraction (char) obtained after pyrolysis at 550 °C, for the copper impregnated carbons, SCu and QCu, and for the analysis of the chemical state of copper species in the carbon matrix for sample SCu5.The analysed samples were previously pulverized in an agate mortar and placed on a metal horizontal sample holder with a cylindrical cavity of about 1 mm deep.

The diffractograms were obtained on a D8 X-ray diffractometer Bruker AXS with automatic data acquisition, equipped with a graphite crystal curved monochromator coupled to a goniometer and using kα1 radiation of a copper bulb (λ = 1.5406 Å). Scans were carried out between 0.7 ° and 6 ° 2θ, with a step size of 0.03 ° 2θ and a time per step of 4 s, operating at 40 kV and 40 mA in the X-ray tube.

A.3.5 Surface pH

The pH$_{PZC}$ of the carbon samples in Article III was determined by mass titration, adapted from the method proposed by Noh and Schwarz (1989). The carbon samples were first dried in an oven at 105 °C overnight. Millipore water (previously degassed with N$_2$ to eliminate the possible presence of CO$_2$), was used to prepare a mixture corresponding to the weight fraction of 10 % of carbon.

The air that was inside the container was also eliminated before sealing. The container was kept closed for at least 24 hours, leaving the mixture under magnetic stirring at room temperature. After this period, the pH of the mixture was measured with a microelectrode (pH meter VWR Symphony SP70P). Then a volume of Millipore water was added to the mixture, repeating the same procedure to obtain mixtures containing mass fractions of 8, 6 and 4 wt. %.

A.3.6 Infrared Spectroscopy

Interferograms of samples S, TiO_2 and TiO_2/S were obtained using a Nicolet Magna-IR560 spectrometer. Spectra were obtained using the attenuated total reflectance method on powdered samples, without KBr addition. Each spectrum was obtained by collecting 300 interferograms with a 4 cm^{-1} resolution.

A.3.7 Diffuse Reflectance Spectroscopy

The optical features of samples S, TiO_2 and TiO_2/S, were determined by UV–vis diffuse reflectance spectroscopy, recorded on a Shimadzu spectrometer (UV-2501) equipped with an integrating sphere and using $BaSO_4$ as a blank reference. Measurements were recorded in the diffuse reflectance mode (R) and transformed to a magnitude proportional to the extinction coefficient through the Kubelka–Munk function, $F(R\infty)$.

The Energy band gap (E_{bg}) of the photocatalysts was calculated as the intersection point of the extrapolation of the linear segment of the plot $(F(R) \times E)^n$ (being n =1/2 for direct allowed transition in n-type semiconductors such as TiO_2) as a function of the energy in eV (López and Gomés, 2012), in the region near the onset of the the light absorption. As an example, the calculation of the E_{bg} for TiO_2 is presented in Figure A.2.

y = 5.42x - 16.38
R^2 = 0.9996
E_{bg}= 5.42/-(16.38)
=3.02
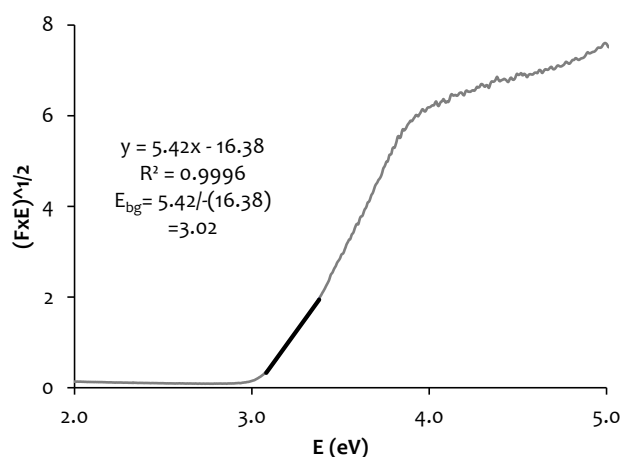
Figure A.2- Graphical representation of a modified Kubelka–Munk function for the experimental determination of the E_{bg} value forTiO₂.

A.3.8 X-ray Photoelectron Spectroscopy

The chemical state of the copper species in sample SCu5 was investigated by X-ray Photoelectron Spectroscopy (XPS) measurements, carried out in high vacuum conditions, with previously dried samples.

A.3.9 Ion Coupled Plasma-Optical Emission Spectrocopy (ICP-OES)

This technique was used to determine the actual copper content of sample SCu5, in a Perkin Elmer Optima 2000 DV equipment.

A.3.10Transmission Electron Microscopy

Transmission Electron Microscopy (TEM) images of samples S and SCu5 were obtained in a Hitachi H-8100 equipment, operating at 200 kV, which corresponds to a point-to-point resolution of 2.7 Å.

A.3.11 Scanning Electron Microscopy

The morphology of the samples and the dispersion of the metallic particles incorporated to the carbon matrices was investigated through Scanning Electron Microscopy (SEM) micrographs of the copper-loaded activated carbons, and EDX (Energy Dispersive X-ray Spectroscopy) analysis (qualitative) of the distribution of heteroatoms on the carbon surface was made using a Ziess DS 942 and a JEOL JSM-7001F equipments, operating at 25 kV. Particles were dispersed on a graphite adhesive tab placed on an aluminum stub. The images were generated in the back scattered electron signal mode, which yielded better quality pictures.

In the following figures (Figure A.3, A.4 and A.5), SEM images obtained for the sisal wastes used as precursor for the preparation of the carbon materials, for carbon S and carbon SCu5, are presented.
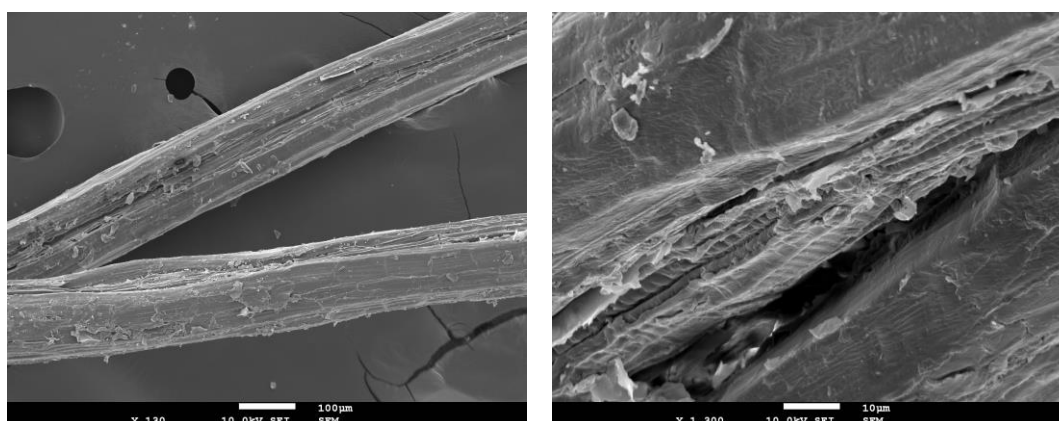

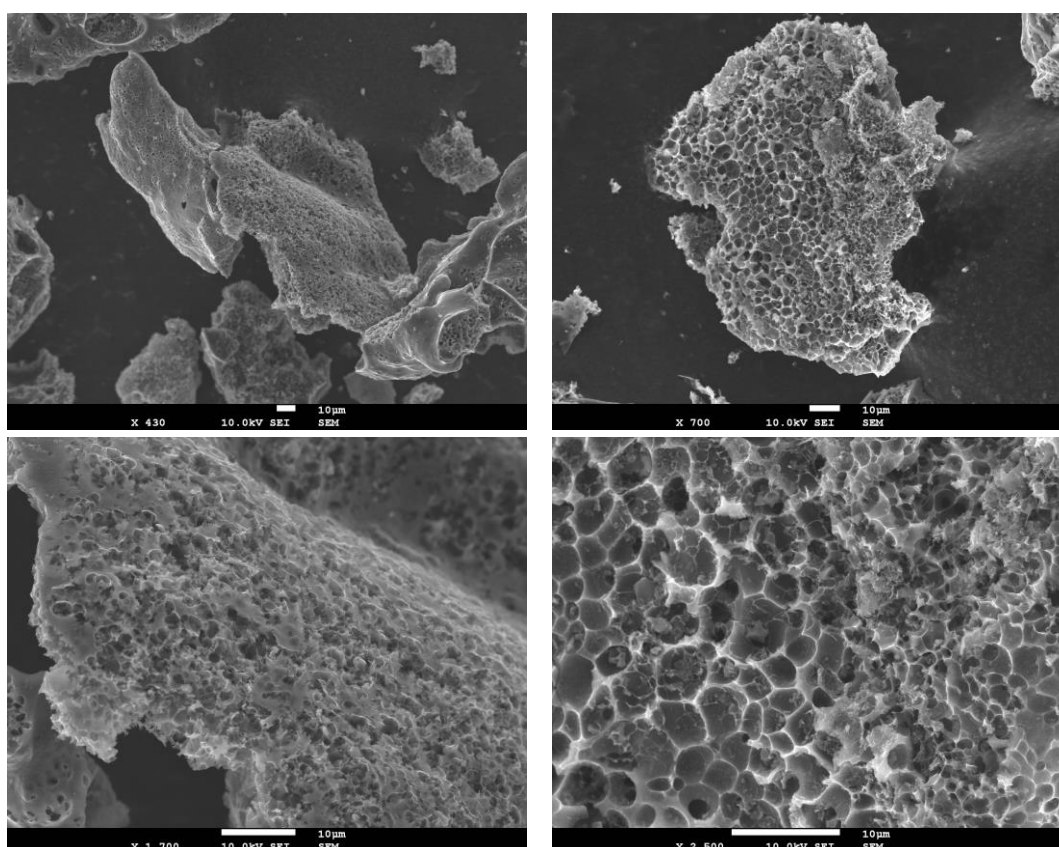**Figure A.3**- SEM images of the pristine sisal wastes.

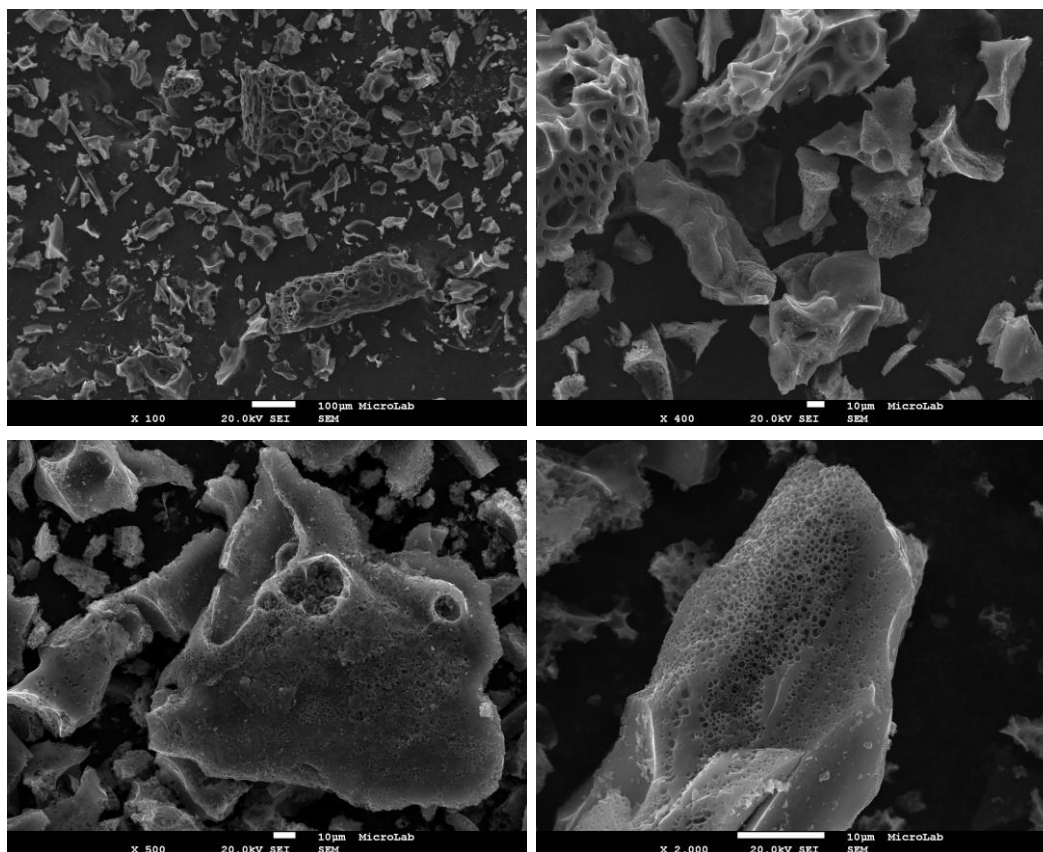**Figure A.4**- SEM images of the unloaded carbon S.

Figure A.5- SEM images of the copper-containing carbon, SCu5.

A.4 Photodegradation experiments methodology

A detailed procedure of the experiments carried out for phenol degradation will be here described. The methodology used included a pre-adsorption step for the activated carbons, before irradiation of the phenol solution. The results obtained from these assays are presented in Article III and IV (Chapter 6).

A.4.1 Photodegradation tests with pre-adsorption

Photodegradation experiments were schematized in order to eliminate the contribution of phenol adsorption within the porosity of the activated carbon; thus, the irradiation of samples was preceded by a pre-adsorption step, to ensure that during irradiation, the contribution of the adsorption process can be minimized, and photocatalysis and photolysis are the only occurring processes.

The activated carbons were put in contact with a phenol solution, with mechanical stirring, during 30 minutes. This contact time was assessed by phenol kinetic adsorption assays, which allowed to determine the time needed to reach phenol adsorption equilibrium. Once phenol adsorption equilibrium was attained, irradiation with UV light was started.

A.4.2 Phenol adsorption kinetics of carbons S and SCu5 in dark conditions

Phenol adsorption studies under dark conditions were initially performed for carbon S and carbon SCu5 (Figure A.6) and the residual concentration of the phenol was determined by UV–vis spectrophotometry (Genesys 10S) at the wavelength corresponding to the maximum absorbance (269 nm) (Figure A.7).
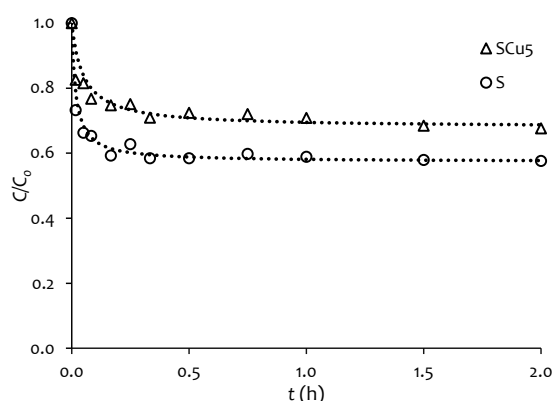
Figure A.6- Phenol concentration decay curves for the studied carbons.
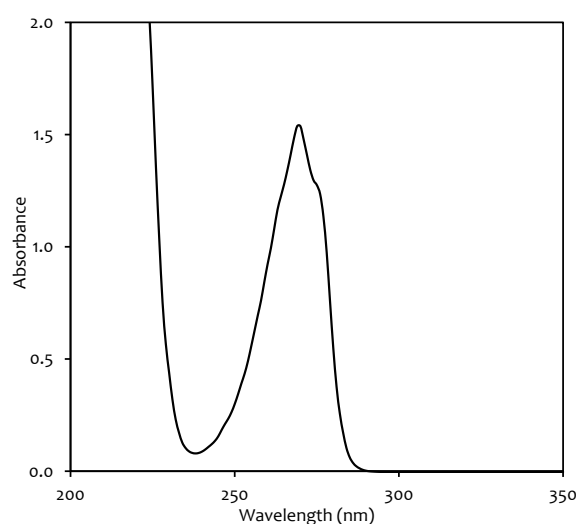
Figure A.7- UV absorption spectra of phenol (C= 100 mg L^{-1}, optical length= 5 mm).

Phenol uptake was calculated according to the following equation:

$$q_t = \frac{(C_o - C_t)}{W} V$$

equation A.1

where q_t is the amount (mg g^{-1}) of phenol adsorbed at time t, C_o is its initial concentration (mg dm^{-3}) and C_t the concentration at time t (mg dm^{-3}), V is the volume (dm^3) of the adsorbate solution and W is the weight (g) of dried carbon. After 30 min of dark exposure to phenol, equilibrium was reached for the two cases. Phenol removal efficiencies achieved were of 42 and 32 % for samples SC and SCu5, respectively. Phenol dark uptake on P25 was also assayed, but its contribution to the amount adsorbed in the case of the composites TiO$_2$/carbon was found to be negligible, which was expected given the non-porous nature of the bare catalyst.

Pseudo-first and pseudo-second order kinetic models, whose theoretic fundamentals are presented in section B.4, were applied to the experimental data. The coefficients of determination of the pseudo-first order (not shown) were very unfavourable, which indicated that this model does not adjust to the experimental data. The fitting results clearly show that the adsorption of phenol onto the activated carbons obeys to the pseudo-second order equation. The kinetic parameters are presented in Table A.2.

Table A.2- Pseudo-second order phenol adsorption parameters for the studied carbons, C_o= 100 mg dm^{-3}. K_2- pseudo-second order rate constant; h- initial adsorption rate; $t_{1/2}$- half-life time; q_e- phenol uptake at equilibrium; C_e- phenol concentration at equilibrium; re- removal efficiency.

Sample	k_2 (g mg^{-1}h^{-1})	R^2	h (g mg^{-1}h^{-1})	$t_{1/2}$ (h)	q_e (mg g^{-1})	C_e (mg dm^{-3})	re (%)
S	0.639	0.9995	5000	0.0177	88.5	59.2	42.4
SCu5	0.316	0.9995	1250	0.0503	62.9	66.4	32.4

A.4.3 Configuration of the photocatalytic reactor

Phenol photodegradation experiments were carried out at room temperature using a photo-reactor of 500 cm^3 capacity; the irradiation source was provided by a high pressure mercury lamp (Helios Italquartz, 125 W, emitting at 313, 360, 404, 436, 546, 577 and 579 nm), whose spectrum is presented in Figure A.8.
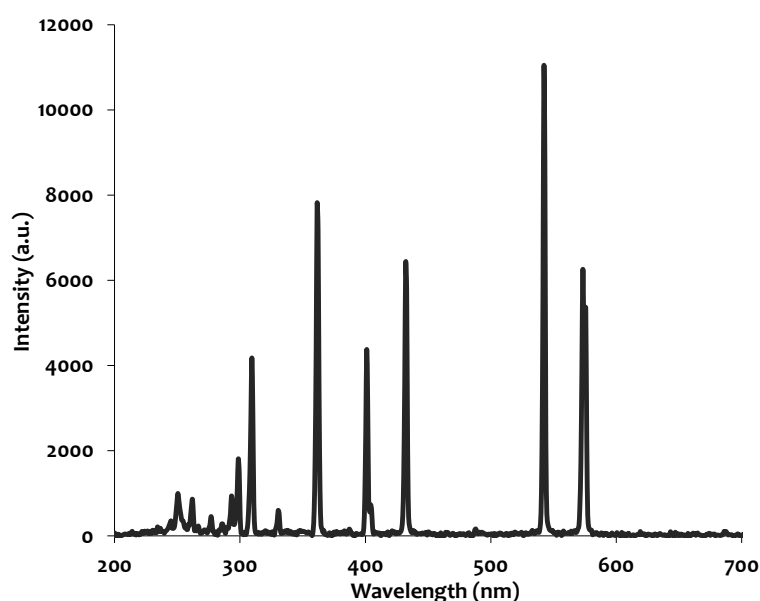
Figure A.8- Emission spectrum of the high pressure mercury lamp (Helios Italquartz, 125 W) used as irradiation source for the photocatalytic experiments.

The lamp was vertically suspended in a cylindrical, double-walled jacket cooled by flowing water, immersed in the solution (Figure A.9). The incident photon flux, evaluated by actinometric determinations was 1.35 x 10^{-5} Einstein s^{-1} and 9.14 x 10^{-6} Einstein s^{-1}, when a Pyrex filter was used. The water cell was used to control the temperature during the experiments, preventing any overheating of the suspension due to the irradiation. The reactor was open to air in all the experiments to ensure that enough oxygen was present in the reaction solution. The catalysts were added to 500 cm^3 of phenol solution under vigorous stirring (900 rpm).

High Performance Liquid Chromatography (HPLC) was used to analyse the aliquots (~ 1 cm^3) taken from the reaction solution at pre-determined time intervals of irradiation. A Shimadzu chromatograph with a reverse phase column (Spherisorb C18, 125 mm x 4 mm) was used, using as mobile phase a mixture of methanol-water, and a detector UV-Vis photodiode array. Coinciding with the respective maximum absorption spectra the selected wavelengths in the detector were 245, 269, 273, 275 and 285 nm for the concentration measurement of benzoquinone, phenol,

resorcinol, catechol and hydroquinone, respectively. All samples were filtered through 0.45 μm pore size membranes prior to chromatographic analysis.

Figure A.9- Irradiation source and photocatalytic reactor used in the experiments.

Total Organic Carbon (TOC) analysis was performed to determine the mineralization degree of the contaminant reached after the photocatalytic process. The equipment used was a Shimadzu TOC-VCPH E200V.
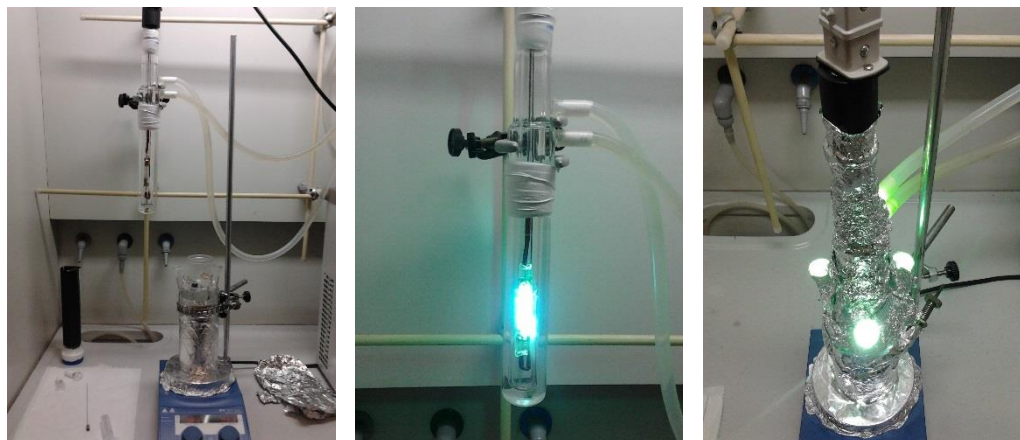
ANNEX B

THEORETICAL FUNDAMENTALS OF THE CHARACTERIZATION METHODS

The full characterization of activated carbons (texture, composition, structure) is quite challenging, given their extreme complexity regarding size and shape of pores, and variety of structures and surface functionalities. However, a good knowledge of the porous structure of activated carbons, and of the factors that control the extent of adsorption, as well as the energy associated with it becomes imperative due to the wide range of application of these materials.

The most effective experimental approach for obtaining information on the adsorption process is the experimental determination of an isotherm, which contains information on the adsorption process. On the other hand, knowledge of the surface chemistry of carbon materials is also of fundamental importance, since their physical and chemical properties are strongly influenced by the presence of chemical species at the surface that will determine many of its applications.

Throughout this section the theoretical fundamentals of the techniques used for the characterization of the activated carbons prepared in the course of this dissertation will be briefly described.

B.1 Textural characterization

B.1.1 Adsorption of gases and vapors

Adsorption is a spontaneous process that occurs whenever the surface of a solid is exposed to a gas or a liquid. More specifically, it can be defined as the adsorptive enrichment of a given fluid, or the increased density of this fluid, in the vicinity of an interface. One of the most suitable methods for the interpretation of the adsorption data, especially for the general characterization of their micro- and mesoporosity of carbon materials, is the adsorption of gases and vapors.

Physical adsorption of gases is fundamentally a thermodynamic phenomenon. Being essentially a spontaneous process, at constant temperature the free energy variation ΔG is negative; on the other hand, adsorption corresponds to an ordering of the molecules on the solid surface, carrying an entropy change, ΔS, also negative. Thus, at constant temperature:

$$\Delta G = \Delta H - T\Delta S \qquad \text{equation B.1}$$

from what it can be concluded that the enthalpy variation, ΔH, should also be negative, indicating that the adsorption processes are exothermic and therefore not favoured by temperature.

B.1.2 General definitions and terminology

The adsorption phenomenon is the result of interaction forces between the solid and gas molecules. According to the nature of such interactions a distinction can be made between physical adsorption (or physisorption) and chemical adsorption (or chemisorption). Some of the key terms and properties associated with the adsorption are presented in Table B.1.

Table B.1- Some definitions regarding the adsorption process.

Term	Definition
Adsorption	Enrichment of the interface in one or more components
Adsorbate	Substance in the adsorbed state
Adsorptive	Substance that will be adsorbed
Adsorbent	The solid material in which adsorption occurs
Chemical adsorption	Adsorption process which involves the formation of a chemical bond with the solid
Physical adsorption	Adsorption process that does not involve the formation of a chemical bond with the solid

Simultaneously with the process of adsorption, which is a surface phenomenon, absorption may occur, with regard to the entire mass of solid. In cases in which it is practically impossible to distinguish between the two processes, it is convenient to use the wider term sorption.

B.1.3 Classification of pores

Porosity may be defined as the ratio between the volume of pores and voids and the volume occupied by the solid. However, a given porosity value can not be regarded as characteristic of the material, since it depends on the method used for its determination. In a way that is necessarily arbitrary, it is considered that the outer area corresponds to the area of the protuberances and cavities which are wider than deep, and the inner area to the walls of the pores and slits having a depth greater than the width. Porous solids usually have an internal area that is of a much higher order of magnitude than the external area. According to IUPAC (Rouquerol, Avnir, *et al.*, 1994), the pores can be classified upon their size as:

- Micropore- Pore of internal width >2 nm;
- Mesopore- Pore of internal width between 2 and 50 nm;
- Macropore- Pore of internal width <50 nm;
- Nanopore- Pore of internal width less than 100 nm.

B.1.4 Chemical and physical adsorption

The distinction between chemical and physical adsorption is based on the interactions between the solid and the molecules that are adsorbed. Physical adsorption always occurs whether or not accompanied by chemical adsorption. Both phenomena can be distinguished by the following characteristics (Rouquerol, Roquerol, *et al.*, 2014):

- Physical adsorption is a general phenomenon with a relatively low degree of specificity, while chemical adsorption is selective, depending on the reactivity of the adsorbent and the adsorbate;
- The adsorbed molecules are chemically bound to the surface active centers, for which adsorption occurs in a monolayer. At high relative pressures, physical adsorption usually occurs in multilayer; a physically adsorbed molecule retains its identity when it desorbs,

returning to its original shape. If a chemically adsorbed molecule undergoes reaction or dissociation, it loses its original identity;

- The energy of chemical adsorption is of the same order of magnitude of the energy of a chemical reaction. The physical adsorption is always exothermic, but the energy involved is not much larger than the energy of the condensing adsorbable. However, this can be considerable high when the physical adsorption occurs at very small pores;

- In chemical adsorption, an activation energy is often involved and at low temperatures, it may not be possible to achieve thermodynamic equilibrium. In physical adsorption equilibrium is reached quickly, since activation energy is not required.

- The chemical adsorption involves the formation of chemical bonds, whereby the heat of adsorption is of the order of magnitude of the heat of reaction.

B.1.5 Adsorption of gases in solids

In the case of gas adsorption on solids, the amount of gas adsorbed by a solid sample is proportional to the mass of the sample and depends on the temperature, T, the pressure, p, and of the nature of the solid and gas. The amount of gas adsorbed at a given temperature, n^{ads} (usually expressed in mmol g^{-1}), is given by:

$$n^{ads} = f(p, T, gas, solid) \qquad \text{equation B.2}$$

where p is the equilibrium pressure, for constant temperature, gas composition and mass of the solid. Alternatively, if the gas is below its critical pressure, the amount adsorbed can be expressed in terms of relative pressure $p/p°$, where $p°$ is the gas saturation pressure at the temperature of the isotherm, replacing p, in equation B.2, by $p/p°$. This form can be advantageous, since for each temperature, $p/p°$ varies between 0 and 1. Equation B.2 is a general expression for an "adsorption isotherm", which represents the relation, at constant temperature, between the amount adsorbed and the equilibrium pressure, or concentration.

B.1.6 Adsorption isotherms

The theory of gas/solid adsorption was developed especially from experimental isotherms, which is the reason why most of the fundamental equations do not include temperature. The experimental determination of adsorption isotherms can be made by static or dynamic methods. In either case, it is necessary to clean the surface of the solid before the analysis and the exact conditions for this depend on the nature of the sample. Nevertheless, degassing under vacuum and applying temperature is the recommended (Sing, Everett, *et al.*, 1985). In static methods, successive amounts of the substance to adsorb are added to a previously evacuated volume in which the sample is located, and the amount adsorbed is determined when equilibrium is reached for each value of pressure. The adsorbed amount may be determined gravimetrically, using a balance, or volumetrically. In this case, the calculation is based on the application of the ideal gas equation, once the volume of the system is known (by prior calibration).

The adsorbed amount may be expressed in different units: moles, cubic centimeters or grams at standard temperature and pressure conditions. It is recommended, however, that the amount adsorbed would be expressed in moles per gram of solid, n^{ads}. There are several mechanisms by which a porous solid can retain a vapor. The physical adsorption originates adsorbed multilayers at low temperature (close to the boiling point). This is the mechanism

responsible for adsorption on meso and macropores, as well as on the geometric surface of the materials.

The dimensions of the micropores are of the same order of magnitude as the dimensions of the molecules, whereby the adsorption on these pores has special characteristics, namely as a result of the overlay of the adsorption potential fields due to the proximity of the walls of the pores. The chemical adsorption energies are high, and the adsorbed is held in a condensed state and the amounts adsorbed at low pressures are relatively very high.

A third mechanism for vapor retention (temperatures below the critical temperature) on porous solids is capillary condensation. In reality, the vapor saturation pressure in the interior of a pore is lower than the value determined in contact with surfaces without curvature. This pressure is as smaller as the pore size, according to the Kelvin equation. When adsorption equilibrium isotherms are determined, as the pressure increases, increasingly larger pores become saturated by condensation of the adsorbed.

The shape of the adsorption isotherm depends not only on pore size distribution but also on the molecular dimensions of the adsorbate molecule. Thus, the critical parameter is not the pore size, but the relation between the pore size and the critical dimension of the adsorbate molecule. Thus, the adsorption isotherm analysis of different molecules in a given adsorbent generates a complete set of information for the characterization of its porous texture.

B.1.7 Classification of adsorption isotherms

In 1940, Brunauer, Deming, Deming and Teller grouped all known isotherms into five types (BDDT classification) (Brunauer, Deming, *et al.*, 1940). The IUPAC included a sixth type of isotherm which had been observed later on (Sing, Everett, *et al.*, 1985). However, given the new characteristic types of isotherms identified and shown to be closely related to particular pore structures, over the past 30 years, a refinement of the original IUPAC classification of isotherms was necessary (Thommes, Kaneko, *et al.*, 2015). The current IUPAC classification of adsorption isotherms is presented in Figure B.1. The existence of hysteresis is associated with the isotherm types IV and V. Each type of isotherm is associated to a particular mechanism (physical adsorption, chemical adsorption, capillary condensation). As a result, from the simple observation of experimental isotherms, some conclusions can be drawn on the porous texture of the material.

Reversible Type I isotherms are given by microporous solids presenting relatively small external surface areas, as is the case of some activated carbons, molecular sieve zeolites and certain porous oxides. A Type I isotherm is concave to the $p/p°$ axis, and characterized by a limiting value of the amount adsorbed, which begins to set at relatively low relative pressure and is extended to the saturation pressure. The threshold corresponds to the complete filling of the micropores, and therefore its height is proportional to the micropore volume. Type I(a) isotherms are given by microporous materials having mainly narrow micropores (of width < ~ 1 nm), while Type I(b) isotherms are characteristics of materials with wider pore size distributions (including wider micropores and narrow mesopores, of width < ~ 2.5 nm). These isotherms also represent chemical adsorption, in which case the threshold value corresponds to the formation of a monomolecular layer adsorbed on the active sites.
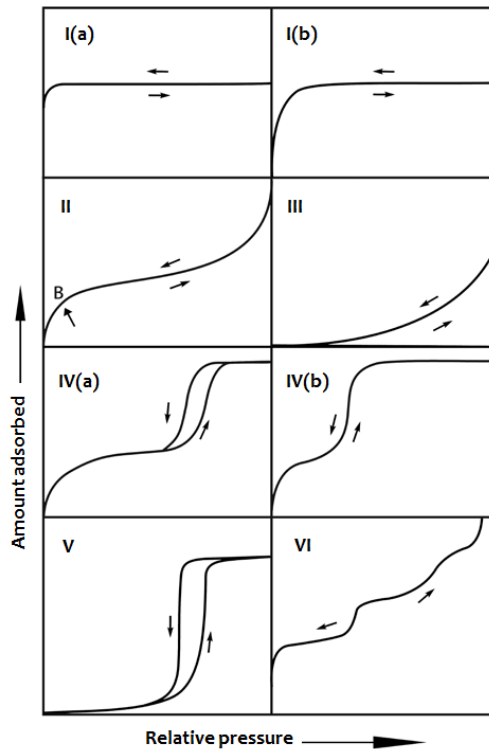
Figure B.1- IUPAC classification of adsorption isotherms (adapted from Thommes, Kaneko, *et al.*, 2015).

Reversible Type II isotherms are characteristics of the adsorption of most gases on non-porous or macroporous adsorbents, with unrestricted monolayer-multilayer adsorption. These isotherms are concave relative to the x-axis up to a certain point, normally referred to as point B, when the middle almost linear section starts. If the knee is sharp, point B usually corresponds to the completion of monolayer coverage, while a less distinctive point B is an indication of a significant amount of overlap of monolayer coverage and the onset of multilayer adsorption. After this almost straight section, the slope increases and the curve becomes convex to the axis of abscissas.

The Type III isotherm is convex in relation to the axis of the abscissas and does not present a point B, with no monolayer formation. This indicates that the adsorbent-adsorbate interactions are relatively weak and the adsorbed molecules are clustered around the most favourable sites on the surface of a non-porous or macroporous solid.

Type IV isotherms are characteristic of mesoporous adsorbents, as many oxide gels, industrial adsorbents and mesoporous molecular sieves. The adsorbent-adsorptive interactions and the interactions between the molecules in the condensed state rule the adsorption behaviour in mesopores. The initial monolayer-multilayer adsorption on the mesopore walls, which is similar to the corresponding part of a Type II isotherm, is followed by capillary condensation, with the existence of a final saturation plateau of variable length. In Type IV(a) isotherms, capillary condensation is accompanied by hysteresis (different equilibrium points obtained for adsorption and desorption), that occurs when pore widths exceeds a certain critical width, depending on the adsorption system and temperature (for nitrogen adsorption at – 196 °C, hysteresis occurs at pores > ~ 4 nm). Completely reversible Type IV(b) are observed for adsorbents having mesopores of smaller width.

B.1.7 Classification of adsorption isotherms

Type V isotherms are, to a certain pressure value, similar to the isotherms of Type III, which is an indication of relatively weak adsorbent-adsorbate interactions. At higher relative pressure values, molecular clustering is followed by pore filling. These isotherms are obtained for water adsorption on hydrophobic microporous and mesoporous adsorbents.

Reversible stepped Type VI isotherms are associated with layer-by-layer adsorption on highly homogeneous non-porous surfaces. The levels, at approximately equal heights, correspond to the formation of successive adsorbed layers, and the sharpness of the step depends on the system and the temperature. Type VI isotherms are typically obtained with argon or krypton at low temperature on graphitized carbon blacks.

The hysteresis phenomenon is a result of the capillary condensation that occurs in the mesopores and results from the fact that condensation and evaporation of the adsorbed gas does not occur at the same relative pressure. Normally this phenomenon is attributed to the thermodynamic effects (formation of metastable vapor states), or constrictions in the porous network (percolation, cavitation), or even a combination of the two effects (Rouquerol, Rouquerol, *et al.*, 2014). In addition, hysteresis may also be caused by the effects of connectivity of the pores (Choma and Jaroniec, 2006).

The original IUPAC hysteresis classification, that reported Types H1, H2, H3 and H4 (Sing, Everett, *et al.*, 1985), was extended to six characteristic types, for carbons or other non-carbonaceous materials, corresponding to different pore structures, in the light of recent findings (Thommes, Kaneko, *et al.*, 2015), as presented in Figure B.2:
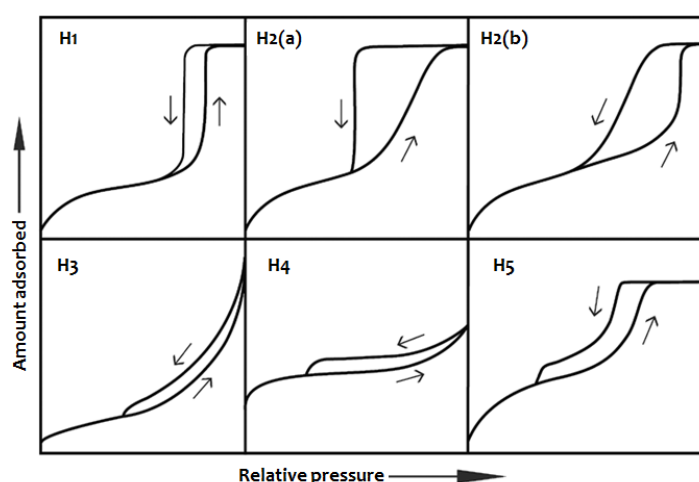
Figure B.2- Classification of hysteresis loops, according to the IUPAC (adapted from Thommes, Kaneko, *et al.*, 2015).

The characteristic features of some types of loop are associated with certain well defined pore structures:

- Type H1 loop is characterized by two almost parallel branches of the isotherm, a clear sign of delayed condensation of the adsorption branch. It is associated to porous materials with a narrow range of uniform pores (e.g., template silicas and ordered mesoporous carbons);
- The Type H2 loop, in which only the desorption branch is almost vertical, is associated to materials with complex pore structures and that tend to be made up of interconnected networks of pores of different size and shape. Type H2(a) displays a very steep desorption

branch, attributed to pore-blocking/percolation in a narrow range of pore necks or to cavitation-induced evaporation, being characteristic of many silica gels and ordered mesoporous materials. In the Type H2(b) loops, also associated with pore blocking, the size distribution of neck widths is much larger. Mesocellular silica foams and certain mesoporous ordered silicas exhibit this type of hysteresis loop;

- Type H3 loop is characterized by the resemblance of the adsorption branch to a Type II isotherm and a lower limit of the desorption branch. This type of loop is usually given by the aggregates of platy particles or adsorbents containing slit-shaped pores;

- Type H4 loop presents an adsorption branch that is a composite of Types I and II, in which the marked uptake at low relative pressures is associated to the filling of micropores. Examples of this type of hysteresis is found for aggregated crystals of some mesoporous zeolites and micro-mesoporous carbons;

- Type H5 loop is rather unusual, although it has a distinctive form associated with certain pore structures containing both open and partially blocked mesopores.

Activated carbons typically have loops of type H4 hysteresis, returning to a zero adsorbed amount after desorption to relative pressures of approximately zero (Marsh and Rodríguez-Reinoso, 2006).

B.1.8 Quantitative Interpretation of Isotherms

In addition to the analysis of the isotherms shape, these must be quantitatively interpreted, so that comparisons between materials can be made. For an analysis of the texture of activated carbon is necessary to know the amount of carbon porosity along with an indication of the type of porosity, namely pore size distribution. Numerous analytical methods for determining the specific surface area from adsorption data are available, which are generally of a semi-empirical character. The methods and models employed in the analysis of the adsorption isotherms of N_2 and CO_2 of materials obtained throughout this work will be described in the next section. A thorough and comprehensive analysis of the many proposed methods for the analysis of adsorption isotherms will not be presented here. The discussion on the characterization techniques of porous solids can be further consulted in a wide bibliography (Rodríguez-Reinoso, McEnaney, *et al.*, 2002; Choma and Jaroniec, 2006; Marsh and Rodríguez-Reinoso, 2006; Rouquerol, Rouquerol, *et al.*, 2014; and references therein).

B.1.9 Assessment of surface area- Model and equation of Brunauer-Emmett-Teller

The most often used mathematical treatment for the determination of the specific surface area, is the model proposed by S. Brunauer, P. H. Emmett and E. Teller, in 1938, which aimed to quantitatively describe the physical adsorption of vapor, and thus, the Type II or Type IV(a) isotherms (Brunauer, Emmett, *et al.*, 1938). Nevertheless, this model has been subjected to a number of criticisms and there is a general awareness of the shortcomings in relation to the underlying theory.

The BET model is based on the kinetic model on the monolayer adsorption proposed by Langmuir. A dynamic equilibrium of adsorption and desorption is recognized, but the possibility of forming adsorbed multilayers is included, an hypothesis that on one hand explains the general shape of a type II isotherm and on the other is not admissible in chemical adsorption, being yet compatible with the phenomenon of physical adsorption. It is based on the following assumptions:

B.1.9 Assessment of surface area- Model and equation of Brunauer-Emmett-Teller

- In each layer, the adsorption rate is equal to the desorption rate;
- The heat of adsorption from the second layer is constant and equal to the vapor condensation heat;
- When $p = p°$, the vapor condenses as a liquid and the ordinary number of adsorbed layers is infinite.

The mathematical equation that results from BET model is generally used in the linear form:

$$\frac{p/p°}{n^{ads}\left(1-(p/p°)\right)}=\frac{1}{n_m c_{BET}}+\frac{c_{BET}-1}{n_m c_{BET}}\left(p/p°\right) \quad \text{where} \quad c_{BET}=e^{\left(\frac{E_1-E_L}{RT}\right)} \qquad \text{equation B.3}$$

where n^{ads} corresponds to the amount adsorbed at the relative pressure $p/p°$, and temperature T, $p°$ corresponds to the vapor saturation pressure at temperature T, n_m is the adsorbed amount needed to fill the monolayer, and c_{BET} is designated the BET constant defined as $(E_1-E_L)/RT$, with E_1 e E_L, being the heat of adsorption of the first layer and the vapor condensation heat, respectively.

The application of this equation to the experimental data, allows the determination of the number of adsorbed moles in the monolayer (n_m); from this value, the area occupied by a monolayer on the surface of a solid (A_{BET}) can be calculated by the expression:

$$A_{BET}=n_m N_A a_m \qquad \text{equation B.4}$$

where N_A is the Avogadro's number (6.02×10^{23} mol^{-1}), n_m is the monolayer capacity, and a_m is the average area occupied by a molecule of adsorbate in the monolayer. For nitrogen at $-196°$ C (the temperature of liquid nitrogen), $a_m = 0.162$ nm^2 (Gregg and Sing, 1982). The value of a_m should be, as much as possible, constant and characteristic of adsorbate, which presupposes the existence of a poorly localized interface. However, the higher the value of the parameter c, more energetic and localized will be the adsorption, and therefore the value of a_m will be more dependent of the adsorbent itself.

The BET equation, originally proposed to describe the Type II sigmoid isotherms, can reproduce the initial part of any of the BDDT isotherms, varying the value of parameter C_{BET}. When the adsorbents are not microporous, this equation usually has a maximum validity in the relative pressure range $p/p°$ =0.05 and $p/p°$ =0.3, respecting to the equation linearity area. At higher or lower pressures, the BET equation provides adsorbed quantities which are, respectively, lower and higher than real.

In the case of microporous adsorbents such as activated carbon, the range of validity of equation is generally much more restricted, usually between values of $p/p°$ from 0.05 to 0.20. In this study the range of relative pressures used was limited to 0.05 < $p/p°$< 0.15. In microporous samples, the surface area determined by the BET method can not have a real physical meaning. This results from the fact that adsorption on this type of materials does not take place by superimposing layers, but rather by microporosity filling. In this context, the surface area determined by the BET method should only be seen as an apparent surface area.

B.1.10 Assessment of microporosity- Dubinin-Raduskhevich equation
The Dubinin-Raduskhevich equation (DR equation) is based on the Polany potential theory and admits that the adsorption process involves the filling the micropore volume and not the formation of several layers on the pore walls, as proposed by the BET or Langmuir models. This equation was proposed in 1947, arguably occupying a central position in the physical adsorption of gases and vapors in microporous solids theory (Theory of Volume Filling of micropores) (Choma and Jaroniec,

2006). The DR equation is different from the BET equation, because it is not based on a model that describes gas physical adsorption, being an empirical method that takes into account the distinct adsorption energies. The fractional filling of the micropore volume, W/W_0, is expressed in the general form:

General form $\qquad$ $W/W_0 = \exp\left[-(A/E)^2\right]$ $\qquad$ equation B.5

Linearized equation $\qquad$ $\ln W = \ln W_0 - (R \cdot T/\beta \cdot E_0)^2 \cdot \ln^2\left(p^{\circ}/p\right)$ $\qquad$ equation B.6

where W is the volume occupied by adsorbed phase, W_0 the microporous volume, A is the adsorption potential ($A = -RT \ln(p/p^{\circ})$, E is the characteristic energy of the system under study and β is an affinity coefficient. Being a linear equation (B.6), the graphical representation of $\ln W$ vs $\ln (p^{\circ}/p)^2$ is a straight line whose intersection with the y-axis allows the determination of the micropore volume (w_0).

Ultramicroporous carbons generally originate linear DR plots, over a wide ranges of p/p°, but the extent of the linear region is much more restricted for most nanoporous carbons. Also, the significance of the empirical parameters of the DR equation is questionable, and as consequence, it must be emphasized que the DR simple plot can not always give a true assessment of the effective micropore volume.

The linearity of the DR equation is only observed at low relative pressures values, since the linearity deviations occur in the case of not exclusively microporous solids, deviations which are accentuated for the progressive increase of pressure values. In many cases the upward positive deviation is associated with the loss of rectangularity in the adsorption isotherm due to a higher contribution of the wider micropores and even mesopores (Rodríguez-Reinoso and Sepúlveda-Escribano, 2001), in which filling occurs through a cooperative mechanism. The most usual explanation for this kind of deviations is the capillary condensation in the mesopores. However, the existence of two types of microporous in the solid, with different dimensions, has also been pointed as a reason for this fact, since it originates the same sort of deviations.

As part of this work, the DR equation was applied to the results obtained for the adsorption of nitrogen at $-196\,°C$ and CO_2 at $0\,°C$, allowing to estimate the total micropore volume and the volume of narrower micropores (ultramicropores), respectively, of the studied activated carbons. The comparison of the micropore volume obtained by applying the DR equation to the nitrogen adsorption isotherm at $-196\,°C$, with the value obtained by applying the same equation to the CO_2 adsorption isotherm at $0\,°C$ for a given carbon material can lead to three different observations (Rodríguez-Reinoso and Sepúlveda-Escribano, 2001):

(i) $W_{0,N2} < W_{0,CO2}$ – This situation occurs when the microporosity is too narrow, and may attributed to the difficulty in achieving equilibrium in the adsorption of N_2 molecules at the low temperature at which the process occurs;

(ii) $W_{0,N2} \approx W_{0,CO2}$ – This case is observed on carbons with intermediate activations. The DR representations of these solids are substantially linear over a wide range of relative pressures, although there may be some positive deviation for the adsorption of nitrogen at high relative pressures. The characteristic curves of the two adsorbates ($\ln W$ vs A^2) can be adjusted by the same

line. The carbons that exhibit this behaviour have relatively narrow microporosity but sufficiently wide to avoid diffusional limitations for N_2 at $-196\,°C$;

(iii) $W_{o,N_2} > W_{o,CO_2}$ – This kind of results is observed for carbons with high degrees of activation. When it is not possible to obtain results for the adsorption of N_2 at $-196\,°C$ at low relative pressures ($p/p° = 0.01$), the extrapolation of the characteristic curve for N_2 at $-196\,°C$ and CO_2 at $0\,°C$ is not coincidental. Thus, the range of relative pressures used for applying the DR equation is not the same, and the micropore volume obtained for N_2 is superior to that obtained with CO_2. These carbons have a very wide microporosity and the adsorption of N_2 at $-196\,°C$ occurs in micropores of larger dimensions than the micropores in which adsorption of CO_2 at $0\,°C$ takes place, due to the fact that different ranges of relative pressures are used.

The resulting uncertainty of the limit of application of the DR equation to the nitrogen adsorption data at $-196\,°C$ in carbons with a wider pore size distribution, resulting from the heterogeneity of the porous system, and consequently, the adsorbate and the range of pressures used, suggests the use of other complementary approaches to the analysis of these adsorption isotherms.

B.1.11 Pore size distribution assessment

There are many methods to calculate the pore size distribution, most of them based on classical methods (i.e., Horvath-Kawazoe and t-plot method for micropores, and those based on the Kelvin equation for the mesoporosity, such as Barrett, Joyner and Halenda (BJH) or Broekhoff and de Boer (BdB), and their modifications (Choma and Jaroniec, 2006).

All pore distribution calculation methods are based on the assumption that the experimental isotherm can be expressed as the sum of the isotherms of individual pores forming the porous solid structure.

In the 80's considerable progress was made on the understanding of fluid behaviour constrained by the presence of walls, which led to the application of the Density Functional Theory (DFT) to the adsorption phenomena (Tarazona, Marconi, *et al.*, 1987; Seaton, Walton, *et al.*, 1989; Lastoskie, Gubbins, *et al.*, 1993). From a mathematical approach, the DFT method applied to the calculation of PSD is based on the integral of the individual isotherms of defined given sizes:

$$n(p) = \int_{W_{min}}^{W_{max}} f(w) \cdot \rho(p, w) \cdot dw \qquad \text{equation B.7}$$

where *n(p)* is the amount of adsorbed gas at a p pressure, w_{min} *and* w_{max} are the minimum and maximum pore widths, *f(w)* is the distribution of pore volumes as a function of the pore width, and $\rho(p,w)$ is the molar density of the adsorbate dependent on *p* and pore width *w*.

The most advanced form of this theory is called the non-local approach (NL-DFT) that that is based on calculating model isotherms that may be used to determine pore size distribution from gas adsorption data. The first approaches made assumptions concerning the functional form of the size distribution; more recently, a generalization was accomplished by numerical deconvolution of the isotherm data using a set of pore shape dependent model isotherms calculated from DFT, each member of the set being representative of a unique, narrow range of pore sizes. Nowadays, the advanced methods based on NLDFT succeed in determining the pore size distribution in the entire

range of pore sizes accessible by the adsorptive molecule (Jagiello and Olivier, 2013a; Jagiello and Olivier, 2013b).

More sophisticated methods based on the DFT have been recently developed for the determination of the pore size distribution, although few studies in the literature are related to CO_2 adsorption in carbon materials. These methods are however difficult to implement due to its mathematical complexity.

In a study by Pinto and coworkers (Pinto, Mestre, *et al.*, 2010), the authors make a comparison of the methods for the determination of pore size distribution of carbonaceous materials from the CO_2 adsorption isotherm, concluding that the results of applying the DR equation to estimate the pore size distribution are highly dependent on the method used to make the adjustment of the experimental data. The authors propose a more suitable method that does not assume a Gaussian distribution (equation B.8).

$$w(A) = \sum_{i=1}^{m} w_{oi} \exp\left[-\left(\frac{A}{\beta E_{oi}}\right)^2\right] \qquad \text{equation B.8}$$

where β ($\beta = E/E_o$) is the affinity coefficient, and E_o is the characteristic energy that depends on the adsorbent. From the practical point of view, it is preferable to always use this method for the determination of pore size distribution of carbon materials, because there often is no previous indication of how developed is the porosity of a new carbon adsorbent (activated carbon or char) and how this could influence the microporous distribution results.

B.2 Chemical and structural characterization

The complexity of the surface of carbon materials makes it difficult to select a single characterization technique to successfully explain all the chemical properties of the surface. There are numerous available techniques to characterize the surface chemistry of activated carbons, such as infrared spectroscopy, Boehm and potentiometric titrations and thermal analysis that provide information about the composition and concentration of surface groups. Other techniques are focused on the crystal structure, as for example, electron microscopy and X-ray spectroscopy. The combination of complementary techniques with chemical analysis is a powerful tool for determining the composition and concentration of functional groups present in carbon materials. A description of the chemical characterization methods used in this study will be presented below.

B.2.1 Elemental analysis and ash content

The amount of heteroatoms present in carbons may result from the raw material, the activation process or some after-treatment. The elements which remain after the complete combustion of a carbonaceous material to constitute the ashes of the material. The quantity and composition (inorganic matter) of the ashes may vary according to the precursor used. Activated carbons may contain up to about 20 wt. % of ash content (Rodríguez-Reinoso and Sepúlveda-Escribano, 2001). In addition to the quantification of inorganic matter by the determination of the ash content, the remaining heteroatoms can also be quantified by elemental analysis, including oxygen, hydrogen, nitrogen and sulfur, as well as carbon, which is the major component.

The elemental analysis of an activated carbon allows the quantification of the heteroatoms present on the carbon matrix, providing first information about the possible functional groups present in the sample. Even though the percentage of heteroatoms is quite low compared to the percentage

of carbon atoms, these atoms, especially oxygen, play a decisive role in the chemical characteristics of the materials.

B.2.2 pH at the point of zero charge

The surface charge of activated carbon is determined by the nature of the surface groups and pH, as the surface may present characteristics of acidic or basic centers, thereby displaying an amphoteric character. The surface chemistry depends essentially on the presence of heteroatoms, and most frequently on the content and nature of oxygen functional groups on the surface. These groups will also determine the hydrophobicity of the carbon and the electronic density of graphenic layers. When an activated carbon is immersed in an aqueous solution it develops a surface charge resulting from the dissociation of surface groups or the adsorption of ions in solution. The surface charge depends on the pH of the solution and the surface characteristics of the material.

The dissociation of acidic surface oxygenated functionalities, such as phenolic or carboxyl groups (Brönsted acids) originates a negative charge. Moreover, the source of a positive surface charge is more uncertain, since in carbons with nitrogenated groups it can be assigned to oxygen surface complexes as pyrones or chromenes, or due to the existence of high electron density regions in the graphenic layers that act as basic Lewis centers, which accept protons from the solution (Marsh and Rodríguez-Reinoso, 2006).

The determination of the surface charge can be achieved by electrokinetic methods or mass titration. These methods are complementary, especially in the case of activated carbons. The former measures the surface charge on the outer surface area of the particle, while the latter provides a measure of the total surface charge. Also, determining the surface pH value of the carbon material can provide useful information on the surface charge distribution. In this regard, the pH value required to present zero surface charge -pH at the point of zero charge - pH_{PZC}- is considered a crucial parameter for the characterization of the electronic charge of the surface of activated carbons. In the model presented by Noh and Schwarz (Noh and Schwarz, 1989), the pH_{PZC} is evaluated in an aqueous suspension. It is assumed that near neutrality, at pH_{PZC} of 7, the pH of the suspension is independent of the mass of carbon. Otherwise the pH variation is due to the dissociation of ionizable groups on the surface of the carbon materials.

Carbons that present a pH_{PZC} < 7 carbons are referred to as acidic ones, while basic carbons are those which have a pH_{PZC} > 7. For an amphoteric material, the surface is positively charged at pH < pH_{PZC} and negatively charged when pH > pH_{PZC}. Thus, it is possible to measure the tendency of a carbon surface to be positively or negatively charged. This is generally considered an indicator of the carbon surface oxidation, as it allows to identify an acidity or basicity increase of the surface after modification treatments.

The pH_{PZC} measurements can be performed independently using solutions with different weight percentages of carbon, or from successive dilutions of the same sample. The pH of the equilibrium in the plateau of the curve pH curve vs mass concentration of the suspension corresponds to the pH_{PZC}. This method presents however some practical limitations, since weight concentrations above 20 % can not be used, because above this value the solutions become too dense to allow pH measurements. A low ionic strength value may also condition the pH value; in these cases the use of support electrolyte solutions may be advantageous.

Finally, the presence of impurities in the carbon may lead to an increase in pH and pH_{PZC} may not be representative.

B.2.3 Thermal Analysis

Thermal analysis is a general term which groups the measurement methods of the physical and chemical properties variations essentially as a function of temperature or time, when the sample is subjected to a controlled temperature program (Brown, 1988).

B.2.3.1 Thermogravimetry

The mass change of a sample as a function of temperature is the basis for thermogravimetry (TG). The sample is subjected to a controlled heating or cooling program, and mass variations are measured continuously (Hill, 1991). The most frequently used procedure consists in subjecting the sample to a constant heating rate. The measuring instrument used (thermogravimetric analyser or thermobalance), consists of a furnace and a microbalance with a control device to measure the temperature and mass of the sample during the test. The gas flow within the thermobalance follows a longitudinal path and is introduced into the upper part of the furnace. The entire scale of the mechanism is in an inert atmosphere, with a carrier gas stream of all the gases generated. The curve obtained for the representation of the weight change versus time or temperature is the thermogravimetric or TG profile.

The information obtained from the thermogravimetric profiles is of empirical nature, since the transition temperatures depend on instrumental parameters and sample characteristics, which makes it difficult to make comparisons between data obtained in different equipments. The thermogravimetric parameters are not intrinsic to a substance, depending on the method used for its acquisition. Among these experimental parameters are the heating rate, reaction atmosphere, the material and the geometry of the sample holder, furnace size and shape.

In the case of carbon materials, TG profiles induce the thermal decomposition of the surface functionalities chemically bound to carbons. These profiles are usually characterized by wide humps. The evolved gases can be analysed by different techniques (mass spectrometry, IR, gas chromatography). CO, CO_2 and H_2O are the dominant desorbed gases although some other compounds (NO, NH_3, SO, SO_2) can also be detected in N- and S-doped carbons. The correlation between the gaseous species detected upon thermal decomposition (the number and temperature of the desorption peaks) and the nature of the carbon surface functionalities has been widely studied (Bandosz and Ania, 2006).

B.2.3.2 Temperature Programmed Reduction

Temperature Programmed Reduction (TPR) with hydrogen is a widely used technique for the characterization of reducible solids and catalysts. This technique is often used in the field of heterogeneous catalysis to find the most efficient reduction conditions. The experimental method of TPR for the investigation of gas/solid reactions is well established and widely used since the 1970s. In TPR experiments, a reducible catalyst or catalyst precursor is exposed to a flow of a reducing gas mixture (typically a few vol. % of hydrogen in an inert gas) while the temperature is linearly increased. The rate of reduction is continuously followed by measuring the composition (H_2 content) of the reducing gas mixture at the outlet of the reactor with appropriate detectors (thermal conductivity detector, mass spectrometer). The experiment allows the determination of the total amount of hydrogen consumed, from which the degree of reduction

and thus, the average oxidation state of the solid after reduction can be calculated (Reiche, Maciejewski, *et al.*, 2000).

B.2.4 Fourier Transformed Infrared Spectroscopy (FTIR)

Infrared (IR) spectroscopy is one of the instrumental analysis techniques most commonly used in the characterization of surface features of activated carbons. The introduction of the Fourier transform increased the range of application of this technique for the qualitative and quantitative analysis of surface functionalities. The infrared region of the electromagnetic spectrum is generally divided into three zones, with respect to the visible region: far (400-10 cm^{-1}), mid (4000-400 cm^{-1}) and near (4000-14000 cm^{-1}). FTIR is applied to the intermediate region of the spectrum, and it may be used for a direct and rapid characterization of solid samples.

When a sample is irradiated, light is selectively absorbed according to the specific frequency vibration (vibrational level) of the molecules, reason why compounds with similar chemical groups exhibit characteristic absorption bands in the IR, giving rise to a spectrum. The absolute reflectance measurements depend, for example, on the experimental conditions, the angle of incidence and reflection, and thickness and state of the sample surface. Since the ratio of the intensities of the bands remains constant with no change of particle size, it is essential to previously prepare the sample, pulverizing it in a mortar.

The assignment of the infrared absorption bands and peaks to different functionalities of the carbon surfaces is made by comparison with the spectra for organic compounds containing similar functional groups. In Table B.3 a summary of bands and peaks assignment corresponding to oxygen functionalities in carbon materials is presented (Fanning and Vannice, 1993; Bandosz and Ania, 2006).

Table B.3- Principal functional groups on carbon surfaces and their corresponding infrared assignments.

Group or functionality	Assignment regions (cm^{-1})		
	100-1500	1500-2050	2050-3700
C-O stretch of ethers	1000-1300		
Ether bridge between rings	1230-1250		
Cyclic ethers containing COCOC groups	1025-1141		
Alcohols	1049-1276		3200-3640
Phenolic groups: C-O stretch O-H bend/stretch	1000-1220 1160-1200		2500-3620
Carbonates; carboxyl-carbonates	1000-1500	1590-1600	
Aromatic C=C stretching		1585-1600	
Quinones		1550-1680	
Carboxylic acids	1120-1200	1665-1760	2500-3300
Lactones	1160-1370	1675-1790	
Anhydrides	980-1300	1740-1880	
Ketenes (C=C=O)			2080-2200
C-H stretch			2600-3000

The main challenge in FTIR analysis of carbon materials is that most of them are too opaque for direct transmission analysis in the mid-infrared spectral region. Partial dilution in an appropriate transparent additive (KBr) is not always satisfactory, for which alternative sampling techniques such as diffuse reflectance, photo acoustic spectroscopy, or attenuated reflectance are extensively used to overcome these problems. Furthermore, in the case of carbon materials IR spectroscopy does not provide quantitative information. The modification of the surface chemistry of carbon materials originated by, for example, oxidation treatments and under different operating conditions, detected by FTIR, have been widely disclosed in the literature.

Although this technique does not provide quantitative information on the carbon surface chemistry, it enables the identification of the groups created or removed during the modification treatment. In addition to oxygen functional groups, nitrogen groups have also been studied, although the interpretation of the spectra is still unclear due to the existence of a broadband where there is an overlap due to the contribution of various bands. This technique was also used for the determination of sulfur compounds present on the surface of activated carbons after adsorption/oxidation with H_2S (Bandosz and Ania, 2006).

B.2.5 UV-vis Diffuse Reflectance Spectroscopy

UV-vis spectroscopy is a useful technique for obtaining information about the electronic structure of the materials and their optical properties. It is based in the electronic absorption of electromagnetic radiation when it interacts with matter in the range of wavelengths of ultraviolet and visible (190-800 nm). In the case of solid catalysts, the most used technique is the diffuse reflectance, observing the transition of electrons from the valence band to the conduction band and therefore, allowing the calculation of the band gap energy.

Diffuse reflectance measurement is defined as the fraction of incident radiation that is reflected in all directions by the sample, due to absorption and dispersion processes and predominates when the materials of the reflecting surface are weak absorbents at the incident wavelength and when the penetration of the radiation is large in relation to the wavelength. Reflection has two components, specular and diffuse, with the latter providing useful information about the sample. The calculation of the diffuse reflectance can be rationalized by the Kubelka-Munk theory (Kubelka and Munk, 1931), which provides a relationship for the reflected radiation based on the absorption (k_{ab}) and dispersion (k_s) constant, according to equation B.9:

$$f(R_L) = \frac{(1-R_L)^2}{2\,R_L} = \frac{k_{ab}}{k_s} \qquad\qquad \text{equation B.9}$$

where R_L is the relative reflectance using a reference pattern.

B.2.6 X-ray Photoelectron Spectroscopy

X-ray Photoelectron Spectroscopy, commonly known as XPS, is an interesting technique for the characterization of solid and powder samples, due to its ability to measure binding energy variations resulting from the surrounding chemical environment. This type of spectrometry is currently a key tool in surface analysis, essentially due to two main characteristics: the possibility of a quantitative analysis and also knowledge of the chemical nature and state of the detected elements. Other advantages of this technique are a highly specificity due to the short range photoelectrons that are excited from the solid and also the fact of being a non-destructive

technique. XPS is able to determine the chemical composition of the surface of various materials by 1 nm in depth, being also possible to know if the material surface is oxidized and what elements are present (Bandosz and Ania, 2006).

The XPS technique uses X-rays to excite electrons from the sample by measuring their kinetic energy. Photons with energy $h\nu$ (the typical energy of the incident photons is 1 to 2 keV) are directed to the sample being absorbed by its atoms, leading to ionization and emission of an electron from an inner layer. By absorbing a photon, an electron is emitted in order to return to its original energy state. The electron ejected retains the energy of the incident photon, thus being able to escape from the atom with a kinetic energy that will depend on its binding energy, the energy of the incident photon and a correction factor. To return to the ground state, the atom can emit another photon (fluorescence) or suffer an Auger transition. Thus, different chemical species can be identified, since the kinetic energy of the ejected electrons depends on its binding energy.

For each element there is a series of characteristic peaks in the photoelectronic spectrum, whose intensity is related to the concentration of the element in the analysed region, allowing a quantitative analysis. However, the analysis of porous samples can sometimes be misleading, since the outer surface of these materials is often found more oxidized or functionalized to its core. In these cases, the quantification corresponds only to the surface of the materials.

XPS is used to characterize the surface chemistry of carbon materials, providing useful information about the binding energies of photoelectrons (i.e., C_{1s}, N_{1s}, O_{1s}, P_{2p}, S_{2p} and so forth) of surface groups. The allocation of bond energies to features of the surface of activated carbon has been extensively reported in the literature (Bandosz and Ania, 2006). The assignment is largely affected by the local environment of the heteroatoms, the state of bonding to neighboring atoms, etc., for which identification is not straightforward. Despite this, XPS analysis can be very convenient to identify any likely changes on the surface of carbon materials during pyrolysis/carbonization treatments, or those arising after long-term uses.

B.2.7 X-Ray Diffraction

The X-radiation is an electromagnetic radiation of the same kind of visible light, strongly energetic due to its short wavelength (0.1 to 100 Å). Generally, the longer wavelength used for inorganic and organic materials studies varies between 0.5 and 2.5 Å due to the interatomic distances of the materials is located in this interval. The X-ray diffraction is the most widely used method to identify crystalline structures. The diffractograms result of the interference between the waves associated with X-ray and the electronic cloud of the constituents of the crystal lattice. The analysis of the diffractograms thus enables to determine the distribution of atoms, ions or molecules in a crystal lattice.

X-ray diffraction is generally considered the "optimal" technique for structural characterization of materials, since it allows to distinguish between the various allotropic forms, but also to determine the graphitization degree of an activated carbon in comparison with the ideal graphite structure. More specifically, the XRD technique reflects the degree of graphitization in terms of the stacking/packaging of basic constituents. The X-ray diffraction has been used to study activated carbon and other carbon materials since the first uses of this technique for the characterization of microstructures (Iwashita, Park, *et al.*, 2004).

In powder diffractometry, the sample is composed by a large number of crystallites whose orientation is statistically random; a number of crystallites are in the Bragg position for a given family of hkl planes, that is, an incidence angle θ such that n λ = 2 d (hkl) sin θ (Bragg's law), where n is an integer number of wavelengths of incident radiation, λ, d represents the distance between the interlattice planes, (hkl) are the Miller indices, of the family of hkl planes, integers numbers corresponding to the ratio between the dimensions of the crystal lattice a, b and c, of the intersection distances of the respective planes in the crystallographic axis, and θ is the Bragg angle, the angle between the incident radiation and the crystal plane (Pecharsky and Zavalij, 2003).

B.2.8 Scanning Electron Microscopy

Scanning electron microscopy, designated as SEM, is a widely used technique for the study of the surface morphology, due to the simplicity of sample preparation, ease of operation, and the high amount of information made available. SEM images have a three dimensional characteristic appearance and are useful to evaluate the surface structure of a given sample (Cahn, 2001). The surface to be analysed is systematically covered by a beam of energetic electrons. When the surface is hit by a beam, secondary electrons are emitted, generating a signal that is used to form an image through a cathode ray tube.

The resolution obtained is much higher than of optical microscopes, since electrons are used, achieving also a high field depth. Given the range of interactions between electrons and matter, it is possible to obtain specific information, depending on the detected signal. The signals commonly used in materials science are: secondary electrons, retrodiffused electrons and X-rays. Secondary electrons have very little energy (0 up to 50 eV), being derived from the more superficial layers of the sample, holding information on the topography of surface. The retrodiffused electrons, more energetic (50 eV to beam energy), "carry" information about the composition of the sample, i.e., are sensitive to the atomic number. Thus, the image obtained can be a reproduction of the sample topography or an image whose contrast is qualitatively related to the chemical composition of the sample (higher atomic number, higher intensity). The characteristic X-rays detected by Energy-Dispersive X-ray spectroscopy (EDX) or Wavelength-Dispersive X-Ray Spectroscopy (WDS) identify and quantify the elements present in the sample.

B.2.9 Transmission Electron Microscopy

Transmission electron microscopy (TEM) is a powerful tool that allows to obtain a great amount of information about the material, such as characterization of the morphology and the crystalline structure, determination and quantitative analysis of the crystalline defects, relating these to specific sample areas. The use of this technique, which is often used in conjunction with SEM, has contributed to the development of advanced materials (Williams and Carter, 1996).

In a transmission electron microscope, a sufficiently thin sample amount (5 nm to 0.5 μm of maximum thickness) is irradiated with a monochromatic electron beam of uniform current density. The energy of the electrons is typically in the range between 100 and 400 keV. The electrons interact strongly with matter through elastic and inelastic dispersions. TEM permits high spatial resolution because the elastic dispersion, predominant in this technique, is a highly localized process. The use of electrons has the major advantage of high resolution, but has implications on the design of this kind of equipment: the lenses used to collimate the beam must be magnetic and the interior of the TEM must be kept in vacuum, assures through several pumps and valves.

At the exit, in addition to a direct or primary beam, several diffracted beams are present. The primary beam, has the same direction of the initial beam, being also called transmitted (although in reality it is involved in the phenomena of successive dispersion). In fact, not only the primary beam gives rise to several diffracted beams that interfere with each other, but these beams themselves also may contribute to the intensity of the so called transmitted beam. The formed image is a two dimensional projection of the sample and its contrast depends on the amplitude and phase of the beams at the output of the sample.

TEM image forming system is constituted, generally, by the same components as an optical transmission microscope: the light source (electron gun), the illumination system (the beam is focused on the sample), the lens objective, with a clear specimen in the middle of its magnetic field (which is to form the image), the magnification and projection system and the detector (screen and/or camera and/or charge-coupled device camera). TEM can be operated in two different modes, so as to form diffraction patterns using the diffraction diaphragm or bright field, dark field or high resolution images.

When the electron beam passes through the crystalline sample it is diffracted according to the Bragg law. The resulting beams are made to converge through the objective lens, forming a diffraction pattern on its back focal plane. Intermediate lenses and projecting form a magnification of the pattern in the fluorescent screen.

B.3 Analytical Techniques for the Photocatalytic Assays

B.3.1 Total Organic Carbon

Since the early 70's, the determination of the Total Organic Carbon (TOC) has been a widely used analytical technique in the evaluation of water quality during the process of drinking water purification. TOC analysis emerged as a rapid and accurate alternative to other more time-consuming analysis, as BOD and COD, traditionally used for the evaluation of potential wastewater pollution. TOC content can be measured directly or can be determined by difference if the total carbon content and inorganic carbon contents are measured.

In the case of the analysis of the total carbon, the sample is injected the sample onto a platinum catalyst at 680 °C in an oxygen rich atmosphere, subjected to a catalytic combustion and a posterior analysis of the generated CO_2 by a non-dispersive infrared detector. For the determination of inorganic carbon, that corresponds to carbonates and dissolved carbon dioxide, the sample is acidified with phosphoric acid (H_3PO_4), and the CO_2 formed is analysed similarly to the previous case.

B.3.2 Reversed-Phase High Performance Liquid Chromatography

High performance liquid chromatography (HPLC) is a type of chromatography that can separate molecules according to their polarity. In the reversed-phase mode, the separation is based on the hydrophobicity of the molecules, and their ability to bind the immobilized hydrophobic ligands attached to a stationary phase. The stationary phase is an apolar matrix commonly constituted by chemically modified silica with saturated or unsaturated hydrocarbons or aromatic compounds, while the mobile phase is polar.

The solute mixture is initially applied to the sorbent in the presence of aqueous buffers, and the solutes are eluted by the addition of organic solvent to the mobile phase. Elution can proceed either by isocratic conditions where the concentration of the organic solvent is constant, or by

gradient elution whereby the amount of organic solvent is increased in time. The solutes are, therefore, eluted in order of increasing molecular hydrophobicity. The most commonly employed column for such applications is a functionalized silica, octadecylsilane, designated as C18.

B.3.3 Actinometry

According to the "Glossary of terms used in photochemistry" (Bravslasky, 2007) an actinometer is a chemical system for the determination of the number of photons absorbed (integral or per time unit) in a defined space of a chemical reactor. This name is generally applied to systems used in the ranges of ultraviolet and visible light. A chemical actinometer is a chemical system (fluid, gas, solid, or in a micro heterogeneous environment) which undergoes a light induced reaction (at a particular wavelength) for which the quantum yield $\Phi(\lambda)$ is accurately measured. The measurement of the velocity of the reaction allows the calculation of the flux of the absorbed photon. The quantum yield of a photochemical reaction is defined as $\Phi(\lambda)$ = number of events, i.e. the change, formation or destruction of molecules divided by the number of absorbed photons at a particular wavelength in the same period of time.

The actinometric determinations carried out in this study were performed according to the standard procedure L31 of liquid phase (Kuhn, Braslavsky, *et al.*, 2004), commonly referred to as ferrioxalate actinometry. This is the most widely accepted actinometric method, consisting in the photoreduction of potassium ferrioxalate and determination of the absorbance at 510 nm of the complex [tris (1,10-phenanthroline) iron (II)] in an acidic buffered solution. The exposure of an ion ferrioxalate solution at a wavelength lower than 490 nm leads to the photodecomposition in accordance with the following equation:

$$2\ Fe^{3+} + C_2O_4^{2-} \rightarrow 2\ Fe^{2+} + 2\ CO_2 \qquad\qquad \text{equation B.10}$$

The iron (II) produced is quantified with 1,10-phenanthroline upon the formation of a reddish ferrous phenanthroline complex which absorbs at 510 nm:

$$Fe^{2+} + 3\ phen \rightarrow \left[Fe\ (phen)_3\right]^{2+} \qquad\qquad \text{equation B.11}$$
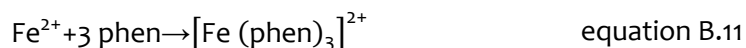
A buffer solution (sodium acetate and H_2SO_4) was used to keep the pH around 5. The experiments were held in a dark room under red safety light, and carried out in duplicate. All solutions were prepared immediately before the beginning of the experimental procedure. A solution of 0.006 M of green crystals of $K_3\left[Fe(C_2O_4)_3\right]\cdot 3H_2O$, was prepared and its spectrum was obtained. Then, a volume (V_1) of this solution was irradiated with vigorous stirring. At predetermined time intervals (0 to 5 min), 1 cm^3 (V_2) of the irradiated solution was taken to a volumetric flask of variable volume (V_3) containing a mixture of a 0.1 % solution of 1,10-phenanthroline (kept in the dark) and a buffer solution, and completed with distilled water. A reference solution is also prepared in the same way, which however is not irradiated. Both solutions are kept in the dark (for about one hour) until the full color development and then the absorbance difference between the two samples is measured at 510 nm [optical path l = 1 cm, ε (510 nm) = 11100 dm^3 mol^{-1} cm^{-1}]. The photon flux, amount basis, $q_{n,p}$ (Einstein s^{-1}), which enters the sample cell is given by (in consistent SI units):

$$q_{n,p} = \frac{\Delta Abs\ V_1 V_3}{\Phi(\lambda)\ \varepsilon(510\ nm)\ V_2 l\ t} \qquad\qquad \text{equation B.12}$$

where ΔAbs is the absorbance difference between the irradiated and the reference solution, measured at 510 nm, $\Phi(\lambda)$ is the quantum yield of production of ferrous ions from potassium ferrioxalate as a function of the excitation wavelength, and t is the time of irradiation. In this case, the value of the photon flux must be divided by the fraction of absorbed light at the irradiation wavelength $(1-10^{-A})$.

B.4 Kinetic Models

B.4.1 *Pseudo-first order kinetic model*

The pseudo-first order kinetic model used to describe the rate of adsorption from liquid phase on a solid adsorbent, was initially proposed in 1989 by Lagergren (Lagergren, 1898) for the adsorption of oxalic and malonic acid on carbon. This is the first known model that describes the adsorption rate based on the adsorption capacity, and in the last four decades has been widely applied to the adsorption of pollutants in aqueous phase (Ho, 2006). The Lagergren equation considers that the driving force is the difference between the concentration of solute adsorbed and the equilibrium concentration of solute adsorbed at a given time, so that the adsorption rate is determined by the following expression (Lagergren, 1898):

$$\frac{dq_t}{dt} = k_1\left(q_e - q_t\right) \qquad\qquad \text{equation B.13}$$

where $k1$ is a constant for pseudo first order rate (h^{-1}), q_e and q_t correspond to the amount of solute adsorbed $(mg\,g^{-1})$ at equilibrium and at time t, respectively. Integrating Equation B.12 for the boundary conditions $q_t = 0$ when t = 0, and $q_t = t$ when t = t, and after rearranging it in the linear form, we obtain the following equation:

$$\ln\left(q_e - q_t\right) = \ln q_e - k_1 t \qquad\qquad \text{equation B.14}$$

Thus, the of pseudo-first order constant rate, $k1$, can be obtained directly from the slope of the representation $(q_e - q_t)$ *vs* t and the amount of solute adsorbed in equilibrium, q_e, it is obtained from the intercept.

B.4.2 *Pseudo-second order kinetic model*

The pseudo-second order was proposed by Ho and McKay (1999) and, as in the case of the pseudo-first order kinetic model, the prefix pseudo indicates that it is based on the adsorption capacity of a solid (Ho, 2006). Thus, a pseudo-second order kinetic can be expressed by the following equation:

$$\frac{dq_t}{dt} = k_2(q_e - q_t)^2 \qquad\qquad \text{equation B.15}$$

where k_2 is the constant of the pseudo-second-order rate $(mg\,g^{-1}\,h^{-1})$, q_e and q_t correspond to the amount of solute adsorbed $(mg\,g^{-1})$ at equilibrium and at time t, respectively. Integrating Equation B.14 for the boundary conditions $q_t = 0$ when t = 0, and $q_t = t$, when t = t, and rearranging it to the linear form, we obtain the following equation:

$$\frac{t}{q_t} = \frac{1}{k_2 q_e^2} + \left(\frac{1}{q_e}\right)t \qquad\qquad \text{equation B.16}$$

The q_e and k_2 values can be estimated from the slope and intercept, respectively, of the representation (t/qt) *vs* t. The product $k_2 q_e^2$ is the Initial adsorption rate, h. The half-life, $t_{1/2}$, that

is, the time required for half the quantity of adsorbate that will be adsorbed in the equilibrium is on the surface of the adsorbent is often used to measure the adsorption speed and is determined by the following equation:

$$t_{1/2} = \frac{1}{k_2 q_e}$$

equation B.17

The pseudo-second order equation has been successfully applied to the adsorption of metal ions, dyes, herbicides, oils and other organic substances in aqueous solution. In the study by Ho and McKay, in which 12 systems of adsorbents and bioadsorbents were used to treat wastewater containing dyes and metal or organic ions also, it is shown that while the pseudo-first order model only shows a good fit to the experimental data for an initial period of the reaction, the pseudo-second order model presents better correlations for all studied systems (Ho and McKay, 1999).

B.4.3 *Langmuir–Hinshelwood kinetics*

Langmuir–Hinshelwood (LH) kinetics is the most commonly used kinetic model for heterogeneous catalytic processes during the photodegradation of organic contaminants in solution. The application of this model to an ideal batch reactor produces the following expression:

$$-\frac{dC}{dt} = \frac{k_r K_e C}{1 + K_e C}$$

equation B.18

where C represents the concentration in solution of the molecule being degraded (mg L^{-1}), k_r is the reaction rate constant (mg L^{-1} min^{-1}) and K_e is the equilibrium constant for the adsorption of the molecule on the catalyst surface at the reaction temperature (L mg^{-1}). The term $k_r K_e$ is globally evaluated as an apparent constant rate (k_{app}; min^{-1}), and thus, Equation B.17 can be rewritten as:

$$-\frac{dC}{dt} = \frac{k_{app} C}{1 + K_e C}$$

equation B.19

In most photocatalytic kinetic studies it is assumed that the low concentration used in the experiments allows that $K_e C \ll 1$, and therefore equation B.20 can be reduced to a classical first-order equation:

$$-\frac{dC}{dt} = k_{app} C$$

equation B.20

To fit the experimental data the following linear form of the integrated equation is generally used:

$$\ln\left(\frac{C_0}{C}\right) = k_{app} C$$

equation B.21

where k_{app} value can be obtained from the representation of ln(C_0/C) *vs* C.

ANNEX C

REFERENCES

Bandosz, T. J. and Ania, C. O., 2006. Surface chemistry of activated carbons and its characterization. In: *Activated Carbon Surfaces in Environmental Remediation*, Bandosz, T. J., (Ed.), Volume 7, Elsevier: New York; Chapter 4, 159-229.

Braslavsky, S. E., 2007. Glossary of terms used in photochemistry. *Pure and Applied Chemistry* 79, 293-465.

Brown, M. E., 1988. *Introduction to Thermal Analysis- Techniques and applications,* Chapman and Hall, Ltd: New York.

Brunauer, S.; Deming, L. S.; Deming, W. E. and Teller, E., 1940. On a theory of the van der Waals adsorption of gases. *Journal of the American Chemical Society* 62, 1723-1732.

Brunauer, S.; Emmett, P. H. and Teller, E., 1938. Adsorption of gases in multimolecular layers. *Journal of the American Chemical Society* 60, 309-319.

Cahn, R. W., 2001. *The coming of materials science*, Pergamon: Amsterdam

Choma, J. and Jaroniec, M., 2006. Characterization of Nanoporous Carbons by Using Gas Adsorption Isotherms. In: *Activated Carbon Surfaces in Environmental Remediation*, Bandosz, T. J. (Ed.), Volume 7, Elsevier: New York; Chapter 3, 107-158.

Fanning, P. E. and Vannice, M. A., 1993. A DRIFTS study of the formation of surface groups by oxidation. *Carbon* 31, 721-730.

Gregg, S. J. and Sing, K. S. W., 1982. *Adsorption, Surface Area and Porosity* (2nd ed.), Academic Press Inc: London.

Hill, J. O., 1991. *For better Thermal Analysis and Calorimetry* (3rd ed.), ICTAC.

Ho, Y. S., 2006. Review of second-order models for adsorption systems. *Journal of Hazardous Materials*, 136, 681-689.

Ho, Y. S. and McKay, G., 1999. Pseudo-second order model for sorption processes. *Process Biochemistry* 34, 451-465.

Iwashita, N.; Park, C. R.; Fujimoto, H.; Shiraishi, M. and Inagaki, M., 2004. Specification for a standard procedure of X-ray diffraction measurements on carbon materials. *Carbon*, 42, 701-714.

Jagiello, J. and Olivier, J. P., 2013a. 2D-NLDFT Adsorption Models for Carbon Slit-Shaped Pores with Surface Energetical Heterogeneity and Geometrical Corrugation. *Carbon* 55, 70-80.

Jagiello, J. and Olivier, J. P., 2013b. Carbon Slit Pore Model Incorporating Surface Energetical Heterogeneity and Geometrical Corrugation. *Adsorption* 19, 777-783.

Kubelka, P. and Munk, F., 1931. Ein Beitrag Zur Optik der Farbanstriche. *Zeitschrift für Technische Physik* 12, 593-601.

Kuhn, H. J.; Braslavsky, S. E. and Schmidt, R., 2004. Chemical Actinometry (IUPAC Technical Report). *Pure and Applied Chemistry* 76, 2105–214.

Lagergren, S., 1898. Zur theorie der sogenannten adsorption gelöster stoffe. *Kungliga Svenska Vetenskapsakad Handlingar* 24, 1-39.

Lastoskie, C.; Gubbins, K. E. and Quirke, N., 1993. Pore Size Distribution Analysis of Microporous Carbons: A Density Functional Theory Approach. *Journal of Physical Chemistry* 97, 4786-4796.

Marsh, H. and Rodríguez-Reinoso, F., 2006. *Activated Carbon*, Elsevier: Oxford.

Noh, J. S. and Schwarz, J. A., 1989. Estimation of the point of zero charge of simple oxides by mass titration. *Journal of Colloid and Interface Science* 130, 157-164.

Pecharsky, V. K. and Zavalij, P. Y., 2003. *Fundamentals of powder diffraction and structural characterization of materials*, Springer: New York.

Pinto, M. L.; Mestre, A. S.; Carvalho, A. P. and Pires, J., 2010. Comparison of methods to obtain micropore size distributions of carbonaceous materials from CO_2 adsorption based on the Dubinin-Radushkevich isotherm. *Industrial & Engineering Chemistry Research* 49, 4726-4730.

Reiche, M. A.; Maciejewski, M. and Baiker, A. 2000. Characterization by temperature programmed reduction. *Catalysis Today* 56, 347-355.

Rodríguez-Reinoso, F.; McEnaney, B.; Rouquerol, J. and Unger, K. K., 2002. *Characterization of Porous Solids VI. Studies in Surface Science and Catalysis*, Volume 144; Elsevier: Amsterdam.

Rodríguez-Reinoso, F. and Sepúlveda-Escribano, A., 2001. Porous carbons in adsorption and catalysis. In: *Handbook of Surfaces and Interfaces of Materials*. Nalwa, H. S. (Ed.), Academic Press;

Rouquerol, F.; Rouquerol, J.; Sing, K., Llewellyn, P. and Maurin, G., 2014. *Adsorption by Powders and Porous Solids - Principles, Methodology and Applications* (2nd ed.), Academic Press.

Seaton, N. A.; Walton, J. P. R. B. and Quirke, N., 1989. A New Analysis Method for the Determination of the Pore Size Distribution of Porous Carbons from Nitrogen Adsorption Measurements. *Carbon* 27, 853-861.

Sing, K. S. W.; Everett, D. H.; Haul, R. A. W.; Moscou, L.; Pierotti, R. A.; Rouquerol, J. and Siemieniewska, T., 1985. IUPAC Reporting physisorption data for gas/solid systems with special reference to the determination of surface area and porosity. *Pure & Applied Chemistry* 57, 603-619.

Tarazona, P.; Marconi, U. M. B. and Evans, R., 1987. Phase equilibria of fluid interfaces and confined fluids. Non-local versus local density functionals. *Molecular Physics* 60, 573-595.

Thommes, M; Kaneko, K.; Neimark, A. V.; Olivier, J. P.; Rodríguez-Reinoso, F.; Rouquerol, J. and Sing, K. S. W., 2015. Physisorption of gases, with special reference to the evaluation of

surface area and pore size distribution (IUPAC Technical Report). *Pure and Applied Chemistry* 87, 1051-1069.

Williams, D. B. and Carter, C. B., 1996. *Transmission Electronic Microscopy- A Textbook for Materials Science*, Plenum Press: New York.

ANNEX D

COMMUNICATIONS IN CONFERENCES

Oral presentations

1.   **Andrade, M. A.,** Mestre, A.S., Nuno Lapa, N., Mendes, B., Ania, C. O., Carvalho, A. P.; Photocatalytic degradation of pharmaceutical compounds by TiO_2: An ecotoxicity assessment; 10ª Conferência de Química Inorgânica da SPQ, Costa da Caparica, Portugal, 11 - 12 April 2014 (also presented in panel).

2.   **Andrade, M.,** Mestre, A. S., Carvalho, A. P., Ania, C.O.; TiO_2/Cu-doped carbon composites as catalysts for phenol photodegradation; XII Reunión del Grupo Español del Carbón, Madrid, Spain, 20-23 October 2013.

3.   **Andrade, M. A.,** Mestre, A. S., Matos, J., Carvalho, A. P., Ania; C. O.; Phenol photocatalytic degradation by TiO_2/Cu-doped carbon composites; The Annual World Conference on Carbon, Carbon 2013, Rio de Janeiro, Brasil, 19-21 July 2013.

Panel communications

1.   **Andrade, M. A.,** Mestre, A. S., Lapa, N., Mendes. B., Carvalho, A.P., Ania, C.O.; Pharmaceutical Compounds Photocatalytic Degradation by TiO_2/Carbon Composites: Ecotoxicity Risk Assessment; The Annual World Conference on Carbon, Carbon 2014, Jeju Island, Korea, 29 June-4 July 2014.

2.   **Andrade, M.,** Mestre, A. S., Haro, M., Carvalho, A. P., Ania, C. O., Copper-doped carbons for environmental remediation; The Annual World Conference on Carbon, Carbon 2012, Krakow, Poland, 17-22 June 2012.

3.   Haro, M., Ruiz, B., **Andrade, M.,** Mestre, A. S., Parra, J. B., Carvalho, A. P., Ania, C. O.; Efecto promotor del cobre en el desarrollo textural durante la gasificación catalítica en aire de carbones activados; XI Reunión del Grupo Español del Carbón 2011, Badajoz, Spain, 24-29 October 2011.

4.   **Andrade, M.,** Ruiz, B., Mestre, A. S., Parra, J. B., Carvalho, A. P., Ania, C. O.; Role of copper as an additive during physical and chemical activation of a lignocellulosic precursor; Characterization of Porous Solids COPS 2011, Dresden, Germany, 5-8 June 2011.
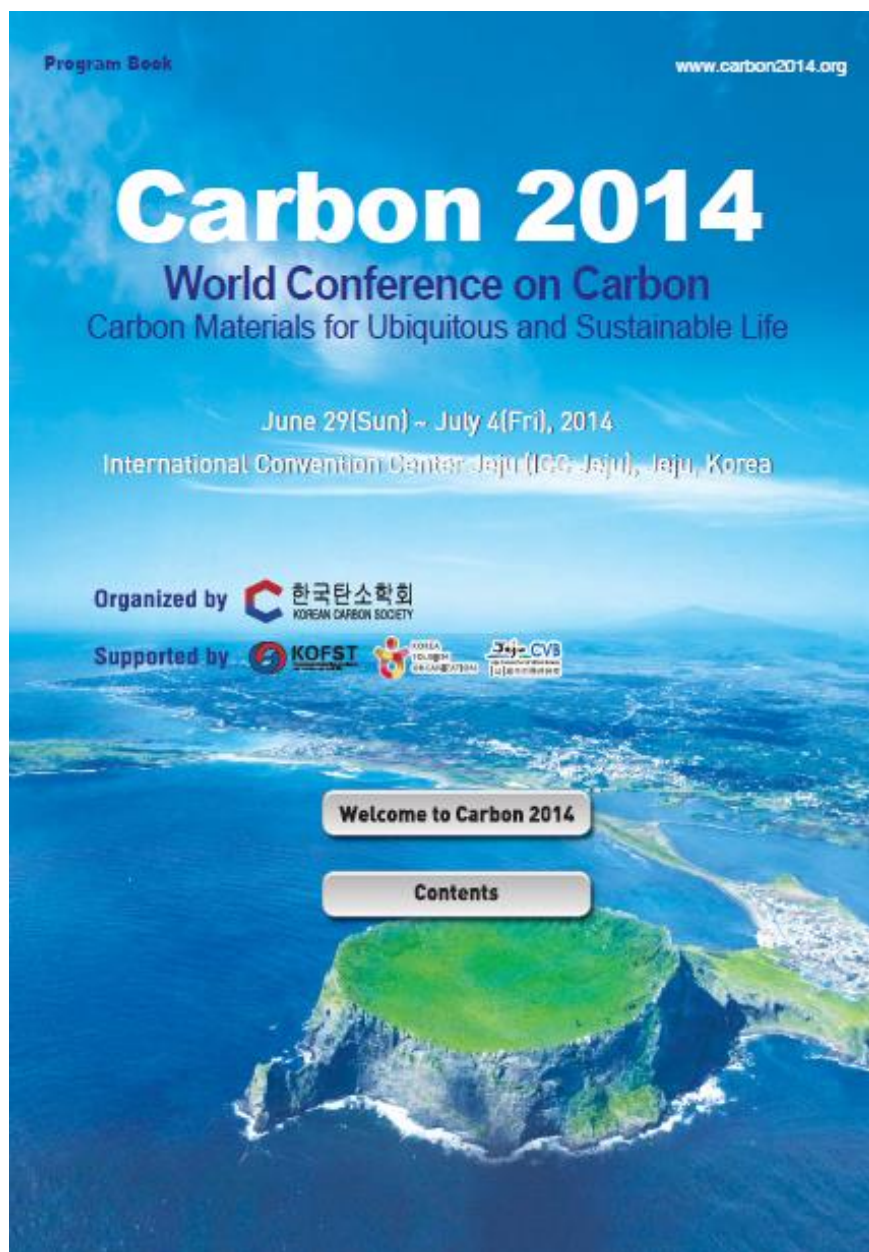
Annex D

Panel

Pharmaceutical Compounds Photocatalytic Degradation by TiO₂/Carbon Composites: Ecotoxicity Risk Assessment

Marta Amaral ANDRADE[1,2*], Ana Sofia MESTRE[1], Nuno LAPA[3],
Benilde MENDES[3], Ana Paula CARVALHO[1], <u>Conchi O. ANIA</u> [2*]

[1]Dpt. Química e Bioquímica and CQB, Faculdade de Ciências da Universidade de Lisboa, Ed. C8 Campo Grande, 1749-016 Lisboa, Portugal, [2]Instituto Nacional del Carbón (INCAR, CSIC) 33011, Oviedo, Spain, [3]DCTB, Faculdade de Ciências e Tecnologia, Universidade Nova de Lisboa, 2829-516 Caparica, Portugal.

*mvandrade@fc.ul.pt, conchi.ania@incar.csic.es

INTRODUCTION

Pharmaceutical and personal care products (PPCPs) are a class of compounds of emerging concern, corresponding in most cases to unregulated contaminants that have recently been detected in water streams worldwide. PPCPs encompass compounds of great consumption, such as over-the-counter medication and many disinfectants that are continuously introduced into the aquatic environment. Amongst Advanced Oxidation Processes, heterogeneous photocatalysis is one of the most promising technologies for the degradation of these compounds in wastewater treatment plants. Carbon materials have been successfully used as supports of photoactive species, and TiO₂/carbon composites have shown quite high efficiencies for the photodegradation of a variety of pollutants. Most of the studies on photocatalysis do not encompass an ecotoxicity evaluation, being more focused on the degradation efficiency and mineralization of the pollutants. Given the usual increase of ecotoxicity accompanying the early stages of oxidation treatments, an assessment of the effluent ecotoxicity is therefore essential. Nevertheless, data on the ecotoxicity of treated effluents after photocatalytic reactions is still scarce. In this context, the aim of the present work is to screen the photocatalytic degradation of ibuprofen (IBU) and sulfamethoxazole (SMX) and mixtures of these compounds (IBU/SMX) using TiO₂/carbon composites as catalysts. The results are interpreted in terms of the compounds mineralization and ecotoxicity levels of the initial and final effluents, focusing on the role of the carbon component on the photocatalytic degradation.

MATERIALS AND METHODS

Catalysts and pharmaceutical compounds

Carbon S, a nanoporous carbon prepared by chemical activation of a lignocellulosic precursor (sisal fibers, discarded from the rope industry), and commercially available titania (P25, Evonik) were used as catalysts for the photoxidation of IBU and SMX (Sigma-Aldrich).

Experimental procedure

IBU, SMX and IBU/SMX photodegradation experiments with titania and titania/carbon (TiO₂/S) composites as catalysts - using a 1:1 weight ratio- were carried out at room temperature in a Rayonet RMR-600 photochemical reactor equipped with eight 350 nm light sources, and an initial concentration of 50 ppm of the pollutant(s) in all cases. To minimize the photolytic reaction, a Pyrex vessel was used. In the case of composites, the suspensions were allowed to equilibrate under dark conditions before being illuminated. After the equilibration step, the suspensions were irradiated for 180 min. Total organic carbon (TOC) of the solution at the end of each run was measured in a TOC Shimadzu 5000. The

ecotoxicity assessment was performed by the bioluminescence inhibition of the bacterium *Vibrio fischeri*, through the evaluation of the Effective Concentration of 50% bioluminescence inhibition for 30 min of exposure (EC_{50}-30 min) in a Microtox equipment.

RESULTS AND DISCUSSION

The results obtained so far reveal that additionally to the individual ecotoxicity of each compound, a positive synergic effect is observed when these compounds are simultaneously present in solution (Table 1). While the individual solutions of IBU and SMX had no ecotoxicity, their mixtures presented lower EC_{50} values, with a significant increase of the ecotoxicity.

Table 1- EC_{50} (%) values for mixtures of SMX and IBU 50 ppm solutions.

% SMX	% IBU	EC_{50}-30 min (% v/v)
-	100	> 100
25	75	90.4
50	50	85.8
75	25	76.5
100	-	> 100

The photodegradation assays with titania/carbon catalysts proved to be effective, since high mineralization rates were achieved (Fig.1) within three hours of irradiation, along with the absence of ecotoxicity of the final solutions (EC_{50}-30 min > 100% v/v).
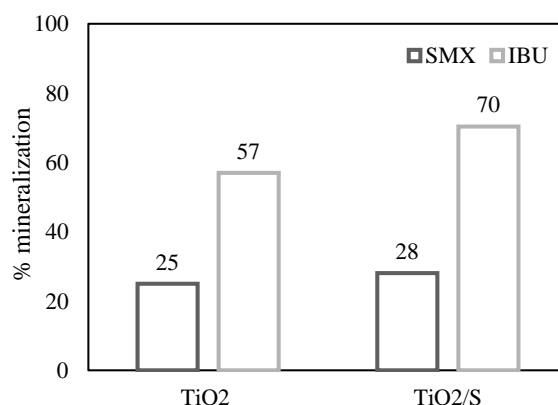

Figure 1- SMX and IBU mineralization rates with a load of 0.125 g L^{-1} of TiO_2.

CONCLUSIONS

The study proceeds with the evaluation of the best operating conditions for the photocatalytic assays, so as to achieve high mineralization along with low ecotoxicity, providing a new insight on the aquatic environment impact of the degradation products of pharmaceutical compounds.

REFERENCES

1. Carvalho, A.P., Mestre, A.S., Andrade, M., Ania, C.O. "Ibuprofen in the aquatic environment: occurrence, ecotoxicity and water remediation technologies" in Wilton C. Carter and Brant R. Brown Ed. Ibuprofen: Clinical Pharmacology, Medical Uses and Adverse Effects. Nova Science Publishers, Inc., **2013**, Ch. 1, p. 1-84. ISBN: 978-1-62618-659-0.

Oral and panel

PFC3 - PHOTOCATALYTIC DEGRADATION OF PHARMACEUTICAL COMPOUNDS BY TiO$_2$: AN ECOTOXICITY ASSESSMENT

Marta A. Andrade[1,2,] **Ana Sofia Mestre**[1], **Nuno Lapa**[3], **Benilde Mendes**[3],
Conchi O. Ania[2], **Ana Paula Carvalho**[1]

[1]*Dpt. Química e Bioquímica and CQB, Faculdade de Ciências da Universidade de Lisboa, Ed. C8 Campo Grande, 1749-016 Lisboa, Portugal.*
[2]*Instituto Nacional del Carbón (INCAR, CSIC) 33011, Oviedo, Spain.*
[3]*Dpt. Ciências e Tecnologia da Biomassa, Faculdade de Ciências e Tecnologia, Universidade Nova de Lisboa, 2829-516 Caparica, Portugal.*

In the last few years, a considerable amount of research has been carried out in the field of advanced oxidation processes (AOPs) to be applied in the removal and degradation of emergent contaminants from wastewaters. Among AOPs, heterogeneous photocatalysis is an effective technology for the degradation of organic pollutants. Compared to other semiconductors, titanium dioxide plays a leading role as photocatalyst due to its cost effectiveness, inert nature and photostability [1]. However, most of the studies on photocatalysis do not encompass an ecotoxicity evaluation, being more focused on the degradation efficiency and mineralization of the pollutants. The possible synergic effects due to the presence of various pollutants in solution are also scarcely addressed. In this context, the aim of the present work is to study the photocatalytic degradation of pharmaceutical compounds using TiO$_2$ as catalyst, and to assess the ecotoxicity variation associated with the process. The target molecules were ibuprofen (IBU), sulfamethoxazole (SMX) and mixtures IBU/SMX, as these compounds are medicines of great consumption, frequently detected in the environment.

The results are interpreted in terms of the mineralization achieved (Total Organic Carbon) and of the ecotoxicity of the initial and final solutions obtained after the photocatalytic assays. The ecotoxicity assessment was performed by the bioluminescence inhibition of the bacterium *Vibrio fischeri* using the Microtox® assay. The results were expressed as the Effective Concentration for 50 % bioluminescence inhibition after 30 min of exposure (EC$_{50}$-30 min).

The initial solutions of IBU and SMX and their mixtures presented high EC$_{50}$ values; the mixtures presented an increase of the ecotoxicity. The photodegradation assays with TiO$_2$ proved to be effective, since high mineralization rates along with the absence of ecotoxicity of the final solutions were achieved. This study will proceed with the evaluation of the best operating conditions for the photocatalytic assays, providing a new insight on the degradation of this class of compounds, as well as on their ecotoxicity for a bacterium of the marine environment.

[1] Carvalho, A.P., Mestre, A.S., Andrade, M., Ania, C.O. "Ibuprofen in the aquatic environment: occurrence, ecotoxicity and water remediation technologies" in Wilton C. Carter and Brant R. Brown Ed. Ibuprofen: Clinical Pharmacology, Medical Uses and Adverse Effects. Nova Science Publishers, Inc., **2013**, Ch. 1, p. 1-84. ISBN: 978-1-62618-659-0.

Oral

20 - 23 OCTUBRE, 2013 / E.T.S.I. DE MINAS Y ENERGÍA

XII reunión

grupo español del Carbón

Madrid 2013

Sección de
Ingeniería Química

E.T.S.I.
de Minas y Energía

Universidad
Autónoma de Madrid

Universidad
Politécnica de Madrid

FACULTAD DE CIENCIAS

UNIVERSIDAD AUTONOMA DE MADRID

POLITÉCNICA

FUNDACION GOMEZ PARDO

CARBUNION

TiO₂/Cu-DOPED CARBON COMPOSITES AS CATALYSTS FOR PHENOL PHOTODEGRADATION

M. Andrade[1,2], A.S. Mestre[1], A.P. Carvalho[1], C.O. Ania[2]

[1]*Dpt. Química e Bioquímica and CQB, Faculdade de Ciências da Universidade de Lisboa, Ed. C8, Campo Grande, 1749-016 Lisboa, Portugal*

[2]*Instituto Nacional del Carbón (INCAR, CSIC) 33011, Oviedo, Spain*

mvandrade@fc.ul.pt

Palabras clave: photocatalysis, copper, titania, activated carbon

The incorporation of transition metals with catalytic activity on the surface of activated carbons is a powerful tool offering great possibilities in the preparation of selective adsorbents and/or catalysts for environmental remediation processes.

The aim of the present work was to investigate the effect of copper on the photocatalytic activity of TiO₂/Cu-doped carbon composites in the degradation of phenol from aqueous medium. Carbons with diferent copper loadings were prepared by a one-pot route consisting in the impregnation of a lignocellulosic industrial residue (carbon precursor) using copper nitrate and K₂CO₃, followed by chemical activation. The obtained materials were characterized by several techniques and resulted to be essentially microporous materials exhibiting a homogenous distribution of copper species (Cu^0/Cu^{2+}) within the carbon matrix. Phenol photooxidation efficiency of the hybrid carbon/titania composites was found to be strongly modified by the incorporation of small amounts of copper in the carbon material. The copper-loaded hybrid composite increased the photodegration rate of phenol in solution, as well as the mineralization rate of the intermediates.

Oral

The Annual World Conference on Carbon

July 14-19, 2013

Windsor Atlântica Hotel - Copacabana

Rio de Janeiro - Brazil

Program and Abstracts

Organization

ABCarb   PETROBRAS

Annex D

318

Phenol photocatalytic degradation by TiO2/Cu-doped carbon composites

Marta Andrade[a,*], Ana S. Mestre[a], Juan Matos[b], Ana P. Carvalho[a], Conchi O. Ania[c]

[a] Dpt. Química e Bioquímica and CQB, Faculdade de Ciências da Universidade de Lisboa, Ed. C8, Campo Grande, 1749-016 Lisboa, Portugal
[b] Dpt. Catalysis and Alternative Energies. Venezuelan Institute for Scientific Research (IVIC), 20632, Caracas 1020-A, Venezuela
[c] Instituto Nacional del Carbón (INCAR, CSIC) 33011, Oviedo, Spain

Heterogeneous photocatalysis is an expanding technology for the removal of toxic pollutants in wastewater treatment plants. Carbons have been successfully used as supports of photoactive species and carbon/semiconductor composites have shown quite high efficiencies for the photodegradation of a variety of pollutants [1,2]. Recently, it has also been reported that certain activated carbons possess a significant level of self-photochemical activity [3]. On the other hand, the incorporation of transition metals with catalytic activity on the surface of activated carbons is a powerful synthesis tool which offers great possibilities in the preparation of selective adsorbents and/or catalysts for processes of environmental remediation, in particular in the adsorption and/or degradation of contaminants. In this context, the aim of the present work was to investigate the photocatalytic activity of composites of TiO_2/Cu-doped carbons on the degradation of phenol from aqueous medium.

Carbons with diferent copper loadings were prepared by a one-pot route consisting in the impregnation of a lignocellulosic industrial residue (carbon precursor) using copper nitrate and K_2CO_3, followed by chemical activation to develop a porous network. The obtained materials were characterized by several techniques (gas adsorption, TEM, XPS, XRD) and resulted to be essentially microporous materials exhibiting a homogenous distribution of copper species within the carbon matrix. The photocatalytic activity of the hybrid carbon/TiO_2 composites towards phenol degradation was found to be strongly modified by the incorporation of copper in the carbon material. The copper-loaded hybrid composite increased the photodegration rate of phenol in solution, as well as the mineralization rate of the intermediates, revealing a copper-promoted enhancement of the carbon/titania synergy effect [4]. These results have been analyzed in terms of the chemical state of the copper species incorporated to the carbon matrix.

[1] R. Leary, A. Westwood, Carbonaceous nanomaterials for the enhancement of TiO_2 photocatalysis, Carbon 49 (3) 2011, p. 741-72.

[2] J. L., Faria, W. Wang, Carbon materials in photocatalysis (chapter 13), in Carbon Materials for Catalysis, (Serp, Ph., Figueiredo, J. L. eds.) Wiley & Sons, 2009.

[3] L.F. Velasco, J.B. Parra, C.O. Ania, Role of activated carbon features on the photocatalytic degradation of phenol, Appl. Surf. Sci. 256 (17) 2010, p. 5254-8.

[4] J. Matos, E. García-López, L. Palmisano, A. García, G. Marcì, Influence of activated carbon in TiO2 and ZnO mediated photo-assisted degradation of 2-propanol in gas-solid regime, Appl. Catal. B: Environ. (99) 2010, p. 170-180.

113

Panel

The Annual World Conference on Carbon
June 17-22, 2012
Krakow, Poland

Program and Abstracts

**Carbon2012**

Polish Carbon Society

ID 599
Copper Doped Carbons for Environmental Remediation
M. Andrade, A.S. Mestre, M. Haro, A.P. Carvalho, C.O. Ania

Copper doped carbons were prepared following a one-step procedure by chemical activation (using copper salts and K_2CO_3) of a lignocellulosic residue (ropes). The adsorption performance of the obtained materials on the removal of caffeine and paracetamol from liquid phase shows theirs potentialities as catalysts for the degradation of pharmaceutical compounds.

Page 112

Panel
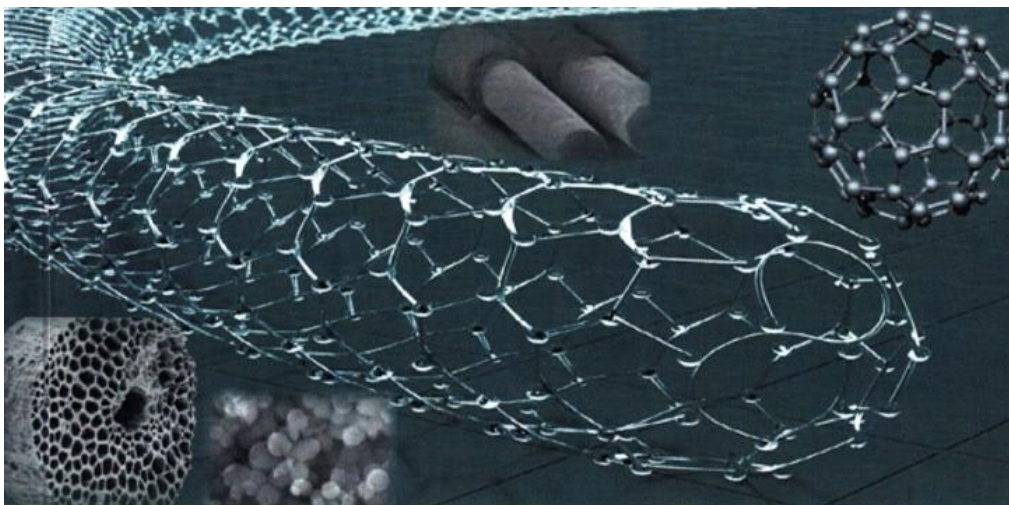
EFECTO PROMOTOR DEL COBRE EN EL DESARROLLO TEXTURAL DURANTE LA GASIFICACIÓN CATALÍTICA EN AIRE DE CARBONES ACTIVADOS

Haro, M.[1], Ruiz, B.[1], Andrade, M.[2], Mestre, A.S.[2], Parra, J.B.[1], Carvalho, A.P.[2*], Ania, C.O.[1*]

[1]*Instituto Nacional del Carbón, INCAR-CSIC, Apdo. 73, 33080-Oviedo, Spain.*
[2]*Departamento de Química e Bioquímica and CQB, Faculdade de Ciências da Universidade de Lisboa, Ed. C8, Campo Grande, 1740-16-Lisboa, Portugal.*

mharo@incar.csic.es

Palabras clave: Cobre, gasificación catalítica, porosidad, carbón activado.

1. Introducción

La incorporación de metales de transición con actividad catalítica en soportes porosos es una herramienta de síntesis que ofrece grandes posibilidades en la preparación de adsorbentes selectivos y/o catalizadores más eficientes para su empleo en procesos de adsorción/degradación de contaminantes [1-3].

En este trabajo se llevó a cabo la preparación de carbones activados dopados con cobre, investigando los mecanismos de interacción del cobre con la matriz carbonosa en función de la naturaleza del carbón activado (carbón mineral o lignocelulósico). Se han evaluado asimismo las propiedades fisicoquímicas y texturales de los carbones dopados obtenidos así como la dispersión del cobre.

2. Experimental

Como materiales de partida se utilizaron dos carbones activados obtenidos a partir de la activación física de un carbón mineral (muestra Q) y de un residuo lignocelulósico (agave sisalana, *sisal*) generado durante la manufacturación de cuerdas (muestra S). La muestras se impregnaron con $Cu(NO_3)_2$ al 1 % en agua durante 24 h y posteriormente fueron sometidas a un tratamiento térmico en aire hasta 325 °C, con un tiempo de residencia de 3 horas (series *Cu*). Todos los materiales preparados fueron caracterizados química y texturalmente. Los análisis inmediato y elemental, fueron realizados en equipos automáticos LECO: TGA-701, CHNS-932 con un módulo para determinación directa de oxígeno VTF-900. La caracterización textural se determinó por adsorción de N_2 a -196 °C y de CO_2 a 0 °C (Micromeritics ASAP 2020 y TriStar 3020). Las muestras se analizaron por difracción de rayos X y análisis térmico en atmósfera inerte y en aire.

3. Resultados y discusión

La gasificación en aire a 325 °C de los carbones activados seleccionados en ausencia de cobre da lugar a dos comportamientos claramente diferenciados en función de la naturaleza del material de partida. En el caso del carbón activado obtenido por activación física de un carbón bituminoso (muestra Q), la temperatura seleccionada es suficientemente baja como para que la reacción de gasificación apenas tenga lugar (Figura 1). Así, no se observan cambios significativos en la composición química o la porosidad, más allá de un leve descenso en el área superficial y un débil incremento del contenido en oxígeno. En cambio, estas condiciones experimentales resultan demasiado drásticas para el carbón activado obtenido a partir del residuo lignocelulósico ya que la gasificación

169

no catalítica a 325 °C da lugar a la calcinación casi completa de la muestra (rendimiento final de carbono del 27 %). El sólido obtenido adquiere un color grisáceo y se produce un colapso total de la porosidad.
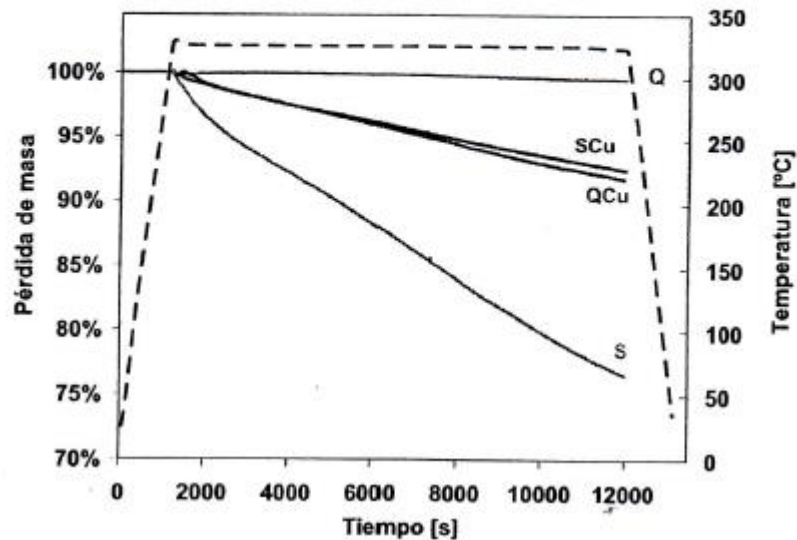

Fig. 1. Perfiles de reactividad en aire de los carbones activados estudiados.

La incorporación de cobre en ambos materiales tiene un efecto doble. En el caso del carbón activado Q, el cobre actúa como catalizador de la gasificación en aire, dando lugar a un desarrollo textural importante con un aumento significativo de la microporosidad [4]. En el caso de la muestra S, la incorporación del cobre actúa como protector de la matriz carbonosa de manera que la muestra dopada tras la calcinación presenta un elevado desarrollo textural, superior al de la muestra de partida. Este cambio en la velocidad de gasificación en aire tras la inmovilización de cobre en función del origen del carbón activado se confirma en los estudios de gasificación isotermal en termobalanza (Figura 1). Además, en ambos casos se consigue una dispersión homogénea de las partículas de cobre, por lo que los carbones activados resultantes poseen propiedades interesantes para su utilización como adsorbentes selectivos y catalizadores.

Bibliografía

[1] J.L. Figueriedo, Carbon Materials for Catalysis, Serp Ph, John Wiley and Sons, New Jersey, 2009.
[2] D. Nguyen-Tahnh, T.J. Bandosz, Microporous Mesoporous Mat. 92 (2006) 47-55.
[3] C.O. Ania, T.J. Bandosz, Energy Fuels. 20 (2006) 1076-1080.
[4] R.T.K. Baker, J.J. Chludzinski Jr, Carbon. 19 (1981) 75-82.

Annex D

Panel

Role of copper as an additive during physical and chemical activation of a lignocellulosic precursor

Andrade M[1], Ruiz B[2], Mestre AS[1], Parra JB[2], Carvalho AP[1], Ania CO[2]

[1] Departamento de Química e Bioquímica and CQB, Faculdade de Ciências da Universidade de Lisboa, Ed. C8, Campo Grande, 1749-016 Lisboa (Portugal)
[2] Instituto Nacional del Carbón (INCAR), CSIC, P.O. 73, 33080 Oviedo, Spain

The incorporation of certain metals to the surface of activated carbons is an approach that allows the preparation of advanced materials with superior performance in many applications (enhanced gas storage and selectivity, improved energy storage ability, induced reactive adsorption or catalytic activity) [1-3]. One of the key aspects is to achieve a high metal dispersion on the carbon matrix, for which several methods have been widely investigated [4,5]. After the incorporation of the metallic species on the material surface, the chemical features and properties are modified; very often the porosity of the porous material is also largely modified during the doping process.

The objective of this work was to investigate the role of copper as an additive during the chemical and physical activation of a lignocellulosic residue. To attain this goal, activated carbons were prepared by physical (CO_2) and chemical activation (K_2CO_3) of a lignocellulosic industrial residue (i.e., ropes). The as-received ropes were cut into small pieces, and their thermal stability was investigated under inert and oxidizing atmosphere. For the chemical activation, the ropes were directly impregnated with ca. 7 mmol of copper (hydroxidcarbonate and acetate salts) and K_2CO_3 (ratio K_2CO_3/precursor 0.5:1) and subsequently heated at 700 °C (10 °C/min) under N_2 atmosphere for 1 hour. For the physical activation, copper impregnation was carried before (raw carbon precursor) and after (char) the carbonization step at 700 °C.

The immobilization of copper during the early stages of the synthetic route allowed a good dispersion and distribution of the metallic species within the porous carbonaceous matrix, along with a few clusters randomly dispersed on the outer surface of the carbon matrix. Due to the reactive atmosphere during the activations, the copper was mainly in the form of oxides; however, some zero valence clusters were also randomly dispersed on the carbon surface. This might be attributed to the low reduction potential of the pair Cu (II)/Cu. Moreover, the incorporation of low amounts of copper to the carbon precursor before activation favoured the development of the microporosity. This catalytic role of copper might be linked to the large amount of oxygen present in the carbon precursor, and the ability of copper species to activate oxygen creating reactive adducts that favour the formation of new pores in the material.

References

[1] Ania, C.O., Bandosz, T.J., Carbon 2006, 44, 2404-2412.
[2] Froudakis, G.E., Nano Letters, 2001, 1, 531–533.
[3] Serp, Ph., Figueiredo, J.L. (edts) in Carbon Materials for Catalysis, Wiley & Sons Inc. Pub., 2008.
[4] Hines, D., Bagreev, A., Bandosz, T.J., Langmuir 2004, 20, 3388–97.
[5] Titirici, M.M., Antonietti, M., Thomas, A., Chem. Mater. 2006, 18, 3808-3812.